The Pennsylvania State University

The Graduate School

Department of Biochemistry and Molecular Biology

PROTEINS AS BIOMARKERS FOR TOBACCO-INDUCED LUNG CANCER DEVELOPMENT AND CHEMOPREVENTION

A Dissertation in

Biochemistry and Molecular Biology

by

James D. Bortner, Jr.

Submitted in Partial Fulfillment
of the Requirements
for the Degree of

Doctor of Philosophy

August 2011

The dissertation of James D. Bortner, Jr. was reviewed and approved* by the following:

Karam El-Bayoumy
Professor of Biochemistry and Molecular Biology
Dissertation Advisor
Chair of Committee

Arunangshu Das
Assistant Professor of Biochemistry and Molecular Biology

Gail Matters
Associate Professor of Biochemistry and Molecular Biology

David Phelps
Professor of Pediatrics

John Richie, Jr.
Professor or Public Health Sciences and Pharmacology

Cara-Lynne Schengrund
Professor Emeritus of Biochemistry and Molecular Biology

Judith S. Bond
Distinguished Professor and Chair
Head of the Department of Biochemistry and Molecular Biology

*Signatures are on file in the Graduate School

ABSTRACT

Background: As discussed in **Chapter 1**, lung cancer continues to be the most common cancer diagnosed in the world and is the leading cause of cancer-related death in both men and women in the United States. The non-small cell lung cancer (NSCLC) subtype adenocarcinoma is the leading histological type clinically diagnosed in the United States, accounting for over 30% of all cases. The primary risk factor associated with lung cancer is related to cigarette smoking; approximately 87% of lung cancer deaths in the United States are attributed to cigarette smoking. Existing approaches using conventional treatment strategies, including surgery, radiation therapy, and chemotherapy, have generated minimally significant results for lung cancer survival; 5-year survival for all stages combined is 16%. Furthermore, the disease is often diagnosed at advanced stages of development, beyond the benefit of current treatment. Therefore, alternative approaches in the management of lung cancer, such as early detection and prevention, are urgently needed. In the present investigation we embark upon two strategies with promising clinical implications: identification of (informative) molecular biomarkers related to the development of tobacco-induced lung cancer and the discovery of novel chemopreventive agents.

Hypotheses: Current clinical protein biomarkers for detection of lung cancer lack sensitivity and specificity. The proteomics field can contribute greatly to the understanding of mechanisms in cancer progression and treatment response. Therefore, in **Chapter 2** we hypothesized that by using proteomic approaches in a well-defined preclinical mouse lung tumorigenesis model induced using the tobacco carcinogen NNK, protein biomarkers could be obtained to provide an accurate view of molecular alterations during lung cancer development. Such biomarkers can provide utility for early detection, but also in the validation of chemoprevention strategies. Smokers are at risk for a variety of health concerns including lung cancer. Non-invasive biological fluids such as blood plasma contains molecular profiles related to current health status.

Therefore, in **Chapter 3** taking advantage of proteomic techniques and proteins identified in Chapter 2, we hypothesized that dynamic changes in protein expression profiles in the blood plasma of smokers characterized by a proteomics approach would assist in identifying early molecular changes related to tobacco-induced diseases such as lung cancer. Selenium-containing compounds are promising chemopreventive agents against lung cancer development. Developments of agents that can target molecular pathways that are critical in lung carcinogenesis, such as nitric oxide synthase (iNOS) and nitric oxide production, known to be involved in the promotion/progression phases of lung carcinogenesis, are needed and may be beneficial in chemoprevention of lung cancer in both smokers and former smokers. Therefore, in **Chapter 4** we hypothesized that substitution of sulfur for selenium in an inducible nitric oxide synthase inhibitor, *S*,*S*'-(1,4-phenylenebis[1,2-ethanediyl])bisisothiourea (PBIT), would enhance its chemopreventive activity.

Methods: (**Chapter 2**) The proteomic techniques two-dimensional differential in-gel electrophoresis (2D-DIGE) and isobaric tags for relative and absolute quantitation (iTRAQ) were employed to achieve a global protein expression profile of the lung during the progression of disease development in the NNK-induced lung tumorigenesis A/J mouse model. Furthermore, the synthetic organoselenium chemopreventive agent 1,4-phenylenebis(methylene)selenocyanate (*p*-XSC) was administered to validate potential protein biomarkers. (**Chapter 3**) In order to gain an understanding of some of the dynamic protein changes in human plasma as a result of chronic exposure to mainstream tobacco smoke, we used iTRAQ and immunoblot analyses in blood plasma samples derived from healthy male smokers and non-smokers. (**Chapter 4**) To compare the efficacy of the novel selenium analog of PBIT (*Se*-PBIT) with PBIT and *p*-XSC, various *in vitro* molecular assays were performed in NSCLC cells including detection of nitric oxide production, cellular proliferation and apoptosis, cell cycle distribution, and protein expression related to important cellular activities.

Results: (**Chapter 2**) We discovered proteins, including the 14-3-3 protein isoforms (θ, ε, σ, and ζ), annexin A5, Clara cell 10 kDa protein (CC10), high mobility group box 1, and carbonyl reductase 2 that were differentially expressed in the lungs of mice treated with the tobacco carcinogen NNK versus vehicle (control)-treated mice during the progression of adenocarcinoma development; some of these changes were further modulated by *p*-XSC. These proteins are involved in a variety of biological functions that are critical in lung carcinogenesis, as well as in its prevention. (**Chapter 3**) We identified differentially expressed plasma proteins in healthy chronic cigarette smokers compared to healthy non-smokers. Several of the proteins identified, including ITI-HC3 and VDBP, associated with immunity and inflammatory responses, and 14-3-3 σ and ζ, identified in Chapter 2, have been shown to be associated with tobacco-related diseases, including chronic obstructive pulmonary disease (COPD) and lung cancer. (**Chapter 4**) We found *Se*-PBIT to be superior to both PBIT and *p*-XSC as an inducer of apoptosis and inhibitor of cell growth in NSCLC cells, as determined by analysis of its effects on important molecular targets involved in cell growth inhibition, induction of apoptosis, and cell cycle regulation.

Conclusions: (**Chapter 2**) Based on our results, we were able to demonstrate the utility of a well-defined animal model in developing candidate protein biomarkers for lung cancer. Such biomarkers may be useful in early detection of the disease, as well as in the efficacy of chemopreventive agents. (**Chapter 3**) Our clinical pilot study results demonstrated for the first time that chronic cigarette smoking can influence the expression profile of the human plasma proteome and these changes may be indicative of future health concerns. (**Chapter 4**) We demonstrated that selenium in the form of *Se*-PBIT is a promising candidate for chemoprevention of NSCLC and appears superior to PBIT and *p*-XSC.

TABLE OF CONTENTS

LIST OF FIGURES

LIST OF TABLES

LIST OF ABBREVIATIONS

1,25-OHD	1,25-dihydroxyvitamin D
2D-DIGE	Two-dimensional differential in-gel electrophoresis
7-mG	7-methylguanine
AAT	α-1-antitrypsin
ABI	Applied Biosystems Inc.
ACE	Angiotensin 1 converting enzyme 1
ACO2	Aconitase 2
ACSL4	Acyl-CoA synthetase long-chain family member 4
ACVP	American College of Veterinary Pathologist
AGT	O^6-alkylguanine-DNA-alkyltransferase
AIN	American Institute of Nutrition
ALDH	Aldehyde dehydrogenase
ANXA5	Annexin A5
ARHGDIA	Rho GDP dissociation inhibitor (GDI) α
ATBC	α-Tocopherol, β-Carotene Trial
ATCC	American Type Culture Collection
ATP5B	ATP synthase, H^+ transporting, mitochondrial F1 complex, β polypeptide
B[a]P	Benzo[a]pyrene
BALF	Bronchoalveolar lavage fluid
C1R	Complement component 1, r subcomponent
C8α, β, γ	Complement component 8 α, β, γ polypeptide
CA1	Carbonic anhydrase 1
Calm1	Calmodulin 1
CALR	Calreticulin
CARET	β-Carotene and Retinol Efficacy Trial
Cbr2	Carbonyl reductase 2
CC10	Clara cell 10 kDa protein
CD34	CD34 molecule
CD36	CD36 molecule

CDK	Cyclin dependent kinase
CDKN2A	Cyclin-dependent kinase inhibitor 2A
CEA	carcinoembryonic antigen
CEACAM6	Carcinoembryonic antigen-related cell adhesion molecule 6
CES1	Carboxylesterase 1
CHAPS	3-[(3-Cholamidopropyl)-dimethylammonio]-1-propane sulfonate
cICAT	cleavable isotope-coded affinity tags
COPD	Chronic obstructive pulmonary disease
COX-2	Cyclooxygenase-2
cPLA2	Cytosolic phospholipase A2
CRP	C-reactive protein
CT	Computed tomography
CYB5B	Cytochrome b5 type B
CYFRA 21-1	cytokeratin fragment 21-1
CYP450	Cytochrome P450
DC	Detergent compatible
DENND4A	DENN/MADD domain containing 4A
DMSO	Dimethyl sulfoxide
DPYSL2	Dihydropyrimidinase-like 2
DTT	Dithiothreitol
ECL	Enhanced chemiluminescence
ECOG	Eastern Cooperative Oncology Group
EDTA	Ethylenediaminetetraacetic acid
EF	Error factor
EGFR	Epidermal growth factor receptor
EGTA	Ethylene glycol tetraacetic acid
eIF2α	Eukaryotic initiation factor 2 α
EIF4A3	Eukaryotic translation initiation factor 4A, isoform 3
EMEM	Eagle’s Minimum Essential Medium
eNOS	Endothelial nitric oxide synthase
ER	Endoplasmic reticulum
ERBB2	v-erb-b2 erythroblastic leukemia viral oncogene homologue 2

ERK	Extracellular signal-regulated kinase
ETS	Environmental tobacco smoke
EUROSCAN	European Study on Chemoprevention of Vitamin A (retinyl palmitate) and *N*-acetylcysteine
F13A	Coagulation factor XIII A chain
F5	Coagulation factor V
FACS	Fluorescence-activated cell sorting
FAM107A	Family with sequence similarity 107, member A
FBS	Fetal bovine serum
FCTC	Frame-work Convention and Tobacco Control
FDA	Food and Drug Administration
FDR	False discovery rate
FMO1	Flavin containing monooxygenase 1
FSPTCA	Family Smoking Prevention and Tobacco Control Act
GRP78	Glucose-regulate protein 78
GSN	Gelsolin
H&E	Hematoxylin and eosin
HMGB1	High-mobility group box 1
HRP	Horseradish peroxidase
HSP90B1	Heat shock protein 90kDa β, member 1
HSPA8	Heat shock protein 70kDa protein 8
IARC	International Agency for Research on Cancer
ID	Identification
IEF	Isoelectric focusing
IFN-γ	Interferon-γ
IL-	Interleukin
iNOS	inducible nitric oxide synthase
ip	intraperitoneal
IPA	Ingenuity Pathway Analysis
IPG	Immobilized pH gradient
ITGB1	Integrin, β 1
ITGB2	Integrin, β 2 (complement component 3 receptor 3 and 4 subunit)

ITI-HC3, 4	Inter-α-trypsin inhibitor heavy chain 3, 4
iTRAQ	isobaric Tags for Relative and Absolute Quantitation
KLST	Kallistatin
KRAS	Kirsten RNA associated rat sarcoma 2 virus gene
LC	Liquid chromatography
L-NA	L-Nitroarginine
LPS	Lipopolysaccharide
LYZ	Lysozyme
MALDI	Matrix assisted laser desorption ionization
MAP	Mitogen-activated protein
MARS	Multiple affinity removal system
MASP-1	Mannan-binding lectin serine protease 1
MBP-C	Mannose-binding protein C
MFAP4	Microfibrillar-associated protein 4
miRNA	microRNA
MS	Mass spectrometry
MTT	3-(4,5-dimethylthiazol-2-yl)-2,5-diphenyltetrazolium bromide
MYC	Myelocytomatosis
MYL6	Myosin, light chain 6, alkali, smooth muscle and non-muscle
NADPH	Nicotinamie adenine dinucleotide phosphate
NBF	Neutral buffered formalin
NCBI nr	National Center for Biotechnology Information non-redundant
NCI	National Cancer Institute
NCL	Nucleolin
NFκB	Nuclear factor-κB
NIH	National Institute of Health
NLF	Nasal lavage fluid
NNAL	4-(methylnitrosamino)-1-(3-pyridyl)-1-butanol
NNAL-Gluc	Glucuronidation of NNAL
NNK	Nicotine-derived nitrosamine ketone, 4-(methylnitrosamino)-1-(3-pyridyl)-1-butanone
nNOS	Neuronal nitric oxide synthase

NO	Nitric oxide
NOS	Nitric oxide synthase
NPR	Nutritional Prevention of Cancer
NSCLC	Non-small cell lung cancer
O^6-mG	O^6-methylguanine
P4HB	Prolyl 4-hydroxylase, β polypeptide
PAH	Polycyclic aromatic hydrocarbon
PANTHER	Protein Analysis THrough Evolutionary Relationships
PARP	Poly (ADP-ribose) polymerase
PBIT	*S*,*S*'-(1,4-phenylenebis[1,2-ethanediyl])bisisothiourea
PBS	Phosphate-buffered saline
PCA	Principal components analysis
PCR	Polymerase chain reaction
PDI	Protein disulfide isomerase
PECAM1	Platelet/endothelial cell adhesion molecule
PET	Positron emission tomography
PI	Propidium iodide
PIC	Protease inhibitor cocktail
PLUNC	Palate, lung and nasal epithelium carcinoma associated precursor
PMSF	Phenylmethylsulfonyl fluoride
POB	Pyridyloxobutylated
ppm	Parter per million
PRDX6	Peroxiredoxin 6
PSEP	Proteomics system performance evaluation pipeline
PSMA5	Proteasome (prosome, macropain) subunit, α type, 5
PTMA	Prothymosin, α
PXN	Paxillin
p-XSC	1,4-phenylenebis(methylene)selenocyanate
RAGE	Receptor for advanced glycation endproducts
RB	Retinoblastoma
REM1	RAS (RAD and GEM)-like GTP-binding 1
RNaseA	Ribonuclease A

RRAD	Ras-related associated with diabetes
S	Sulfur
SCGB1A1	Secretoglobin, family 1A, member 1 (uteroglobin, CC10)
SCLC	Small cell lung cancer
SCX	Strong cation exchange
SDS	Sodium dodecyl sulfate
SE	Standard error
Se	Selenium
SELECT	Selenium and Vitamin E Cancer Prevention Trial
SELENBP1	Selenium binding protein 1
Se-PBIT	*Se*,*Se*'-(1,4-phenylenebis[1,2-ethanediyl])bisisoselenourea
SHBG	Sex-hormone binding globulin
SILAC	stable isotope labeling with amino acids in cell culture
T20	Tween-20
TBS	Tris-buffered saline
TCA	Trichloroacetic acide
TCEP	Tris-(2-carboxyethyl)phosphine
TEAB	Triethylammoniumbicarbonate
TLN1	Talin 1
TNF-α	Tumor necrosis factor-α
ToF	Time-of-flight
TSNA	Tobacco-specific nitrosamine
UPR	Unfolded protein response
UV	Ultraviolet
VDBP	Vitamin D-binding protein
VEGF	Vascular endothelial growth factor
VIM	Vimentin
VTN	Vitronectin
WHO	World Health Organization
YWHAD, Q, Z, E	Tyrosine 3-monooxygenase tryptophan 5-monooxygenase activation protein δ, θ, ζ, ε polypeptide

AKNOWLEDGEMENTS

The journey through graduate school was filled with lots of frustration and stress (as indicated by the gray and white hairs that appeared on the top of my head beginning from year 1), but also with plenty of joy and excitement. However, provided the opportunity to work with a number of caring and supportive individuals over the years, I was able to overcome any obstacle in my path.

I would like to express my deepest gratitude to my mentors Dr. Karam El-Bayoumy and Dr. Arunangshu (Arun) Das for their patience, guidance, and support. The work ethic and enthusiasm that Karam brings to the field of science is absolutely contagious. There was never an instance that he was too busy during the day and couldn't find the time to discuss science. Working with Arun has been an absolute pleasure. He has become a great friend and truly someone I am fortunate to have met in my life. He has taught me valuable skills not only in the laboratory, but also in everyday life.

I would like to thank the members of my committee, Dr. Gail Matters, Dr. David Phelps, Dr. John Richie, and Dr. Cara-Lynne Schengrund for their positive support and guidance.

I would also like to thank Todd Umstead, Dr. Bruce and Anne Stanley, and everyone associated with the El-Bayoumy laboratory. The working relationship and friendships I have developed with these individuals made my graduate school career very enjoyable.

And last but not least, I would also like to my family and friends for their relentless encouragement and love throughout this exhaustive journey. Without these people in my life this would not have been possible.

Chapter 1

Introduction

Etiology of Lung Cancer and Current and Alternative Approaches in Disease Management

1. Lung cancer

1.1 Cancer statistics

Lung cancer continues to be a major global health burden. Among all cancers diagnosed yearly, lung cancer accounts for 12% of all new cases (1). In contrast to the 1980s, when developed countries experienced the most cases of lung cancer (69%), the incidence is now fairly proportionate with 49.9% occurring in developing countries (2). Men in Eastern Europe, North America, and Russia experience the highest incidence, whereas in women, high incidence occurs in North America, the Scandinavian countries, and China (1). Despite lower levels of smoking compared to European countries (3), the higher incidence of lung cancer observed in Chinese women is largely due to poor air quality as a result of unventilated coal-fueled stoves and cooking fumes (4). Worldwide, it is the leading cause of cancer death in men and the second leading cause of cancer death in women with about 975,000 men and 376,000 women estimated to have succumbed to the disease in 2007 alone (1).

In the United States, an estimated 222,520 new cases of lung cancer were diagnosed and 157,300 individuals died of lung cancer in 2010 (5). Although men have seen declines in incidence and mortality beginning in the mid-1990's, incidence rates in women are still increasing, and mortality rates have stabilized, as observed from 2003 to 2005 (6). Survival following a lung cancer diagnosis has only changed slightly, with an overall 5-year relative

survival rate for all stages combined increasing from 12.4% in 1974-1976 to 15% in 1996-2002 (7), and currently rests at 16% (5). This minimal improvement in survival reflects limited advances in screening and current conventional treatment modalities, including surgery, radiation, and chemotherapy, and thus, emphasizes the need to pursue alternative approaches for the management of lung cancer.

1.2 Molecular pathogenesis of cancer

The development of lung cancer results from an accumulation of numerous molecular abnormalities over a relatively long period of time caused by a variety of factors (8). In general, early preneoplastic lesions in the lung appear morphologically distinct before becoming clinically overt lung cancer. The progression of these preneoplastic lesions begins with transformation from a normal cell to hyperplasia to metaplasia to dysplasia to carcinoma *in situ* and finally, invasive cancer (9). In the bronchial epithelium and adjacent tissue, early preneoplastic events are often associated with instability of the genome, including gene silencing through methylation, DNA sequence changes, amplifications, deletions, and whole chromosomal gains or losses. These events can cause inactivation of specific tumor suppressor genes, such as *P53* and *P16*, the activation of specific oncogenes, such as myelocytomatosis (*MYC*) and Kirsten RNA associated rat sarcoma 2 virus gene (*KRAS*), and the expression of hormone receptors and growth factors, such as epidermal growth factor receptor (*EGFR*), necessary for cancer development (8).

1.3 Cancer etiology

Although the development of lung cancer can be caused by a variety of factors including occupational and environmental, e.g. asbestos, air pollution, and radiation, and genetic, the most important risk factor is unequivocally related to tobacco use (5,10,11). Worldwide, cigarette smoking accounts for approximately 80% of lung cancer cases in men and 50% in women (1). In the United States, smoking accounts for 87% of lung cancer deaths (5). Besides lung cancer, the International Agency for Research on Cancer (IARC) has designated smoking to be causally

associated with at least 14 other cancers, including that of the larynx, oral cavity, esophagus, bladder, kidney, liver, and pancreas (12). Tobacco consumed in any form, but particularly when smoked, is carcinogenic (13). The strong association between cigarette smoking and lung cancer was first established in two historical large-scale case control studies by Wynder et al. (14) and Doll et al. (15) over half a century ago and was subsequently followed up in a report by the United States Surgeon General on smoking and health (16). Since then numerous studies have embarked on investigations to understand the carcinogenic properties of smoking and the responsible constituents. The risk of developing lung cancer as a male or female smoker is approximately 23 and 13 times higher, respectively, compared to lifelong non-smokers (5). For smokers, both the age at which smoking was initiated and the duration of exposure increases risk (5,17). In addition, due to the extensive damage caused by smoking, individuals with a history of smoking, i.e. former smokers, are still at an elevated risk for several years following cessation compared to a never smoker (18).

2. Tobacco smoking and lung cancer

Despite the association between lung cancer and smoking, global tobacco use continues to rise (13). It is estimated that 1.3 billion people in the world currently smoke tobacco (1). China represents the largest group containing one third of all smokers worldwide (19). In the United States, approximately 46 million adults, representing 20.6% of the population, are active smokers, and it is estimated that another 1,000 adolescents become new smokers each day (20).

In general, many current smokers wish to quit, however, in the United States of those 70% that wish to quit only 40% actually try and less than 5% succeed each year (13,21). Nevertheless, comprehensive tobacco control programs to inform the public at large as to the harmful effects of smoking have had some success as indicated by the increasing number of former smokers observed in the United States (48.1 million). Furthermore, from 1998 to 2008, the proportion of adult cigarette smokers in the United States dropped substantially from 24.1%

to 20.6% (a 3.5% total decrease) (20). However, upon further review, the proportion of cigarette smokers actually began to increase from 2007 (19.8%) to 2008 (20.6%) (20), pointing to a need to develop more awareness and newer strategies for prevention of initiation in young adults and treatments for cessation. To this end, both in the United States and globally, extensive efforts to better tobacco control programs have been made. For example, under the Family Smoking Prevention and Tobacco Control Act of 2009 (FSPTCA) signed by President Obama in June 2009, the U.S. Food and Drug Administration (FDA) now has regulatory authority over all tobacco products in the United States. With this authority, the FDA has the jurisdiction to moderate changes to tobacco products in order to protect public health. And globally, the World Health Organization (WHO) has organized the Frame-work Convention and Tobacco Control (FCTC) health treaty to regulate tobacco supply and demand by evidence-based strategies. By 2009, the FCTC was endorsed by 168 countries (13). However, the war on tobacco will continue as long as the tobacco industry is still able to devise its myriad of tactics to increase tobacco use, targeting both youth and developing countries (13). Without a doubt, lung cancer will remain among the top killers for decades unless drastic reductions in smoking prevalence are achieved (22).

2.1 Clinical classification and histopathology of lung cancer

Clinically, lung cancer is grouped into two main histological types: small cell lung cancer (SCLC), accounting for 14% of cases and non-small cell lung cancer (NSCLC), accounting for 85% of cases (5). SCLC and NSCLC exhibit major differences in tumor histopathological characteristics as determined by their distinct patterns of genetic lesions (23). For example, in NSCLC cases, the most common genetic alterations involve loss of genomic regions of chromosomes 3p and 9p, deletions of chromosomal arm 5p and mutations of *P53*, *P16*, and the oncogene *KRAS*. Loss of these chromosomal regions can prohibit expression of important genes involved in DNA repair and tumor suppression (8). The tumor suppressor gene

P53 is mutated in over 60% of lung cancers leading to dysregulation of cell-cycle control and apoptosis. *P16*, also an important regulator of the cell-cycle, is inactivated in over 40% of NSCLCs. SCLCs are aggressive lung carcinomas with neuroendocrine features that primarily develop in the peribronchial region of the lungs. They have a distinctive histologic appearance and are often diagnosed at rather advanced stages (24,25). NSCLCs are typically divided into three major subtypes: large-cell carcinoma, squamous cell carcinoma, and adenocarcinoma (24,26). Large-cell carcinomas account for 10% of all lung cancers and are poorly differentiated and appear in any part of the lungs (27). About 30% of all lung cancers are squamous cell carcinomas. Squamous cell carcinomas develop mainly in the central airways and exhibit features such as intercellular bridging, squamous pearl formation, and individual cell keratinization (25,26). Lung adenocarcinomas are currently the leading histological type diagnosed in the United States, accounting for over 30% of all cases. Adenocarcinomas consist of a histologically heterogeneous mass composed of progenitor cells of the bronchioles (Clara cells) or alveoli (Type II pneumocytes) or from mucin producing cells located in the peripheral regions of the lung (25-27). In lung adenocarcinomas, *KRAS* mutations are highly prevalent, occurring in 30% of cases, and are often found in alveolar atypical hyperplasia, a proposed early precursor lesion to adenocarcinoma development (8). KRAS is involved in various signal transduction pathways such as the extracellular signal-regulated kinase mitogen-activated protein (ERK/MAP) pathway responsible for cellular growth (9). Persistance of these cellular changes can lead to transformation and clonal expansion, and ultimately, solid tumor development.

Small cell carcinomas, squamous cell carcinomas, and adenocarcinomas are the most common histological variants of lung cancer related to smoking (28). Until the late 1950s squamous cell carcinomas were the major histological type diagnosed in smokers (14). However, over the past several decades there has been a shift towards an increased prevalence of lung adenocarcinomas (28-30). It is now widely accepted that this shift is associated with changes in

cigarette design and composition and have led to smokers modifying their smoking patterns. For example, filtered cigarettes with lower nicotine yields in smoke influence smokers to inhale more intensely to satisfy their nicotine craving; nicotine is the addictive component of tobacco (31,32). This modification results in relatively greater exposure to smoke carcinogens, and because of the deep inhalation of the smoke, these carcinogens reach the peripheral parts of the lung where adenocarcinoma primarily develops (28-30). Moreover, changes in cigarette composition have led to a relative increase in the smoke of the type of nicotine-derived carcinogenic *N*-nitrosamines that are known to induce adenocarcinoma in laboratory animals (30,33). These nitrosamines may play a significant role in the induction of adenocarcinoma in the lung of cigarette smokers (33,34).

2.2 Cigarette smoke composition

Cigarette smoke is composed of primarily two phases: a gas-vapor phase and a particulate phase. The gas-vapor phase is arbitrarily defined as the portion of the smoke that passes through a Cambridge glass fiber filter. The particulate phase is the portion that is trapped on the glass fiber filter; the size of particles ranges from 0.1 to < 0.1 μm in diameter. The gas-vapor phase accounts for up to 96% of the weight of the mainstream smoke of a non-filter cigarette and contains carbon monoxide, carbon dioxide, benzene, ammonia, formaldehyde, hydrogen cyanide, various nitrogen species, including nitrogen dioxide, and some volatile sulfur compounds. Major compounds of the particulate phase include nicotine, other nicotiana alkaloids, metals, and compounds specific to solanaceae (29). In addition, the particulate phase contains most of the carcinogenic, co-carcinogenic, and tumor-promoting compounds found in cigarette smoke (10,29,35). Both phases of cigarette smoke are also a rich source of free radicals that are thought to play an important role in carcinogenesis (10,36,37). Altogether, these components elicit some of the harmful effects imposed by cigarette smoking that support the development of lung cancer (Figure 1.1).

Of the roughly 4,000 chemical compounds found in cigarette smoke, 81 have been identified to harbor carcinogenic capabilities (11,29,38). Most of these agents are found in mainstream smoke taken up by smokers, i.e. the smoke emitted at the mouth end of the cigarette during puffing; however, they are also present in the sidestream smoke emitted from the burning cone of the cigarette, but at lower levels compared to mainstream smoke (34). Sidestream smoke constitutes most of the environmental tobacco smoke (ETS) that also causes lung cancer (34). Central to the development of tobacco-induced lung cancer is the generation of harmful DNA adducts induced by various tobacco carcinogens. If these adducts persist resulting in gene mutations, alterations in critical homeostatic pathways necessary for cellular balance may occur, and ultimately, lead to cancer development (34) (Figure 1.1).

The most important lung carcinogens in cigarette smoke are the polycyclic aromatic hydrocarbons (PAHs) and the tobacco-specific nitrosamines (TSNAs). These strong carcinogens are present at 1-200 ng per cigarette compared to the weaker carcinogen, acetaldehyde, which is present at 1 mg per cigarette. Overall, however, each cigarette contains 1-3 mg of carcinogens, similar to the amount of nicotine found in cigarettes (0.5-1.5 mg) (34); nicotine dependence provides the link through which smokers are repeatedly exposed to carcinogenic agents on a daily basis (31) (Figure 1.1).

2.3 Carcinogenicity and metabolic activation of NNK

One of the most potent and remarkably lung specific carcinogens in cigarette smoke is the TSNA, 4-(methylnitrosamino)-1-(3-pyridyl)-1-butanone (more commonly known as nicotine-derived nitrosamine ketone, NNK) (33). NNK is formed from the oxidation and nitrosation of nicotine during the curing process of tobacco and pyrosynthetically from nicotine during smoking (39). Independent of the route of administration (e.g. intragastric, intravenous, intravesicular, or topical application to skin or oral cavity), NNK specifically induces adenomas and adenocarcinomas of the lung in animal models, including rat, mouse, and hamster (33,40). More

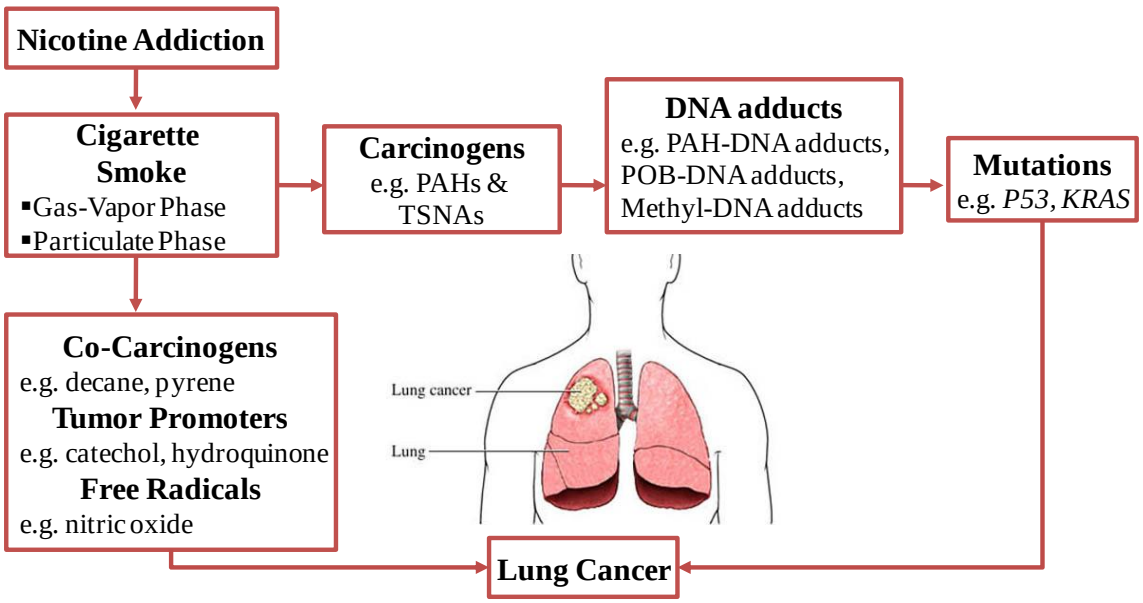

Figure 1.1 Scheme associating cigarette smoking to lung cancer development. Adapted from S.S. Hecht (34,35).

importantly, these tumors posses both morphological and molecular similarities to those observed in humans (41) and the doses of NNK administered are comparable to the exposure encountered by a smoker during his/her lifetime (40,42).

The uptake and metabolism of NNK in humans is clearly observed by detection of the metabolite, 4-(methylnitrosamino)-1-(3-pyridyl)-1-butanol (NNAL) and the NNAL glucuronidation product, NNAL-gluc, in biological fluids. Accordingly, both NNAL and NNAL-Gluc are detected at higher levels in smokers than in non-smokers (43-45). In addition, of particular interest is the findings of the results of two nested case-control studies that have demonstrated a significant relationship between levels of total serum or urinary NNAL to lung cancer risk (46,47). After performing an odds ratio analysis on serum levels of total NNAL collected at baseline in 100 lung cancer cases and 100 controls who smoked at baseline, Church et al. found that higher levels of total NNAL were significantly associated with an increased risk

of lung cancer development (odds ratio=1.57; 95% CI, 1.08-2.28; the odds ratio is a measure of the probability that a certain event is the same for two groups with a ratio greater than 1 indicating that the event is more likely to occur) (46). Moreover, a statistically significant association between total NNAL and the histological subtype adenocarcinoma was also found (46). Similarly, Yaun et al. evaluated total NNAL in a case-control study using two cohorts of Chinese cigarette smokers in which urine samples were collected from lung cancer cases and controls at baseline (47). The results of this study showed that urinary levels of total NNAL were higher in lung cancer cases than in control subjects and in combination with total urinary cotinine levels, total NNAL could independently and significantly predict lung cancer risk with an 8.5-fold increased risk for lung cancer development in individuals with the highest values of urinary metabolites (47). Thus, as a result of conclusive evidence over several decades, NNK has been designated as "carcinogenic to humans" (group 1) by the IARC and an important risk factor for lung cancer in tobacco users (48).

Extensive *in vitro* and *in vivo* investigations have demonstrated the capability of NNK to impose a variety of lethal factors to instigate and/or promote the multi-step lung carcinogenesis process. NNK itself, however, is a procarcinogen and requires metabolic activation to elicit its largely mutagenic, and carcinogenic, effects. Metabolism of NNK follows three primary, and well-understood, pathways: i) carbonyl reduction, ii) α-hydroxylation (hydroxylation of carbons adjacent to the *N*-nitroso group), and iii) pyridine *N*-oxidation (Figure 1.2). The major metabolic pathway in the liver and lung of rodents and humans is carbonyl reduction of NNK by carbonyl reductases, such as 11-β-hydroxysteroid dehydrogenase, to generate the aforementioned *N*-nitroso alchohol NNAL (33). Both NNK and NNAL have similar mutagenic activity due in part to the intermediates generated during cytochrome P450 (CYP450) enzyme mediated α-hydroxylation (49). The current human pulmonary CYP450 enzymes responsible for α-hydroxylation include CYP2A6/CYP2A13, CYP2B6, CYP3A4/3A5, and CYP2E1 (33,50). Alpha-hydroxylation is

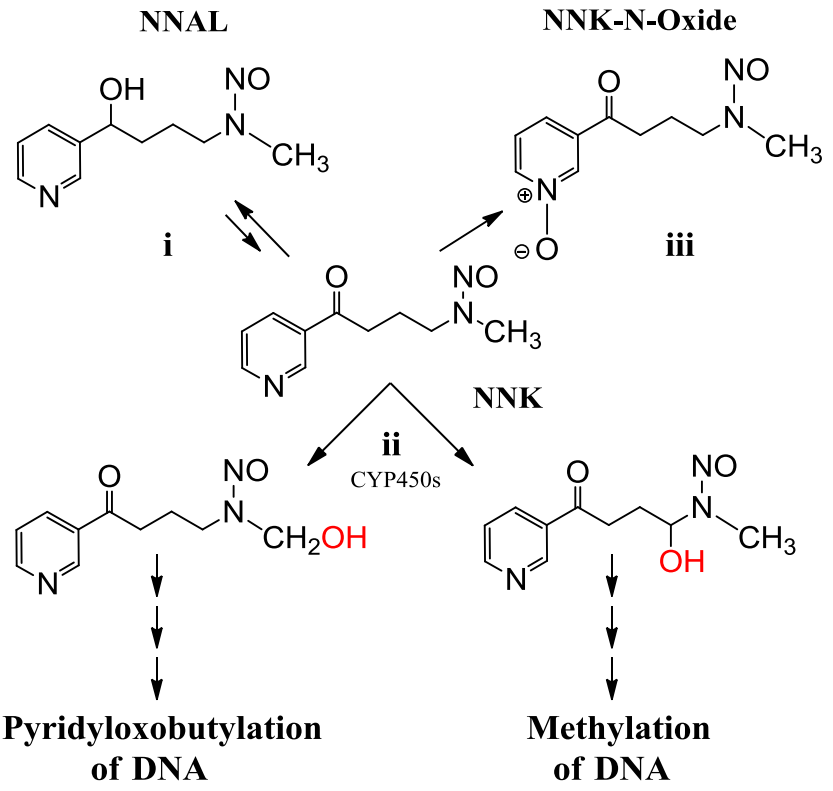

Figure 1.2 Metabolism of the tobacco-specific nitrosamine NNK.

the major route of the metabolic activation of NNK and NNAL that generates species that either methylate or pyridyloxobutylate bases of DNA (Figure 1.2). Methylated (methyl) bases found in the lung tissue of NNK-treated animals include 7-methylguanine (7-methyl-dG), O^6-methylguanine (O^6-methyl-dG), and O^4-methylthymine (O^4-methyl-dT) (33). Pyridyloxobutylated (POB) bases identified include O^6-POB-dG (51), O^2-POB-dT (52), 7-POB-dG, N^2-POB-dG, and O^2-POB-dC (53). Seven-methyl-dG adducts are hydrolytically unstable, and following spontaneous depurination, produce abasic sites and single strand breaks in DNA (54). If unrepaired, abasic sites can potentially cause mutations in mammalian cells (55-57). Both O^6-methyl-dG and O^6-POB-dG primarily induce G→A transition mutations (58-60) as observed in the *K-ras* oncogene after NNK treatment in mice (33), while O^6-POB-dG also

induces G→T transversion mutations (60). Furthermore, POB adducts inhibit AGT-mediated repair of O^6-methyl-dG lesions (61-63). Previous studies have observed a correlation between the formations of O^6-methyl-dG adducts in Clara cells and lung tumor multiplicity in laboratory animals treated with NNK (64,65). In human lung tissue, higher levels of O^6-methyl-dG are associated with smokers compared to non-smokers, and are suggested, in part, to be a result of the activity of NNK (66). Finally, the pyridine *N*-oxidation pathway and the glucuronidation of NNAL (NNAL-Gluc) are considered as the means of detoxification of NNK and NNAL. Metabolites of NNK and NNAL *N*-oxidation can be readily detected in the urine of rodents, but in humans only NNAL and NNAL-Gluc are detected (33). In addition, activation of NNK has also been found to generate oxidative damage as measured by the formation of 8-hydroxy-2́-deoxyguanosine (8-OHdG) lesions (67-70), which are also known to induce G→T transversions (36), as well as induce chromosomal instability (71), suppress immunologic responses (72), and interfere with critical cellular pathways necessary for growth and cellular stability (73,74).

3. Existing modalities in the management of lung cancer

Compared with other major types of cancer in the Western countries, such as colon, breast, and prostate cancers, the clinical outcome of conventional therapies such as surgery, radiotherapy, and chemotherapy still remains poor for lung cancer despite the major efforts to improve treatment modalities during past decades. Several reasons can account for the lack of improvement in prognosis, such as the difficulties in making the early-stage diagnosis of lung cancer and the high recurrence rate after curative treatment (75).

3.1 Screening

There are currently no approved screening procedures available for lung cancer. Existing strategies with current technologies that include chest X-rays and computed tomography (CT) scans have not yet demonstrated efficacy in reducing lung cancer mortality and have, however, only raised major concerns regarding overdiagnoses and unnecessary anxiety, radiation exposure,

and high expenses (27). As a result, organizations such as the American Cancer Society do not recommend screening for lung cancer (5).

Nevertheless, efforts to improve the design of current technologies and to discover newer ones continue. Recently, the National Cancer Institute (NCI), a part of the National Institute of Health (NIH), discovered that enhanced detection with low-dose helical CT (also referred to as spiral CT) can reduce lung cancer deaths by 20%, a standard that has not been reached with other convential strategies (76); low-dose helical CT scans provide better resolution images of the lungs compared to standard CT (77). The study (the National Lung Screening Trial, NLST), which began in August 2002, was a large randomized clinical trial involving more than 53,000 current (≥ 30 pack years) and former (quit ≥ 15 years previously) heavy smokers, ages 55 to 74 (78). In addition, many newer screening technologies are currently being explored. These include fluorescence bronchoscopy (79), molecular analysis of sputum, and detection of genetic alterations in circulating DNA (77). Together, these different modalities may provide information complementary to results of CT screening tests.

3.2 Detection and diagnosis

Lung cancer is often detected and diagnosed at rather advanced stages of the disease when noticeable symptoms begin to develop, including persistent cough, sputum streaked with blood, and possibly development of chest pain. However, in some cases these symptoms are presented in earlier stages, but are unfortunately overlooked by the patient and left unattended (5,27). Initial detection and diagnosis of lung cancer includes sputum cytology and noninvasive radiographic imaging with chest X-ray, CT, and positron emission tomography (PET) scans. For more decisive diagnoses invasive procedures such as bronchoscopy and fine-needle biopsy are performed (5,27).

3.3 Treatment

Treatment for lung cancer is provided based on the histologic type of cancer, the stage at presentation, and the patient's pulmonary function evaluation that includes forced expiratory volume in one second (FEV_1) and diffusion lung capacity for carbon monoxide (DLCO) measurements (27). SCLC, whether in a limited or extensive disease stage, is treated primarily with chemotherapy and/or radiotherapy (24). Conversely, NSCLC is better treated according to its stage. NSCLC is classified into three primary stages: local (IA, IB, IIA), locally advanced (IIB, IIIA, IIIB), and advanced (IIIB, IV). These stages are further broken down into categories related to the size of the tumor, lymph-node status, and presence of metastases. In general, surgical resection is the most effective treatment for NSCLC at earlier stages of the disease including stages I through IIIA (24,27). The 5-year survival rate following surgery ranges from 23% for Stage IIIA disease to 67% for Stage IA disease (80), thus emphasizing the benefit of early detection. For Stages II and III, the use of adjuvant chemotherapy is also highly supported; however for Stage I, controversy still exists among experts (81). NSCLC deemed inoperable requires treatment with either chemotherapy and/or radiotherapy. The most effective chemotherapeutic agents are platinum-based, such as cisplatin – atypical alkylator – that causes cross-linking of DNA to initiate cellular apoptosis (24). In addition, targeted therapies, such as erlotinib (Tarceva®), which targets the growth factor receptor EGFR that is often overexpressed in cancers, are also implemented with chemotherapy and have demonstrated some efficacy (5,27).

4. Alternative approaches to lung cancer management

Since current modalities are unable to effectively reduce lung cancer mortality, alternative approaches are urgently needed. Two such strategies with promising clinical implications include the identification of sensitive, specific, and reliable biomarkers for early detection and the development of more effective and less toxic cancer preventive agents, i.e. chemoprevention.

4.1 Biomarkers

Biomarkers are defined as molecular changes that are objectively measured and evaluated as an indicator of a biological state (82). Biomarkers are especially important in the case of a disease such as cancer, in which the molecular profile of a cancer cell drastically differs from that of a normal cell (83). Molecular changes are often detected at both the DNA and protein level and are measured primarily by alterations in structure, expression, and/or function. For example, DNA-based biomarkers include those derived from chromosomal changes, hypermethylation, or mutations that can ultimately lead to a loss or gain in gene expression. Similarly, protein biomarkers are identified from changes in expression, but are also derived from post-translational modifications such as glycosylation, phosphorylation, ubiquitination, methylation, and acetylation that can also impair functionality (84). In the case of lung cancer, biomarkers have the potential to play an important role in a variety of situations including early diagnosis, staging, disease course progression, and determination of efficacy of preventative and therapeutic targeting agents.

4.1.1 Current clinical biomarkers

Many genetic and protein biomarkers have been discovered for lung cancer, but only a few have reached a clinical setting. Current clinical biomarkers include carcinoembryonic antigen (CEA), cytokeratin fragment 21-1 (CYFRA 21-1), squamous cell carcinoma antigen, neuron-specific enolase, progastrin-releasing peptide, tumor M2-pyruvate kinase, and C-reactive protein (CRP) (85). These biomarkers have demonstrated efficacy with regards to distinguishing histological types and predicting reoccurrence and prognosis, as well as in response to therapy. However, these markers lack sensitivity and specificity to lung cancer and are thus, not recommended or encouraged for use by clinicians (85).

4.1.2 Biomarker discovery for cancer

Cancer biomarkers can be obtained from a variety of distinct areas of research including genetics, epigenetics, proteomics, and metabolomics, as well as through imaging technology and general physical examination. Among these research areas, genomics and proteomics have contributed the most to biomarker discovery by providing a large list of many potential candidates. The primary focus of genomics is to detect the activation of oncogenes or inactivation of tumor-suppressor genes using DNA microarrays and polymerase chain reaction (PCR). Accordingly, DNA biomarkers for lung cancer include the previously mentioned *KRAS* and *P53*, as well as the cell cycle regulator retinoblastoma (*RB*) and the transcriptional factor *MYC*. However, despite their frequency in lung cancer, many genes are also correlated with other types of cancers and tests to evaluate their expression have lacked sensitivity and selectivity in clinical settings (84).

Proteomics allows for a global identification of physiological changes that are associated with a given disease state and it is proposed that a more accurate view of the cellular state is best taken at the protein level (86). Gene transcription does not always correlate to protein expression and in fact in a study comparing mRNA expression in lung tumors to corresponding protein expression in the same tumors this was clearly observed as only a small percentage of genes actually had a strong correlation to protein expression (87). Proteins carry out numerous cellular activities and their function is dependent on post-translational modifications (i.e. phosphorylation, acetylation), sub-cellular compartmentalization, and interactions with other proteins and ligands (84). In addition, proteins are not only the end product of the expression of a gene, but also the major targets for diagnostic, therapeutic, and chemoprevention strategies. Thus, proteomics may provide a better means with which to identify novel lung cancer biomarkers.

4.1.3 Proteomic technologies in biomarker discovery

A number of proteomic techniques have been developed to help in the discovery of novel protein biomarkers. Many of these approaches incorporate gel-, and/or liquid chromatography (LC)-based separation procedures in combination with mass spectrometry (MS) or MS alone for the quantitation and identification of proteins (86,88). However, there does not appear to be a clear understanding as to which technology is superior, as all have proven to provide important information regarding potential biomarkers in disease development and provide complementary data to each other based on each technique's advantages (88,89). Ultimately, the selection of one technology or a combination can offer valuable information to provide answers to the intended biological questions that are being asked. Two commonly used techniques are further discussed below.

The use of two-dimensional electrophoresis (2D PAGE), which allows for separation of proteins on the basis of their isoelectric point and molecular mass in a polyacrylamide matrix, was one of the first techniques that offered a view of proteomes. Protein spots indicated not only abundance, but also the visualization of proteins in their diverse isoforms. Since then, improvements of 2D PAGE have allowed for multiplexing and enhancement of quantitation of proteins. One such improvement includes the use of 2D differential in-gel electrophoresis (2D-DIGE). 2D-DIGE has been used extensively in a variety of applications for quantitative proteomic analysis (90). 2D-DIGE utilizes two or three spectrally distinct, charge, and mass-matched fluorescent dyes known as CyDye DIGE fluors to label proteins from two or more samples thereby, allowing for the loading of more than one sample per gel. There are currently two types of labeling techniques available for 2D-DIGE: saturation labeling and minimal labeling. Saturation labeling is used for situations in which protein abundance is a limiting factor such as in the case of laser-microdissected samples which may contain as little as 5 μg of protein (91). The two dyes used here, Cy3 and Cy5, have a maleimide reactive group that reacts with

available cysteine groups on proteins and adds a mass of approximately 677 Da to the labeled protein. A high dye-to-protein labeling ratio is required to effectively label the cysteine residues, which are prevalently low in proteins and respond well to the chemical modification (92). Minimal labeling, however, uses dyes Cy2, Cy3, and Cy5 (Figure 1.3A) with an *N*-hydroxy succinimidyl ester group that reacts with the ε-amine groups of lysine residues (Figure 1.3B) and requires a low dye-to-protein ratio (add approximately 500 Da to the labeled protein). Although lysine residues are readily available, based on optimized labeling conditions, only 2-5% of the total numbers of lysine residues are labeled (92). By having three dyes, minimal labeling also allows for one of the dyes, typically Cy2, to label a pooled standard containing an equal amount of protein from each sample in a study. The internal pool standard is critical to this technique as it represents an average of all of the samples being compared and is used to normalize protein abundance across multiple gels in an experiment. This substantially reduces the effects of gel-to-gel variation regarding the quantitation of a protein spot on a gel. Following labeling with either procedure, visualization of proteins in a resolved gel is performed by exciting the different dyes at their specific excitation wavelength using a Typhoon variable mode imager. The images produced show protein spot intensities corresponding to relative protein expression. These images can be quantified by differential analysis software (e.g. Progenesis SameSpots) to compare the relative protein expression among sample groups under examination (90). Finally, to determine the identification of the proteins pertaining to the observed spots, a separate 2D gel can be run with representative non-labeled samples. The spots from this gel, once matched to the experimental spots, can then be excised from the gel and identified by MS techniques (90). Figure 1.4 summarizes the procedure of the 2D-DIGE proteomic technique.

Mass spectrometry is another principle method of protein separation used in proteomics. Mass spectrometry measures the mass to charge ratio (m/z) from ionized proteins or peptides. The subsequent ratios can be utilized for identification, as well as quantitation purposes. In

general, MS is conducted with instruments comprised of components necessary for sample ionization, separation (mass analyzer), and detection. Ionization technologies include matrix assisted laser desorption ionization (MALDI), which utilizes a light absorbing matrix to mix with

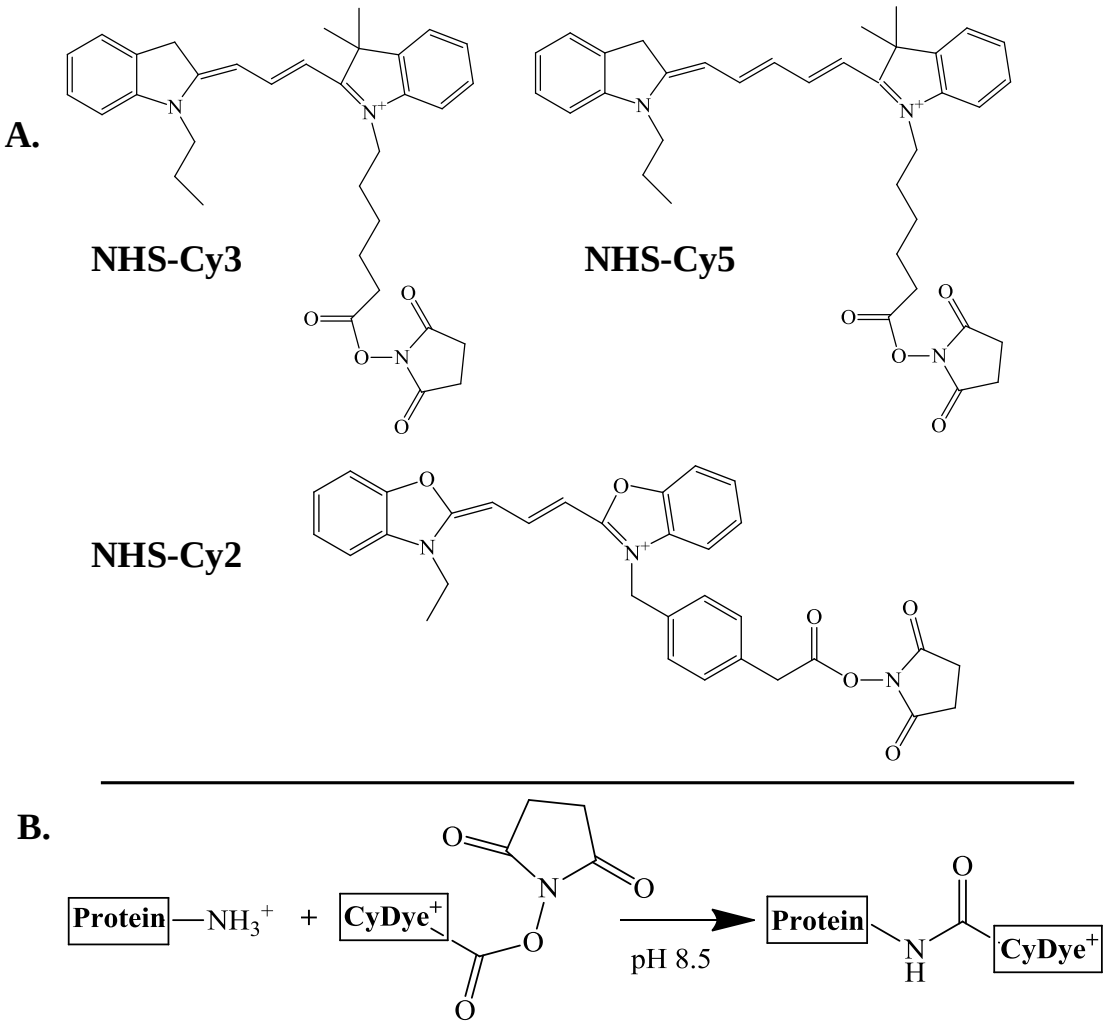

Figure 1.3 CyDye 2D-DIGE fluors used in minimal labeling of lysine residues of proteins. (A) *N*-hydroxy succinimidyl esters of propyl Cy3 and methyl Cy5 and Cy2. (B) CyDyes react with the ε-amine groups of lysine residues in the target protein through a nucleophilic substitution reaction at an optimal pH of 8.5. Adapted from Timms et al. (89) and Chakravarti et al. (93).

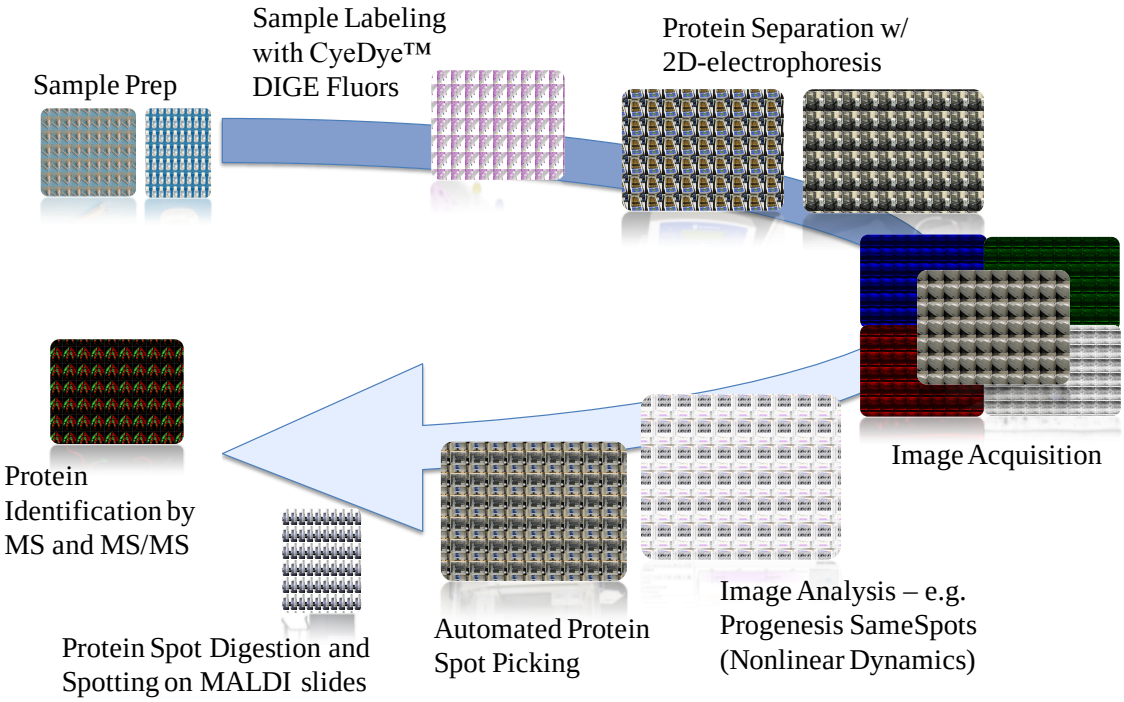

Figure 1.4 Two-dimensional differential in-gel electrophoresis (2D-DIGE) workflow.

protein samples to form crystals; upon pulsation with a laser, the crystal matrix donates a single proton to the proteins. These protonated proteins are then desorbed (ejected) into the gas phase and into a mass analyzer (94). A commonly used mass analyzer is time-of-flight (ToF). The ToF mass analyzer separates ions according to the speed with which the ions travel; this is proportional to the mass of the ion. Therefore, the ions with a higher m/z ratio will travel faster to the detector. By combining a series of ToF analyzers the accuracy of m/z measurements and sensitivity towards low abundance ions can be increased (95). Finally, detectors, such as electron multipliers are used to change the kinetic energy of the ions into an electrical current that can be measured and imported into a computer for subsequent analyses (94).

One of the more sensitive proteomic techniques currently available is the MS-based isobaric Tags for Relative and Absolute Quantitation (iTRAQ) approach (88). iTRAQ utilizes a reporter ion set of amine reactive isobaric tags to label proteins from different sample groups

thus, allowing for multiplexing of proteomic studies; currently 4-plex (m/z 114-117) or 8-plex (m/z 113-119,121) reporter ion sets exists (a tag of m/z 120 is skipped because that mass represents the ammonium ion of phenylalanine). Therefore, in any given experiment up to eight different conditions can be analyzed simultaneously (Figure 1.5). The tags are designed to derivatize all peptides in a digested mixture (e.g. digestion with trypsin) at the N-terminus and ε-amino group of lysine side-chains (96) using different combinations of ^{13}C and ^{15}N heavy isotopes in the different iTRAQ tag portions to give a unique mass representing the contribution of any peptide from each of the samples included in the analysis (Figure 1.5). In contrast to other heavy-isotope quantitation methods, such as stable isotope labeling with amino acids in cell culture (SILAC) or cleavable isotope-coded affinity tags (cICAT) where the addition of different labels confers different masses to the same peptides from each sample labeled, upon MS analysis of combined iTRAQ labeled samples, any specific peptide sequence has the same mass (isobaric) no matter which iTRAQ tag was used to label it. Furthermore, upon fragmentation of peptides using a technique known as tandem MS (MS/MS), the fragmented ions used to decipher the peptide sequence also have the same mass no matter which iTRAQ tag was used to label the peptide (Figure 1.6). This increases the sensitivity of the iTRAQ assays because the amounts of lower abundance peptides are not split into multiple mass signals, but instead show up as a single m/z peak, which includes the summed contributions for each peptide mass from each of the samples labeled. These peptides can then be searched against a protein database to identify the proteins being quantified (Figure 1.6). In addition, during MS/MS fragmentation additional signature ions (i.e. m/z 114-117 for 4-plex or 113-119, 121 for 8-plex) are generated that provide quantitative information about relative amounts of each peptide arising from each sample (88) (Figure 1.6).

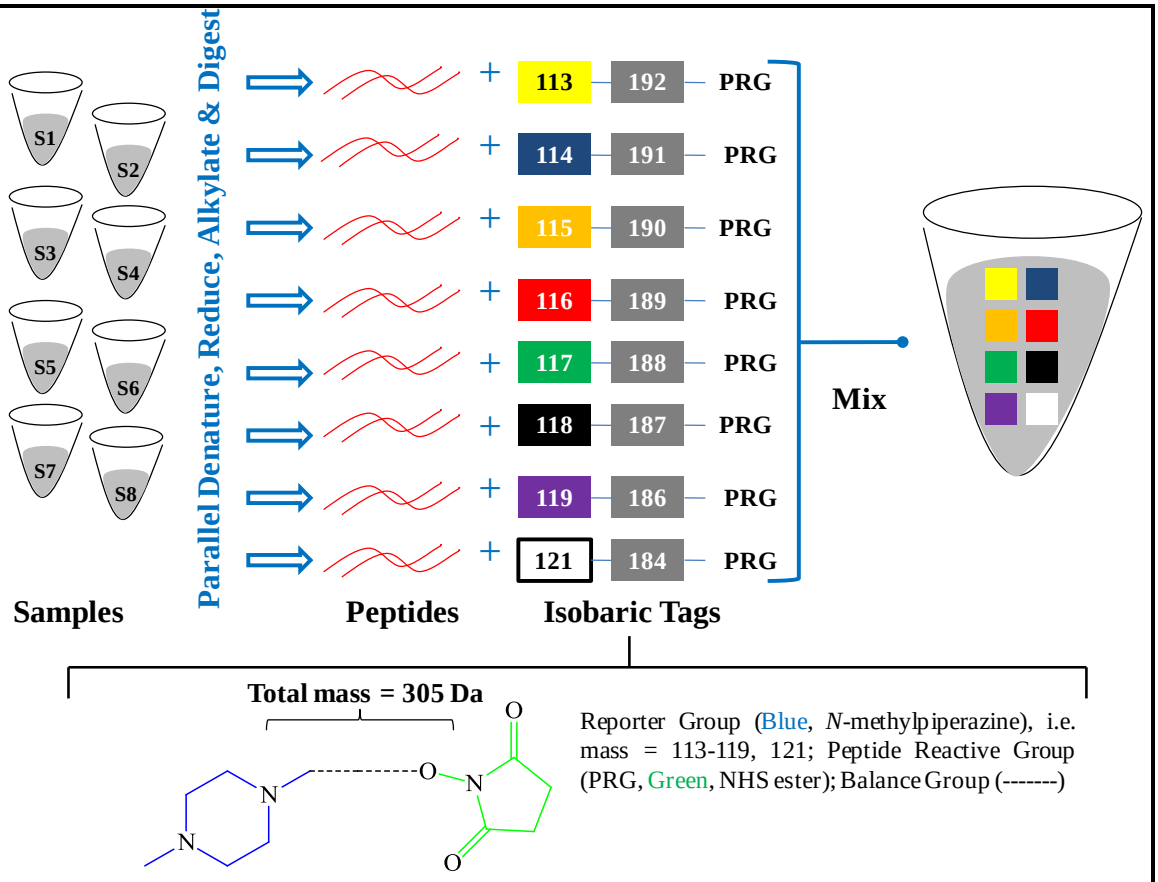

Figure 1.5 Multiplexed isobaric tagging chemistry for iTRAQ analysis. Up to 8 samples can be labeled with one of the isobaric tags following sample protein processing and digestion with trypsin. Isobaric tags are comprised of three groups: a reporter group, a peptide reactive group, and a balance group; the balance group allows for each tag to have the same mass. After labeling, samples are ready for MS analysis.

4.2 Chemoprevention

Since lung cancer is a multi-step disease affecting numerous cellular pathways over a long period of time (up to 20 to 30 years (97)), compounds able to interfere at any point in the carcinogenic process would prove to be beneficial in terms of prevention-based approaches. Chemoprevention is defined as the use of natural or synthetic agents to reduce or prevent the initiating and/or promotional events that occur during the process of carcinogenesis (98). In

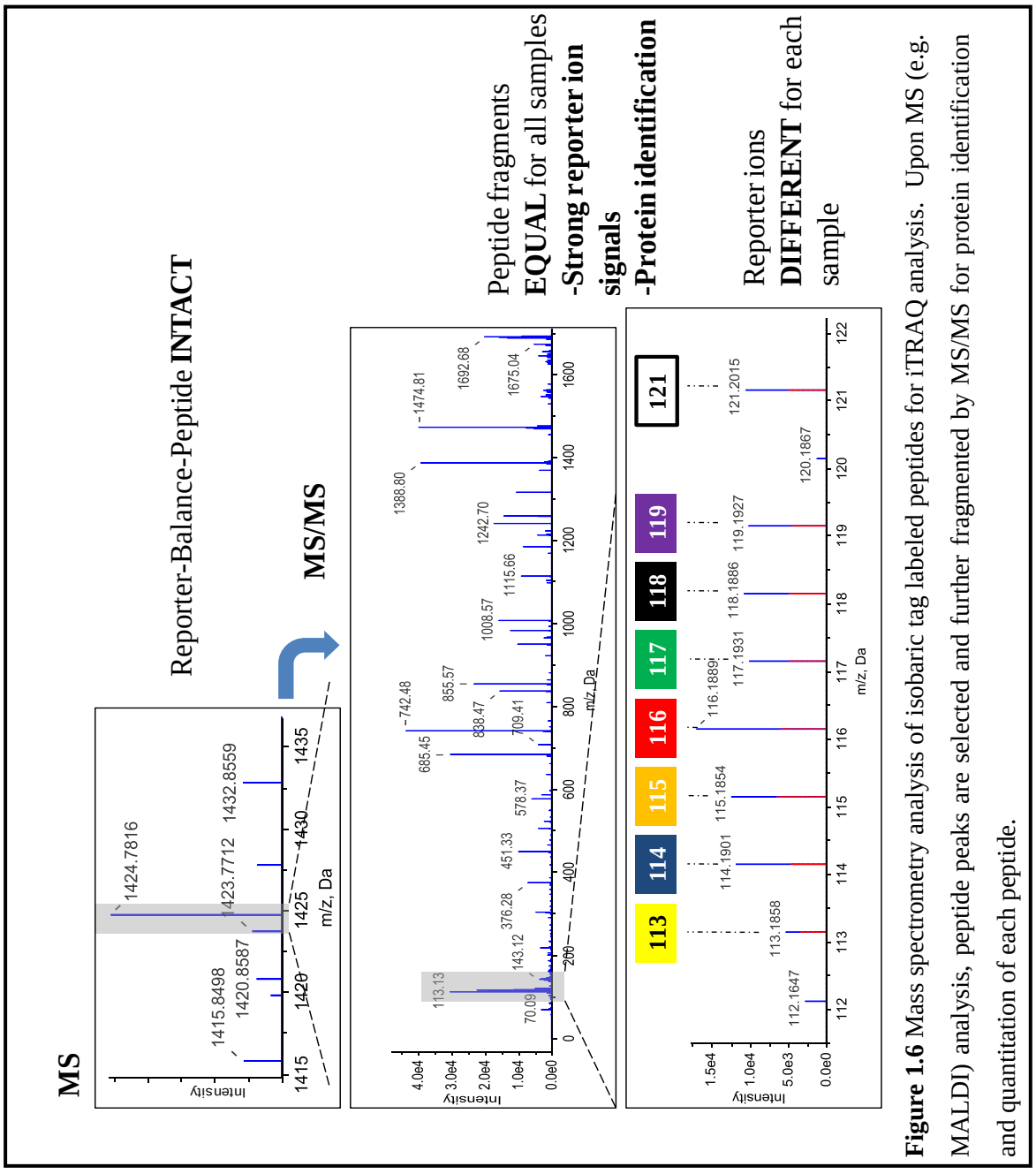

Figure 1.6 Mass spectrometry analysis of isobaric tag labeled peptides for iTRAQ analysis. Upon MS (e.g. MALDI) analysis, peptide peaks are selected and further fragmented by MS/MS for protein identification and quantitation of each peptide.

general, these agents are broadly grouped as either blocking agents or suppressing agents. Blocking agents prevent the interactions of exogenous or endogenous carcinogens with target sites such as DNA by altering carcinogen metabolism or enhancing carcinogen detoxification, whereas suppressing agents prevent the down-stream effects following carcinogen exposure that include inflammation and proliferation, as well as suppression of apoptosis (98,99). In

experimental systems, blocking agents are primarily effective when administered before or during treatment with carcinogens and therefore, the timing of administration in relationship to carcinogen exposure is important for their activity. On the other hand, suppressing agents are active when given after carcinogen exposure and thus, have the potential to be effective against a variety of carcinogens that impact a particular tissue (98). Surpressing agents have the potential to be highly useful in former smokers. Several agents are known to function as both blocking and suppressing agents (100). Ultimately, the use of a single agent or a combination of agents to target cancer is a main goal (100).

Various chemopreventive agents alone, and in combination, have demonstrated clinical efficacy in individuals against breast (tamoxifen) (101), prostate (finasteride) (102), and colon [celecoxib (103); difluoromethylornithine plus sulindac (104)] cancer development, but none have been validated to be effective against lung cancer. Therefore, the development of novel chemopreventive agents against lung cancer is urgently needed.

4.2.1 Chemoprevention of cancer: trials and tribulations

Ultimately, the prevention of smoking initiation and the act of quitting the habit are the best approaches against lung cancer development and constitute a goal of primary prevention (13). Chemoprevention, however, serves as a plausible secondary prevention approach to target addicted smokers, as well as high risk former smokers (10).

Early efforts to identify candidate chemopreventive agents against lung cancer development were derived from epidemiological and case-control studies regarding diet intake. These studies demonstrated that diets high in fruits and vegetables were associated with a reduced risk of lung cancer (105). As a result, extensive investigations identified numerous components of these foods that had the potential to generate this preventative effect. A majority of the focus was aimed at nutrients with known cellular maintenance, anti-oxidant, immunomodulatory, and anti-chemical carcinogenic properties and included Vitamins A (retinol, retinyl palmitate,

isotretinoin) and E (α-tocopherol) and β-carotene (97,106,107). Given the benefit these compounds provided, several chemoprevention trials were conducted. Four large chemoprevention trials included the Finland-based Alpha-Tocopherol, Beta-Carotene (ATBC) trial (108), the United States-based β-Carotene and Retinol Efficacy Trial (CARET) (109), and the Physician's Health and Women's Health trials involving β-carotene (110,111). In the ATBC trial, 29,133 male smokers ages 59-60 were randomly administered daily supplementation of 50 mg of α-tocopherol or 20 mg of β-carotene or a combination of both for five to eight years. At the conclusion of the study, both agents were found ineffective against reduction of lung cancer (108). Similar results were also obtained from the CARET study. After four years of supplementation with 30 mg of β-carotene and 25,000 IU of retionol, smokers, former smokers, and workers exposed to asbestos did not receive any benefit from these agents regarding lung cancer (109). Unexpectedly, the ATBC and CARET studies also showed that β-carotene actually increased lung cancer incidence 18% and 28%, respectively, and mortality 8% and 17%, respectively, and these adverse effects were primarily associated with heavy cigarette smoking (108,109,112,113). In addition, further meta-analysis of the β-carotene trials revealed that an increased risk of lung cancer occurred in current smokers (114). However, both the Physician's Health and Women's Health trials showed that healthy men and women administered β-carotene for several years does not confer harm, but again, confirmed no provided benefit either (110,111). Subsequent chemoprevention trials have yielded similar disappointing results. The European Study on Chemoprevention of Vitamin A (retinyl palmitate) and *N*-acetylcysteine (EUROSCAN) study showed no reduction of lung cancer incidence in patients receiving retinyl palmitate and/or *N*-acetylcysteine with previously resected lung cancer (115) and a Phase III trial indicated that the retinoid isotretinoin was actually harmful in current smokers (116). Subsequent studies in animal models and human archived tissue have thus far indicated that the negative effect associated with β-carotene supplementation in smokers may, in part, exist as a result of pro-oxidant formation,

increased phase I carcinogen metabolizing enzyme, reduced retinoid signaling, and increased aberrant cell growth (117-121). These studies emphasize the necessity of thorough preclinical investigations and carefully designed early phase human trials of agents using biomarker validations before entering large-scale clinical settings and costly Phase III clinical chemoprevention trials.

4.2.2 Selenium compounds as representative chemopreventive agents

Several agents, including selenium-containing compounds, have demonstrated the success of the chemoprevention approach in lung carcinogenesis and have been reviewed and described in the literature (97,100,122). Selenium is an essential trace element needed for production of selenoproteins involved in antioxidant and redox status regulation of molecules (123). In excess, i.e. over 400 μg per day, selenium can be toxic, and thus, its recommended dietary allowance in the United States is 55 μg for adult men and women (124). Dietary selenium is obtained from plants, meats, fish, poultry, grains, and nuts. Based on epidemiological, preclinical, and some clinical studies, selenium appears to provide some protection against a variety of cancers, including lung cancer (123,125-127). A well-documented clinical trial supporting selenium's protective effect against lung cancer came from a study published by the late Larry Clark (128). In the Nutritional Prevention of Cancer (NPC) trial, selenium supplementation, in the form of selenized-yeast (200 μg per day for a mean of 4.6 years), was tested against the incidences of basal and squamous cell carcinomas of the skin in 1,312 subjects with a history of these lesions. At the conclusion of the study, Clark's group found that there was no significant effects against reduction in skin cancer, however secondary endpoints indicated that selenium reduced total cancer mortality to 50%, total cancer incidence to 47%, and incidence of lung cancer to 46% (128). It was later shown that in this trial those individuals in the low baseline selenium population (<106 ng/ml in plasma) supplemented with selenium benefited the most in reduction of lung cancer incidence (129). Furthermore, a meta-analysis of several

epidemiological studies confirmed the protective potential of selenium in individuals with below average selenium levels (<100 ng/ml) (130). These studies, as well as others, have prompted more recent clinical investigations to take place with selenium in order to determine its role against lung cancer, including a phase III chemoprevention trial of selenium supplementation in persons with resected stage I NSCLC sponsored by the Eastern Cooperative Oncology Group (ECOG; NCI: NCT00008385). Preliminary results from this study, using selenized-yeast (200 μg per day), have thus far indicated that no apparent benefit exists (131). However, contrary to results from the Selenium and Vitamin E Cancer Prevention Trial (SELECT) (132) and the NPC (128) trials that indicated there was an association between selenium and an increased occurence in type II diabetes mellitus (133), selenium in the ECOG trial was safe and provided some benefit (5-year overall survival rate was 87% versus 83% for placebo users), although not significant, against lung cancer to individuals that never smoked (131).

Several preclinical studies with selenium have indicated that both the dose and form of selenium plays an important role in its protection against lung cancer development (126,134). At doses well above the physiological requirement necessary for the production of selenoproteins, various organic and inorganic forms of selenium, including the selenium-containing amino acid selenomethionine found in selenized-yeast and the inorganic sodium selenite, have demonstrated chemopreventive efficacy (Figure 1.7) (127). The anti-cancer effects of such selenium-containing compounds have been explained in part by the formation of the metabolite methyselenol to induce apopotosis and cell cycle arrest. In addition, their distinct chemical structures also confer different anti-cancer activity, as well as inherent toxicity (135). In an effort to further increase chemopreventive efficacy and overcome the toxicity concerns associated with existing forms of selenium, our laboratory pioneered the development of synthetic organoselenium compounds (125). The basis for the design of the first generation organoselenium compounds evolved from substitution of oxygen or sulfur atoms with selenium in

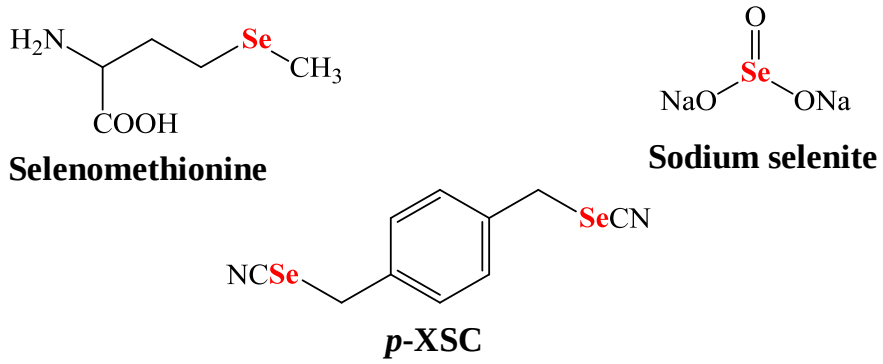

Figure 1.7 Stuctures of selenium-containing compounds.

known inhibitors of carcinogenesis. The subsequent selenium analogs were more effective than the parent compounds (125).

One of the most promising second generation compounds developed in our laboratory is 1,4-phenylenebis(methylene)selenocyanate (*p*-XSC). *p*-XSC is an aromatic selenium compound with two methyleneselenocyanate groups positioned in a *para*- configuration to each other (Figure 1.7) (125). Its toxicity is very minimal relative to that of other selenium compounds tested (134). Metabolic breakdown of *p*-XSC in mice and rats has revealed production of the metabolite tetraselenocyclophane (TSC); proposed pathway: *p*-XSC→glutathione conjugate (*p*-XSeSG)→a selenol (*p*-XSeH)→TSC (136,137). Accordingly, the formation of the selenol moiety intermediate (*p*-XSeH) was proposed to be an important entity in cancer chemoprevention by *p*-XSC (138).

Our laboratory showed that selenium in the form of *p*-XSC significantly inhibited lung tumorigenesis in A/J mice treated with NNK (139). In contrast, we showed that other forms (selenized-yeast and several of its components, such as selenomethiomine, Se-methylselenocysteine, and sodium selenite) under identical conditions had no effect on NNK-induced lung tumors (139,140). The protective effect of *p*-XSC when fed throughout the

bioassay was due, in part, to its ability to inhibit NNK-induced covalent DNA adducts and DNA oxidative damage (139). Furthermore, it was later determined that *p*-XSC enhanced the levels of glutathione (GSH), a major intracellular antioxidant, in the lung (141). Our laboratory, using microarray and real-time PCR analysis, also showed that *p*-XSC altered several molecular markers involved in inhibition of cell growth and induction of apoptosis, including Akt, COX-2, and NF-κB, *in vitro* using human NSCLC cell lines (142). In addition, mass spectrometry combined with computer modeling demonstrated that the inhibition of the transcriptional factor NF-κB by the organoselenocyanate compound benzyl selenocyanate (BSC; structurally similar to *p*-XSC minus a selenocyanate group) was due to covalent binding of selenium with the sulfur of Cys^{62} of the p50 subunit of NF-κB (143). Altogether, the results of these studies support the chemopreventive efficacy of the selenium-containing compound, *p*-XSC.

Our laboratory has also taken the initiative to develop novel forms of selenium-containing compounds that can specifically target important mediators and pathways involved in the multi-step lung carcinogenesis process such as nitric oxide synthase (iNOS) and nitric oxide (NO) production (144,145). These entities play a pivotal role in the promotion/progression phases of lung carcinogenesis. However, before selenium-containing compounds, including *p*-XSC, are used in a clinical setting it is of utmost importance to better understand their mechanisms of activity. Such mechanisms can provide informative biomarkers to evaluate efficacy of numerous chemopreventive agents. Currently, our knowledge regarding the mechanisms that may account for cancer prevention by various forms of selenium is poorly understood and is based primarily on animal model studies and assays conducted on cancer cells (125,126,146). However, central to the use of selenium-containing compounds is that both the dose and form of selenium are critical determinents in cancer prevention (126,134). Therefore, much caution should be taken when subsequent stages of chemopreventive agent development are followed regarding selenium supplementation. For example, SELECT, mentioned previously,

was halted due to a concern with an increase in diabetes mellitus in individuals supplemented with selenium in the form of selenomethionine (200 μg daily for a mean of about 5 years) (132). However, the results of this study, as well as others, can be avoided provided that adequate interpretation of existing preclinical data, further mechanistic studies, and subsequent clinical pilot studies are performed (147).

5. Research objectives and specific aims

The poor 5-year survival rate for lung cancer reflects a lack of reliable screening methods and the inadequacy of current conventional treatment strategies. As a result, alternative strategies in the management of the disease are urgently needed. Two such strategies with promising clinical implications include the discovery of reliable, sensitive, and selective biomarkers (e.g. proteins) for early detection and the discovery of novel chemopreventive agents.

Biomarkers have shown utility in the management of breast (cancer antigen 15-3), liver (α-fetoprotein), colon (CEA), and prostate (prostate-specific antigen) cancers (148), however, none have been identified for lung cancer. In addition to sensitivity and specificity concerns, a primary reason for this is due in part to the identification of proteins that may be the consequence of tumor development rather than a cause of cancer induction. Therefore, the main objective of this project is to use a proteomic approach to discover reliable proteins that are involved in the development of lung cancer, and more specifically tobacco carcinogen-induced adenocarcinoma. Such proteins, monitored throughout the progression of the disease and related to lung carcinogenesis, may be useful biomarkers for early detection and in the evaluation of preventative and therapeutic treatments. **Specific Aim 1** of this study is to use a well-established tobacco carcinogen (NNK)-induced lung tumorigenesis mouse model to identify proteins in the lung that are differentially expressed as a function of disease development. To validate the utility of biomarkers, the chemopreventive organoselenium compound *p*-XSC that previously demonstrated efficacy against lung tumorigenesis will be employed. Ultimately, the goal of this

research is to be able to translate our preclinical findings to a clinical setting. However, unlike animals in which tissue is easily and readily obtained, collection of human lung tissue requires invasive procedures which is not practical in a clinical setting. Therefore, collection of blood plasma using non-invasive procedures is more suitable. Smokers are at high risk for a number of respiratory diseases, including lung cancer. Currently, there are no reliable protein biomarkers that can be used to detect the damage caused by cigarette smoke leading to disease development. To this end, **Specific Aim 3** of this study will identify differentially expressed proteins in human blood plasma of smokers compared to non-smokers using the iTRAQ proteomic approach. Currently, there are no effective chemopreventive agents in the clinic to inhibit lung cancer development. **Specific Aim 2** is to develop more effective selenium-containing chemopreventive agents to target specific mechanisms involved in lung carcinogenesis. As an initial preclinical investigation we developed a novel selenium analog of an established inducible nitric oxide synthase (iNOS) inhibitor *S,S'*-(1,4-phenylenebis[1,2-ethanediyl])bisisothiourea (PBIT) and tested it *in vitro* against human NSCLC cells; iNOS and its product NO are positively correlated with the development of a number of human cancers, including lung cancer (144,145).

Chapter 2

Preclinical Development of Lung Cancer Protein Biomarkers

1. Objectives

Lung cancer continues to be a deadly disease as a result of late diagnosis and the inability of current conventional treatment strategies to effectively increase survival. However, early detection of lung cancer allows for current treatment, as well as preventative strategies, such as chemoprevention, to be more effective. Although protein biomarkers related to disease development have been of some success in the early detection of a number of cancers, none have been sensitive enough and specific for detection of lung cancer. A primary concern is that of the protein biomarkers detected for lung cancer thus far, many may be a consequence of tumor development rather than a cause of cancer and therefore, be of no utility for early detection. Therefore, molecular changes at the protein level related to lung cancer development are needed. Following the progression of lung cancer in an adequate number of high risk humans (e.g. current or former smokers) under controlled conditions to identify critical molecular changes for biomarker discovery is impractical. Animal models, on the other hand, provide ample sample collection and manipulation, and can develop lung cancer that resembles the major histological type classified in humans, e.g. adenocarcinoma. As a result, in this chapter we hypothesized that by using a well-defined, tobacco carcinogen-induced, preclinical, lung carcinogenesis model and proteomics approaches, reliable biomarkers could be obtained to provide an accurate view of molecular alterations during different histopathological stages of disease development. We further validate the utility of candidate biomarkers identified in the selected animal model by the synthetic organoselenium chemopreventive agent *p*-XSC.

2. Background

2.1 Lung cancer protein biomarkers: the discovery phase

The utility of proteins as biomarkers in both targeted and surrogate tissue to reflect an individual's current health status has long been used in clinical settings for diagnostic tests. Proteins ultimately dictate the phenotype of cellular activity and thus, any change in relative expression and/or alteration in structure (i.e. post-translational modifications, including phosphorylation, glycosylation, and proteolytic processing) can have major implications dependent on the protein affected and its biological role. In the case of lung cancer, genetic alterations can regulate proteins involved in cell growth, invasion/metastasis, differentiation, cell cycle processes, apoptosis, and angiogenesis (8). Identification of these proteins not only provides information in understanding the mechanism behind lung cancer development, but also in providing biomarkers to monitor disease progression (84).

In general, lung cancer protein biomarker discovery platforms have been based on model systems which employ *in vitro* cell lines, animal models, or human tissue. Each model system has its advantages and disadvantages. For example, carefully handled cell lines and animal models lack genetic and lifestyle factors, whereas human lung tissue represents the heterogeneous nature of the disease and can contain a variety of cell types. Furthermore, collection of sufficient samples from cell lines and animal models can be performed with greater ease than from tissue obtained from human subjects (84).

Although early attempts to discover novel biomarkers characteristic of lung cancer development have been reported (P16, KRAS, retinoblastoma, fragile histidine triad) (149), no single marker has so far met sufficient specificity and sensitivity to be recognized for clinical significance for diagnostic purposes (85). A primary reason for this stems from the fact that lung cancer is a heterogeneous disease that demonstrates high variability among patients, cancer types, and stages (24). Therefore, large-scale characterization of proteins using proteomic approaches

has been utilized for lung cancer biomarker discovery purposes. As discussed in Chapter 1, the field of proteomics has developed a variety of techniques that analyze the global protein profile of disease states (86). More importantly, both the gel-based 2D-DIGE and MS-based iTRAQ approaches have been used extensively in a variety of applications for quantitative proteomic analysis of diseases, including lung cancer (150-153).

2.2 The NNK-induced lung tumorigenesis model in the A/J mouse

Mouse models have been successfully used to study human lung carcinogenesis processes of both NSCLC and SCLC. These include spontaneous, carcinogen-induced, transgenic, and knockout mouse models (154). Most of the spontaneous and chemically induced lung tumors developed in mice resemble that of human lung adenocarcinomas (41), the major histological type diagnosed in humans today. Lung tumors generated in mouse models exhibit similar features to that of human tumors at both the molecular (i.e. mutational profiles and gene/protein expression) and pathological levels (155,156). For example, genetic alterations of the tumor suppressor genes *p53* and *p16* and the proto-oncogene *Kras2* are often observed in both mouse and human lung cancer (157).

The A/J mouse is an inbred mouse strain that is highly susceptible to lung tumor development; greater susceptibility has been linked to the mouse *Pas1* (pulmonary adenoma susceptibility) gene and a polymorphism in the second intron of the *K-ras2* gene that appears to confer different nuclear protein binding abilities that may influence gene expression (158-162). The A/J strain develops a large number of tumors spontaneously with age and produces a strong lung tumor response after treatment with certain carcinogens in a relatively short time (159). The A/J mouse has been utilized extensively to study the carcinogenic effects of numerous tobacco smoke carcinogens, including benzo[a]pyrene (B[a]P) and NNK, and the effects of intervention strategies, most notably chemoprevention (33,100,159). Activating *KRAS* mutations, often observed in potentially precancerous lesions of human lung adenocarcinoma (163), appear in

greater than 80% of lung tumors in untreated A/J mice and virtually all chemically treated A/J mice (164).

NNK is a tobacco carcinogen commonly used to induce lung tumors in A/J mice. The potency and specificity of NNK can be demonstrated after a single intraperitoneal (ip) dose (10 μmol) in which mice develop up to 7-12 lung tumors sixteen weeks after carcinogen treatment (33). Moreover, after 50 weeks post-NNK treatment, these lesions are predominantly characterized as adenocarcinomas (164). In addition, models to mimic a human exposure situation (continuous exposure of NNK) have also been developed (139,165). In these models, NNK can be administered in a chronic manner for several weeks (i.e. 3 μmol once weekly for eight weeks, total dose 24 μmol), after which adenocarcinoma development can be observed 18 weeks post-NNK treatment (139). Extensive studies in the NNK-A/J mouse model have also led to the identification of specific histopathological stages of lung tumor development, i.e. from hyperplasia to adenoma and from adenoma to adenocarcinoma (33,166,167) (Figure 2.1). These stages closely resemble the progression of human NSCLC (168). This feature allows for identification of characteristic effects occurring at specific stages of disease development, as well as in the evaluation of appropriate intervening points with preventative (i.e. chemoprevention) and therapeutic agents.

As discussed in Chapter 1, previous clinical chemoprevention trials of lung cancer using several agents have been unsuccessful; however, selenium – depending on the form – appears to provide some protection (122). Based on epidemiological, preclinical, and some, but not all, clinical studies, selenium has been shown to have a preventive effect against a variety of cancers, including lung cancer (126,127,129,132). Our laboratory has consistently shown that the synthetic organoselenium compound *p*-XSC is the most potent inhibitor, as compared to other forms of selenium, against lung tumorigenesis in A/J mice treated with NNK. This effect is

evident during the initiation phase of lung carcinogenesis supporting the role of *p*-XSC as a blocking agent; however, it was weakly effective as a suppressing agent (139,169).

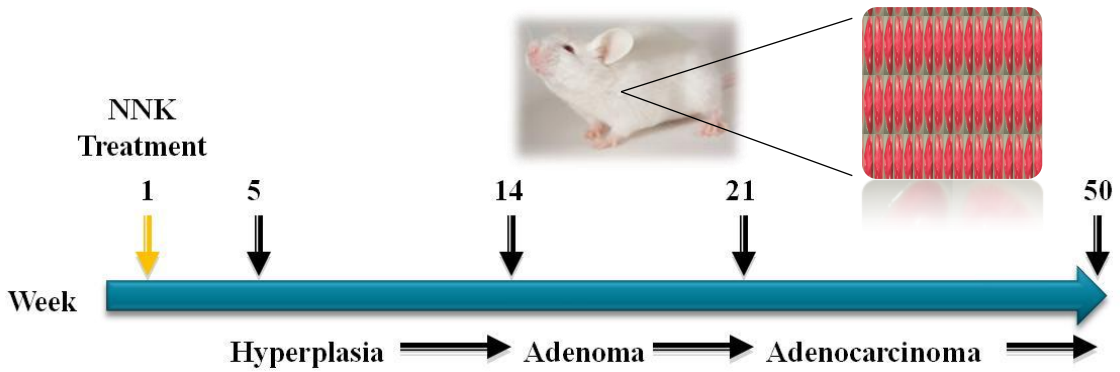

Figure 2.1 The NNK-induced lung tumorigenesis A/J mouse model. Independent of the route of administration, NNK specifically induces lung adenocarcinomas. In this illustration, after a single ip dose of NNK (10 μmol) the various histopathological stages of lung adenocarcinoma development can be followed (33).

3. Rationale

As indicated in Chapter 1, alternative approaches to lung cancer management are gravely needed to combat this disease. Early treatment of lung cancer using current strategies has provided some resolve for prognosis; however, diagnosis often occurs at rather advanced stages of the disease (27). Therefore, detection of the disease in its earliest stages is urgently needed. Molecular changes related to the development of lung cancer (i.e. biomarkers) are lacking (149). In this chapter we focused our attention on identifying more reliable biomarkers by utilizing a mouse model (strain A/J) in which the stages of disease development are well-characterized following lung cancer induction with the tobacco-specific carcinogen NNK. Lung tissue was collected at various histopathological stages and analyzed for protein expression using proteomics approaches. We initially analyzed end-stage lung tissue comprised of primarily adenocarcinoma

using 2D-DIGE; however these proteins may be a consequence of tumor formation rather than a cause of cancer induction. We then targeted earlier stages of lung carcinogenesis, i.e. hyperplasia/atypia and adenoma using immunoblot and iTRAQ analysis. Such proteins can provide a better understanding of the mechanism of the disease, but may also help in early detection of the disease, as well as in the evaluation of preventative and therapeutic strategies. Clinical chemopreventive agents have demonstrated success against various cancers, however no agent has demonstrated sufficient efficacy against lung cancer. A synthetic form of selenium, *p*-XSC, has demonstrated chemopreventive efficacy in the A/J lung tumorigenesis model with various tobacco carcinogens, including NNK alone or in combination with B[a]P (139,170). Therefore, to validate the utility of protein biomarkers we also analyzed protein expression in mice treated with NNK plus dietary adminstration of *p*-XSC.

4. Experimental design

4.1 2D-DIGE: Analysis of protein expression in A/J mouse lung comprised of adenocarcinomas induced by NNK

4.1.1 Reagents

All reagents were of analytical grade and stored appropriately prior to use according to manufacturers' recommendations. All reagents for performing 2D-DIGE were purchased from GE Healthcare (Piscataway, NJ). Reagents for immunoblot assays were purchased from Bio-Rad Laboratories (Hercules, CA). Primary and secondary antibodies were purchased from Abcam (Cambridge, MA), Cell Signaling (Danvers, MA), and Santa Cruz Biotechnology (Santa Cruz, CA). Chemiluminescent immunodetection reagents and autoradiography films were purchased from GE Healthcare and Imaging Resources, Inc. (Seattle, WA), respectively.

4.1.2 Animals and treatments

The 2D-DIGE study was performed on lung tumor tissue comprised primarily of adenocarcinomas collected at termination from a previous study (139). Briefly, five-week old female A/J mice (Jackson Laboratories, Bar Harbor, ME) in groups 1 and 2 were fed a control diet (American Institute of Nutrition, AIN-76A, Dyets Inc., Bethlehem, PA) and mice in group 3 were fed an experimental diet containing *p*-XSC (10 ppm as selenium). At 7 weeks of age, mice in groups 2 and 3 received NNK (3 μmol) in 0.1 ml cottonseed oil by intragastric administration, once weekly, for 8 weeks (total dose: 24 μmol/mouse). Twenty-six weeks after the first administration of NNK, mice were fasted overnight, anaesthetized with a solution of ketamine-xylazine, and then killed by cervical dislocation and necropsied. Figure 2.2 illustrates the design of the animal bioassay. Lungs were excised and tumors were counted. The lungs were then frozen in liquid nitrogen and stored at -80°C.

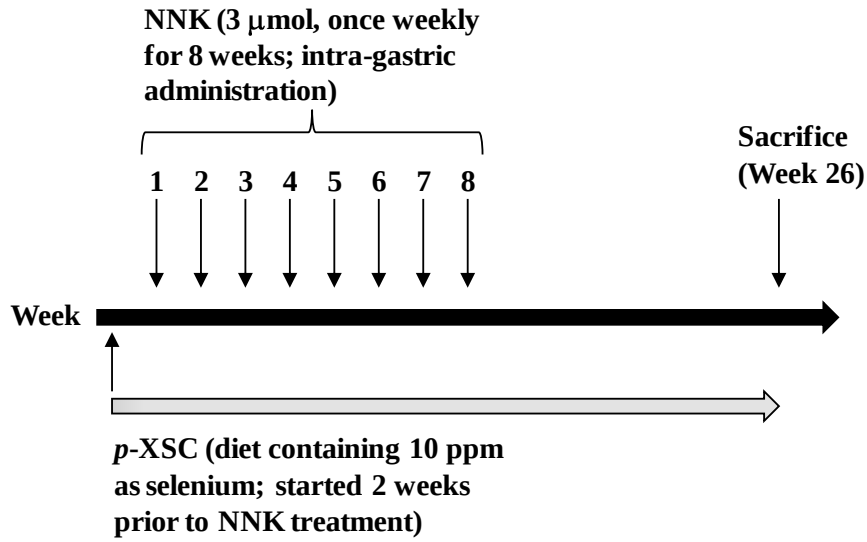

Figure 2.2 NNK treatment regimen to induce lung tumors in the A/J mouse (139). Mice in groups treated with NNK received a total dose of 24 μmol. Dietary administration of *p*-XSC was provided 2 weeks prior to the administration of NNK and continued throughout the bioassay until termination. Diets were provided *ad libitum*.

4.1.3 Minimal labeling of total lung protein with CyDye DIGE fluors

Whole frozen mouse lungs from groups 1, 2, and 3 (four lungs/group) from the aforementioned study (139) were individually processed. To isolate total lung protein for CyDye labeling, lungs were placed in liquid nitrogen and pulverized using a mortar and pestle (Bessman Tissue Pulverizers, Spectrum Laboratories, Inc., Rancho Dominquez, CA). The pulverized tissue from each mouse was weighed and resuspended in 1 mL of cell lysis buffer (30 mM TrisCl, 2 M thiourea, 7 M urea, 4% (w/v) CHAPS, adjusted to pH 8.5 with dilute HCl) for every 100 mg of tissue. The homogenate was then gently vortexed, briefly sonicated on ice for 10 sec, and centrifuged at 150 x g for 10 min at 4°C to pellet cellular debris. Recovered supernatants containing protein were aliquoted and distributed for protein concentration or frozen at -80°C. Protein concentration was determined using the Bio-Rad Protein Assay Dye Reagent Concentrate (Bio-Rad Laboratories).

In our investigation, we recovered an ample amount of protein from each sample and therefore, used the minimal labeling procedure, described in Chapter 1. Fifty micrograms of total protein from each lung was collected and labeled by incubation for 30 min on ice with 400 pmol CyDye DIGE fluor minimal dyes Cy3 or Cy5 (diluted 400 pmol/μl with dimethylformamide). Samples were randomized to Cy3 and Cy5 to ensure no dye-based artifacts in quantitation (171) (Table 2.1). An additional aliquot (29.2 μg) from each sample was used for an internal standard pool and labeled with Cy2 (400 pmol). The labeling reaction was stopped by the addition of 1 μl of 10 mM L-lysine for 10 min on ice.

4.1.4 2D separation of total lung protein

Group samples were combined randomly in pairs (Table 2.1) and diluted with an equal volume of 2X sample buffer (2 M thiourea, 7 M urea, 4% (w/v) CHAPS, 1.2% (v/v) DeStreak Reagent (GE Healthcare), IPG (Immobilized pH Gradient) Buffer 4-7 (GE

Healthcare) and the final volume brought up to 450 µl with Destreak Rehydration Solution (GE Healthcare). Immobiline DryStrips (24 cm, IPG 4-7; GE Healthcare) were rehydrated for 15 hrs with 450 µl DeStreak Rehydration solution (GE Healthcare) containing0.5% pH 4-7 IPG buffer. The labeled samples were applied to the Immobiline Drystrips for isoelectric focusing (IEF) in the first dimension using an ETTAN IPGphor3

Table 2.1 2D-DIGE experimental design. Six 2D-gels were loaded with CyDye-labeled samples. Each 2D-gel contained individual mouse whole lung protein homogenates from two of the three groups (group 1, vehicle [control]; group 2, NNK; group 3, [NNK + *p*-XSC]), as well as the internal pooled standard containing lung protein from each mouse involved in the study. Six gels were needed to accommodate number of mice in study (n=12). Gel no. 7 was loaded with unlabeled pooled lung protein from each mouse for corresponding protein spot identification.

2D-gel #	Cy3-labeled Samples (group # and mouse ID)	Cy5-labeled Samples (group # and mouse ID)	Cy2
1	group 1, 3-5	group 2, 15-4	Pooled Standard
2	group 1, 4-3	group 3, 25-3	Pooled Standard
3	group 2, 14-4	group 1, 3-4	Pooled Standard
4	group 2, 15-5	group 3, 25-5	Pooled Standard
5	group 3, 24-5	group 1, 4-5	Pooled Standard
6	group 3, 25-4	group 2, 16-1	Pooled Standard
7	Unlabeled Pool for Picking		

(GE Healthcare) as follows: active rehydration for 12 hrs at 30 V, followed by IEF conducted at 300 V for 3 hrs, 1,000 V for 7 hrs, 800 V for 4 hrs, and 100 V for 10 hrs until the system reached 50-60 kV/h in total. After IEF, the strips were equilibrated with gentle shaking in an equilibration buffer (75 mM tris, 6 M urea, 30% (v/v) glycerol, 2% (w/v) sodium dodecyl sulfate (SDS), 0.5% (w/v) DTT) and then in a second equilibration buffer) similar to the previous equilibration buffer, but with DTT replaced with 4.5% (w/v) iodoacetamide) for 15 min each. For second dimension separation by molecular weight, the IEF strips were placed on 12.5% homogeneous

polyacrylamide gels and separated at a constant wattage of 7 W at 20°C for 19 hrs in an Ettan DALTtwelve System (GE Healthcare).

4.1.5 2D gel scanning and image analysis

2D gels were imaged using the Typhoon 9410 Variable Mode Imager (GE Healthcare) for appropriate wavelengths (Cy2, 520 nm; Cy3, 580 nm; Cy5, 670 nm) at a resolution of 100 µm. All images were cropped to exclude peripheral gel artifacts arising from the IEF strips and the bromophenol blue front and were imported into Progenesis SameSpots v2.0 (Nonlinear Dynamics USA, Inc., Durham, NC) for spot matching and differential expression analysis, as previously described (172). Images were aligned by selecting a Cy2-labeled image from which all subsequent gels were aligned to for reference. Quantitation of spots was accomplished using a ratiometric normalization method (Progenesis SameSpots v2.0, PG240). In this approach, ratiometric spot volumes were calculated by expressing each spot volume as a ratio of the volume of the corresponding spot on the internal standard image from the same multiplex group. The ratios were subsequently multiplied by a normalizing factor to account for total spot volume differences between gel images.

4.1.6 Statistical analysis and interpretation of 2D gel spots

Statistical analysis comparing spots between experimental groups was performed using Student's *t* test. A filter was set to select for spots that demonstrated statistically significant difference ($p<0.05$, average ratio or fold-change >1.5 or <-1.5) and can be used to distinguish one group from the other.

Using the expression data for spots altered in a statistically significant manner, the relationship of the groups to each other was assessed by Principal Components Analysis (PCA). PCA involves a mathematical procedure that transforms a number of (possibly) correlated variables into a (smaller) number of uncorrelated variables called *principal components*. The first principal component accounts for as much of the variability in the data as possible, and each

succeeding component accounts for as much of the remaining variability as possible (173). PCA by group was performed using GeneSpring GX 7.3 (Agilent Technologies, Santa Clara, CA) and mean centered and scaled. Each axis was scaled according to the variance incorporated in that component. An expression heat map was also generated from the group mean expression values for spots altered in a statistically significant manner. The groups were clustered by an average linkage algorithm with distance used as the similarity measure using GeneSpring GX 7.3 (Agilent Technologies). The spots were clustered in the same manner.

4.1.7 Protein identification of 2D gel spots by mass spectrometry (MS)

Candidate protein spots were picked from a preparative gel (gel #7, Table 2.1) loaded with a representative lung protein homogenate from each group (166 µg/group). The picking gel was prepared on a plate that was first treated with Bind-Silane solution (80% ethanol, 0.02% glacial acetic acid, and 0.001% Bind-Silane (GE Healthcare)) containing reference markers for spot picking. After completion of electrophoresis, the preparative/picking gel plate was then fixed overnight in 30% ethanol and 7.5% glacial acetic acid. Next, the preparative/picking gel was stained for 2 hrs with Deep Purple Total Protein Stain (GE Healthcare) and preserved in an acid solution containing 15% ethanol and 1% citric acid (pH 2.3) for 30 min. Finally, the gel was imaged with the Typhoon 9410 Variable Mode Imager (GE Healthcare) using the Deep Purple filter (610 nm) at a resolution of 100 µm, and imported into Progenesis SameSpots v2.0 (Nonlinear Dynamics) for alignment and spot picking coordinate assignment as previously described (172). Spots of interest were picked from the gel using a spot-picking robot (Ettan Spot Picker, GE Healthcare).

Spots were identified by matrix-assisted laser desorption ionization time-of-flight/time-of-flight mass spectrometry (MALDI-ToF/ToF MS) as described previously (172) in the Penn State Hershey Cancer Institute Proteomics/Mass Spectrometry Shared Resource Core (Hershey, PA). Gel plugs picked from the gel were prepared by washing twice with 200 mM ammonium

bicarbonate/400 mM acetonitrile for 30 min at 37°C and then drying with 75% acetonitrile for 20 min, followed by removal of the acetonitrile solution and air drying at 30°C for 30 min. The gel plugs were then digested with 20 µg/mL trypsin (Sigma-Aldrich, St. Louis, MO) in 40 mM ammonium bicarbonate/40% acetonitrile overnight at 37°C. After protein digestion, peptides were extracted with 50% acetonitrile/0.1% trifluoroacetic acid and desalted and concentrated using C_{18} ZipTips (Millipore, Billera, MA). The clean peptides were then spotted onto an Opti-TOF™ 384 Well Insert MALDI plate (Applied Biosystems Inc., ABI, Foster City, CA). Each sample was spotted three times and prepared for MS analysis by drying in 0.7 µl of matrix solution (2 mg/ml ACH-Cinnamic Acid and 10 mM ammonium phosphate, monobasic). Peptides were analyzed using a 4800 Proteomics Analyzer (ABI). For each sample, an initial mass spectrum was collected. Based on the initial mass spectrum, up to 15 precursors were selected for tandem mass spectrometry (MS/MS) analysis. Using GPS Explorer v3.6 software (ABI), the MS and MS/MS data were submitted to a MASCOT search engine (v1.9, Matrix Science, London, UK) for identification. The National Center for Biotechnology Information non-redundant (NCBI nr) database and the *Mus musculus* taxonomy were used for sequence comparison searches. If the MASCOT confidence interval was greater than 95% for at least two MS/MS data sets along with a protein score >180, the spot was confidently identified as the corresponding protein.

We also used nanoflow capillary liquid LC tandem MS (LC/MS/MS) to sequence and identify spots on the preparative/picking gel. For those spots identified by LC/MS/MS, gel plugs were processed by ITSI Biosciences (Johnstown, PA). Each spot was in-gel digested with trypsin using an automated spot handling workstation (Ettan ProSpot, GE Healthcare) as previously described (174). Nanoflow capillary LC/MS/MS was performed with Nanobore electrospray columns on digested peptides. Nanobore electrospray columns were constructed from a 360 mm

o.d. (outside diameter), 75 mm i.d. (inner diameter) fused silica capillary with the column tip tapered to a 15 mm opening. The columns were packed with 200 Å 5 μm C_{18} beads (Michrom BioResources, Auburn, CA.), a reverse-phase packing material, to a length of 10 cm. The mobile phase used for gradient elution consisted of (A) 0.3% acetic acid, 99.7 % water and (B) 0.3% acetic acid, 99.7 % acetonitrile. The flow through the column was split pre-column to achieve a flow rate of 350 nL/min. Tandem mass spectra were acquired on a Thermo LTQ ion trap mass spectrometer (Thermo Corp., San Jose, CA). Needle voltage was set at 3 kV. Ion signals above a predetermined threshold automatically triggered the instrument to switch from MS to MS/MS mode for generating fragmentation spectra (175). Tandem mass spectra were acquired on a Thermo LTQ ion trap mass spectrometer (Thermo Corp., San Jose, CA) and searched against the NCBI nr sequence database using the SEQUEST computer algorithm (176). A spot identified with >3 unique peptides was considered to be a positive identification for the protein under examination (peptide probability >95%).

4.1.8 Validation of 2D-DIGE results by immunoblot analysis

In order to validate the utility of the 2D-DIGE proteomic technique, we performed immunoblot analyses using specific antibodies for some of the proteins identified. In addition to whole tissue, we also determined if the modulation in protein expression was taking place in tumor tissue of specific histological type. Tumors in the NNK-treated group were carefully removed under a dissecting microscope and were classified by an American College of Veterinary Pathologists (ACVP) diplomate pathologist as adenocarcinomas. Proteins from dissected adenocarcinomas and from whole lung of mice treated with the vehicle control or (NNK + *p*-XSC) were obtained by grinding tissue with a glass hand homogenizer (Ten-Broeck, Wheaton, Millville, NJ) and lysing with standard cell lysis buffer (20 mM Tris-HCl (pH 7.5), 150 mM NaCl, 1 mM Na_2EDTA (ethylenediaminetetraacetic acid), 1 mM ethylene glycol tetraacetic acid (EGTA), 1% triton, 2.5 mM sodium pyrophosphate, 1 mM β-glycerophosphate, 1 mM

Na_3VO_4, and 1 μg/mL leupeptin; 1 mL of cell lysis buffer/100 mg of homogenized tissue) (Cell Signaling, Danvers, MA) with freshly added 1 mM phenylmethylsulfonyl fluoride (PMSF) overnight at 4°C. Protein was collected following centrifugation at 14,000 x g for 10 min at 4°C and concentrations were determined using the Bio-Rad Protein Assay Dye Reagent Concentrate (Bio-Rad Laboratories). For each sample, 40 μg of total protein was denatured and resolved on a 12% or 15% SDS-PAGE gel (100 V for 100-140 min) and transferred to a nitrocellulose membrane (100 V for 65 min) (Amersham Biosciences, Piscataway, NJ). Membranes were blocked with 2.5% non-fat dry milk in Tris-Buffered Saline (TBS) containing 0.5% Tween-20 (TBS-T20) overnight at 4°C. To probe for proteins of interest, membranes were cut according to the molecular weight of the proteins. The following antibodies, diluted in 0.5% bovine serum albumin in TBS-T20, were used: anti-14-3-3 σ (1 μg/ml) from Abcam, anti-14-3-3 ε (1:1000) and anti-14-3-3 θ (1:1000) from Cell Signaling, and anti-annexin V (1:2000), anti-CC10 (1:1000) and anti-β-actin (1:2000) from Santa Cruz. Following incubation with primary antibodies overnight at 4°C, membranes were washed 3x with TBS-T20 and corresponding secondary antibodies conjugated to horseradish peroxidase (HRP) were added at a 1:2000 dilution in 0.5% bovine serum albumin in TBS-T20. Membranes were again washed 3x with TBS-T20 and bands were detected using enhanced chemiluminescence reagents (ECL, GE Healthcare) and developed with autoradiography film (Imaging Resources, Inc). For densitometric analysis, films were scanned using Bio-Rad's GS800 Calibrated Densitometer. Quantitation of protein levels was carried out using the Quantity One v4.5.0 1-D Analysis Software (Bio-Rad Laboratories) and normalized to β-actin levels. Data is presented as mean ± standard error (SE). Statistical significance ($p<0.05$) was determined using Student's *t* test.

4.1.9 Network and gene product ontology analyses of 2D-DIGE identified proteins

To determine the biological effect and the important pathways impacted by differentially expressed proteins identified from the 2D-DIGE study, proteins were imported into the Protein

Analysis THrough Evolutionary Relationships (PANTHER) classification system (http://www.pantherdb.org/, SRI International, Menlo Park, CA) and Ingenuity Pathway Analysis (IPA) Software v7.1 (Ingenuity Systems, Mountain View, CA). In PANTHER, proteins were grouped accordingly to associated biological processes. Human Genome Organization (HUGO) or Swiss-Prot accession numbers and official gene symbols were inserted into the IPA software along with corresponding comparison ratios between groups. The software identified various groupings for the gene products with respect to cellular location and components, and reported or suggested biochemical, biologic, and molecular functions. The identified proteins were mapped to associated network functions that were generated from existing literature from the Ingenuity Systems Knowledge Base. These networks are scored for degree of relevance with values >3 having a 99.9% confidence level of not being generated by random chance alone. The genetic networks that were created describe functional relationships between gene products based on known associations in the literature.

4.2 Immunoblot and iTRAQ: Analysis of protein expression at early stages (hyperplasia/atypia and adenoma) of lung adenocarcinoma development

4.2.1 Diets, chemicals, and reagents

For the NNK-A/J mouse model, NNK was purchased from Toronto Research Chemicals Inc. (North York, Ontario, Canada), cottonseed oil from Acros Organics (Morris Plains, NJ), and the AIN-76A diet from Dyets Inc. *p*-XSC was prepared in house as reported previously (177). All iTRAQ reagents and buffers were obtained from ABI, Promega (Madison, WI), and Sigma-Aldrich. Reagents and buffers for immunblot assays were purchased from Invitrogen (Carlsbad, CA) and Bio-Rad Laboratories. Primary and secondary antibodies were purchased from Abcam, Cell Signaling, and Santa Cruz Biotechnology. Chemiluminescent immunodetection reagents and

autoradiography films were purchased from GE Healthcare and Imaging Resources, Inc., respectively.

4.2.2 Animals and treatments

Female A/J mice (n=160) (five-weeks old) were obtained from The Jackson Laboratory to determine protein expression profiles in lung tissue of mice treated with NNK as a function of disease stage (hyperplasia/atypia, adenoma); we further examined the impact of the chemoprevention intervention agent *p*-XSC on protein profiles. Following quarantine for two weeks, mice were distributed by weight into three experimental treatment groups (40 mice /group) as follows: **group 1**, vehicle-treated; **group 2**, NNK-treated; **group 3**, NNK-treated plus *p*-XSC (10 ppm as selenium, selected based on demonstrated efficacy and dose tolerance without any adverse side effects (139))(Table 2.2). Mice were housed in poly-carbonated cages in a ventilated rack caging system (5/cage) under controlled conditions with a 12 hour light/dark cycle

Table 2.2 Treatment groups for NNK-induced lung tumorigenesis A/J mouse model

group	no. of mice	chemopreventive agent	carcinogen	administration of chemopreventive agent
1	40	none	none	None
2	40	none	NNK	none
3	40	*p*-XSC (10 ppm as Se)	NNK	continuous

at 50% humidity and 21°C temperature. Mice in groups 1 and 2 were fed *ad libitum* a control diet (AIN-76A) and mice in group 3 were fed *ad libitum* AIN-76A diet supplemented with *p*-XSC (Table 2.2). The AIN-76A diet was prepared in powder form from ingredients supplied by Dyets Inc. The final AIN-76A diet contained 1% vitamin mix, 3.5% mineral mix, 5% cellulose, 20% casein, 55% dextrose, 0.3% DL-methionine, 0.2% choline bitartrate, 15% corn starch, and 50 ml corn oil/kg diet. For preparation of experimental diet, lyophilized *p*-XSC was added to AIN-76 diet and thoroughly mixed with a Hobart blender to ensure uniform distribution (Offenburg, Germany). Diets were prepared as needed and stored at 4^{o}C. The stability of *p*-XSC in the diet at

room temperature and 4°C was reported previously by HPLC analysis (178) and under previous bioassay feeding conditions >97% of *p*-XSC can be recovered from the diet (177). Fresh diet was provided and food consumption was monitored as performed previously (139). At 7 weeks of age, mice in NNK-treated groups received 3 µmol NNK in 0.1 ml cottonseed oil by intragastric administration, once weekly for 8 weeks (total dose: 24 µmol per mouse) to induce lung tumors; vehicle-treated mice were given cottonseed oil alone. To perform intragastic administration, mice were positioned on their back and a gavage needle (a 3.8 cm long needle with a stainless steel ball affixed to the tip to prevent accidental rupture of esophagus) was inserted into the mouth, through the esophagus, and finally to the stomach where NNK was introduced. Body weights were recorded weekly until termination of the bioassay. To follow the progression of lung tumor development, mice were sacrificed by CO_2 asyphyxiation at five specific time points during which histopathological stages of disease in the lungs were expected to be prominent, i.e. hyperplasia/atypia, adenoma, and adenocarcinoma (33,166,167). The sacrifice times were during NNK treatment (week 4), 2 weeks after last dose of NNK (week 10), 11 weeks after last dose of NNK (week 19), 17 weeks after last dose of NNK (week 25), and 24 weeks after last dose of NNK (week 32). Figure 2.3 illustrates the design of the animal bioassay. At the time of sacrifice, both blood and lung tissue was collected. Blood was obtained by cardiac puncture in lithium heparin (anticoagulant) tubes and centrifuged at 4°C for 10 min at 3,000 rpm to recover plasma. Blood plasma was aliquoted into tubes containing 10 µl of a protease inhibitor cocktail (PIC, Sigma-Aldrich) to limit protein degradation and stored at -80°C. To remove blood constituents from the lungs, mice were perfused with approximately 20 mL of cold phosphate-buffered saline (PBS). Visible tumors (1-3 mm) on the outer surface of the lungs were tabulated during necropsy by carefully examining lungs under a dissecting lamp. Tumor incidence and multiplicity were calculated for each group; incidence was presented as the percentage of tumor-bearing mice and multiplicity as the average number of lung tumors per mouse, including non-tumor-bearing mice.

For tumor multiplicity, a Poisson regression was used to statistically compare the number of tumors between mice among the four treatment groups. To maximize the use of the lungs, the five lobes (one left lobe and four right lobes: apical, cardiac, diaphragmatic, and azygous) were separated. For protein analysis and histology, the left and right apical lobes were selected and each lobe was cut in half and processed accordingly. Lungs were flash frozen in liquid nitrogen and stored at -80°C for protein analysis or fixed in 10% neutral buffered formalin (NBF) for 24 hrs for histology.

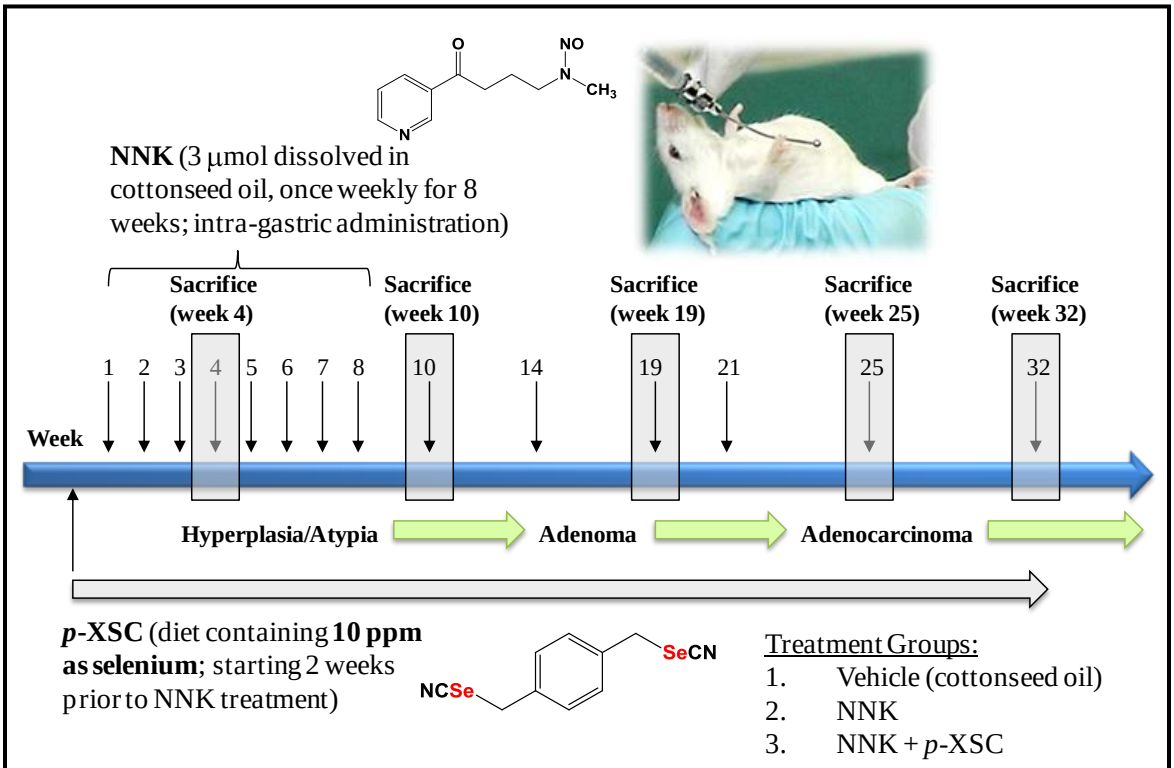

Figure 2.3 Experimental design to collect lung lesions at different stages of disease in the NNK-induced lung tumorigenesis A/J mouse model. NNK was administered weekly for 8 weeks. *p*-XSC was administered in the diet 2 weeks prior to the start of NNK treatment. During specific time points of the bioassay in which specific histopathological stages of lung cancer were reached, 7-10 mice/group were sacrificed and evaluated for histopathology and/or protein expression. Sacrifice time points are highlighted according to the start of the NNK treatment schedule.

4.2.3 Histological examination of lung tissue obtained at different stages of disease development

In order to determine the histopathological stage of lung lesions at the various sacrifice time points, tissue was submitted to the Penn State Hershey College of Medicine Comparative Medicine Department. Briefly, lung tissues fixed in 10% NBF were processed in an automated Tissue-Tek VIP processor and paraffin-embedded with a Tissue-Tek TEC embedding station. Paraffin blocks containing tissue were then cut into 5 µm thick sections on a microscope slide and stained with hematoxylin and eosin (H&E); H&E staining is a routine staining procedure used by pathologist for tissue diagnosis in which hemotoxylin stains the nuclei of cells and eosin stains intracellular and extracelluar structures.

All H&E stained tissues (one slide/animal) were examined by an ACVP diplomate pathologist blinded to treatment/genotype/intervention. Images of lung tissue were obtained with an Olympus BX51 microscope and DP71 digital camera using MicroSuite Basic 2.6 imaging software (Olympus America, Inc.). Lung tissue sections were scored using standardized criteria to confirm extent of pathological stage (41). Definitions and descriptions of tissue for this study were adapted from Nitikin et al. (41). **Epithelial hyperplasia**: Increase in number of cuboidal, columnar, ciliated or mucous cells without atypia. Cells maintain normal architecture of bronchioles and alveoli. **Airway hyperplasia**: Number of respiratory epithelial cells is increased diffusely or focally. Frequently luminal protrusions are observed, sometimes forming papillae. A regenerative phenotype consisting of small cuboidal cells with cytoplasmic basophilia, open nuclei and increased nucleus:cell (N:C) ratio can also be present. **Alveolar hyperplasia**: Solitary or multiple foci of increased cellularity distal to terminal bronchioles. The background of bronchoalveolar architecture remains detectable, and epithelial cells are usually single layered. Round to oval hypertrophic type II pneumocytes with abundant eosinophilic cytoplasm line the alveolar walls. Macrophages may be present in the alveolar lumens. **Atypia** included

karyomegaly, nuclear hyperchromasia, increased N:C ratio, abnormal nuclear shape, pseudoinclusions, cellular crowding, indistinct cell borders, anisokaryosis, prominent hobnail appearance, and non-basal mitotic figures. Atypia and hyperplasia were graded independently on a semi-quantitative scale of 0 (normal) to 4 (severe) which reflected both the number of cells affected as well as the degree of hyperplasia/atypia. Grade 1 (minimal) lesions consisted of low grade changes in scattered individual epithelial cells within a few airways or alveoli. Grade 2 (mild) consisted of a greater degree of cytologic changes in small clusters of epithelial cells in several airways or alveoli. Grade 3 (moderate) consisted of a majority of epithelial cells within most airways or alveoli. Grade 4 (severe) was a diffuse process. **Adenoma**: Well circumscribed areas consisting of cuboidal to columnar cells lining alveoli. The size is usually less than 5 mm in diameter and retains preexisting alveolar structure. An adenoma was considered adenoma with progression when a distinct clone of cells (10 or more) appeared with hyperchromatic nuclei and nuclear size greater than those found in cells of the adenoma (179). **Adenocarcinoma**: Compared with adenomas, adenocarcinomas show greater cytological atypia, increased frequency of mitoses, regional variation in growth pattern, more papillary structures, sizes over 5 mm in diameter, invasion of vessels, large airways or pleura, as well as lymphatic and hematogenous metastases.

4.2.4 Protein extraction from lung tissue

Total lung protein from mice was collected by homogenizing tissue with a Ten-Broeck glass hand homogenizer (Wheaton) in standard cell lysis buffer (Cell Signaling) containing 5 µl PIC (Sigma-Aldrich). The resulting homogenate was vortexed thoroughly and placed at 4^{o}C overnight. To pellet cellular debris, samples were again vortexed and centrifuged at 14,000 x g for 10 min at 4^{o}C. Supernatants containing protein were aliquoted and distributed for protein concentration or frozen at -80°C for further protein analysis. Protein concentrations were

determined by the *DC* (detergent compatible) Protein Assay (Lowry Assay, Bio-Rad Laboratories).

4.2.5 Immunoblot analysis of differentially expressed proteins discovered in our 2D-DIGE study

To identify molecular changes at early histopathological stages of lung tumor development in the NNK-A/J mouse model, we selected lungs from mice sacrificed 2 weeks after the last dose of NNK (week 10) and 17 weeks after the last dose of NNK (week 25) (Figure 2.3); at week 10 mice treated with NNK alone exhibited an increase in the alveolar hyperplasia/atypia and at week 25 the transition to adenoma development was apparent based on histological analysis of lung tissue. We initially focused on determining the modulation of proteins that were identified as being down-regulated in lung tissue comprised primarily of lung adencarcinomas from our 2D-DIGE study (e.g. CC10 and the 14-3-3 protein isoforms ε, θ, and σ). Individual lung samples (n=3 mice /treatment group), 25-45 µg of total protein was denatured and resolved on a NuPAGE® 4-12% gradient gel (Invitrogen) (200 V for 60 min) and transferred to a nitrocellulose membrane (100 V for 72 min) (Amersham Biosciences). Membranes were blocked with 5% non-fat dry milk in TBS containing 0.5% TBS-T20 at room temperature for 1 hr. To probe for proteins of interest, membranes were cut according to the molecular weight of the proteins. The following antibodies, diluted in 0.5% bovine serum albumin in TBS-T20 as recommended by the manufacturers, were used: anti-14-3-3 σ (1 µg/ml) from Abcam, anti-14-3-3 ε (1:1000) and anti-14-3-3 θ (1:1000) from Cell Signaling, and anti-CC10 (1:1000), anti-annexin V (1:2000), and anti-β-actin (1:2000) from Santa Cruz. Following incubation with primary antibodies overnight at 4°C, membranes were washed 3x with TBS-T20 and corresponding secondary antibodies conjugated to HRP were added at a 1:2000 dilution in 0.5% bovine serum albumin in TBS-T20. Membranes were again washed 3x with TBS-T20 and bands were detected using ECL reagents (GE Healthcare) and developed with autoradiography film (Imaging Resources, Inc). For

densitometric analysis, films were scanned using Bio-Rad's GS800 Calibrated Densitometer. Quantitation of protein levels was carried out using the Quantity One v4.5.0 1-D Analysis Software (Bio-Rad Laboratories) and normalized to β-actin levels. Data are presented as mean ± SE. Statistical significance ($p<0.05$) was determined using Student's *t* test.

4.2.6 Acetone precipitation of lung proteins for iTRAQ analysis

To identify additional molecular changes at early histopathological stages of lung tumor development we used the same lung tissue used for the immunoblot analysis above to perform an iTRAQ analysis. Prior to using protein samples in proteomic studies it is strongly recommended that potentially interfering agents including salts, nucleic acids, lipids, etc. be removed. As a result, a variety of techniques have been developed including ultrafiltration and conventional precipitation with acetone or trichloroacetic acid (180); weak acids such as trichloroacetic acid decrease sample pH, resulting in denaturation and consequently precipitation of protein (181). Acetone precipitation is a widely used procedure with high protein recovery and sample concentration (180) and is recommended by ABI for protein precipitation prior to iTRAQ analysis. Equal amounts of protein were pooled from five mice in each group during both time points and precipitated with cold acetone as follows. Six volumes of 100% acetone (chilled, kept at -20^{o}C) was added to each sample, vortexed, and placed at -20^{o}C for approximately 2 hrs. To collect precipitated protein, samples were centrifuged at 16,000 x g for 10 min at 4^{o}C. Protein pellets were then vortexed twice with a 4:1 acetone-to-water solution and recovered by centrifugation. The last wash was followed by drying in a centrifugal vacuum concentrator. Final protein pellets were resuspended in Milli-Q water, 0.1% SDS, and 1M urea. Protein recovery was determined by the *DC* Protein Assay (Lowry Assay, Bio-Rad Laboratories).

Lung tissue protein pools from the three treatment groups at the two different sacrifice time points were allocated to individual isobaric tags for an 8-plex iTRAQ experiment as indicated in Table 2.3.

Table 2.3 8-Plex iTRAQ experimental design using total lung protein collected from vehicle and NNK- treated A/J mice

isobaric tag	week of sacrifice	treatment group
113	10	Vehicle
114	10	NNK
115	10	NNK + *p*-XSC (10 ppm as Se)
117	25	Vehicle
118	25	NNK
119	25	NNK + *p*-XSC (10 ppm as Se)

4.2.7 Preparation of lung proteins prior to isobaric tag labeling of peptides

Prior to protein labeling with iTRAQ tags a series of sample preparation steps are required. These include denaturation (unraveling of proteins), reduction (addition of hydrogen atoms), alkylation (transfer of alkyl group for inhibition of disulfide bond formation), and digestion (breaking of proteins into separate peptide fragments). All of the steps were performed according to the recommendations of ABI with appropriate modifications suggested by the Penn State Hershey Cancer Institute Proteomics/Mass Spectrometry Shared Resource (Hershey, PA). For each sample, 150 µg of protein was dried with a centrifugal vacuum concentrator and then resuspended in 50 µl of 0.5 M triethylammoniumbicarbonate (TEAB) pH 8.5. Following resuspension of samples, 1 µl of denaturant (2% SDS) and 1 µl of reducing reagent (5 mM tris-(2-carboxyethyl) phosphine, TCEP) were then added to each sample and incubated for 1 hr at 37°C. To block cysteine side chains from disulfide bridging, 1 µl of freshly prepared 84 mM iodoacetamide solution (alkylating agent) was then added and incubated for 30 min at room temperature under dark. Digestion of proteins at the carboxyl side of the amino acids lysine and arginine was performed with the serine protease trypsin. Sequencing grade trypsin (Promega) was reconstituted in 50 mM acetic acid (supplied by Promega) at a concentration of 1 µg/µl. Trypsin was added to each sample (1:15, trypsin:protein) and allowed to incubate overnight at

48°C. Efficient digestion of samples was visualized by coomassie G-250 staining (Bio-Rad Laboratories) on a 10% SDS-PAGE gel (Figure 2.4).

4.2.8 iTRAQ labeling of protein peptides

After protein samples were carefully prepared, as described above, iTRAQ labeling was performed according to the recommendation of ABI with appropriate modifications suggested by the Penn State Hershey Cancer Institute Proteomics/Mass Spectrometry Shared Resource. iTRAQ tags (mass=113-119, 121) were reconstituted in 50 µl of isopropanol. The contents of one iTRAQ tag was transferred to one sample tube and mixed thoroughly; samples and corresponding tags are listed in Table 2.3. The labels and samples were allowed to incubate at

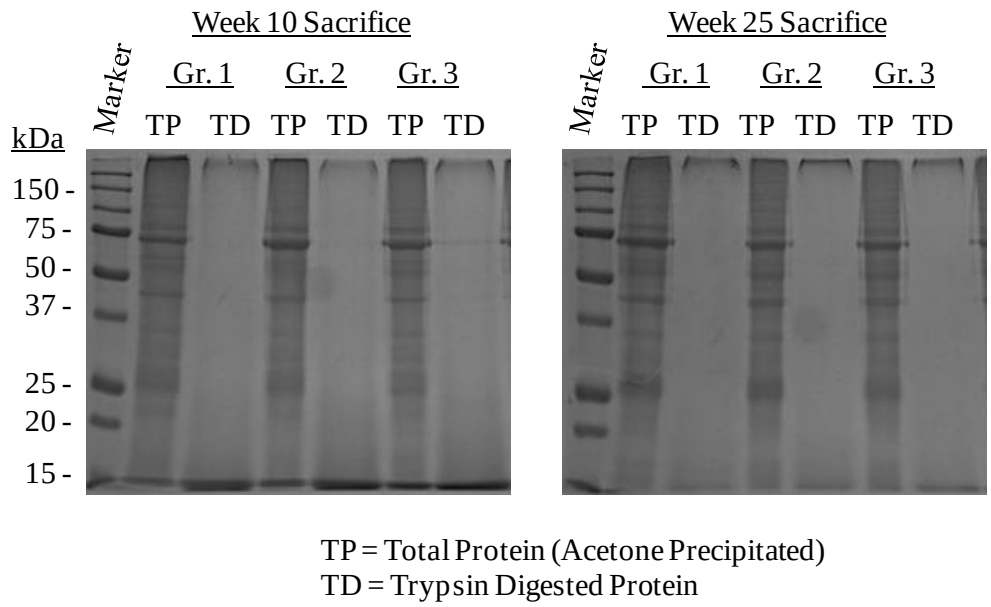

Figure 2.4 Digestion of lung proteins with trypsin prior to iTRAQ labeling. Total lung protein samples from week 10 and week 25 sacrifice time points before and after digestion with trypsin were resolved on a 10% SDS-PAGE gel and stained with coomassie. Two lanes are present for each group (Vehicle, Gr. 1; NNK, Gr. 2; (NNK + *p*-XSC, Gr. 3); the first lane contains total lung protein (TP, 15 µg) and the adjacent lane contains the total lung proteins following digestion with trypsin (TD).

room temperature for 2 hrs. To quench the reactions, 100 µl of Milli-Q water was added to each tube and allowed to incubate at room temperature for 30 min. The contents of each iTRAQ reagent-labeled sample were then combined into one tube and dried using a centrifugal vacuum concentrator. Two 100 µl washes with Milli-Q water were performed before further processing. The dried pool of iTRAQ reagent-labeled samples representing 1,200 µg of total protein was resuspended in 500 µl of Cation Exchange Buffer (ABI) and adjusted to the appropriate pH of 2.5 to 3.3 using 1 M HCl.

4.2.9 2D-LC fractionation of iTRAQ labeled peptides

To increase the detection of peptides from low abundance proteins, the labeled peptide mixtures were fractionated in the Penn State Hershey Cancer Institute Proteomics/Mass Spectrometry Shared Resource Core using strong cation exchange (SCX) LC in the first dimension. SCX was carried out on a passivated Waters 600E HPLC system, using a 4.6 x 250 mm PolySULFOETHYL Aspartamide column (PolyLC, Columbia, MD) at a flow rate of 1 ml/min. Two buffers were prepared to separate samples: Buffer A, contained 10 mM ammonium formate, pH 2.7, in 20% acetonitrile/80% water and Buffer B, contained 666 mM ammonium formate, pH 2.7, in 20% acetonitrile/80% water. The HPLC separation gradient was as follows: Buffer A at 100% (0-22 minutes following sample injection), 0%→40% Buffer B (16-48 min), 40%→100% Buffer B (48-49 min), then isocratic 100% Buffer B (49-56 min), then at 56 min switched back to 100% A to re-equilibrate for the next injection. The first 26 ml of eluent (containing all flow-through fractions) was combined into one fraction and then 14 additional 2-ml fractions were collected. All 15 of these SCX fractions were dried down completely to reduce volume and to remove acetonitrile and volatile ammonium formate salts, followed by resuspension in 9 µl of 2% (v/v) acetonitrile, 0.1% (v/v) trifluoroacetic acid.

For 2D separation by reverse phase nanoflow-LC, each SCX fraction above was autoinjected onto a Chromolith CapRod column (150 x 0.1 mm, Merck, Gibbstown, NJ) using a 5

µl injector loop on a Tempo LC MALDI Spotting System (Applied Biosystems Inc-MDS/Sciex). Additional buffers, C and D, were prepared. Buffer C contained 2% acetonitrile, 0.1% trifluoroacetic acid, and Buffer D contained 98% acetonitrile, 0.1% trifluoroacetic acid. The elution gradient was prepared as follows: 95% C/5% D (2 µl per minute flow rate from 0-3 min, then 2.5 µl per minute from 3-8.1 min), 5% D→38% D (8.1-40 min), 38% D→80% D (41-44 min), 80% D→5% D (44-49 min) (initial conditions). Flow rate was 2.5 µl/min during the gradient, and an equal flow of MALDI matrix solution (7 mg/ml recrystallized CHCA (α-cyano-hydroxycinnamic acid), 2 mg/ml ammonium phosphate, 0.1% trifluoroacetic acid, 80% acetonitrile) was added post-column. The combined eluent was automatically spotted onto a stainless steel MALDI target plate every six seconds (0.6 µl per spot), for a total of 370 spots per original SCX fraction.

4.2.10 MS analysis of peptides

MS analyses of peptide fractions for subsequent identification and quantitation were performed in the Penn State Hershey Cancer Institute Proteomics/Mass Spectrometry Shared Resource Core. MALDI target plates (15 per experiment) containing peptides were analyzed in a data-dependent manner on an ABI 4800 MALDI TOF/TOF Analyzer along with 13 calibrant spots (ABI 4700 Mix). As each plate entered into the instrument, a plate calibration/MS Default calibration update was performed, followed by MS/MS default calibration. MS Spectra were taken from 5,500 MALDI Spots, using 500 laser shots per spot and laser intensity of 3,400. A plate-wide interpretation was automatically performed in which the highest peak of each observed m/z value was chosen for subsequent MS/MS analysis. MS/MS spectra were derived from 2,500 laser shots at a laser power of 4,000. Fragmentation of labeled peptides was induced by the use of atmosphere as a collision gas with a pressure of 1.2 to 1.3 x 10^{-6} Torr. A total of 14,861 MS/MS spetra were taken from experimental samples.

4.2.11 Database search for protein identification from MS and MS/MS spectra

Protein identifications from MS spectra were performed using the Paragon Algorithm (182) as implemented in Protein Pilot™ v4.0 software (ABI-MDS Sciex). Protein Pilot™ was programmed to provide a thorough search of proteins taking into account parameters for cysteine alkylation of proteins by iodoacetamide and any potential biological modifications. MS and MS/MS spectra were searched using the *Mus musculus* NCBI nr database sequences containing 30,008 protein sequences (version 2011-03), plus concatenated reverse versions of itself, and common human and laboratory contaminants (ABISciex_ContaminantDB_20070711); total of 60,328 protein sequences. Identifications of proteins were only accepted with a Protein Pilot™ Unused Score of >1.3 (>95% confidence interval). The Unused Score is a measure of the protein confidence for a detected protein, calculated from the peptide confidence for peptides from spectra that are not already completely "used" by higher scoring winning proteins (Protein Pilot™ v4.0). In addition, accepted protein identifications needed to have a "Local False Discovery Rate (FDR)" estimation of no higher than 5%, as calculated by the PSEP (Proteomics System Performance Evaluation Pipeline) Algorithm (183) from the rate of accumulation of "hits" from the Decoy (reversed) database. The Local or "Instantaneous" FDR estimates the "local" error rate around a given identification. This indicates the likelihood that the specific identification is incorrect based on the use of Decoy Database searches (either Reversed or Randomized version of the same Forward/Normal database used for searching), presumably containing no real sequences, with the assumption that the number of identifications of Decoy (not real) peptides or proteins at a particular threshold accurately estimates the number of FALSE identifications from the Forward/Normal database (184). This Local FDR estimate combined with the Pro Group™ Algorithm included in Protein Pilot™ v4.0 gives a very conservative and fully Minimum Information About a Proteomics Experiment (MIAPE)-compliant list of proteins identified (185).

4.2.12 Quantitation and statistical analysis of proteins identified from MS results

iTRAQ reporter ion abundances in MS/MS scans were evaluated using Protein Pilot™ v4.0 software (ABI) for relative quantitation of proteins. For each peptide used for protein identification, areas of peaks at m/z 113-115 and 117-119 were calculated. Peptides shared among different protein groups were removed before quantitation. To correct for experimental errors in amount of protein included in each sample group, a bias correction was performed on the Pro Group™ Algorithm results. This was performed by calculating the median peptide ratio for all peptides reported, adjusting to unity, and then applying the same bias factor to all ratios (performed within Protein Pilot™ v4.0). This normalizing factor is based on the assumption that most of the protein levels between groups should be similar with the exception of those that are influenced by the different treatments. Relative abundances of each protein were therefore expressed as the average iTRAQ ratios of all informative peptides from the given protein. *P*-values and error factors (EFs) for statistical comparison between the profiles of the various times of sacrifice and treatment regimens was performed by Protein Pilot™ v4.0 software. The EF, also known as the standard deviation, defines the quantitative 95% confidence interval of a ratio, which is the range within which the true protein value is to appear. An EF <2 is the same as a standard deviation of the quantitation below 20%. Quantitative iTRAQ data were then exported into Microsoft Excel 2007 (Bellevue, WA) for further analysis. Significant differences in protein levels between groups were only accepted based on a filtering criteria which included a *p*-value <0.05, an EF<2 (i.e. standard deviation <20%), and a >1.2 or <0.8 fold-change. Furthermore, proteins of interest required identification and quantitation with ≥2 peptides. For protein ontology classification, proteins were imported into the PANTHER classification system (http://www.pantherdb.org/, SRI International). Proteins were grouped accordingly to associated molecular functions and biological processes were described.

5. Results

5.1 Protein profiling during NNK-induced lung adenocarcinoma development

5.1.1 2D-DIGE of A/J mouse lung tissue comprised primarily of adenocarcinomas

The 2D-DIGE technique was utilized to discover changes in the lung tissue proteome of A/J mice treated with the highly potent tobacco carcinogen NNK to induce lung adenocarcinoma formation and further validate selected protein biomarkers using the chemopreventive agent *p*-XSC (186). The tissue was obtained from a study in which we demonstrated previously that dietary *p*-XSC significantly inhibited both lung tumor multiplicity (from 10.4 ± 0.6 tumors per mouse in the NNK-treated group to 2.7 ± 1.5 in mice in the (NNK + *p*-XSC) group) and incidence (from 96% in the NNK-treated group to 68% in the (NNK + *p*-XSC) group) (139). Whole lung tissue was homogenized and used in the 2D-DIGE analysis.

Figure 2.5 shows representative images of a 2D-DIGE gel containing two samples, one labeled with Cy3 (total protein from the whole lung of mice treated with the vehicle control, Figure 2.5A) and the other with Cy5 (total protein from whole lung of mice treated with NNK, Figure 2.5B), and an internal standard pool labeled with Cy2 (total protein combined together from all of the lungs obtained from the three experimental groups, Figure 2.5C). These images were analyzed by the image analysis program Progenesis SameSpots v2.0 to compare the differential expression of proteins between groups. Spot matching (100%) between all of the gels (6 gels including 12 images) led to the identification of 796 protein spots (Figure 2.5D).

Quantitative analysis of individual spots was performed using the average normalized expression volume calculated from four lung samples for each group. The data was filtered according to significant ($p<0.05$) changes in expression between groups as well as a change beyond 50% (i.e. average ratio or fold-change >1.5 or <-1.5), and therefore 191 protein spots

were included for subsequent analysis. With these 191 protein spots, an unsupervised, multivariate data analysis method known as PCA was used to analyze the union of all potential

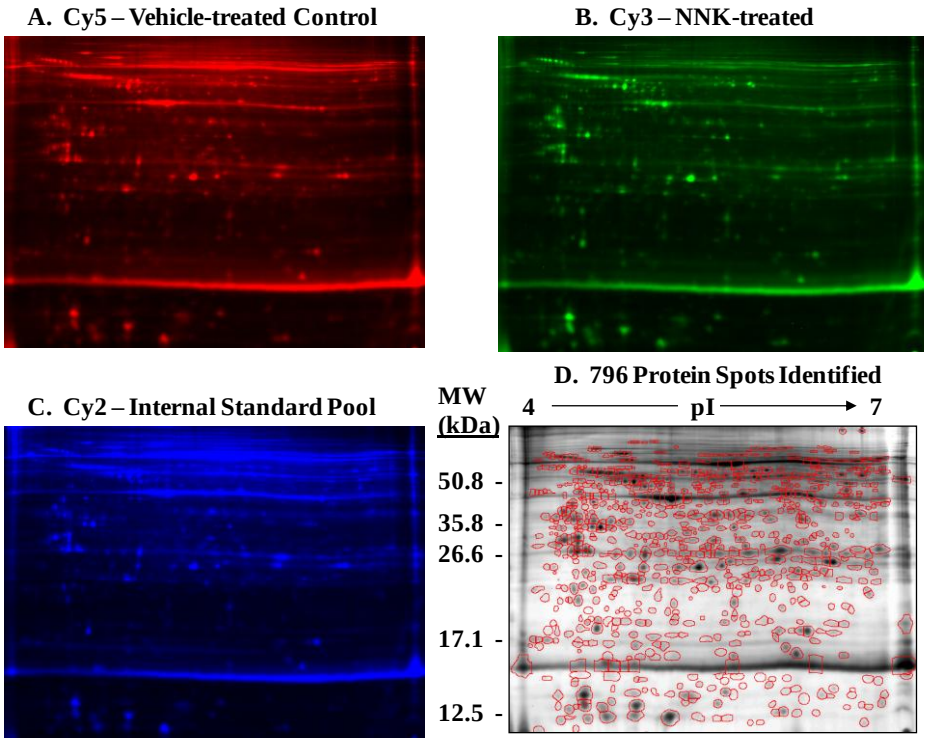

Figure 2.5 Proteomic profiling of the A/J mouse lung using the 2D-DIGE approach to identify differentially regulated proteins in NNK-treated and (NNK + *p*-XSC)-treated mice. Representative images of a 2D-DIGE gel scanned for different CyDye fluorophores illustrating fractionated lung proteins from different groups. (A) The vehicle-treated control sample was labeled with Cy5 (red). (B) The NNK-treated sample was labeled with Cy3 (green). (C) An internal pool standard, consisting of all samples in the study, was labeled with Cy2 (blue). (D) Automatic and manual spot detection led to the identification of 796 protein spots outlined in red. Figure was published in reference (186).

protein expression changes from the statistical analyses and establish a cluster for each group (Figure 2.6). The location of each of the three treatment group markers represents the weighted average of the values of the two principal components for all samples within each group (four mice/treatment group). The first component represented the greatest variance between the groups

(x-axis, 92%). The second component (y-axis), encompassing about 8% of the variance between the groups, had little effect in separating the three experimental groups. The PCA plot demonstrates that the proteomic shifts for the vehicle-treated control and (NNK + *p*-XSC) samples were similar to each other. On the other hand, the NNK-treated group exhibited its own unique proteomic shift that was considerably separate from the other two treatment groups. Further analysis of the 191 protein spots was performed by expression heat map and hierarchical clustering analysis (Figure 2.7). This further demonstrated that each group had its own unique protein profile expression pattern for this particular set of proteins and that the vehicle-treated control and (NNK + *p*-XSC)-treated groups were related to each other, separate from the NNK-treated group.

After comparing the vehicle-treated control and NNK-treated groups, 138 protein spots were found to be differentially regulated. Of these, 10 protein spots were significantly up-regulated and 128 were significantly down-regulated in the lungs of mice treated with NNK. However, after comparing the vehicle-treated control and (NNK + *p*-XSC) groups, only 22 protein spots were differentially regulated. Of these, 13 protein spots were significantly up-regulated and 9 were significantly down-regulated in the (NNK + *p*-XSC) group. After comparing the NNK and (NNK + *p*-XSC)-treated groups, 136 proteins spots were differentially regulated. Of these, 126 protein spots were significantly up-regulated and 10 were significantly down-regulated in the (NNK + *p*-XSC) group. Interestingly, expression levels of 83 proteins negatively regulated by NNK were recovered to levels that were equal to or greater than those observed in the lungs of vehicle-treated control mice.

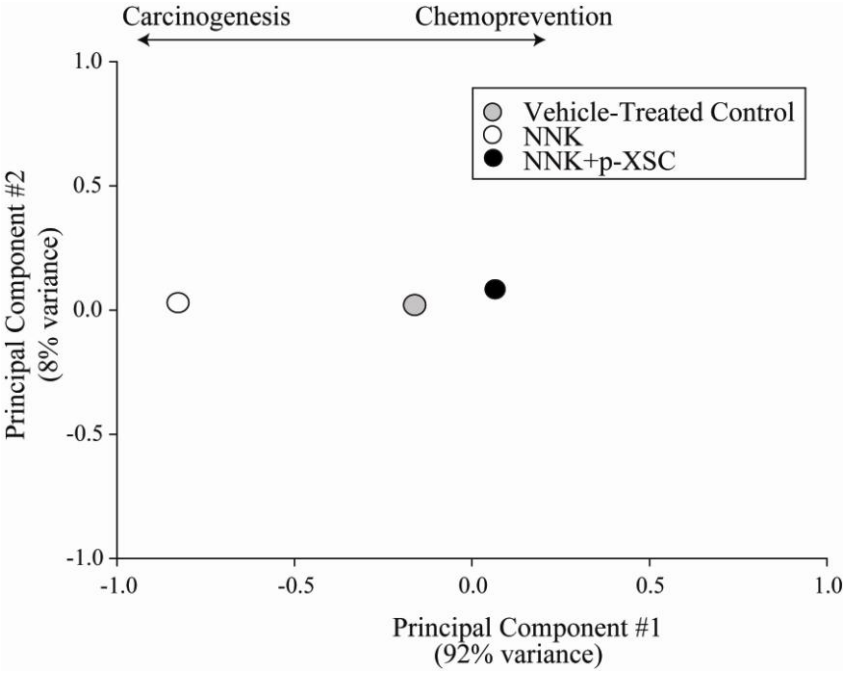

Figure 2.6 Principal Components Analysis (PCA) of 191 significant differentially expressed protein spots with either carcinogenesis or chemoprevention-based relationships. The two greatest study variances between the three groups are represented on the x- and y- axes (x-axis, 1st principal component, 92%; y-axis, 2nd principal component, 8%). Each spot represents the compressed weighted average of the principal components of the 191 proteins for each sample in each treatment group; the vehicle-treated control group (shaded circle), the NNK-treated group (open circle), and the (NNK + *p*-XSC)-treated group (closed circle). Figure was published in reference (186).

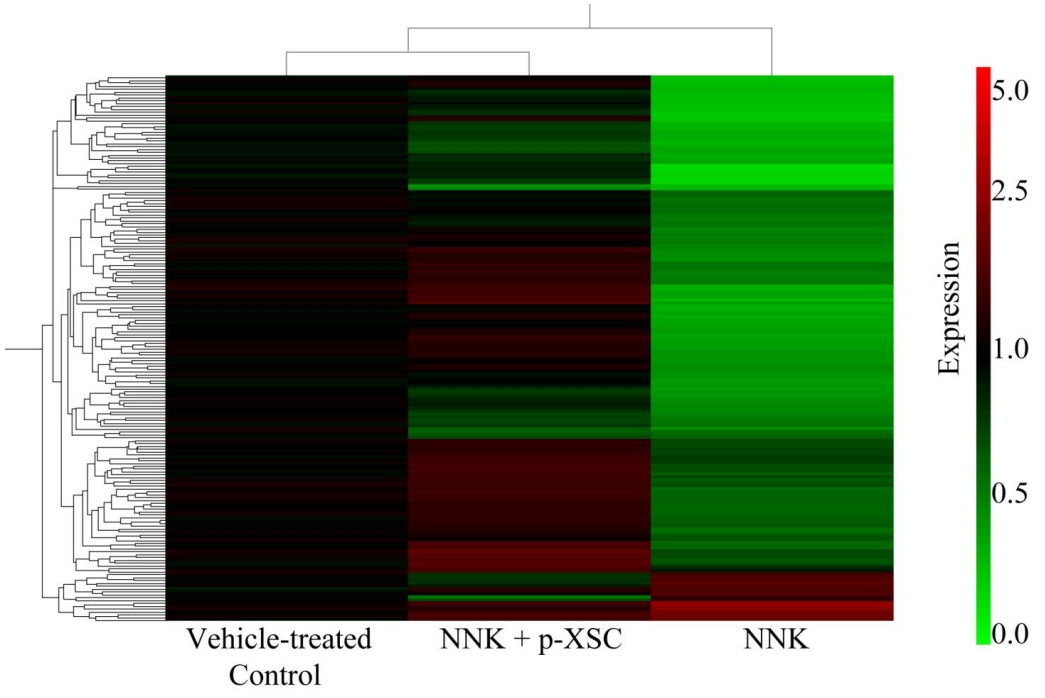

Figure 2.7 Protein expression heat map for 191 protein spots that were differentially regulated between the three treatment groups (Vehicle-treated Control, NNK-treated, and (NNK + *p*-XSC)-treated). Up-regulated proteins are in red and down-regulated proteins are in green. Hierarchial clustering of protein expression was performed in two dimensions. The first dimension (top dendrogram) shows the similarity in protein expression profiles of the groups and the second dimension (left hand side dendrogram) shows individual protein expression profiles. Figure was published in reference (186).

5.1.2 Identification of protein spots modulated by NNK individually and in combination with *p*-XSC

After statistical analysis was completed using the Progenesis SameSpots v2.0 software, a select group of significant, differentially expressed protein spots were excised and identified using MALDI-ToF/ToF MS. Figure 2.8 shows the location of 16 candidate protein spots that were selected for MS analysis. After analysis by MALDI-ToF/ToF MS and subsequent searching of fragments in the NCBI nr and *Mus musculus* databases, 10 proteins were identified and are

listed in Table 2.4 (Table was published in reference (186)). Figure 2.9A shows a representative peptide mass fingerprint match spectrum and MS/MS spectrum of the corresponding amino acid sequence YLAEFATGNDRK used in the identification of 14-3-3 ε protein. Of particular interest concerning these proteins is that they were down-regulated in the lungs of mice treated with NNK compared to vehicle-treated control mouse lungs, but were significantly up-regulated in the group receiving (NNK + *p*-XSC); this is clearly shown in Figure 2.9B. The proteins identified in this study are known to be involved in a variety of biological processes, as noted using the PANTHER ontology database (www.pantherdb.org), including cholesterol, nucleic acid, protein, and fatty acid metabolism (SEC14-like 3, dihydropyrimidinase-like 2, proteasome subunit α type 5, and annexin A5, respectively), signal transduction (the 14-3-3 protein isoforms consisting of ε, ζ, and θ, and Rho GDP dissociation inhibitor α), muscle contraction (myosin light polypeptide 6), and intracellular protein trafficking (tubulin-α-1).

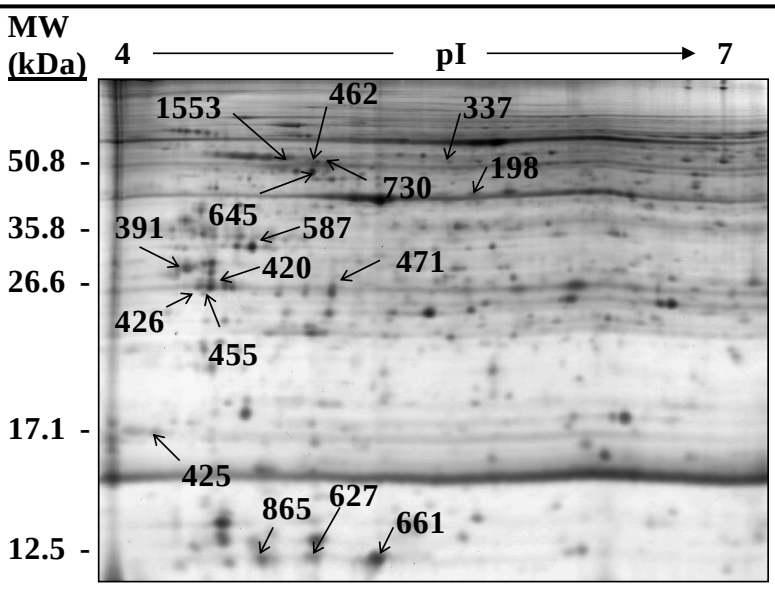

Figure 2.8 2D-DIGE reference gel image. A selected group of protein spots (indicated by arrows, total number 16) that were differentially regulated between vehicle-treated and NNK-treated mice were excised and identified using mass spectrometry methods. Figure was published in reference (186).

Table 2.4 Proteins that are differentially expressed (fold-change) in NNK and (NNK + *p*-XSC) groups as identified by 2D-DIGE and MALDI-TOF/TOF MS & MS/MS

spot no.	identified protein	accession co.*	Vehicle-treated Control vs NNK: average ratio	Vehicle-treated Control vs NNK: *p*-value	Control vs (NNK + *p*-XSC): average ratio	Control vs (NNK + *p*-XSC): *p*-value	NNK vs (NNK + *p*-XSC): average ratio	NNK vs (NNK + *p*-XSC): *p*-value	protein score/C.I.%†	total ion score/C.I.%‡	protein MW/pI§	protein coverage(%)¶	biological function‖
198	SEC14-like 3	gi|71480138	**-2.79**	0.009	1	0.977	**2.78**	0.040	569/100	422/100	46.5/5.6	32.7	Cholesterol Metablolism
337	dihydropyrimidinase-like 2	gi|40254595	**-1.84**	0.021	1.24	0.412	**2.29**	0.033	533/100	400/100	62.6/6.0	26.6	Nucleoside, Nucleotide, Nucleic Acid Metabolism
455	protesome subunit α type 5	gi|7106387	**-1.61**	0.045	1.21	0.145	**1.95**	0.010	348/100	298/100	26.6/4.7	24.9	Protein Metabolism and Modification
587	annexin A5	gi|6753060	-1.23	0.105	1.09	0.178	**1.34**	0.030	1260/100	1041/100	35.8/4.8	51.7	Lipid, Fatty Acid and Steroid Metabolism
391	14-3-3 ε	gi|5803225	**-1.98**	0.002	1.09	0.666	**2.15**	0.025	419/100	302/100	29.3/4.6	23.1	Signal Tranduction, Protein Targeting, Cell Cycle
420	14-3-3 ζ	gi|1841387	**-1.85**	0.027	1.12	0.326	**2.07**	0.017	525/100	393/100	27.9/4.7	30.2	Signal Tranduction, Protein Targeting, Cell Cycle
426	14-3-3 θ	gi|51593617	**-1.84**	0.037	1.12	0.427	**2.06**	0.016	483/100	343/100	30.2/4.9	35.1	Signal Tranduction, Protein Targeting, Cell Cycle
471	Rho GDP dissociation inhibitor (GDI) α	gi|13435747	**-1.52**	0.019	1.24	0.073	**1.88**	0.008	363/100	290/100	23.4/5.1	33.3	Rho Protein Signal Transduction, Negative Regulation of Cell Adhesion
425	myosin light polypeptide 6	gi|17986258	-1.99	0.055	1.03	0.748	**2.06**	0.028	325/100	245/100	17/4.6	25.8	Muscle Contraction
462	tubulin-α-1	gi|6755901	-1.14	0.576	**1.69**	0.005	**1.92**	0.014	481/100	388/100	50.8/4.9	18.8	Intracellular Protein Traffic, Cell Cycle, Cell Structure and Motility

Ratios in **bold** are statistically significant ($p < 0.05$)

* National Center for Biotechnology Information (NCBI)

† Sum of the scores of the peptide mass fingerprint match and MS/MS peptide fragment ion matches; scores >95 are considered significant

‡ Scores of the quality of the MS/MS fragment ion matches only; scores >20 are considered significant

§ Theoretical values from MASCOT

¶ The percent of the residues in each protein sequence that have been identified

‖ PANTHER ontology database

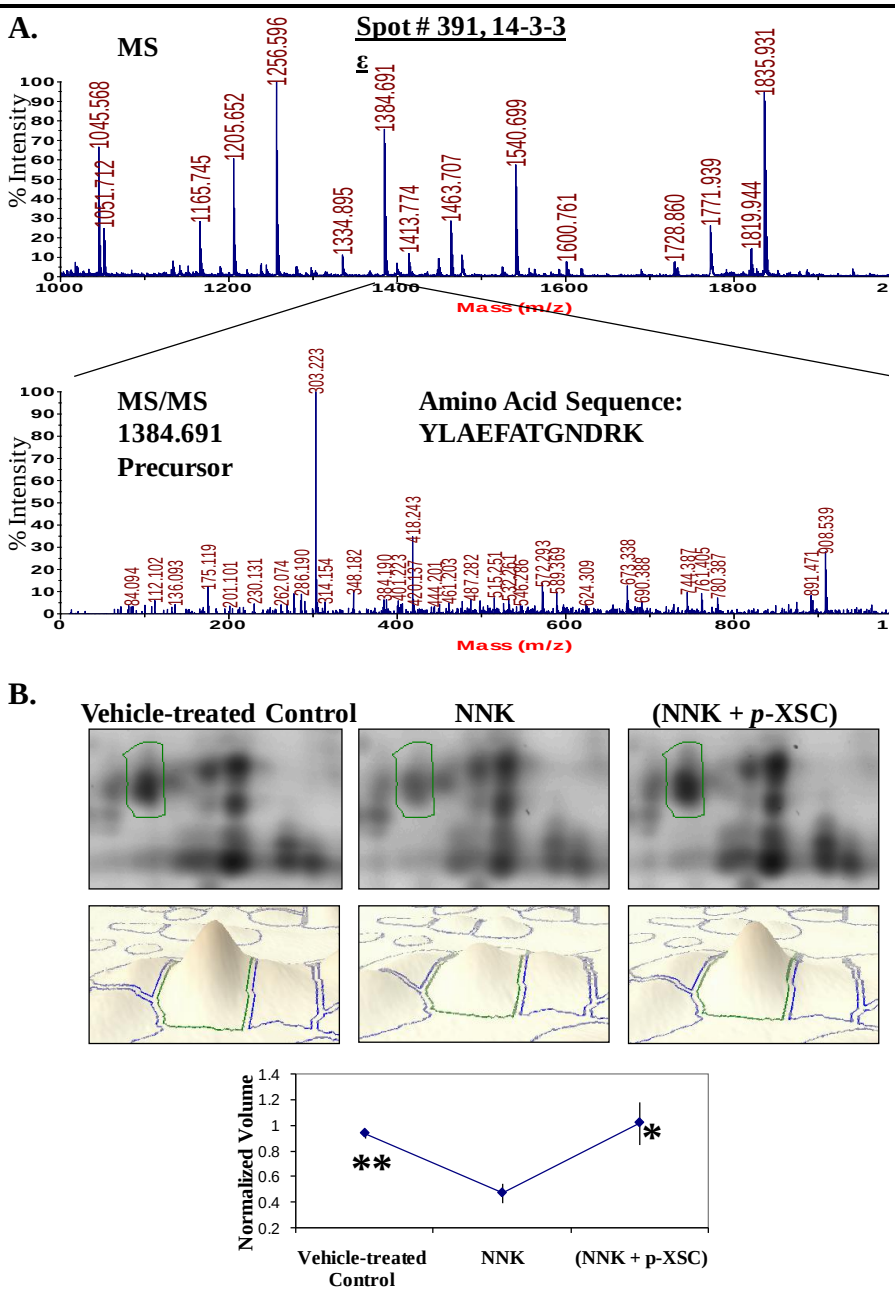

Figure 2.9 Identification of 2D-DIGE gel spot #391 (14-3-3 ε). (A) Representative MALDI-ToF/ToF MS and tandem MS spectra used in the identification of the 14-3-3 ε proteins. The peptide sequence YLAEFATGNDR was unique to the 14-3-3 ε protein. (B) 2D-DIGE gel images of 14-3-3 ε expression for all three experimental groups. The three dimensional and graphical presentations of the normalized spot volume for the 14-3-3 ε protein illustrates the expression differences found between the vehicle-treated control, NNK, and (NNK + *p*-XSC)-treated groups. **p*<0.05; ***p*<0.005 (Student's *t* test). Figure was published in reference (186).

In addition to MALDI-ToF/ToF MS described above, LC/MS/MS analysis was employed for the identification of low abundant proteins on the preparative/picking gel and four additional protein spots were identified as vimentin, Atp5b protein, serine (or cysteine) peptidase inhibitor clade A member 1c (commonly known as α-1-antitrypsin, AAT) and Clara cell 10 kDa protein (CC10) (Table 2.5; table was published in reference (186)). Three isoforms of CC10 were also identified and verified by immunoblot analysis. Interestingly, vimentin expression was 1.64-fold and 2-fold greater in the (NNK + *p*-XSC) group compared to both vehicle-treated control and NNK-treated groups, respectively. Atp5b protein and AAT were only 1.2-fold higher in expression in the (NNK + *p*-XSC) group compared to the vehicle-treated control group. Atp5b, which is involved in ATP biosynthesis, was up-regulated in the NNK-treated group 2.36-fold and 1.92-fold compared to both the vehicle-treated control and (NNK + *p*-XSC) groups, respectively, but this was found to be non-significant. All three isoforms of CC10 were down-regulated in the NNK group compared to vehicle-treated control and remained at comparable levels in the (NNK + *p*-XSC) group.

5.1.3 Immunoblot verification of modulated protein levels found in 2D-DIGE

To verify the identity of proteins described above, we performed an immunoblot analysis on select proteins that have been suggested to be involved in various cancers. To determine if these changes are specifically occurring in tumor tissue as compared to normal tissue, dissected tumors from the NNK-treated group were compared to vehicle-treated control lung tissue. The tumors were classified histopathologically as adenocarcinomas, papillary type (Figure 2.10). Quantification of the protein bands indicated that the 14-3-3 proteins (θ and ε) were expressed at lower levels in lung adenocarcionomas in the NNK-treated group compared to normal lungs of mice in the vehicle-treated control group (Figure 2.11A and B). The 2-fold change in expression observed for for 14-3-3 θ and ε by immunoblot analysis was similar to the fold-change observed in our 2D-DIGE analyses. We also focused on the analysis of the 14-3-3 protein isoform σ, since

Table 2.5 Proteins that are differentially expressed (fold-change) in NNK and (NNK + *p* -XSC) groups as identified by 2D-DIGE and LC-MS/MS

spot no.	identified protein	accession no.*	Vehicle-treated Control vs NNK: average ratio	Vehicle-treated Control vs NNK: *p* -value	Vehicle-treated Control vs (NNK + *p* -XSC): average ratio	Vehicle-treated Control vs (NNK + *p* -XSC): *p* -value	NNK vs (NNK + *p* -XSC): average ratio	NNK vs (NNK + *p* -XSC): *p* -value	no. of peptides†	protein MW	biological function‡
730	vimentin	gi|2078001	-1.22	0.441	**1.64**	0.011	**2.00**	0.016	15	51.6	Intermediate Filament-based Process
645	Atp5b protein	gi|23272966	2.36	0.225	**1.2**	0.006	-1.92	0.295	11	56.7	ATP Biosynthetic Process
1553	Serine (or cysteine) peptidase inhibitor, clade A member 1c (AAT)	gi|15012149	1.03	0.922	**1.2**	0.046	1.16	0.577	5	52	Serine Protease Inhibitor
865	Clara cell 10kDa protein (CC10)	gi|627855	-1.72	0.067	**-1.64**	0.007	1.05	0.874	1	12.5	Ligand Mediated Signaling, Anti-inflammatory
661	Clara cell 10kDa protein (CC10)	gi|627855	**-2.27**	0.028	**-2.09**	0.006	1.08	0.839	1	12.5	Ligand Mediated Signaling, Anti-inflammatory
627	Clara cell 10kDa protein (CC10)	gi|627855	**-2.54**	0.031	**-2.64**	0.024	-1.04	0.929	1	12.5	Ligand Mediated Signaling, Anti-inflammatory

Ratios in **bold** are statistically significant ($p < 0.05$)

* National Center for Biotechnology Information (NCBI)

† No. of peptides that match the theoretical digest of the primary protein identified

‡ PANTHER ontology database

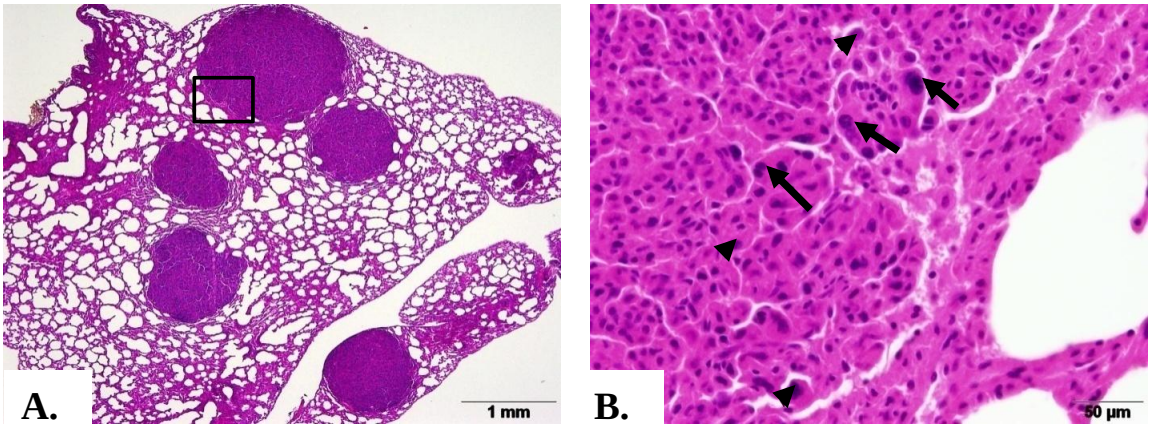

Figure 2.10 Histopathological analysis of H&E stained NNK-induced lung tumors in the A/J mouse. (A) Tumor section surrounded by normal tissue; tumors were classified as adenocarcinomas, papillary type (magnification, X100). (B) Magnified region of box in (A) (magnification, X600); arrows, indicating multinucleate tumor cells; arrowheads, highlighting variation in nuclear size (anisokaryosis), a feature of dysplasia. Figure was published in reference (186).

it has been shown to be frequently modulated in human cancers, including lung cancer (187,188). Although we did not identify this protein in our 2D-DIGE study, we were able to show that it was significantly down-regulated in adenocarcinomas induced by NNK in our immunoblot analysis compared to the vehicle-treated control group (Figure 2.11A and B). Annexin A5 was also found to be significantly down-regulated in the NNK-induced adenocarcinomas compared to the vehicle-treated control group (Figure 2.11B); this significant down-regulation was not observed in our 2D-DIGE analyses. We also observed a significant decrease in CC10 expression in the adenocarcinomas compared to the vehicle-treated control group (Figure 2.11B); this, however, takes into account total CC10, whereas in our 2D-DIGE analyses three isoforms were evaluated. We observed that those proteins down-regulated in the NNK-induced tumors were restored to normal lung tissue expression levels, except for CC10, in the (NNK + *p*-XSC)-treated group (Figure 2.11C and D). Although it was not statistically significant, except for 14-3-3 σ, it should

be mentioned that these expression levels exceeded those observed for the vehicle-treated control group (Figure 2.11D). Furthermore, a non-significant increase in annexin A5 (approximately 1.2-fold) in the lungs of mice treated with (NNK + *p*-XSC) compared to mice treated with vehicle was observed in our immunoblot analyses, whereas in our 2D-DIGE analyses this change was significant.

5.1.4 Network analysis of identified proteins

In order to understand the biological association of the identified proteins within context to each other and potential pathways in which they may be involved, we used the Ingenuity Systems Inc. software, IPA. The proteins that were statistically different and had a 1.5 fold-change in expression between the lungs of mice treated with the vehicle control and NNK, including annexin A5 and vimentin, were included in this analysis. IPA identified an associated cancer-related network regarding tumor morphology and cell morphology between 11 of these proteins with a score of 25. Figure 2.12 shows the cellular location of these proteins along with direct or indirect relationships exhibited by the proteins with each other within the network. In particular, the down-regulated 14-3-3 protein isoforms we identified in the lungs of NNK-treated mice compared to the vehicle-treated group bind to numerous proteins, including each other, to modulate the bound protein's activity. Interestingly, the 14-3-3 θ isoform binds to the oncogenic MYC protein (189), a transcriptional regulator known to play an enhancing role in cancer development (190). MYC was also found to exhibit associations with annexin A5, 14-3-3 ε, and proteasome subunit α type 5.

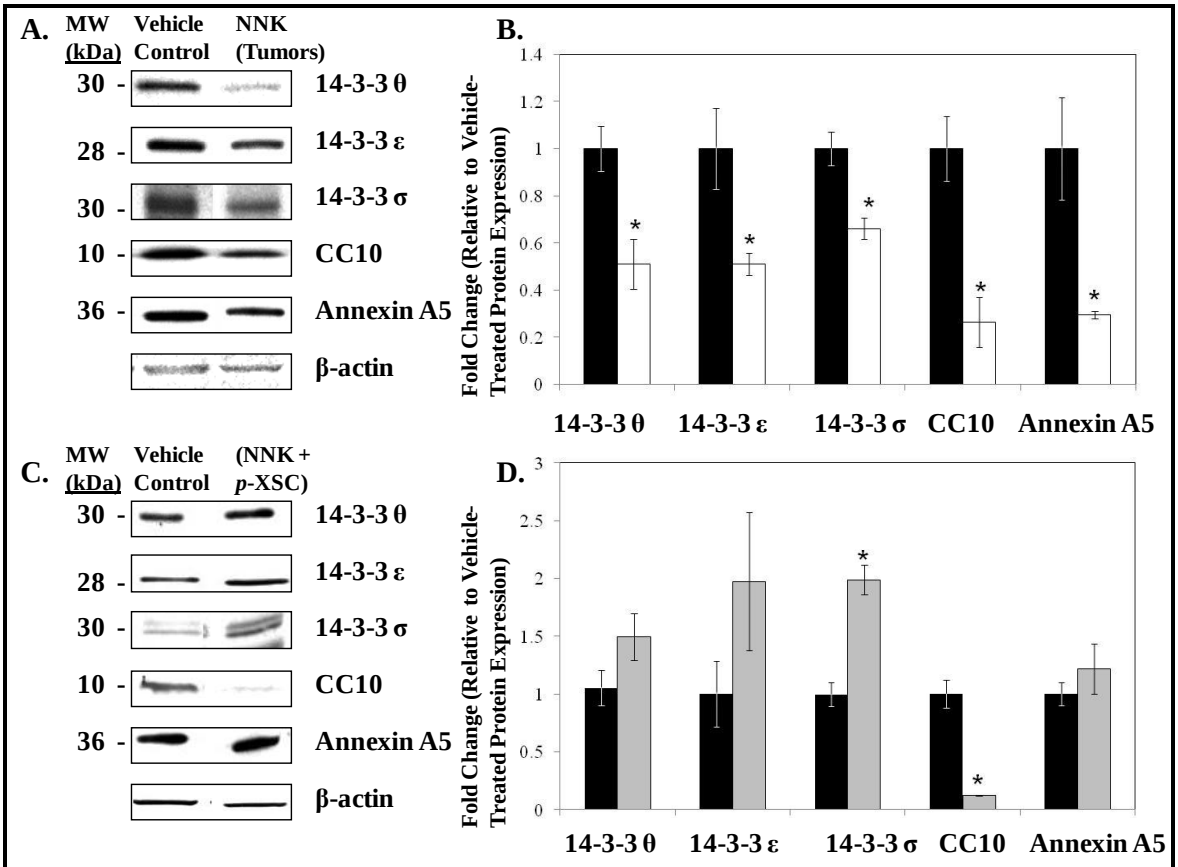

Figure 2.11 Validation of 14-3-3 isoforms θ, ε, and σ, CC10, and annexin A5 under-expression by immunoblot analysis. (A) Representative immunoblot analysis from three experiments of expression of 14-3-3 θ, ε, and σ, CC10, and annexin A5 in dissected NNK-induced lung adenocarcinomas and vehicle-treated control lung tissue. Forty micrograms of total lung protein were loaded into each lane for each sample. (B) Fold-change in mean protein band expression from immunoblot for 14-3-3 θ, ε, and σ, CC10, and annexin A5 in lung tissue from mice treated with vehicle (solid bars) or tumors from mice treated with NNK (open bars). (C) Representative immunoblot analysis from three experiments of expression of 14-3-3 θ, ε, and σ, CC10, and annexin A5 in vehicle-treated lung tissue and (NNK + *p*-XSC)-treated lung tissue. Forty micrograms of total lung protein were loaded into each lane for each sample. (D) Fold-change in mean protein band expression from immunoblot for 14-3-3 θ, ε, and σ, CC10, and annexin A5 in lungs from mice treated with vehicle (solid bars) or (NNK + *p*-XSC) (gray bars). For comparison between protein expression levels between groups, the fold-change was calculated relative to vehicle-treated control levels and normalized with respect to β-actin protein expression levels. $^{*}p<0.05$ (Student's *t* test; n=3). Figure was published in reference (186).

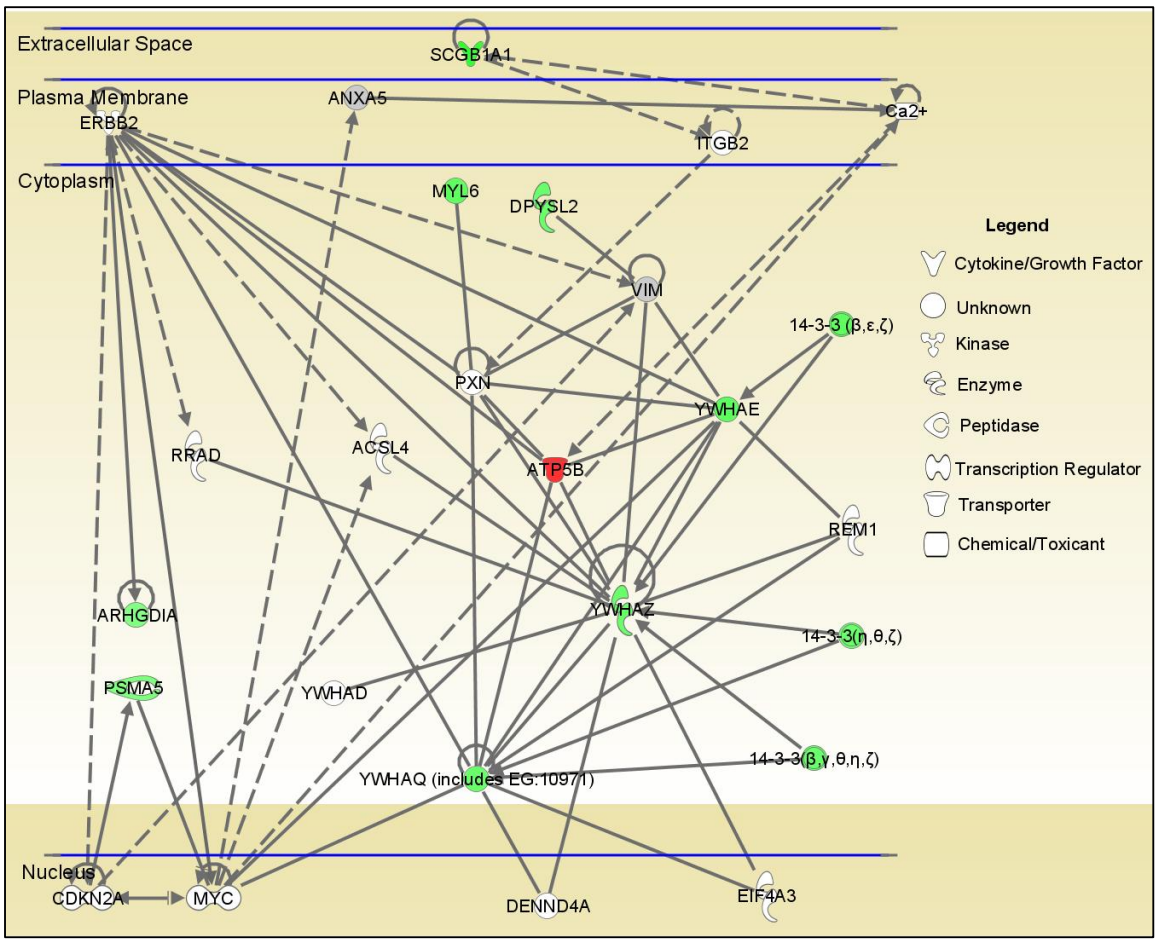

Figure 2.12 Network analysis of differentially expressed proteins using IPA software. Proteins that were found to be significantly different between lungs of mice treated with the vehicle control versus NNK were analyzed using IPA. The proteins were classified in a cancer, tumor morphology, and cell morphology associated network, along with corresponding protein-to-protein direct (solid lines) or indirect (dashed lines) interactions/regulations, based on information published in the literature. The proteins shown in green were down-regulated and those in red were up-regulated in the NNK-treated group compared to the vehicle-treated control group. Proteins were given shapes related to functionality and were also grouped with respect to cellular location: extracellular space, plasma membrane, cytoplasm, and nucleus. Figure was published in reference (186).

5.2 Protein profiling during NNK-induced lung hyperplasia/atypia and adenoma development

5.2.1 Body weights and overall survival of A/J mice

To evaluate the health of the A/J mice used in our study we observed them weekly until the termination of the bioassay. No observable changes in physical appearance and/or behavior were noted in any group to indicate signs of discomfort or toxicity. There were no significant changes in body weights between mice treated with vehicle (group 1) compared to NNK-treatment alone (group 2) (Figure 2.13). Mice treated with (NNK + *p*-XSC) (group 3) did not gain as much weight compared to the other groups (Figure 2.13); reasons for this may be due in part to the initial dietary level of *p*-XSC first administered, as well as in the lower consumption of food. In the original design of this study, *p*-XSC was added to the diet at a concentration of 15 ppm as selenium; this dose is 60% of the maximum tolerated dose and has not exhibited toxicity in our previous studies (140,169,191). However, in the present study, the decrease in average body weight raised a concern as to using selenium at 15 ppm in the form of *p*-XSC. Therefore, after week six, mice were switched to a diet containing *p*-XSC at a concentration of 10 ppm as selenium. We also noted that mice receiving dietary *p*-XSC consumed less food compared to the other groups (group 1, 2.5 g/mouse/d; group 2, 1.9 g/mouse/d; group 3, 1.2 g/mouse/d). This could be due to the poor palatability of the selenium-based diet. As a result, the average body weights never reached those observed in the group 1, but did, however, increase during the progression of the bioassay (Figure 2.13).

5.2.2 Incidence and multiplicity of lung tumors

In this investigation, the incidence of tumors in mice treated with NNK alone reached 60% eleven weeks after the last dose of NNK (week 19) and by week 25, mice in all groups exhibited tumors in the lung. At weeks 19, 25, and 32, tumors on the surface of lungs were

visible and select portions of lung tissue was histologically analyzed as adenomas and adenocarcinomas. The number of tumors per mouse (tumor multiplicity) was significantly lower in mice treated with (NNK + *p*-XSC) at weeks 25 and 32 (Figure 2.14). The results from the present study are consistent with those reported by our group previously (139,141).

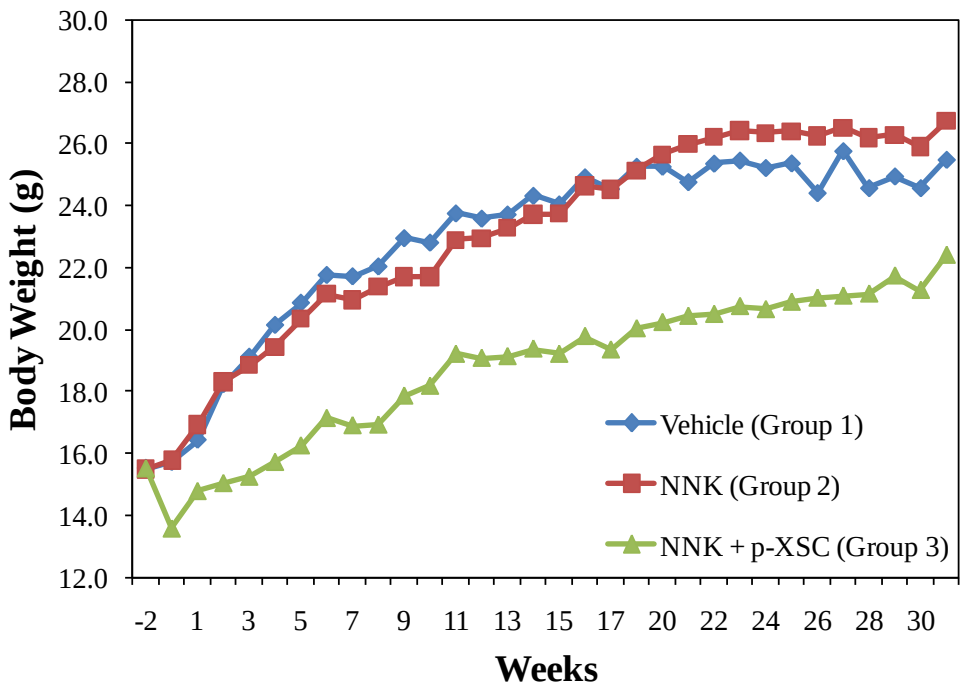

Figure 2.13 The effect of NNK treatment and administration of dietary *p*-XSC on body weights of A/J mice. Body weights were measured weekly. Values from all live mice were averaged for each group at each time point. Mice were treated with 3 μmol of NNK per week for eight weeks (total dose: 24 μmol) starting at week 1 and ending at week 8. Mice in (NNK + *p*-XSC) group received *p*-XSC at 15 ppm as *Se* in the diet for the first eight weeks of the study and were then switched to a diet containing *p*-XSC at 10 ppm as *Se* continuing throughout the bioassay. Significant reduction of body weight by (NNK + *p*-XSC) was observed throughout the bioassay. Diets and drinking water were available *ad libitum*. (n=43/group weeks [-2]-4; n=33/group weeks 5-10; n=23/group weeks 11-19; n=16/group weeks 20-25; n=6-9/group weeks 26-32)

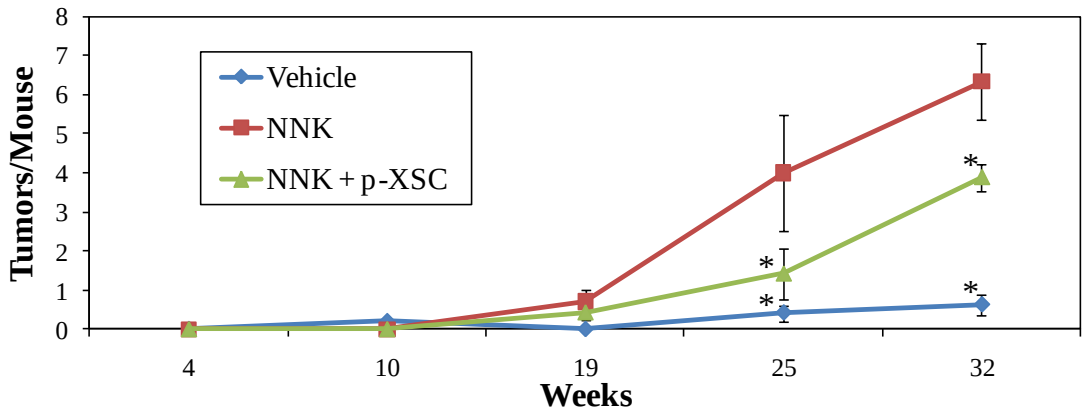

Figure 2.14 The effect of NNK and dietary administration of *p*-XSC on lung tumor multiplicity (gross lesions) in A/J mice. All mice receiving NNK (n=6-10) developed tumors as observed at week 19. Spontaneous tumors were detected in vehicle-treated mice at weeks 10, 25, and 32. At weeks 25 and 32, *p*-XSC reduced tumor multiplicity in mice that had received NNK. *$p<0.05$ (Poisson Regression) compared to NNK alone treated mice.

5.2.3 Progression of pulmonary lesions

The basis of this investigation was to analyze protein expression in lung tissue at various histological stages of lung tumor development (i.e. hyperplasia, adenoma, and adenocarcinoma). The selection of sacrifice times was based primarily on histopathological knowledge of the A/J mouse model from previous studies following carcinogen administration (33,166,167). Lung tissue was collected from mice (n=5-9) at five time points during the bioassay from each group. The tissue was grossly evaluated and analyzed microscopically for histopathology by a board certified veterinary pathologist. Lung tissue was scored according to presence, as well as severity, for airway and alveolar epithelial hyperplasia and atypia (Figure 2.15), adenoma, and adenocarcinoma (Figure 2.16).

To determine the transition of NNK-induced lesion development, lesion multiplicities were tabulated for each group at each point of sacrifice. Epithelial hyperplasia and atypia were

combined into one category and those of alveolar origin were of primary focus based on location of adenocarcinoma development (41). Lung tissue collected from NNK-treated mice exhibited an increase in alveolar hyperplasia/atypia up to week 19 followed by a prominent drop at week 25 and then again an increase at week 32 (Figure 2.17A). The drop in alveolar hyperplasia/atypia at week 25 coincided with an increase in adenoma formation (Figure 2.17A); at this point, the transition from hyperplasia/atypia to adenoma was evident. By comparison, alveolar hyperplasia/atypia in the lungs of vehicle and (NNK + *p*-XSC)-treated mice followed a similar trend to that observed in NNK alone treated mice (Figure 2.17B and C); however, at week 10 the lungs of mice treated with NNK + *p*-XSC had the greatest increase in alveolar hyperplasia/atypia. For pulmonary adenoma development, in mice treated with vehicle, spontaneous adenomas developed at week 25 (Figure 2.17B), whereas in mice treated with (NNK + *p*-XSC), adenomas were present at week 19 (Figure 2.17C). In the present bioassay adenocarcinomas were present at week 32 in NNK-treated mice, but the numbers detected by histology were too low to report with confidence. Histological changes in tumor development during the progress of the bioassay were not evaluated statistically due to limited number of mice. Overall, this analysis indicated that we could identify different histopathological stages of lung carcinogenesis during the progression of the bioassay.

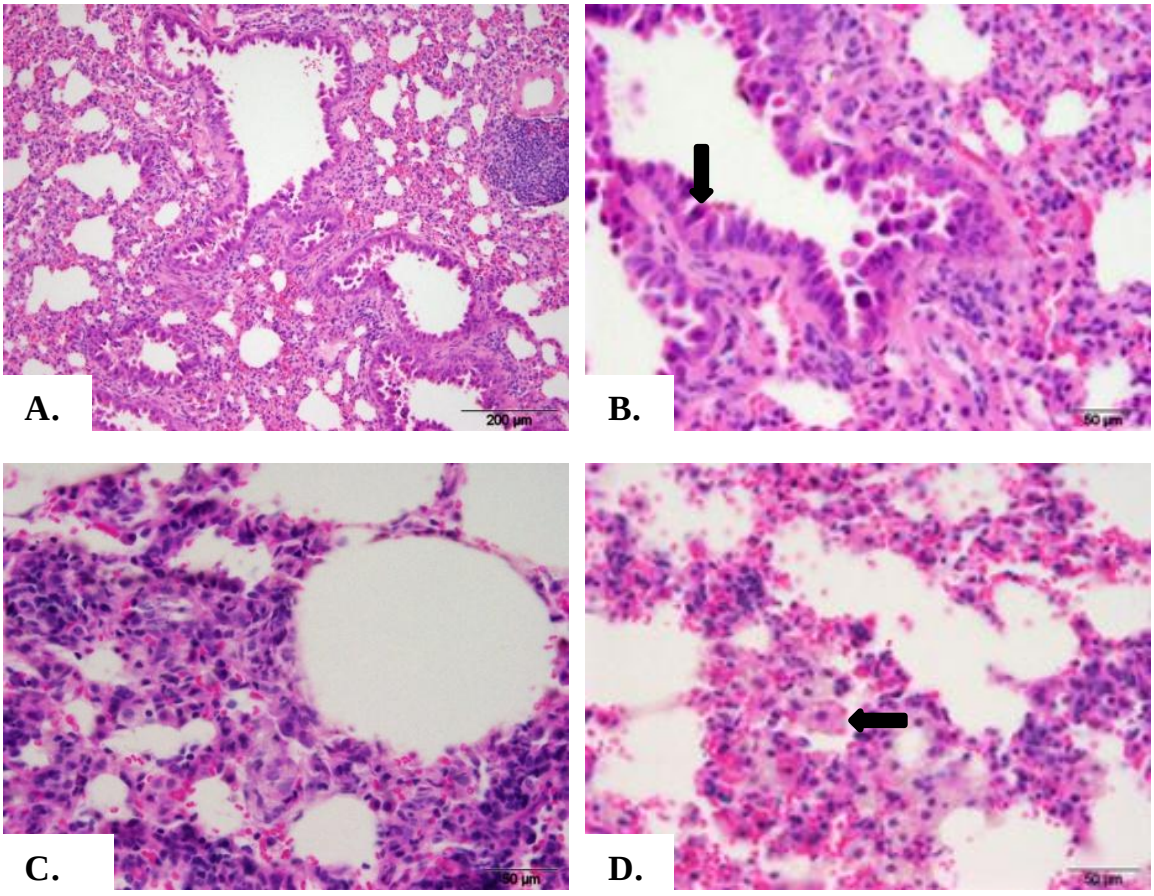

Figure 2.15 Photomicrographs of airway and alveolar epithelial hyperplasia and atypia in lungs of NNK-treated A/J mice. (A, B) **airway epithelial hyperplasia** - characterized as a diffuse or focal increase in number of respiratory epithelial cells creating a crowded appearance, frequently luminal protrusions were observed, sometimes forming papillae. A regenerative phenotype consisting of small cuboidal cells with cytoplasmic basophilia, open nuclei and increased nucleus:cytoplasm (N:C) ratio was also present. **Airway atypia** included karyomegaly, nuclear hyperchromasia, increased N:C ratio, abnormal nuclear shape, pseudoinclusions, cellular crowding, indistinct cell borders, anisokaryosis, prominent hobnail appearance (closed arrow, B), and non-basal mitotic figures. (C, D) **alveolar epithelial hyperplasia** - characterized by solitary or multiple foci of increased epithelial cellularity distal to terminal bronchioles. The background of bronchioloalveolar architecture remained unaltered, and epithelial cells were usually single layered. Round to oval hypertrophic type II pneumocytes with abundant eosinophilic cytoplasm lined the alveolar walls. Macrophages were present in the alveolar lumina (closed arrow, D).

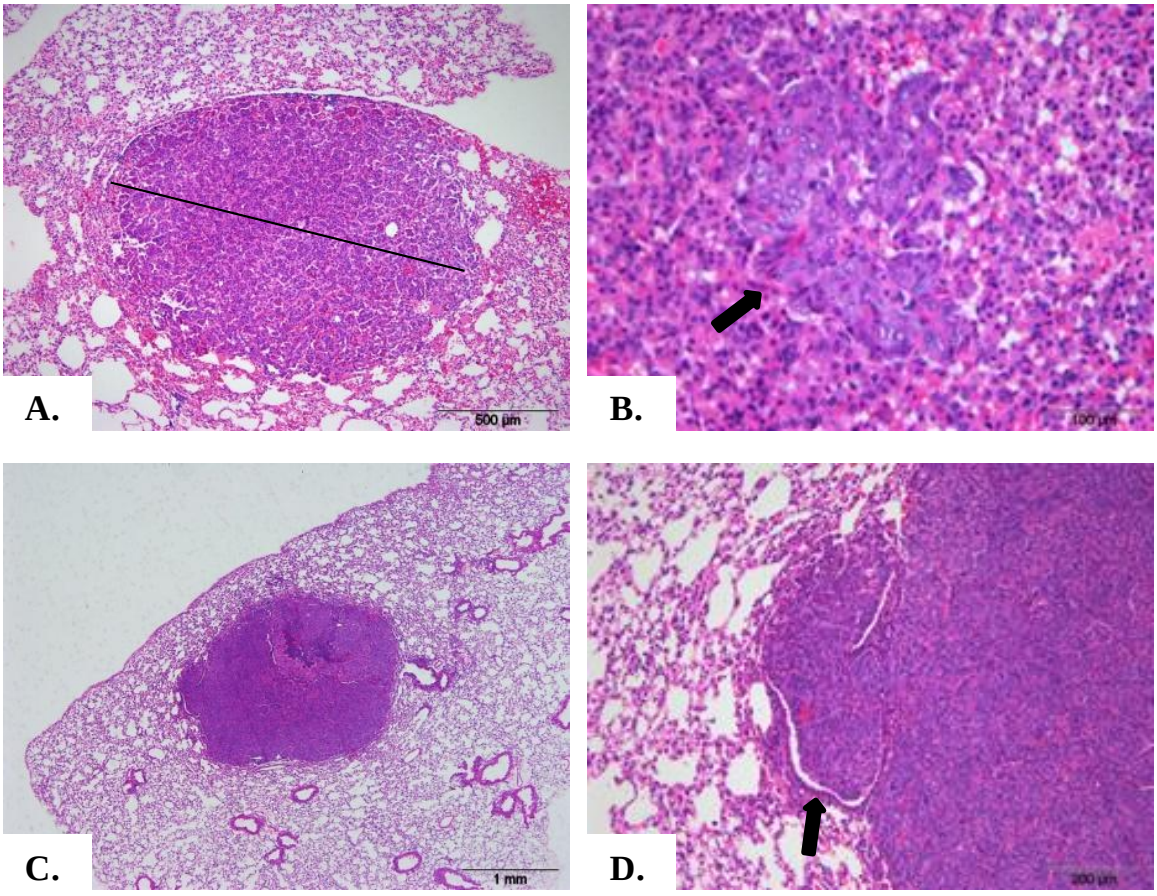

Figure 2.16 Photomicrographs of adenomas and adenocarcinomas in lungs of NNK-treated A/J mice. (A, B) **adenomas** – characterized as well circumscribed areas consisting of cuboidal to columnar cells lining alveoli. The size was usually less than 5 mm in diameter and retained preexisting alveolar structure. The adenoma in this figure had a diameter of 1.5 mm. (B) Adenoma with progression in which a distinct clone of cells (10 or more) appeared with hyperchromatic nuclei and nuclear size greater than those found in cells of the adenoma (closed arrow). (C, D) **adenocarcinomas** – characterized by cytological atypia, increased frequency of mitoses, regional variation in growth pattern, papillary structures, sizes over 5 mm in diameter, invasion of vessels, large airways or pleura, as well as lymphatic and hematogenous metastases. (D) Adenocarcinoma with airway invasion (closed arrow).

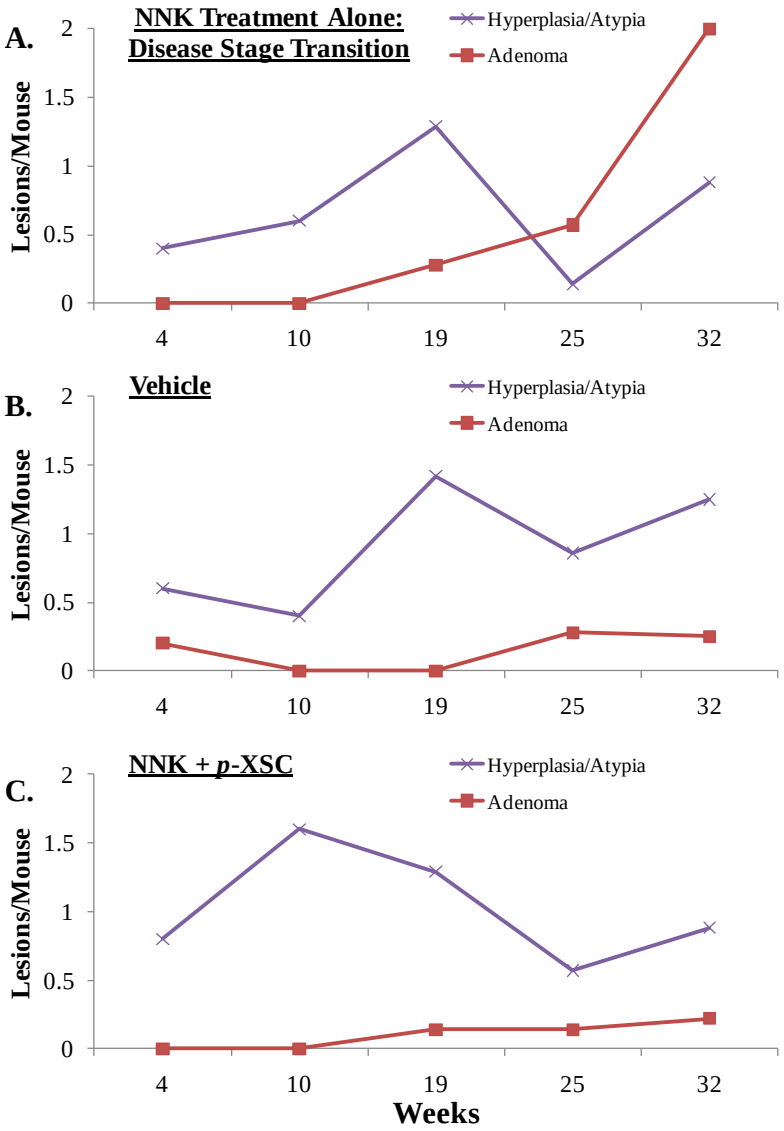

Figure 2.17 NNK-induced pulmonary lesion progressions in A/J mice. The lesion multiplicity data correspond to histological observations from n=5-9 mice. Hyperplasia/atypia are of alveolar epithelial origin, the proposed precursor lesions of adenoma and adenocarcinoma development (41). (A) NNK alone treated mice, (B) Vehicle-treated mice, (C) (NNK + *p*-XSC)-treated mice.

5.2.4 Immunoblot analysis of proteins in the lung during NNK-induced alveolar hyperplasia/atypia and adenoma development

In our initial 2D-DIGE and immunoblot analysis of mice treated with NNK, both lung tissue comprised primarily of adenocarcinomas and isolated adenocarcinomas exhibited down-

regulation of the 14-3-3 protein isoforms ε, θ, and σ, annexin A5 and the lung specific protein CC10 compared to lungs of vehicle-treated mice. Furthermore, *p*-XSC was able to recover the expression of the 14-3-3 protein isoforms (186). Therefore, in a follow-up experiment we next determined the expression of these proteins during early stages of disease progression in the NNK-induced lung tumorigenesis model. Based on our histological analysis of lung tissue, we selected lungs from mice sacrificed 2 weeks after the last dose of NNK (week 10) and 17 weeks after the last dose of NNK (week 25); at week 10, mice treated with NNK alone exhibited an increase in the alveolar hyperplasia/atypia and at week 25, the transition to adenoma development from alveolar hyperplasia/atypia was evident (Figure 2.17A).

In our immunoblot analysis (n=3 mice/group), in lung tissue comprised primarily of alveolar hyperplasia/atypia, mice treated with NNK alone did not show any significant modulation in expression of CC10, 14-3-3 ε, θ, or σ compared to vehicle-treated control mice (Figure 2.18A-D); however, CC10 appeared to be down-regulated and 14-3-3 σ appeared to be up-regulated (Figure 2.18A). In contrast, lung tissue of mice treated with (NNK + *p*-XSC) exhibited significant down-regulation of CC10 compared to both vehicle- and NNK alone treated mice and up-regulation of 14-3-3 σ compared to vehicle-treated mice (Figure 2.18A and D). Annexin A5 expression levels were inconsistent.

In lung tissue comprised primarily of adenomas, NNK treatment alone did not appear to have any effect on the expression of pulmonary CC10, 14-3-3 ε, θ, or σ compared to vehicle-treated control mice (Figure 2.19A-D). CC10 expression appeared to be down-regulated only in the lungs of mice receiving (NNK + *p*-XSC); however, the difference was not statistically significant. In contrast, lungs of mice treated with (NNK + *p*-XSC) exhibited significant up-regulation of the 14-3-3 protein isoforms compared to those treated with NNK alone or vehicle. In addition, CC10 appeared to be down-regulated, but this was not statistically significant.

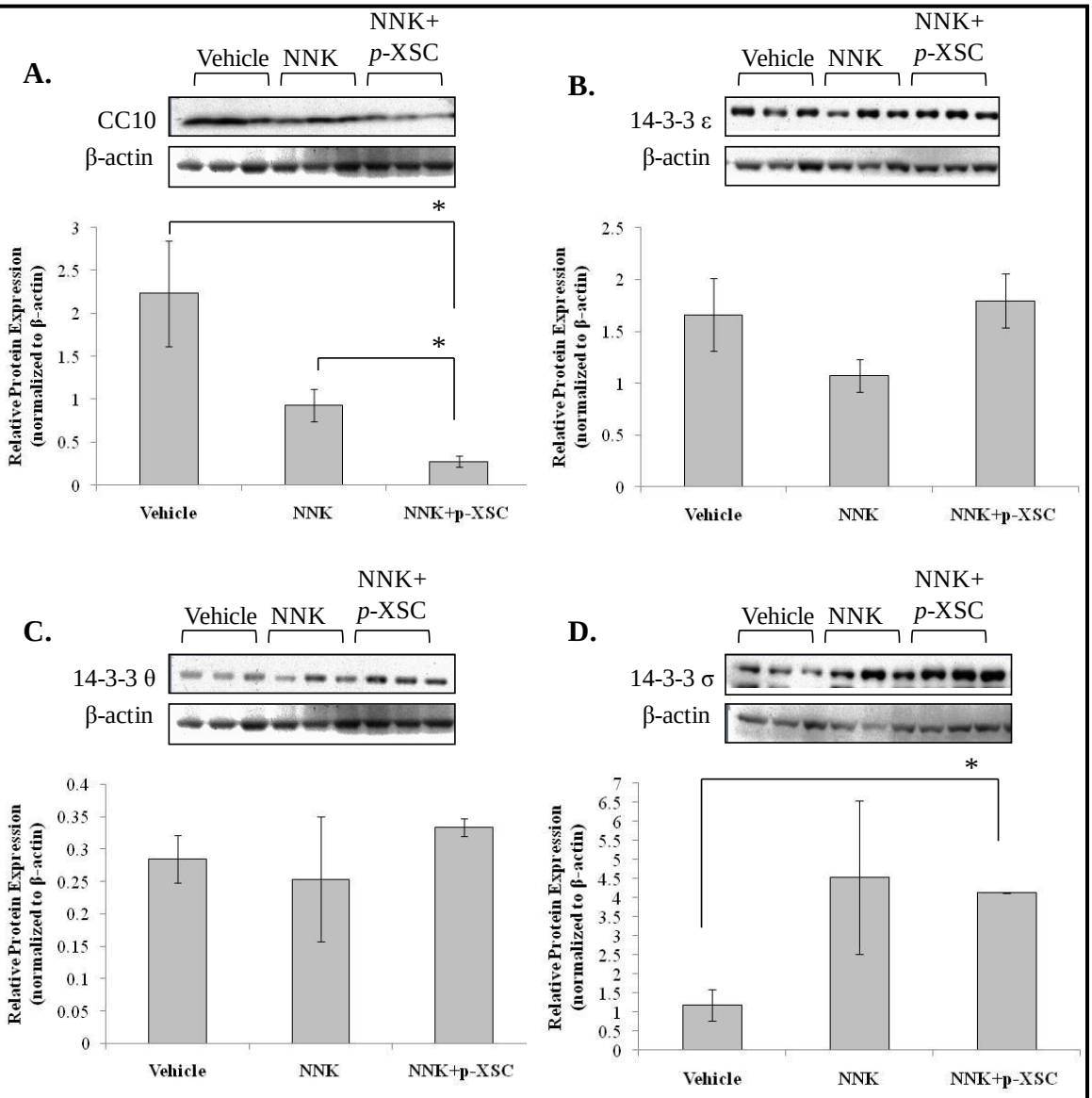

Figure 2.18 Immunoblot analyses of proteins in lung tissue comprised primarily of alveolar hyperplasia/atypia in the A/J mouse. Total lung protein from mice in each treatment group (n=3) were probed with antibodies against (A) CC10 and the 14-3-3 protein isoforms (B) ε, (C) θ, and (D) σ. The average expression of each protein (normalized to β-actin) for each group is presented in the graphs along with ± SE. **p*<0.05 (Students *t* test)

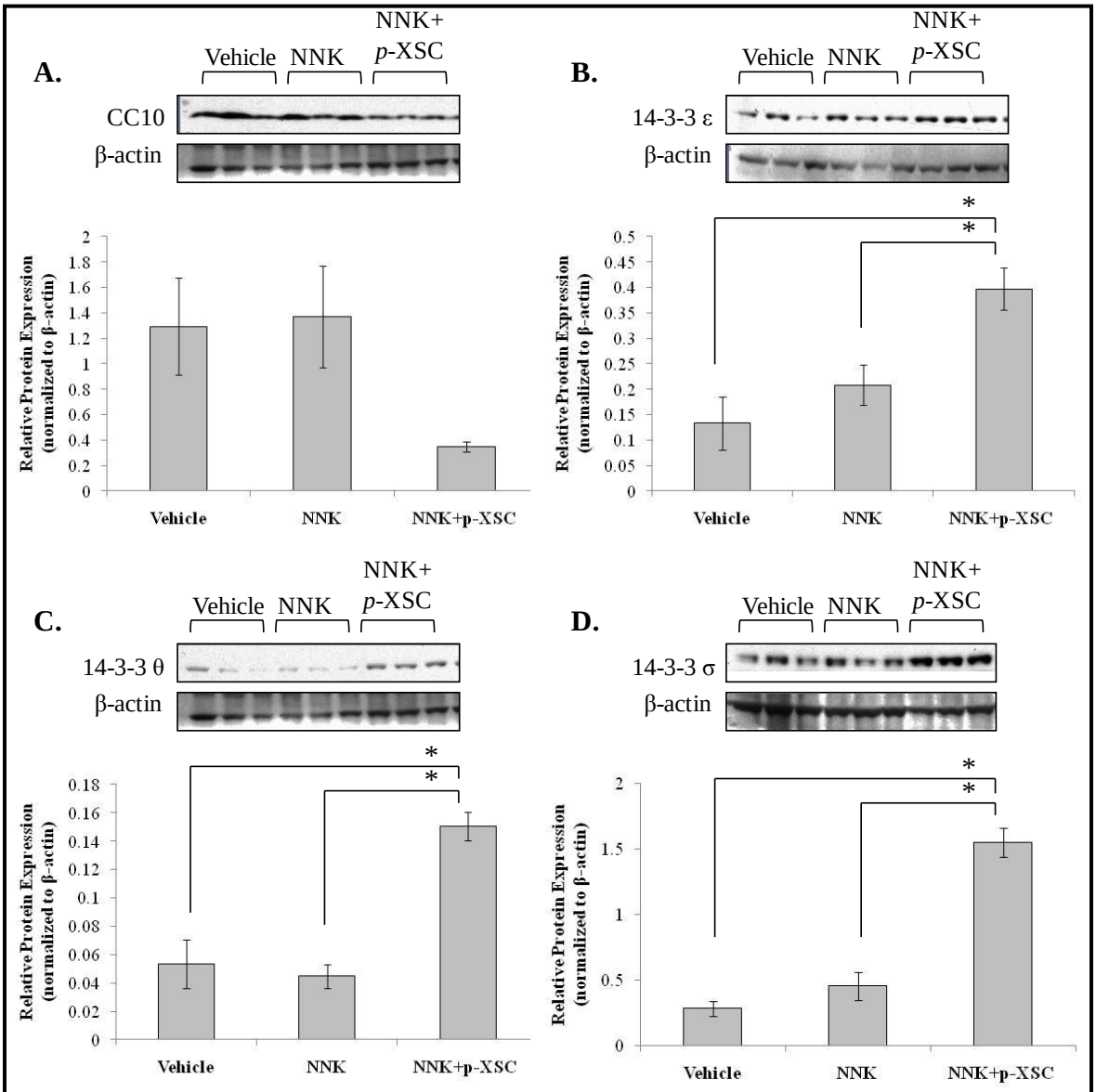

Figure 2.19 Immunoblot analyses of proteins in lung tissue comprised primarily of adenomas in the A/J mouse. Total lung protein from mice in each treatment group (n=3) were probed with antibodies against (A) CC10 and the 14-3-3 protein isoforms (B) ε, (C) θ, and (D) σ. The average expression of each protein (normalized to β-actin) for each group is presented in the graphs along with ± SE. *$p<0.05$ (Students *t* test)

5.2.5 Identification and quantitation of iTRAQ-labeled proteins during NNK-induced disease progression in the A/J mouse lung by MALDI-ToF/ToF MS & MS/MS

To identify additional molecular changes at early histopathological stages of lung tumor development in the NNK-induced lung tumorigenesis A/J mouse model, we performed iTRAQ analysis on lungs from each group collected from week 10 and week 25. The iTRAQ experiment performed on pooled lung tissue collected from mice (n=5 mice/ treatment group) at weeks 10 and 25 led to the identification of 710 proteins with >95% confidence and had a Local FDR estimation of no higher than 5%. The lowest ranking protein in the generated list had a less than 5% chance of being a false positive identification. These proteins were used for expression analysis between experimental groups (Figure 2.20).

To assess proteomic changes, pairwise comparisons between groups was performed by using the areas under the peaks at m/z 113-115 and 117-119 Da, which are the masses of the reporter ions that are derived from the iTRAQ reagents that were attached to peptides, and represent the expression level of proteins. An example of an MS and MS/MS spectrum used in the identification and quantitation of the carbonyl reductase [nicotinamide adenine dinucleotide phosphate, NADPH] 2 is shown in Figure 2.21. The iTRAQ reporter ion peak areas at m/z 113-115 and 117-119 Da were used to measure the relative expression of carbonyl reductase [NADPH] 2 protein in lung tissues from vehicle-, NNK-, and (NNK + *p*-XSC)-treated mice at both sacrifice time points. The identified proteins selected for comparisons were submitted to a filter to further determine which proteins were of significance regarding a relationship to carcinogenesis at the 10 week or 25 week sacrifice time points. The filtering criteria included the following: minimum of two peptides for the calculation of iTRAQ ratios, ratios with EF <2 (StdDev<20%), *p*-values <0.05, and a change beyond 20% (>1.2 or <0.8)

(Figure 2.20); the change beyond 20% has been considered a real change in the A/J mouse lung previously (192,193).

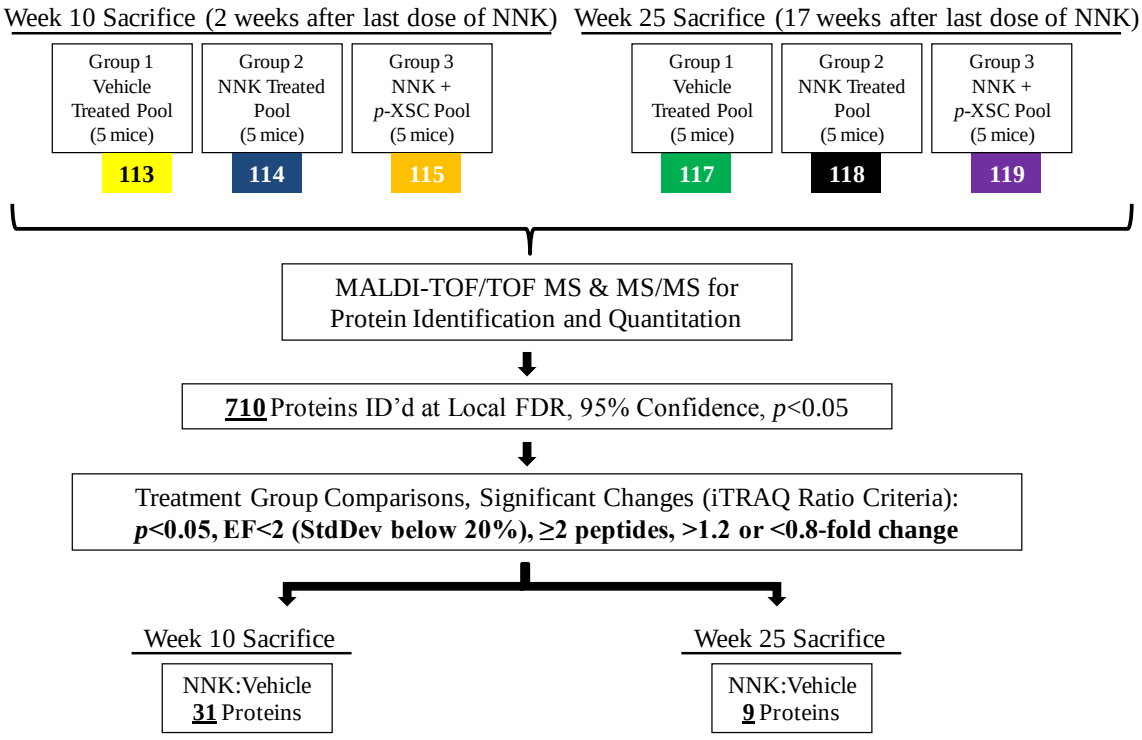

Figure 2.20 8-Plex iTRAQ experimental summary. Total pulmonary proteins were collected from each treatment group at 10 and 25 weeks of the NNK-induced lung tumorigenesis bioassay and were subjected to isobaric tag labeling (m/z 113-115 and 117-119). Proteins were simultaneously identified and quantified by MS. Only proteins identified with high confidence were used for quantitation between groups. At each sacrifice point, a ratio of protein expression between group comparsions for each protein was calculated based on labeled peptide levels for that protein. Significantly modulated proteins (p<0.05) between NNK- and vehicle-treated group comparisons were determined by the expression ratio NNK:Vehicle for both sacrifice time points.

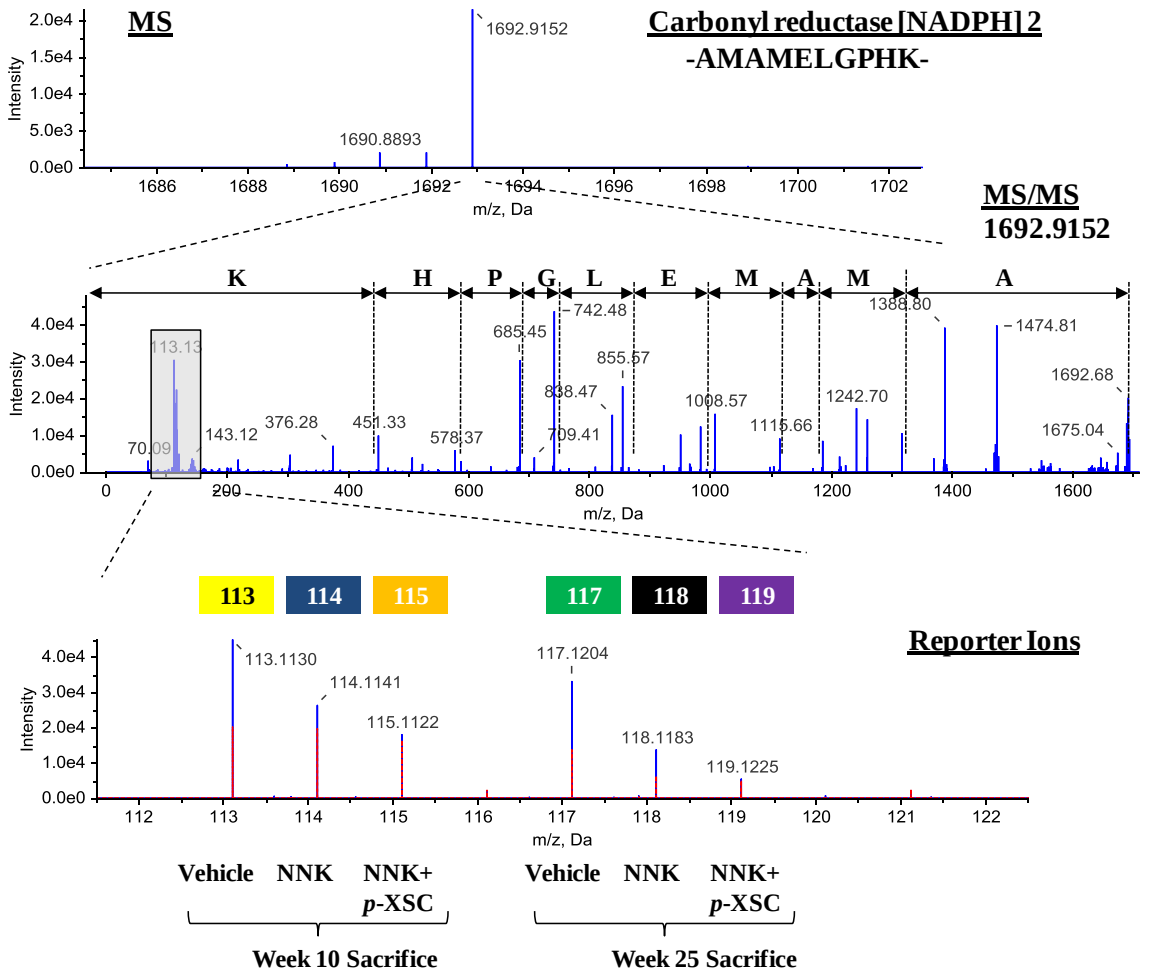

Figure 2.21 Identification of carbonyl reductase [NADPH] 2 from iTRAQ experiment. Representative MALDI TOF/TOF MS (*upper panel*) and tandem MS spectra (*middle panel*) used in the identification of the carbonyl reductase [NADPH] 2 protein. The peptide sequence AMAMELGPHK was unique to the carbonyl reductase [NADPH] 2 protein. Quantification was derived from the intensities of the eight iTRAQ reporter ions (*lower panel*). Reporter ions m/z 113-115 Da correspond to groups sacrificed at week 10 and reporter ions m/z 117-119 Da correspond to groups sacrificed at week 25.

5.2.6 NNK-induced proteomic profile changes detected by iTRAQ in lung tissue comprised primarily of alveolar hyperplasia/atypia and the effect of *p*-XSC

After applying our filtering criteria (Figure 2.20), we found significant changes in the relative expression of 31 proteins in the lung tissue of NNK-treated mice compared to vehicle-treated controls at week 10 during which early development of alveolar hyperplasia/atypia was prominent; of these proteins, 5 were up-regulated and 26 were down-regulated (Table 2.6). Proteins that were up-regulated in the lungs of NNK-treated mice at week 10 were those involved in mitochondrial processes such as electron transport (CYB5B, ATP5B) and carbohydrate metabolism (ACO2), stress-mediated chaperonage (HSP90B1), and cytoskeletol organization (VIM). In contrast, levels of several proteins in the lung were down-regulated in NNK alone treated mice and were involved in a variety of processes; these included, stress-mediated chaperonage (HSPA8), xenobiotic metabolism (FMO1, Cbr2), cholesterol metabolism (SEC14-like 3), protein metabolism (PDIA3, P4HB, CALR, ACE), cell cycle control (Calm1, NCL), immune defense (SELENBP1, LYZ, CES1, MFAP4), intracellular signaling (HMGB1), cell redox homeostasis (PRDX6), and cell adhesion (PECAM1, CD34, CD36) .

At week 10 a majority of the proteins modulated in the lungs of mice that had received NNK were not altered by the dietary administration of the chemopreventive agent *p*-XSC compared to the lungs of vehicle-treated mice; i.e. the same trend of being up- or down-regulated compared to the lungs of vehicle-treated mice, regardless of administration of *p*-XSC, was similar to that of NNK alone treated mice (Table 2.6). These results suggest that the proteomic profile related to NNK treatment to induce alveolar hyperplasia/atypia lesion development was not strongly affected by *p*-XSC.

Table 2.6 Differentially expressed proteins in lung tissue comprised primarily of alveolar hyperplasia/atypia in NNK-induced A/J mice compared to normal lung tissues and the effect of *p*-XSC

				iTRAQ Ratio			
accession*	**identified protein**	**symbol**	**% coverage†**	**NNK:Vehicle (114:113)**	**NNK+*p*-XSC:Vehicle (115:113)**	**NNK+*p*-XSC:NNK (115:114)**	**molecular function‡**
	Up-regulated						
gi|31542438	cytochrome b5 type B (outer mitochondrial membrane)	CYB5B	56.8	**1.28**	1.10	0.86	Oxidoreductase
gi|18079339	aconitase 2, mitochondrial	ACO2	26.8	**1.41**	1.19	0.79	Hydro-Lyase
gi|6755863	heat shock protein 90kDa β (Grp94), member 1	HSP90B1	27.8	**1.66**	1.41	0.80	Chaperone
gi|31980648	ATP synthase, H+ transporting, mitochondrial F1 complex, β polypeptide	ATP5B	37.4	**1.74**	1.42	0.83	Hydrolase
gi|31982755	vimentin	VIM	40.3	**2.29**	1.80	0.76	Cytoskeletol Protein
	Down-regulated						
gi|19526792	CD34 molecule	CD34	11.3	**0.79**	0.94	1.17	Cell Adhesion
gi|31981690	heat shock 70kDa protein 8	HSPA8	58.5	**0.74**	0.26	0.31	Chaperone
gi|71480138	SEC14-like 3 (S. cerevisiae)	SEC14L3	59.9	**0.73**	0.21	0.24	Transporter
gi|74024915	platelet/endothelial cell adhesion molecule	PECAM1	15.4	**0.70**	0.55	0.77	Cell Adhesion
gi|6753890	flavin containing monooxygenase 1	FMO1	25.4	**0.67**	0.59	0.86	Oxidoreductase
gi|227116353	CD36 molecule (thrombospondin receptor)	CD36	28.2	**0.67**	0.35	0.48	Receptor Activity
gi|6754208	high-mobility group box 1	HMGB1	59.5	**0.66**	0.66	1.02	Transcripton Factor
gi|8393866	ornithine aminotransferase	OAT	42.4	**0.65**	**0.58**	0.88	Transaminase
gi|31982186	malate dehydrogenase 2, NAD (mitochondrial)	MDH2	61.5	**0.64**	**0.41**	0.59	Oxidoreductase
gi|61743961	AHNAK nucleoprotein	AHNAK	65.4	**0.63**	**0.34**	0.45	Protein Binding
gi|31981302	annexin A6	ANXA6	58.4	**0.63**	0.19	0.25	Calcium Ion Binding
gi|31543113	lymphocyte cytosolic protein 1 (L-plastin)	LCP1	28.2	**0.63**	**0.42**	0.69	Cytoskeletol Protein
gi|6753244	calmodulin 1	Calm1	74.5	**0.61**	0.53	0.83	Calcium Ion Binding
gi|255003777	glyoxalase domain containing 4	GLOD4	43.3	**0.60**	0.32	0.52	Lyase
gi|21313152	microfibrillar-associated protein 4	MFAP4	15.6	**0.59**	0.30	0.49	Kinase Regulator
gi|112293264	protein disulfide isomerase family A, member 3	PDIA3	57.8	**0.59**	**0.38**	0.61	Isomerase
gi|6680027	glutamate dehydrogenase 1	GLUD1	43.2	**0.56**	0.56	0.99	Oxidoreductase
gi|84875537	nucleolin	NCL	18.3	**0.56**	0.46	0.79	DNA/RNA Binding
gi|6680836	calreticulin	CALR	50.7	**0.55**	0.14	0.23	Calcium Ion Binding
gi|117553604	carboxylesterase 1	CES1	38.8	**0.50**	0.20	**0.38**	Hydrolase
gi|42415475	prolyl 4-hydroxylase, β polypeptide	P4HB	58.0	**0.50**	0.29	0.54	Isomerase
gi|22164798	selenium binding protein 1	SELENBP1	70.6	**0.50**	0.22	0.36	Immune Defense
gi|46559389	angiotensin I converting enzyme 1	ACE	18.8	**0.49**	0.08	0.14	Peptidase
gi|6671688	carbonyl reductase 2	Cbr2	87.7	**0.42**	0.18	**0.33**	Oxidoreductase
gi|8393739	lysozyme	LYZ	56.1	**0.41**	0.61	1.50	Hydrolase
gi|6671549	peroxiredoxin 6	PRDX6	90.6	**0.26**	0.30	0.78	Oxidoreductase

*NCBI gi number (genInfo identifier); †Percent of residues in each protein sequence that have been identified; ‡PANTHER ontology designation;
Ratios in **bold** are statistically significant ($p<0.05$); Ratios in red were statistically significant, but had an EF>2.

5.2.7 NNK-induced proteomic profile changes detected by iTRAQ in lung tissue comprised primarily of adenomas and the effect of *p*-XSC

After using the same filtering criteria as week 10 group comparisons (Figure 2.20), 9 proteins were found to be significantly modulated in the lungs of NNK-treated mice compared to vehicle-treated mice at week 25 during which adenoma development was prominent; of these proteins, 3 were up-regulated and 6 were down-regulated (Table 2.7). Similar to week 10, the stress-mediated chaperone protein HSP90B1 was up-regulated, whereas the transmembrane cell adhesion CD36 protein and the immune defense protein SELENPB1 were down-regulated. Conversely, the transcriptional factor HMGB1 protein, which was down-regulated at week 10, was found to be up-regulated in the lungs of NNK-treated mice at week 25. Furthermore, the ITGB1 protein, which is involved in signal transduction and cell adhesion, was up-regulated in the lungs of NNK-treated mice at week 25 and proteins involved in pH regulation (CA1), lipid, fatty acid, and steroid metabolism (ANXA5), transcriptional regulation (PTMA), and cellular structure (TLN1) were down-regulated.

At week 25, lungs from NNK-treated mice receiving dietary administration of *p*-XSC had expression levels of HSP90B1 and CA1 similar to those observed in lungs of vehicle-treated mice while HMGB1 was down-regulated compared to NNK-treated mice (Table 2.7).

6. Discussion

Cancer development is a multi-step process characterized by abnormal protein expression ultimately leading to phenotypic changes (84). These changes are caused by a large number of proteins rather than a single protein change alone. Therefore, it is of paramount importance to understand the proteome as a whole.

Table 2.7 Differentially expressed proteins in lung tissue comprised primarily of adenomas in NNK-induced A/J mice compared to normal lung tissues and the effect of *p*-XSC

				iTRAQ Ratio			
accession*	**identified protein**	**symbol**	**% coverage†**	**NNK:Vehicle (118:117)**	**NNK+*p*-XSC:Vehicle (119:117)**	**NNK+*p*-XSC:NNK (119:118)**	**molecular function‡**
	Up-regulated						
gi|45504394	integrin, β 1	ITGB1	22.7	**1.32**	0.37	0.29	Receptor Activity
gi|6755863	heat shock protein 90kDa β (Grp94), member 1	HSP90B1	27.8	**1.41**	1.04	0.73	Chaperone
gi|6754208	high-mobility group box 1	HMGB1	59.5	**2.00**	0.08	**0.05**	Transcription Factor
	Down-regulated						
gi|145301561	carbonic anhydrase I	CA1	13.4	**0.75**	1.11	**1.46**	Hydro-Lyase
gi|6753060	annexin A5	ANXA5	76.2	**0.73**	0.32	0.47	Calcium Ion Binding
gi|7110705	prothymosin, α	PTMA	49.5	**0.71**	0.65	0.90	Transcription Regulator
gi|227116353	CD36 molecule (thrombospondin receptor)	CD36	28.2	**0.68**	0.84	1.26	Receptor Activity
gi|227116327	talin 1	TLN1	36.6	**0.53**	**0.38**	0.75	Cytoskeletol Protein
gi|22164798	selenium binding protein 1	SELENBP1	70.6	**0.52**	**0.32**	0.65	Immune Defense

*NCBI gi number (genInfo identifier); †Percent of residues in each protein sequence that have been identified; ‡PANTHER ontology designation;
Ratios in **bold** are statistically significant ($p<0.05$); Ratios in red were statistically significant, but had an EF>2.

In this chapter our goal was to identify important molecular changes at the protein level in the lung to better understand the mechanisms that could account for tobacco carcinogen (NNK)-induced adenocarcinoma development; such proteins may serve as biomarkers to help in the early detection of the disease and to monitor efficacy of chemopreventive and therapeutic agents. We have utilized the well-established NNK-induced lung tumorigenesis model in A/J mice to identify changes in protein expression in the lung during cancer development (33). Animal models provide an opportunity to analyze critical molecular changes in various organs without the effect of experimental artifacts related to genetic background and environment that are a concern when working with human samples (84). In addition, as in the case of lung cancer, many animal models closely follow the histological and molecular changes associated with human disease pathology (41).

Our study began by looking at protein expression changes in mouse lung tissue at end-stage tumor development during which adenocarcinomas are primarily the histological type classified. To globally analyze the plethora of proteins that may contribute to lung tumor development we used the gel-based proteomic approach, 2D-DIGE. Using this approach, we analyzed over 700 protein spots for differential protein expression among three experimental groups: vehicle-treated control, NNK-treated, and (NNK + *p*-XSC)-treated groups. We next filtered for only those significant ($p<0.05$), differentially expressed protein spots (average ratio or fold-change >1.5 or <-1.5) between group comparisons and identified 191 proteins spots of interest. A large number of the 191 proteins (97%) were down-regulated in the lungs of mice treated with NNK compared to vehicle-treated controls. However, after the dietary administration of *p*-XSC in NNK-treated mice, a majority of these proteins (65%) were restored to similar or even higher expression levels compared to those observed in the vehicle-treated control group. MS analysis of select, excised, protein spots identified 14 proteins (Tables 2.4 and 2.5) involved in a variety of biological functions including metabolic, signal transduction, cell

cycle regulation, muscle contraction, protein trafficking, anti-inflammation, intermediate filament-based processes, ATP biosynthesis, and serine protease inhibition activities. Furthermore, pathway analysis indicated that 11 of the proteins are involved in a cancer-associated network based on current literature (Ingenuity Systems Knowledge Base).

A group of proteins consistently showing down-regulation in expression in lung tissue comprised primarily of adenocarcinomas of mice treated with NNK were the 14-3-3 protein isoforms ε, ζ, and θ. Although we did not identify the 14-3-3 σ isoform in our 2D-DIGE study, we were able to detect its expression in our immunoblot study. We determined that 14-3-3 σ was significantly up-regulated in (NNK + *p*-XSC) treated lungs compared to both vehicle-treated control and NNK-treated groups. There are three other known 14-3-3 isoforms, including β, γ, and η, (194) but their expression levels were not examined in this study. The 14-3-3 proteins are ubiquitously expressed regulatory proteins that primarily function by binding to protein ligands and as a result, interfere with or enhance the ligand's normal activities. Some of the proteins to which 14-3-3 proteins bind play various roles in apoptosis, mitogenic signal transduction, DNA replication, and cell-cycle control (194). Interestingly, many of the ligands that 14-3-3 proteins bind to are proto-oncogene or oncogene products (194) suggesting a potential role in carcinogenesis. However, previous studies have provided inconsistent views as both tumor promotion and tumor suppression activities have been attributed to the 14-3-3 proteins (195-197). It appears that the lack of consistency may be dependent on the specific 14-3-3 isoform, the type of tissue examined, and the experimental approach used (187). In lung cancer, 14-3-3 protein isoforms have been found in all major histological types, but at different expression levels (187,188,198). In our study, we identified 14-3-3 protein isoforms ε, ζ, θ, and σ in all lungs of the three experimental groups [vehicle-treated control, NNK, and (NNK + *p*-XSC)-treated groups]. Our 2D-DIGE results, also confirmed by our immunoblot analysis, indicated that these isoforms were down-regulated in lung adenocarcinomas of mice treated with NNK, but dietary *p*-

XSC was capable of providing the necessary environment to restore expression to basal levels noted in the vehicle-treated (normal) control lungs. Of particular significance, the 14-3-3 proteins have been shown to play a role in inducing G2 arrest under DNA damaging scenarios through Cdc2 inactivation (194,199). In our case, the NNK-induced tumor environment may be favorable with a reduced level of these particular isoforms to avoid cell cycle arrest. Reports have also shown that over-expression of 14-3-3 σ can lead to tumor growth suppression in breast cancer (200-202). In the present study, lungs collected from A/J mice that had been treated with (NNK + *p*-XSC) exhibited a significant increase in the levels of the 14-3-3 σ protein. This suggests that over-expression of this protein may provide protection against the development of lung tumorigenesis.

Annexin A5 (ANXA5) is a phospholipid binding protein that efficiently binds to phosphatidylserine. During early events of apoptosis, phosphatidylserine, which normally resides on the inner leaflet of the plasma membrane, becomes externalized to the outer leaflet of the plasma membrane where ANXA5 can bind to it. By binding to phosphatidylserine on the outer leaflet of the plasma membrane, ANXA5 essentially marks the cell for safe removal from the system by macrophages (203). Interestingly, the use of ANXA5 as a clinical tool for visualization of cell death has been suggested to be important in monitoring pathologies such as atherosclerosis, myocardial infarction, and cancer (204). In our study we observed a decrease in ANXA5 expression in lung adenocarcinomas of mice treated with NNK compared to the vehicle-treated control group. In addition, we noted that *p*-XSC administration to mice treated simultaneously with NNK increased ANXA5 expression in lungs. These results are in line with our previous report demonstrating that *p*-XSC is a powerful inducer of apoptosis (126) .

CC10 is a homodimeric protein predominantly secreted in the lungs and comprises approximately 7% of the total protein in bronchoalveolar lavage fluid (BALF). CC10 has been assigned a multitude of protective roles in the lung, including anti-inflammatory, anti-oxidant,

and immunomodulatory functions. Exposure to tobacco smoke and lung carcinogens have been associated with reduced levels of CC10 and numerous studies have indicated that decreased levels of CC10 exist in both BALF and serum in smokers and lung cancer patients compared to healthy nonsmokers (205). Chen et al. (206) showed that the levels of CC10 in plasma and BALF could be restored following smoking cessation, suggesting that some of the damage caused by tobacco smoke could be repaired. Furthermore, it has been shown that high levels of CC10 are associated with improvement of bronchial dysplasia and sputum cytometric assessments in individuals at high risk for lung cancer (207). In addition, CC10 has also been implicated as an inhibitor of lung carcinogenesis (205,208). Our results agree with those found in other laboratories regarding CC10 down-regulation in rodent lungs following NNK treatment (205), as well as NNK in combination with another lung carcinogen (benzo[a]pyrene) (193). However, CC10 levels were unchanged by dietary *p*-XSC (this study) or by other putative chemopreventive, such as N-acetyl-*S*-(*N*-2-phenethylthiocarbamoyl)-L-cysteine and the isothiocyanates, *myo*-inositol and indole-3-carbinol (193). We also detected three isoforms of CC10 in the A/J mouse lung. Previous studies have indicated the presence of three to four isoforms for CC10 in mammals (209,210), but the role of each isoform in carcinogenesis is not entirely understood. All three isoforms were down-regulated in the NNK-treated group compared to the vehicle-treated control group. Although *p*-XSC was unable to restore CC10 expression, CC10 still warrants further investigation as a potential biomarker because it is primarily a lung-specific protein and can be detected in surrogate tissue, such as BALF and serum (211).

Apparently conflicting observations have been reported concerning AAT and lung cancer. Some groups have shown a positive correlation between high levels of AAT in plasma and lung cancer risk (212), while others have shown that a genetic deficiency in AAT is associated with an increased risk for development of lung cancer (213). Our results showed that AAT was significantly increased in the lung in (NNK + *p*-XSC)-treated mice compared to

vehicle-treated control group, but was not significantly increased when compared to the NNK-treated alone group. AAT is a serine-type endopeptidase inhibitor responsible for neutralizing the effects of proteases in a number of organ systems, including the lung, protecting them from damage. Its primary protease counterpart in the lower respiratory tract is neutrophil elastase (214). The balance between these molecules has been suggested to be critical in facilitating the cancer causing effects of cigarette smoke (215). Therefore the increased expression of AAT in the presence of *p*-XSC might be critical in providing the necessary protection to the lung from carcinogens in cigarette smoke, such as NNK.

Vimentin and tubulin-α-1 are both components of the cytoskeleton and play various roles in intermediate filament based processes and intracellular protein trafficking, respectively. Previous reports have indicated that aberrant expression of vimentin is consistent with increased motility, invasive behavior, and poor prognosis in tumors and transformed cell lines (216-218). Tubulin-α-1 was previously found to be informative in characterizing different histological types of lung cancer (219). In our study, we found both vimentin and tubulin-α-1 to be increased in the lungs of mice treated with (NNK + *p*-XSC) compared to both the vehicle-treated group and the NNK-treated group lungs. The increased expression exhibited in the lungs of mice treated with (NNK + *p*-XSC), for both of these proteins, may further define the protective property elicited by this chemopreventive agent. In addition, since our model addresses adenocarcinoma, restoration of tubulin-α-1 may be inhibitory to the development of this histological type of lung cancer.

Dihydropyrimidinase-like 2 is involved in nucleoside, nucleotide, and nucleic acid metabolism by hydrolytic catalysis activity. It is typically studied in the brain as its decreased expression has been observed in Alzheimer's disease, Down Syndrome and Schizophrenia (220). Although its modulation in lung cancer has been identified in other proteomic studies (193), the role of dihydropyrimidinase-like 2 in lung cancer remains questionable.

Like many studies, including our own (186), most biomarker development approaches for lung cancer have been pursued at end-stage points (e.g. the formation of adenocarcinomas) and as as a result may be a consequence of tumor development rather than a cause of cancer induction. Therefore, we next directed our attention towards identifying whether the proteins we identified in lung tissue comprised primarily of adenocarcinomas in the A/J mouse as being down-regulated (i.e. CC10, ANXA5, 14-3-3 isoforms ε, θ, and σ) were also differentially expressed at earlier stages of disease development (hyperplasia/atypia and adenoma). Ultimately, changes in protein profiles during earlier stages of disease development would provide more reliable biomarkers for early detection as these proteins may be directly involved in the lung carcinogenic process.

Based on literature pertaining to lung tumor development following NNK treatment (33,166,167), we initiated an NNK-induced lung tumorigenesis model in the A/J mouse and sacrificed mice at specific time points during the progress of the bioassay to obtain lung tissues at earlier stages of lung tumor development. At each sacrifice time point we examined and confirmed the histological state of the lungs in mice for each group. After 2 and 17 weeks following the last dose of NNK administration we observed alveolar hyperplasia/atypia and adenoma development, respectively, in the lungs of the mice; such lesions are proposed precursors of adenocarcinoma development (41). We also included dietary administration of *p*-XSC to NNK-treated mice to determine its ability to modulate protein expression at earlier stages of disease development; consistent with previous studies, *p*-XSC was effective in reducing lung tumor multiplicity in this model (139,141).

Immunoblot analyses of proteins present in lungs taken from mice at the NNK-induced alveolar hyperplasia/atypia and adenoma stages indicated that the expression of CC10 and the 14-3-3 protein isoforms ε, θ, and σ was not significantly modulated compared to lungs of vehicle-treated mice; however, there did appear to be a reduction of CC10 expression during alveolar hyperplasia/atypia development, but this was not significant (Table 2.8). This suggests that at

earlier stages of disease development, at least in whole lung homogenates, it is unlikely that CC10 or the 14-3-3 protein isoforms analyzed in the current study will be useful as biomarkers for NNK-induced lung carcinogenesis. However, it may be necessary to detect the expression of these proteins in the lesions alone, without the presence of normal tissue. Normal tissue may be skewing the levels being modulated in the lesions. More specifically, CC10 has been shown previously to be down-regulated along the epithelium of conducting airways of the lungs of animals treated with NNK prior to atypia and tumor formation (205). In addition, it may be beneficial to identify more proteins in the 2D-DIGE study in terms of finding a protein that may serve as a cell marker for the epithelium that could serve as a denominator/correction factor. In contrast, *p*-XSC had a significant effect on the proteins analyzed by immunoblot in whole tissue comprised primarily of hyperplasia/atypia or adenomas. During alveolar hyperplasia/atypia development, the lungs of (NNK + *p*-XSC)-treated mice showed significant down-regulation of CC10 and up-regulation of 14-3-3 σ compared to lungs of NNK treated mice. Furthermore, during adenoma development, *p*-XSC also significantly up-regulated 14-3-3 ε and θ compared to the lungs of NNK-treated mice. The up-regulation of the 14-3-3 protein isoforms may be important to the chemopreventive activity elicited by *p*-XSC, and more so during stage progression from adenoma to adenocarcinoma. The inability of *p*-XSC to enhance expression of CC10 is unfortunate considering its protective role in the lung; however future studies should be pursued to identify agents that can positively influence its expression. In summary, the results from our study suggest that in whole lung tissues primarily classified as hyperplasia/atypia and adenoma, CC10 and the 14-3-3 proteins isoforms ε, θ, and σ were not altered by NNK; these results differ from those obtained following the analysis of lung adenocarcinoma (Table 2.8). However, the 14-3-3 protein isoforms ε, θ, and σ were up-regulated by *p*-XSC, which is consistent with our observations in adenocarcinomas (Table 2.8). Therefore, these proteins may be important to monitor response to chemoprevention treatment.

Table 2.8 Summary of candidate protein biomarkers identified by immunoblot analysis in lung tissue of A/J mice during different stages of NNK-induced lung adenocarcinoma development and the effect of *p*-XSC

group	lung tissue comprised primarily of hyperplasia/atypia	lung tissue comprised primarily of adenoma	lung tissue comprised primarily of adenocarcinoma
NNK vs Vehicle	14-3-3 ε → 14-3-3 θ → 14-3-3 σ → CC10 ↓*	14-3-3 ε → 14-3-3 θ → 14-3-3 σ → CC10 →	14-3-3 ε ↓ 14-3-3 θ ↓ 14-3-3 σ ↓ CC10 ↓
NNK + *p*-XSC vs NNK	14-3-3 ε → 14-3-3 θ → 14-3-3 σ → CC10 ↓	14-3-3 ε ↑ 14-3-3 θ ↑ 14-3-3 σ ↑ CC10 ↓*	14-3-3 ε ↑ 14-3-3 θ ↑ 14-3-3 σ ↑ CC10 →

→, no change; ↓, decreased; ↑, increased; *, trend is evident, but not significant

In an effort to identify additional candidate protein biomarkers we analyzed lung tissue samples collected during alveolar hyperplasia/atypia and adenoma development using the MS-based proteomic approach, iTRAQ. With this MS-based approach over 700 lung proteins, similar to the number of protein spots identified with 2D-DIGE, were simultaneously identified and quantitated for each treatment group. Because each treatment group was labeled with a different iTRAQ tag, group comparisons were possible and were provided as expression ratios. At each stage of lung tumorigenesis development, we identified a profile of proteins which were significantly ($p<0.05$) and differentially expressed (changes beyond 20%, >1.2 or <0.8) and corresponded to changes induced by NNK alone or in combination with *p*-XSC; changes tabulated in iTRAQ experiments beyond 20% have been considered a real change in the A/J mouse lung (192,193). As indicated in Tables 2.6 and 2.7 many proteins were identified as differentially expressed at earlier stages of NNK-induced lung tumorigenesis development with a vast array of important molecular and biological functions including electron transport, carbohydrate, protein, and cholesterol metabolism, stress-mediated chaperonage, xenobiotic metabolism, cell cycle control, immune defense, intracellular signaling, cell redox homeostasis, cell adhesion, pH regulation, transcriptional regulation, and cellular structure. In general, it

appears that *p*-XSC had little effect on the profile of proteins that showed significant modulation in the lungs of NNK treated mice compared to vehicle-treated mice. However, further studies with the iTRAQ data will address the extent of the effect of dietary *p*-XSC administration in comparison to NNK-treated mice to identify proteins that may be signature to the protective effect of *p*-XSC.

The iTRAQ analysis provided many proteins to evaluate regarding molecular functions related to lung carcinogenesis and as candidate biomarkers to monitor disease progression. We identified the heat shock protein HSP90B1 which was up-regulated during both alveolar hyperplasia/atypia development and adenoma development, while CD36 and SELENBP1 were down-regulated during both stages. In addition the xenobiotic metabolizer Cbr2 and transcription factor HMGB1 were down-regulated during alveolar hyperplasia/atypia development and unaffected or up-regulated, respectively, during adenoma development. Such proteins may be candidate lung carcinogenesis progression biomarkers. To limit the scope of this thesis just two proteins with strong relationships to lung cancer, HMGB1 and Cbr2, are discussed. Future studies will be performed to determine the relationship of the other proteins identified.

Carbonyl reductase 2 (Cbr2) is in the class of oxidoreductase proteins that are part of the family of short-chain dehydrogenaseses/reductases that are abundant in several tissues including the liver and lung (221). They are found in the cytoplasm and mitochondria and utilize NADPH to reduce aldehyde and ketone groups of many endogenous and exogenous xenobiotic carbonyl compounds and can provide protection against ROS (221). For example carbonyl reductases can reduce and consequently detoxify reactive aldehydes such as 4-oxo-2-nonenal generated during lipid peroxidation (222). Carbonyl reductases have been suggested to play an important role in tumor development. At mRNA and protein levels, Cbr was found to be down-regulated in mouse lung adenocarcinomas compared to adjacent normal tissue (223,224). Furthermore, low levels of Cbr in mouse lung adenocarcinoma cell lines have higher metastatic potential than cells with

higher levels of Cbr (225) and low levels of Cbr have been correlated with a poor prognosis in human NSCLC (226). In our iTRAQ experiment, we found Cbr2 to be significantly down-regulated in the lungs of mice treated with NNK and comprised primarily of alveolar hyperplasia/atypia. In contrast in mice treated with NNK, the lungs comprised primarily of adenomas exhibited no change in Cbr2 levels compared to the lungs of vehicle-treated mice. This suggests that loss of Cbr2 expression, which provides protection to the lung from tissue damage, occurs early in the lung carcinogenic process, and may be a supporting factor in NNK-induced neoplastic cell development.

High-mobility group box 1 (HMGB1) is a highly conserved nuclear protein that binds to DNA to promote access to transcriptional protein assemblies on specific DNA targets to regulate gene expression (227). HMBG1 can also be secreted from cells and through interaction with the receptor for advanced glycation endproducts (RAGE) activate the NF-kB pathway to promote inflammation (228). The HMGB1-RAGE interaction has also been associated with cancer cell proliferation, invasion, and migration (229,230). Consequently, many cancers have been found to overexpress HMGB1, including breast (231) and colon (232). In contrast, low levels of HMGB1 in advanced stages of NSCLC have been associated with poor therapeutic outcome during chemotherapy and radiotherapy (233). We found HMGB1 to be down-regulated in the lung during alveolar hyperplasia/atypia development in NNK-treated mice followed by an up-regulation during adenoma development compared to the lungs of vehicle-treated mice. In addition, we also identified RAGE to be significantly up-regulated during adenoma development with a 1.16 fold-change compared to vehicle-treated mice. In the lungs of mice treated with (NNK + *p*-XSC) HMGB1 levels were similar to those of NNK-treated mice during alveolar hyperplasia/atypia development. However, during adenoma development HMGB1 levels were lower in (NNK + *p*-XSC)-treated mice compared to both groups. This suggests that during adenoma development, the protective effect of *p*-XSC may be elicited by modulation of HMGB1.

Certain proteins identified in the lung in our 2D-DIGE study were also identified using iTRAQ. Vimentin was significantly up-regulated during NNK-induced alveolar hyperplasia/atypia development, followed by a down-regulation in lungs during adenoma development (0.22 fold-change; however, EF>2). We observed vimentin to be up-regulated in lung tissue comprised primarily of adenocarcinomas in (NNK + *p*-XSC)-treated mice, suggesting that this structural protein is lost during adenoma development, but can be recovered by *p*-XSC during adenocarcinoma development. The apoptotic marker ANXA5, which was down-regulated in NNK-induced lung adenocarcinomas, was also significantly down-regulated in the lungs of NNK-induced alveolar hyperplasia/atypia (0.82-fold; significant, but <20% change) and adenoma development and *p*-XSC appeared to have no effect at either time stage. These results support the hypopthesis that throughout the stages of cancer development avoidance of cellular apoptosis is critical for cancer cell survival (83). Although, *p*-XSC was unable to increase the expression of ANXA5 at the stages of alveolar hyperplasia/atypia or adenoma development, *p*-XSC was able to demonstrate its apoptotic effect at the stage of adenocarcinoma development.

In terms of biomarkers, it is apparent that a panel of proteins will be the most informative, as no single marker has proven to be sensitive and specific enough for lung cancer. Therefore, our study provides a significant step towards utilizing a well-defined animal model to identify potentially biologically relevant lung cancer biomarkers for a variety of purposes including early detection and chemopreventive/therapeutic efficacy. By utilizing proteomic approaches we were able to view the modulation of expression of hundreds of proteins during the various stages of lung tumorigenesis. As is the case with many of the proteomic methodologies currently in use, there are certain limitations to this study. First, we identified roughly 700 proteins under our experimental conditions, which represent a small fraction of the protein-encoding transcripts expected in the mouse genome (~20,000) (234). Secondly, some of the proteins we identified in this study are not lung-specific. Therefore, it will be necessary to further

delineate which proteins are both primarily important to understanding the cellular state of lung tissue and provide a molecular profile to carcinogenesis-related changes. Nonetheless, these findings provide a pivotal step towards understanding the changes taking place at the proteomic level in the target tissue cellular environment that plays an important role in cancer development (235). Some of the proteins identified in this study have been previously implicated in lung carcinogenesis supporting their potential usefulness as promising biomarkers to monitor lung cancer progression. Future studies in the NNK-A/J mouse model will need to be aimed towards analyzing these proteins in surrogate tissue such as BALF and plasma and at different stages of disease (hyperplasia/atypia, adenoma, and adenocarcinoma). If these proteins are found in surrogate tissue they could prove useful for the early detection of lung adenocarcinoma and in clinical chemoprevention trials. Therefore, to extend our research to a clinical setting, studies described in Chapter 3 were aimed toward determining the impact of cigarette smoking on plasma proteins in humans.

Chapter 3

The Effect of Cigarette Smoking on the Human Plasma Proteome: A Clinical Pilot Study

1. Objectives

Cigarette smoking is a primary risk factor for many diseases, and more so in the development of respiratory diseases such as chronic obstructive pulmonary disease (COPD) and lung cancer. The damage caused by chronic cigarette smoking and its harmful constituents, including NNK as discussed in chapters 1 and 2, can lead to a variety of molecular alterations disrupting normal tissue physiology, and ultimately lead to disease development. However, to view these changes at the target tissue level is highly invasive, especially in healthy asymptomatic subjects. In addition, no current imaging technologies, including X-ray and CT, are sensitive enough to detect early damage that may be of potential significance. Detection of molecular biomarkers in biological fluids such as blood plasma, however, provides an alternative and non-invasive approach. Plasma contains a variety of molecular entities such as proteins that are present at varying levels depending on current health conditions and thus, are routinely used in hospitals for diagnostic purposes. Given the harmful effects of cigarette smoking, we hypothesized that identification of protein expression profile changes in blood plasma in individuals at high risk (i.e. smokers and former smokers) will assist in early detection as well as in optimizing future preventive (e.g. chemoprevention) and treatment strategies. Therefore, similar to our approach in preclinical settings (Chapter 2), we utilized the iTRAQ proteomic approach to identify differentially expressed proteins in blood plasma between individuals that are chronic smokers and individuals that do not smoke. These proteins may serve as candidate

biomarkers in combination with current screening technologies to monitor damage induced by cigarette smoking leading to disease development.

2. Background

2.1 Cigarette smoking revisited

Cigarette smoking is a major public health concern worldwide and is responsible for 5 million deaths each year (5,236). Currently, in the United States there are approximately 46 million adult smokers (20) and efforts to reduce the prevalence of smoking among adults has been one of the major goals targeted in national health objectives (20). Although the number of adult, as well as adolescent, cigarette smokers in the U.S. has declined substantially in recent years, the rate of decline has begun to slow recently (20). In general, the vast majority of smokers desire to quit, however, less than 5% are successful using current modalities, which include nicotine replacement therapy and counseling (13,21).

Cigarette smokers are at a very high risk for the development of numerous respiratory diseases, including lung cancer and COPD, as well as coronary disease and cerebrovascular disease; cigarette smoking accounts for 87% of lung cancer deaths (5). The harmful compounds found in cigarette smoke constitute the primary reason smokers are at such a high risk. Cigarette smoke contains over 4,000 compounds (cf Chapter 1), some of which are toxic and carcinogenic, including PAHs, TSNAs, aromatic amines, aldehydes, phenols, and volatile hydrocarbons (34). The effects of these compounds are systemic and can be acute or chronic dependent on the extent of damage and an individual's inherent repair capacity (237,238). Furthermore, the degree of damage caused by cigarette smoking is best represented in former smokers who are still at an elevated risk for lung cancer development for several years following cessation (10).

The damage elicited by cigarette smoke is quite diverse and in most cases can be repaired following cessation (238). Cigarette smoke contains compounds such as B[a]P and NNK that can form DNA adducts or strand breaks in tissue. In most cases DNA adducts can be repaired, but

under certain circumstances in which they persist, DNA adducts can cause detrimental mutations (34). Cigarette smoke also contains a large number of oxidants and free radicals such as NO and H_2O_2 that induce oxidative stress; a single puff contains approximately 10^{17} oxidant molecules (239). These molecules can damage tissue by causing nitration of vital proteins and inducing oxidative degradation of lipids. Consequently, levels of 3-nitrotyrosine, a marker of NO-dependent oxidative damage, and F_2-isoprostane, a product of free radical-catalyzed lipid peroxidation, are higher in the plasma of chronic smokers (10,238). Furthermore, the oxidative stress caused by these agents is reflected in the imbalance of reduced and oxidized glutathione levels (240) and reduction of vitamins A and C (238). Cigarette smoke also causes inflammation as indicated by the numerous inflammatory markers, including CRP, fibrinogen, and IL-6, that have been found to be elevated in smokers (237,238); CRP, an important liver protein involved in the activation of the complement system, continues to be elevated in former smokers after 10 to 20 years following cessation (238). In addition, cigarette smoke induces aberrant stimulation of inflammatory cells such as neutrophils and leukocytes which can provide an overprotective, and consequently, harmful response (237). Conversely, anti-inflammatory related processes are also initiated by components in cigarette smoke. For example, carbon monoxide has demonstrated a suppressive effect on eosinophils and several inflammatory cytokines (e.g. TNF-α, IFN-γ, and IL-2) (237).

2.2 An "omic" view of the molecular effect of cigarette smoking on human lung tissue

Many studies have analyzed the primary target organ of cigarette smoke, the lung, through genomic/transcriptomic (241), proteomic (242-244), and whole-genome microRNA (miRNA) expression (245) approaches to identify important molecular changes associated with exposure and/or disease development. Such biomarkers would be beneficial in characterizing an individual's susceptibility to disease development related to COPD and lung cancer. Spira et al.

collected human airway epithelial cells by bronchoscopy in non-smoking and smoking subjects and identified 97 cigarette smoke-induced changes in gene expression by microarray analyses (241). Many of the genes up-regulated in individuals that smoked were involved in xenobiotic metabolism such as CYP1B1, antioxidant activity such as glutathione peroxidase-2 and aldehyde dehydrogenase 3 family, member A1 (ALDH3A1), and electron transport such as NADPH-oxidase. Interestingly, several putative oncogenes such as the cell adhesion molecule carcinoembryonic antigen-related cell adhesion molecule 6 (CEACAM6) and the zinc metalloenzyme carbonic anhydrase 12 were also up-regulated. Contrary to systemic effects, down-regulated genes were primarily involved in inflammation; however, several putative tumor suppressor genes such as family with sequence similarity 107, member A (FAM107A) and growth arrest specific 6, both involved in regulation of cell growth, were down-regulated. In addition, Spira et al. also defined genes whose expression correlated to cumulative pack-years of smoking and genes whose expression were not recovered upon smoking cessation including CEACAM6 and FAM107A, suggesting an increased susceptibility to carcinogenesis (241). In a follow-up study, Steiling et al. used 1D PAGE coupled with LC-MS/MS to identify proteins differentially expressed in the airway epithelial cells between non-smokers and smokers (243). Proteins of significance that were decreased in smokers included the upper respiratory-specific palate, lung and nasal epithelium carcinoma associated precursor (PLUNC), the detoxification enzyme ALDH3B1, a gene previously shown to be highly expressed in the lung, and CC10 (243), a protein we identified in mouse lung in Chapter 2. Using 2D PAGE, Kelsen et al. analyzed protein expression in whole lung tissue focusing on proteins involved in the "unfolded protein response" (UPR) (244). UPR is a compensatory response elicited by cells to manage reactive oxygen species in cigarette smoke from interfering with protein folding in the endoplasmic reticulum (ER) (246). Failure of UPR has been suggested to be a contributor to the development of COPD and lung cancer (244,247). Several ER-related proteins were up-regulated in chronic

smokers compared to non-smokers including the chaperones, glucose-regulated protein 78 (GRP78) and calreticulin, the foldase, protein disulfide isomerase (PDI), and enzymes involved in antioxidant defense (244). Moreover, GRP78, calreticulin, and PDI levels were also lower in former smokers compared to current smokers suggesting that smoking cessation may help to reverse the effects of cigarette smoking on UPR. Interestingly, the 14-3-3 protein isoform, σ, which was down-regulated in our animal model in Chapter 2 in lung adenocarcinomas, was up-regulated in smokers (244); there are several isoforms (cf Chapter 2) of 14-3-3 and their individual roles in cancer development have not been clearly defined (248). Finally, Schembri et al. analyzed miRNA expression in bronchial airways and discovered twenty-eight miRNAs that were differentially expressed between smokers and non-smokers (245). A majority of the miRNAs identified were down-regulated in smokers, including mir-218. Upon further *in vitro* investigation, mir-218 was inversely correlated with corresponding targeted mRNA expression related to transcriptional regulators and cellular structure in primary bronchial epithelial cells and the NSCLC cell line, H1299 (245).

2.3 A proteomic view of the molecular effect of cigarette smoking characterized in biological fluids

Biological fluids obtained from less-invasive and non-invasive approaches are readily accessible and preferable in a clinical setting compared to tissue collection for biomarker applications. In some cases, similar molecular profile changes occurring at the tissue level and related to exposure and/or disease development can also be obtained in proximal fluids, i.e. those adjacent to tissue, as well as in the blood and urine. This occurs as a result of direct secretion and/or release into the microenvironment (249). In addition, biological fluids can also provide an overview of the systemic response to critical disease-related changes in the body (249).

Proteins are easily detected in biological fluids and form the basis of commonly used tests to screen for and monitor health conditions. Thus, laboratories have also analyzed BALF

(250,251), nasal lavage fluid (NLF) (252), exhaled breath condensate (253), and urine (254) in smokers and non-smokers to identify proteomic profile differences related to the effects of smoke exposure. In smokers, increased levels of the inflammatory proteins S100A8, salivary proline-rich peptide P-C, and lysozyme C have been detected in BALF compared to non-smokers, whereas salivary proline-rich peptide P-D and CC10 have been reduced (251); CC10 has also been found to be reduced in NLF (252) and serum of smokers (205). Furthermore, Merkel et al. also found that the S100A8 protein was elevated in the BALF of smokers with COPD compared to BALF from asymptomatic smokers (251). Ghafouri et al. identified anti-inflammatory and proteinase inhibitors elevated in the NLF of smokers compared to non-smokers, including a truncated variant of lipcortin-1, three acidic forms of AAT, and one phosphorylated form of cystatin S (252). In addition, PLUNC, which was down-regulated in bronchial epithelial cells of smokers mentioned previously (243), was increased in NLF of smokers (252). In exhaled breath condensate, Gianazza et al. found many forms of keratin, an important structural protein, up-regulated in smokers by as much as three times the amount found in non-smokers (253). Identification of cigarette smoking effects on the urinary proteome identified many proteins involved in inflammatory processes (254). Up-regulated proteins in smokers included S100A8, inter-α-trypsin inhibitor heavy chain 4 (ITI-HC4), and CD59; the zinc-α-2-glycoprotein was found down-regulated in smokers (254).

Although previous studies that employed various biological fluids have provided valuable information pertaining to the effect of cigarette smoking, there are no studies that have been conducted to compare the plasma proteome of healthy asymptomatic smokers and non-smokers for biomarker discovery. A primary reason for this stems from the fact that plasma is quite complex and very dynamic (249). Only a small number of proteins compose greater than 90% of the protein in plasma, which can consequently impede the assessment of lower abundant proteins (255). In many studies, it is often observed that the higher abundant proteins tend to mask and

interfere with the identification of the lower abundant and biologically relevant proteins (256). In spite of this, strategies to fractionate plasma proteins, e.g. immunoaffinity columns and ultracentrifugation techniques, are available and thus, provide a means with which to enrich for potential protein biomarkers of interest (257-259). Therefore, the utility of plasma for biomarker discovery should not be overlooked, as it is a rich source of information containing most, if not all, human proteins (255).

3. Rationale

In Chapter 2, a single carcinogen in cigarette smoke, NNK, was used to study the progression of lung tumorigenesis in the A/J mouse model. This model allowed for the target tissue, the lung, to be collected and analyzed by proteomic approaches to identify candidate biomarkers for related to cancer development. However, such studies cannot be conducted so easily in a clinical setting. For instance, humans are exposed to whole tobacco smoke rather than a single agent. In addition, lung tissue collection is not practical in healthy asymptomatic smokers, even though they are classified as high risk for numerous diseases, including lung cancer (5). Biomarkers indicative of the harmful effects of cigarette smoke and involved in disease development must therefore be found in surrogate tissue such as blood plasma. Plasma collection is a minimally invasive procedure and readily available for clinical use (255). Therefore, in this study, our objective was to assess the effect of chronic cigarette smoking on the global expression of proteins in human plasma for biomarker discovery related to disease development. We utilized the 8-plex iTRAQ proteomic methodology and MS analysis in combination with immunblotting to identify, quantitate, and validate differentially expressed plasma proteins between healthy asymptomatic smokers and non-smokers.

4. Experimental design

4.1 Human blood plasma samples from smokers and non-smokers

Subjects used in this investigation were from a participatory-based study of smoking and health from 1995-2004. A detailed description of each subject is provided in Table 3.1 (Table was published in reference (260)). The study design and the biological collection and processing protocols were described previously (240,261). In brief, subjects were non-Hispanic white adult male smokers and non-smokers who lived in Yonkers, Mt. Vernon or their surrounding communities in New York. Current smokers were defined as those having smoked at least five cigarettes per day for one or more years and did not use other tobacco products. Trained interviewers administered a structured questionnaire that contained items on cigarette smoking history including cigarettes smoked per day and total years of smoking. All subjects signed a consent form that was approved by the Institutional Review Board of the Institute for Cancer Prevention.

Blood samples were collected from an antecubital vein into tubes containing EDTA as an anticoagulant and immediately placed on ice. The blood was centrifuged at 2,100 x g for 15 minutes at 4ºC to obtain plasma. The plasma was removed, aliquoted and immediately frozen at -80ºC until further processing. Smoking status was confirmed by analysis of plasma and urine cotinine, the major metabolite of nicotine.

4.2 Reagents and chemicals

All reagents were of analytical grade and stored appropriately prior to use according to manufacturers' recommendations. With regard to depletion chromatography, the depletion column and corresponding buffers were obtained from Agilent Technologies Inc. (Palo Alto, CA). Trichloroacetic Acid (TCA) and acetone were obtained from Fisher Scientific (Pittsburgh, PA). All iTRAQ reagents and buffers were obtained from ABI, Promega, and Sigma-Aldrich.

Table 3.1 Subject characteristics of smokers and non-smokers used in iTRAQ study.

subject ID	gender	condition	race	age (yrs)	weight (lbs)	height (in)	BMI*	years smoking	cigarettes per day (#)	age started smoking (yrs)	brand	menthol present in cigarettes (Y/N)	fagerstrom score†	plasma cotinine (ng/ml)
390	M	Non-Smoker	White	60	155	63	27.5	0	—	—	—	—	—	0
401	M	Non-Smoker	White	65	165	70.5	23.4	0	—	—	—	—	—	0
412	M	Non-Smoker	White	47	170	71	23.8	0	—	—	—	—	—	0
415	M	Non-Smoker	White	65	200	72	27.6	0	—	—	—	—	—	0
426	M	Non-Smoker	White	77	125	63	22.2	0	—	—	—	—	—	0
429	M	Non-Smoker	White	36	175	68	26.7	0	—	—	—	—	—	0
434	M	Non-Smoker	White	50	150	67	23.5	0	—	—	—	—	—	0
638	M	Smoker	White	36	190	68	28.9	15	14	21	Marlboro	N	3	73
705	M	Smoker	White	53	200	68	30.4	36	10	17	Marlboro	N	3	47
899	M	Smoker	White	21	190	69	28	4	12	17	Marlboro lights	N	2	46
995	M	Smoker	White	18	135	72	18.3	6	20	12	Marlboro	N	6	71
2027	M	Smoker	White	38	190	71	26.5	20	10	17	Parliament Lights	N	2	87
2031	M	Smoker	White	18	135	68	20.5	4	25	14	Newport	Y	7	635
2058	M	Smoker	White	20	125	68	20.2	5	10	15	Newport lights	Y	5	166

*BMI (body mass index), BMI = mass (lbs) x 703/height $(in)^2$.

†The fagerstrom score is used to measure an individual's nicotine dependence through six self-reported measures; the scale ranges from 0-10 with 0 being a very low nicotine dependence and 10 being a very high dependence for nicotine.

Reagents for immunoblot assays were purchased from Invitrogen and Bio-Rad Laboratories, and primary and secondary antibodies were purchased from Abcam, Santa Cruz Biotechnology, and Cell Signaling. Chemiluminescent immunodetection reagents and autoradiography films were purchased from GE Healthcare and Imaging Resources, Inc., respectively.

4.3 Depletion of abundant proteins in plasma

In order to span a larger range of the plasma proteome and lesser abundant proteins, fourteen of the most abundant human plasma proteins (albumin, IgG, α1-antitrypsin, IgA, transferrin, haptoglobin, fibrinogen, α2-macroglobulin, α1-acid glycoprotein, apolipoprotein AI, and AII, IgM, transthyretin, and complement C3) were depleted from human plasma samples by using a Multiple Affinity Removal System (MARS) Column (Hu-14, 4.6 x 100 mm), from Agilent Technologies Inc (Figure 3.1). All samples were passed through the same Hu-14 column in order to minimize technical variation; however, following each sample run a thorough washing procedure with a pH 7.4 phosphate salt-containing buffer (Buffer A, equilibration/load/wash buffer) was performed to prevent any carryover effects (Agilent Technologies, Inc.). Removal of protein from the column was monitored by ultraviolet light (UV) chromatogram (ÄKTA Prime Plus HPLC System, Amersham Biosciences). Prior to loading the samples onto the column, samples (~80 µl) were first diluted 1:12 in Buffer A, followed by filtration through a 0.2 µm low-protein-binding Acrodisc syringe filter to remove any interfering particulate matter (Pall Life Sciences, Ann Arbor, MI). The filtrate was then loaded onto the column assembled on an ÄKTA Prime Plus HPLC System (Amersham Biosciences). Samples were run through the system according to the manufacturer's instructions. Collection of flow-through fractions (F1) was performed with Buffer A at 0.2 ml/min and eluted bound fractions (E1) with a low pH (~2.5) urea buffer (Buffer B, elution buffer, Agilent Technologies, Inc.) at 1 ml/min. Fractions containing

protein (F1 and E1) were verified by ultraviolet light absorption (280 nm) (Figure 3.2) and placed on ice. Depleted protein fractions (F1) from multiple runs were combined into one tube for each subject and stored at -80°C until further processing.

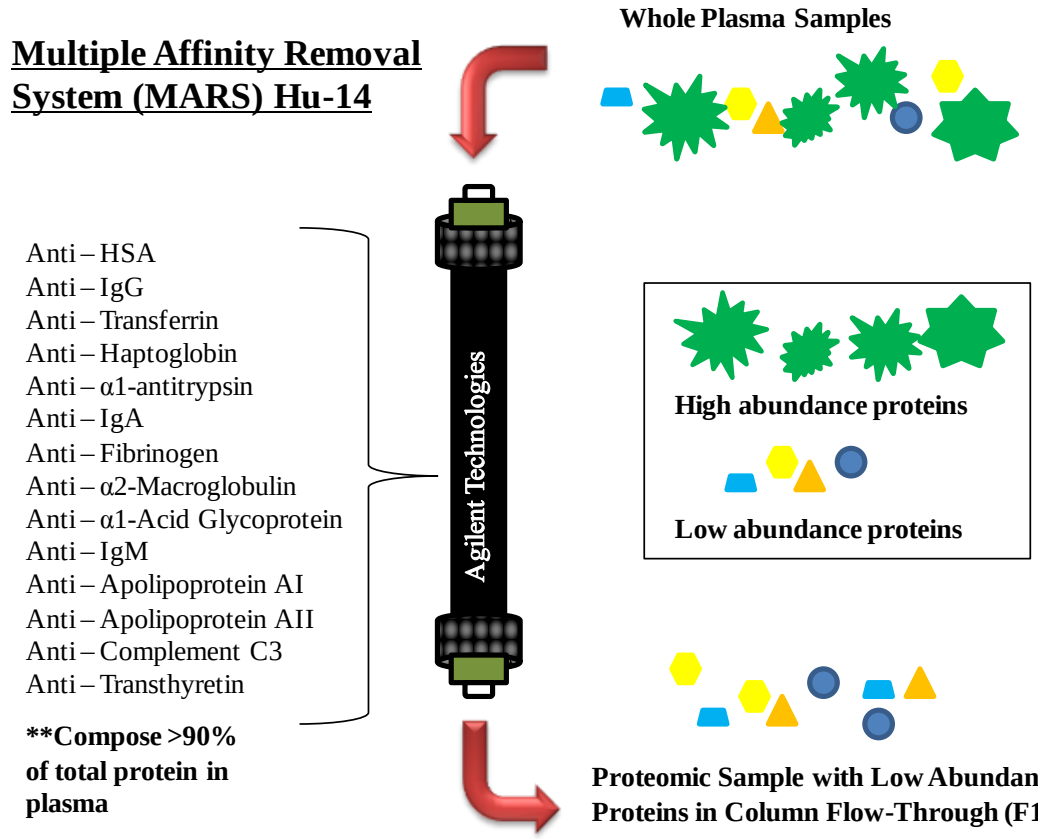

Figure 3.1 Scheme showing the use of the Hu-14 MARS column to remove highly abundant proteins from human plasma samples.

4.4 Trichloroacetic acid (TCA) precipitation of plasma proteins for iTRAQ analysis

TCA precipitation is a widely used procedure with high protein recovery and sample concentration, similar to that of acetone that was used in Chapter 2 (180). However, compared to

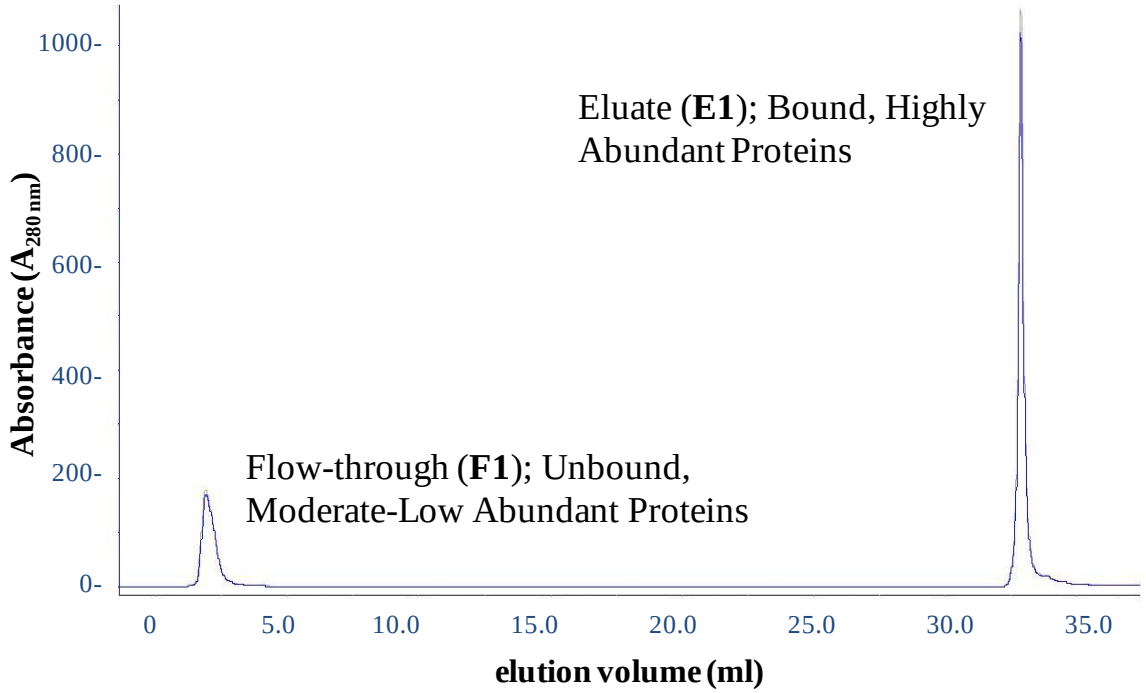

Figure 3.2 Representative UV chromatogram of depletion of protein from plasma samples using Agilent Technologies Hu-14 column.

acetone, TCA works better with diluted samples (180), such as our depleted plasma. Therefore, we selected TCA precipitation for our plasma protein samples.

Prior success using TCA precipitation with biological fluids, such as BALF, was demonstrated (172) and thus, this protocol was followed. One volume of ice cold 100% TCA was added to four volumes of each protein sample. The samples were thoroughly vortexed and placed overnight at 4°C. Following overnight incubation, precipitated proteins were centrifuged at 15,000 x g for 15 min at 4°C. The protein pellets were then washed with 250 µl of chilled acetone, centrifuged again, allowed to dry for approximately 10 min, and then resuspended in 100 µl of Milli-Q water. From this suspension, total protein content was determined using the *DC* Protein Assay (Lowry Assay, Bio-Rad Laboratories). Enrichment of lower abundance proteins

following depletion and acetone precipitation was visualized by silver-staining (Amersham Biosciences) on a 10% SDS-PAGE gel (Figure 3.3).

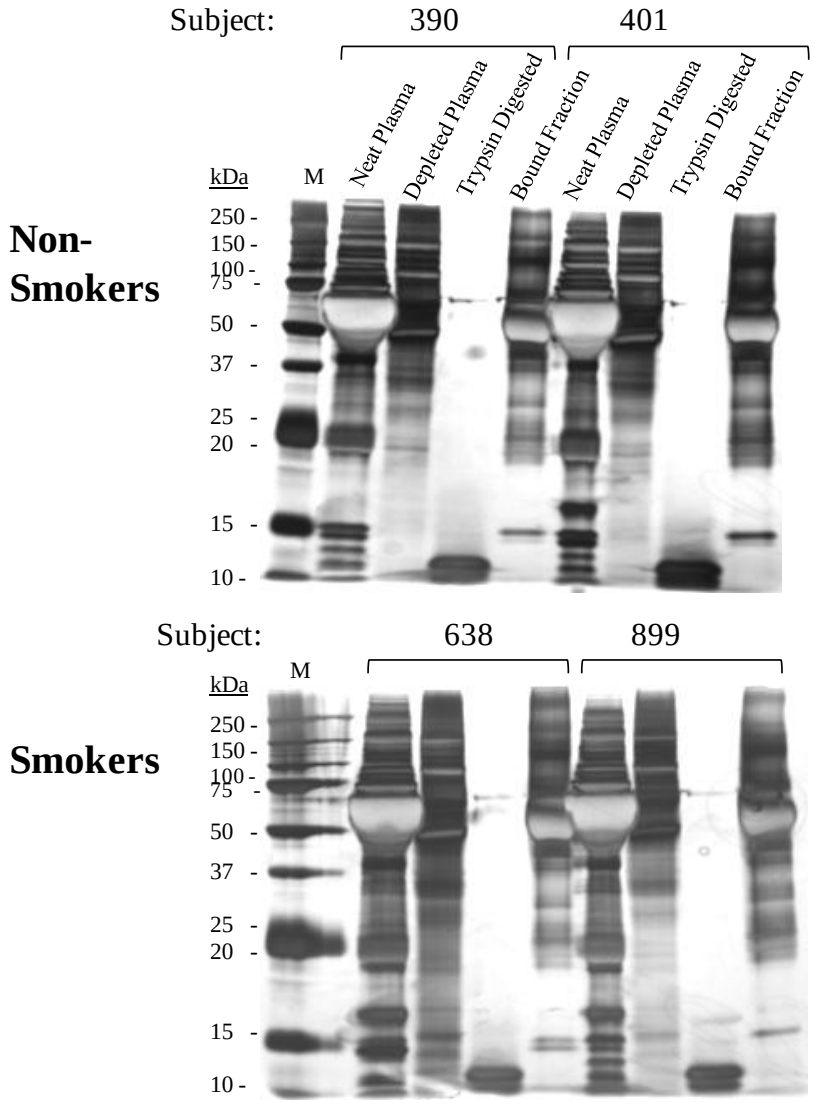

Figure 3.3 Human plasma protein samples from two representative non-smokers (subjects 390 and 401) and two smokers (subjects 638 and 899) resolved on a 10% SDS-PAGE gel and stained with silver nitrate. Lane 1 in each gel is a molecular weight marker. Subsequent lanes represent neat (whole) plasma proteins, depleted plasma proteins (F1), trypsin digested plasma proteins, and bound fraction plasma proteins (E1) for each subject; i.e. four lanes for each subject in order listed above.

4.5 Sample distribution for iTRAQ analysis

The plasma protein samples were divided into two 8-plex experiments with four non-smokers and three smokers in one set (Set A, Table 3.2) and three non-smokers and four smokers in another set (Set B, Table 3.2). A reference pool consisting of an aliquot of each sample (smokers and non-smokers, 50 µl/sample) was allocated to each 8-plex experiment using the same labeling tag (113), and the individual samples were allocated to the remaining tags (114-119, 121) (Table 3.2). Table 3.2 was published in reference (260).

Table 3.2 iTRAQ experimental design for plasma of non-smokers (n=7) and smokers (n=7)

experimental set	isobaric tag	subject ID	condition
Set A	113	Pool of all samples	Smoker/Non-Smoker
	114	390	Non-Smoker
	115	401	Non-Smoker
	116	412	Non-Smoker
	117	415	Non-Smoker
	118	638	Smoker
	119	705	Smoker
	121	899	Smoker
Set B	113	Pool of all samples	Smoker/Non-Smoker
	114	426	Non-Smoker
	115	429	Non-Smoker
	116	434	Non-Smoker
	117	995	Smoker
	118	2027	Smoker
	119	2031	Smoker
	121	2058	Smoker

4.6 Preparation of plasma proteins prior to isobaric tag labeling of peptides

All of the steps were performed according to the recommendations of ABI with appropriate modifications suggested by the Penn State Hershey Cancer Institute Proteomics/Mass Spectrometry Shared Resource (Hershey, PA). The procedure performed in Chapter 2 for iTRAQ

setup was followed accordingly with minor modifications. For each sample, 50 µg of depleted protein was resuspended in 20 µl of 0.5 M TEAB pH 8.5 and boiled for 5 min. Following resuspension of samples, 1 µl of denaturant (2% SDS) and 1 µl of reducing reagent (5 mM TCEP) were then added to each sample and incubated for 1 hr at 60°C. One microliter of freshly prepared 84 mM iodoacetamide solution was then added and incubated for 30 min at room temperature in the dark. Sequencing grade trypsin (Promega, Madison, WI) was reconstituted in 50 mM acetic acid (supplied with Promega trypsin) at a concentration of 1 µg/µl. Trypsin was added at a 5:1 (protein:trypsin) concentration to each sample and allowed to incubate overnight at 48°C. Efficient digestion of samples was visualized by silver-staining (Amersham Biosciences) on a 10% SDS-polyacrylamide gel (Figure 3.3).

4.7 iTRAQ labeling of protein peptides

Details of this approach are described in Chapter 2, section 4.2.9.

4.8 2D-LC fractionation of iTRAQ labeled peptides

Details of this approach are described in Chapter 2, section 4.2.10.

4.9 MS analysis of peptides

MS analysis of peptide fractions for subsequent identification and quantitation was performed in the Penn State Hershey Cancer Institute Proteomics/Mass Spectrometry Shared Resource Core. MALDI target plates (fifteen per experiment) containing peptides were analyzed in a data-dependent manner on an ABI 4800 MALDI TOF/TOF along with thirteen calibrant spots (ABI 4700 Mix). As each plate entered into the instrument, a plate calibration/MS Default calibration update was performed, followed by MS/MS default calibration. MS spectra were taken from 5,500 MALDI spots, using 500 laser shots per spot at a laser intensity of 3,800. A plate-wide interpretation was automatically performed in which the highest peak of each observed m/z value was chosen for subsequent MS/MS analysis. MS/MS spectra were derived from 2,500

laser shots at a laser power of 3,500 for samples in Set A (Table 3.2) or 4,600 for samples in Set B (Table 3.2). Fragmentation of labeled peptides was induced by the use of atmosphere as a collision gas with a pressure of 1.2 to 1.3 x 10^{-6} Torr. A total of 10,680 MS/MS spetra were taken for Set A (Table 3.2) and 10,833 MS/MS spectra were taken for Set B (Table 3.2).

4.10 Database search for protein identification from MS and MS/MS spectra

Protein identifications from MS spectra were performed using the Paragon algorithm as implemented in Protein Pilot™ v3.0 software (ABI-MDS Sciex) (182). Protein Pilot™ search parameters were set to account for cysteine alkylation of proteins by iodoacetamide and any potential biological modifications. MS and MS/MS spectra were searched using the Human NCBI nr database sequences containing 498,411 protein sequences (version 2009-07-05), plus concatenated reverse versions of itself, and common human and laboratory contaminants (ABISciex_ContaminantDB_20070711); total of 995,248 protein sequences. Identifications of proteins were only accepted with a Protein Pilot™ Unused Score of >1.3 (>95% confidence interval) and a Local FDR estimation of no higher than 5% as described in Chapter 2.

4.11 Quantitation of proteins identified from MS results

iTRAQ reporter ion abundances in MS/MS scans were evaluated using Protein Pilot™ v3.0 software (ABI) for relative quantitation of proteins. For each peptide used for protein identification, peak areas for peaks at m/z 113-119 and 121 were calculated. To correct for experimental errors in amount of protein included in each sample group, the bias correction was performed on the Pro Group™ Algorithm results. This was performed by calculating the median peptide ratio for all peptides reported, adjusting to unity, and then applying the same bias factor to all ratios (performed within Protein Pilot™). This normalizing factor is based on the assumption that most of the protein levels in the plasma from white male smokers should be similar to those from white male non-smokers with the exception of those that are influenced by smoking. For proteins with two or more qualified peptide matches, seven average peak area ratios, 114/113,

115/113, 116/113, 117/113, 118/113, 119/113, and 121/113, were calculated using the peak area ratios of the peptides originating from the same protein.

4.12 Immunoblot analysis to validate iTRAQ results and determine expression of 14-3-3 isoforms (σ and ζ)

Total protein content in whole plasma (non-depleted) samples was determined using the *DC* Protein Assay (Lowry Assay, Bio-Rad Laboratories). For each plasma sample, approximately 60 µg of total protein was denatured and resolved on a NuPAGE® 4-12% gradient gel (Invitrogen) (200 V for 60 min) or a 10% SDS-PAGE gel (100 V for 120 min). Thereafter, proteins were transferred to a nitrocellulose membrane (Amersham Biosciences) (100 V for 65 min) and blocked with 5% non-fat dry milk (Bio-Rad Laboratories) in TBS-T20 for 1 hr. To probe for proteins of interest, membranes were cut according to the molecular weight of the proteins. The membranes were then probed with the following antibodies diluted in 0.5% bovine serum albumin in TBS-T20: anti-ITI-HC3 (Santa Cruz), anti-vitamin D-binding protein, anti-14-3-3 σ (Abcam), anti-14-3-3 ζ (Cell Signaling). Following incubation with primary antibodies overnight at 4°C, membranes were washed 3x with TBS-T20 and corresponding secondary antibodies conjugated to HRP were added at a 1:2000 dilution in 0.5% bovine serum albumin in TBS-T20. Membranes were again washed 3x with TBS-T20 and bands were detected using enhanced chemiluminescence reagents (ECL, GE Healthcare) and developed with autoradiography film (Imaging Resources, Inc). For densitometric analysis, films were scanned using Bio-Rad's GS800 Calibrated Densitometer. Quantitation of protein levels was carried out using the Quantity One v4.5.0 1-D Analysis Software (Bio-Rad Laboratories) and normalized to total protein content.

4.13 Statistical analysis, molecular function, and biological processes of proteins

The protein lists from the two iTRAQ experiments (Set A and Set B, Table 3.2) were merged with ratios calculated to the reference pool (labeled with iTRAQ reagent 113 in both sets). Only proteins common to both sets of iTRAQ experiments were analyzed. Quantitative data were exported into Excel (Microsoft, Bellevue, WA) for further analysis. The log ratios were compared between the profiles corresponding to smokers and non-smokers using Student's two-sample, two-tailed *t* test and proteins with a *p*-value smaller than 0.05 were considered significant for quantification differences.

PCA was conducted on the expression data for iTRAQ proteins with *p*-values smaller than 0.05 between smokers and non-smokers. PCA by subject was performed using XLSTAT 2010 in Microsoft Excel® (Addinsoft, New York, NY). Each axis was scaled according to the variance incorporated in that component. For protein ontology classification, proteins were imported into the PANTHER classification system (http://www.pantherdb.org/, SRI International). Proteins were grouped accordingly to associated molecular functions and biological processes (262).

For immunoblot analysis, statistical significance was determined using Student's *t* test and results were considered significant for *p*-values less than 0.05.

5. Results

5.1 iTRAQ analysis to detect differentially expressed proteins in plasma of smokers and non-smokers

We analyzed plasma protein expression profiles of seven smokers and seven non-smokers using the 8-plex iTRAQ proteomic technique. The average pack years (± SD) for smokers was 7.8 (± 6). To account for the number of samples, two 8-plex iTRAQ experiments (Set A and Set B, Table 3.2) were performed and a reference pool in each set allowed for cross-

set comparison. This method of using a pooled reference standard in plasma biomarker discovery studies using iTRAQ labeling reagents has been established (263).

Prior to the start of the iTRAQ experiments, we depleted fourteen of the most abundant plasma proteins, including albumin, IgG, α1-antitrypsin, IgA, transferrin, haptoglobin, fibrinogen, α2-macroglobulin, α1-acid glycoprotein, apolipoprotein AI and AII, IgM, transthyretin, and complement C3, from each sample, as well as the reference pool, to enhance the detection of the lower abundance proteins. On average, approximately 3.2% of the starting total protein sample was recovered, representing the moderate to lower abundance proteins. We selected fifty micrograms of each sample for iTRAQ labeling and analysis as recommended from previous studies utilizing human plasma (264).

iTRAQ protein identification and quantitative ratios for both sets of experiments, A and B, were determined using Protein Pilot™ v3.0. In the first iTRAQ data set (Set A, Table 3.2), identification of 120 proteins were assigned and in the second set (Set B, Table 3.2) identification of 131 proteins were assigned with high confidence using the Protein Pilot™ v3.0 Unused Score of greater than 1.3 (greater than 95% confidence interval) and a Local FDR of no higher than 5%. The proteins identified from the two-iTRAQ data sets were subsequently combined and 113 proteins that were commonly identified between the two data sets were further analyzed. The coefficient of variation for these proteins was less than 30% for each iTRAQ data set and within smoking and non-smoking conditions. Highly abundant proteins not completely depleted from samples, i.e. complement component C3, transthyretin, etc., were not included in the subsequent analyses. Figure 3.4 shows a representative MS and peptide MS/MS spectrum of the corresponding amino acid sequence -EVSFDVELPK- used in the identification and quantitation of one of the proteins identified in this study, the inter-α-trypsin inhibitor heavy chain H3 (ITI-HC3) protein. The relative intensities of the iTRAQ reporter ions used to quantify the relative ITI-HC3 protein expression for each subject is also presented in Figure 3.4.

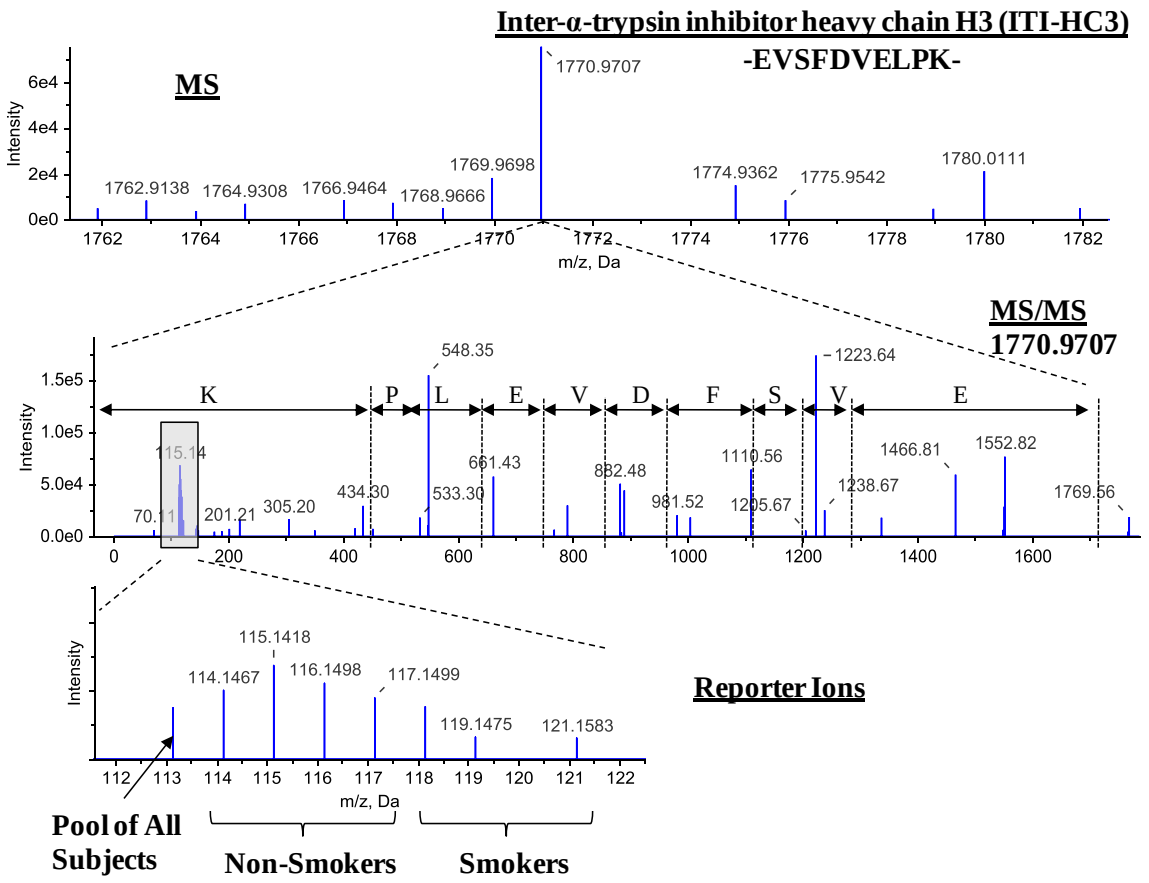

Figure 3.4 Identification of inter-α-trypsin inhibitor heavy chain H3 (ITI-HC3) from iTRAQ experiment. Representative MALDI TOF/TOF MS (*upper panel*) and tandem MS spectra (*middle panel*) used in the identification of the ITI-HC3 protein. The peptide sequence EVSFDVELPK was unique to the ITI-HC3 protein. Quantification was derived from the intensities of the eight iTRAQ reporter ions (*lower panel*). Reporter ions 114-117 are non-smokers and reporter ions 118-121 are smokers. Reporter ion 113 is the pool of all subjects in the study. Figure was published in reference (260).

Based on statistical comparisons, sixteen proteins were found to have *p*-values less than 0.05 between smokers and non-smokers (Table 3.3; table was published in reference (260)). Using these sixteen proteins, an unsupervised, multivariate data analysis method, known as PCA,

Table 3.3 Differentially expressed (p <0.05) proteins in plasma between adult white male smokers and adult white male non-smokers.

accession no.*	description	p-value	fold-change (relative to non-smokers)
	Up-Regulated		
gi|55962663	Complement component 8, γ polypeptide (C8γ)	0.011	1.2
gi|68067608	Kallistatin (KLST)	0.018	1.2
gi|158258917	Complement component 8, β polypeptide (C8β)	0.024	1.2
gi|736249	Gelsolin (GSN)	0.028	1.2
gi|124375948	Complement component 8, α polypeptide (C8α)	6.21E-04	1.3
gi|6683456	Mannan-binding lectin serine protease 1 (MASP1)	0.038	1.6
gi|85360967	Mannose-binding protein C (MBL2)	0.040	1.8
	Down-Regulated		
gi|62896541	Complement component 1, r subcomponent (C1R)	0.030	1.1
gi|36579	Vitamin K-dependent protein S (PROS)	0.020	1.2
gi|78070482	Inter-α-trypsin inhibitor heavy chain H3 (ITI-HC3)	0.037	1.3
gi|189053440	Coagulation factor XIII A chain (F13A)	0.014	1.3
gi|88853069	Vitronectin (VTN)	0.041	1.4
gi|32187679	Apolipoprotein B (APOB)	0.009	1.5
gi|93163358	Apolipoprotein A-IV (APOA4)	0.041	2.0
gi|85566866	Sex hormone-binding globulin (SHBG)	0.001	2.2
gi|639896	Vitamin D-binding protein (VDBP)	0.003	2.4

*National Center for Biotechnology Information (NCBI)

was used to analyze the union of all potential protein expression changes from the statistical analyses and establish a cluster for each subject (Figure 3.5). The first two principal components accounted for 44.6% and 14.3% variances, respectively. The first principal component clearly separated subjects based on their condition as smokers or non-smokers. Further analysis of the expression ratios of the subjects also indicated no difference in protein expression levels between subjects within the same group for the sixteen proteins analyzed as a function of age (± SD), except for the mannan-binding lectin serine protease 1 (MASP-1), which was higher in younger smokers (18.6 ± 1) compared to older smokers (42.3 ± 9).

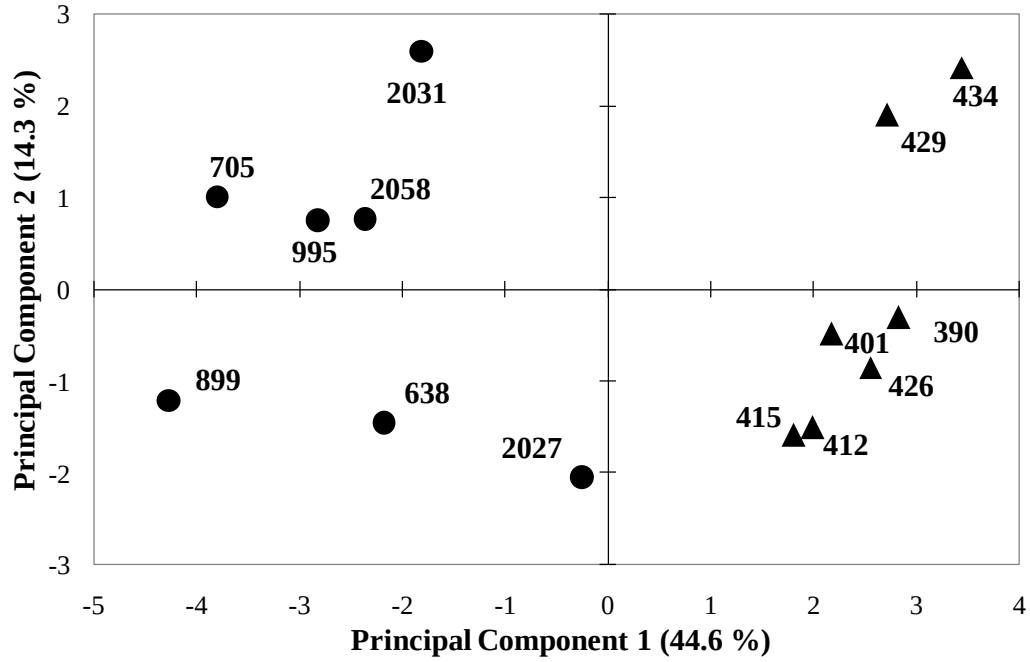

Figure 3.5 PCA of the significantly (p<0.05) modulated proteins identified between smokers and non-smokers. PCA of sixteen proteins identified as differentially expressed between chronic cigarette smokers (n=7) and non-smokers (n=7). Each marker (▲-non-smokers, ●-smokers) represents the compressed weighted average of the principal components of the proteins analyzed for each subject (number indicates the ID of the study subject) in both conditions. Figure was published in reference (260).

5.2 The effect of heavy smoking on protein modulation in plasma

To determine the effect of heavy smoking on protein expression in plasma, iTRAQ ratios for three heavy smokers and three age-matched non-smokers were compared. Heavy smokers were subjects with greater than or equal to 10 pack years of cumulative tobacco exposure; this distinction has also been arbitrarily assigned by other laboratories (265). Heavy smokers were 44.3 ± 7.4 and non-smokers were 42.3 ± 9.3 years old (mean ± SD). Seven proteins were identified as having *p*-values less than 0.05. Five of the proteins identified in Table 3.3 were again modulated in this subset of smokers, including sex hormone-binding globulin (SHBG, down-regulated 2.6-fold), complement component 8 γ polypeptide (C8γ, up-regulated 1.1-fold), vitamin D-binding protein (VDBP, down-regulated 3.0-fold), coagulation factor XIII A chain (F13A, down-regulated 1.6-fold), and apolipoprotein A-IV (APOA4, down-regulated 3.6-fold). In addition, we also identified coagulation factor V (F5) to be up-regulated 1.7-fold (*p*-value=0.024) in smokers and apolipoprotein E (APOE) to be down-regulated 1.3-fold (*p*-value=0.049) in smokers. A PCA plot using these proteins demonstrated a clear separation between the heavy smokers and non-smokers, with the first principal component exhibiting a variance of 81.3% (Figure 3.6).

5.3 Verification of proteins found in iTRAQ studies by immunoblot analysis

Although, proteomic studies using technologies such as iTRAQ have demonstrated great efficiency in both protein identification and quantitation, it is a common practice to verify the results by specific immunodetection techniques, i.e. immunblot, immunohistochemistry, and ELISA. Therefore, to verify our iTRAQ results we performed an immunoblot analysis of individual whole plasma samples from four smokers and four non-smokers; due to limited sample quantity, not all subjects from the iTRAQ analysis could be used for immunoblot analysis. The immunoblots confirmed the results obtained from the iTRAQ analysis for VDBP and ITI-HC3. Relative quantification of VDBP (Figure 3.7A) and ITI-HC3 (Figure 3.7B) indicated that these

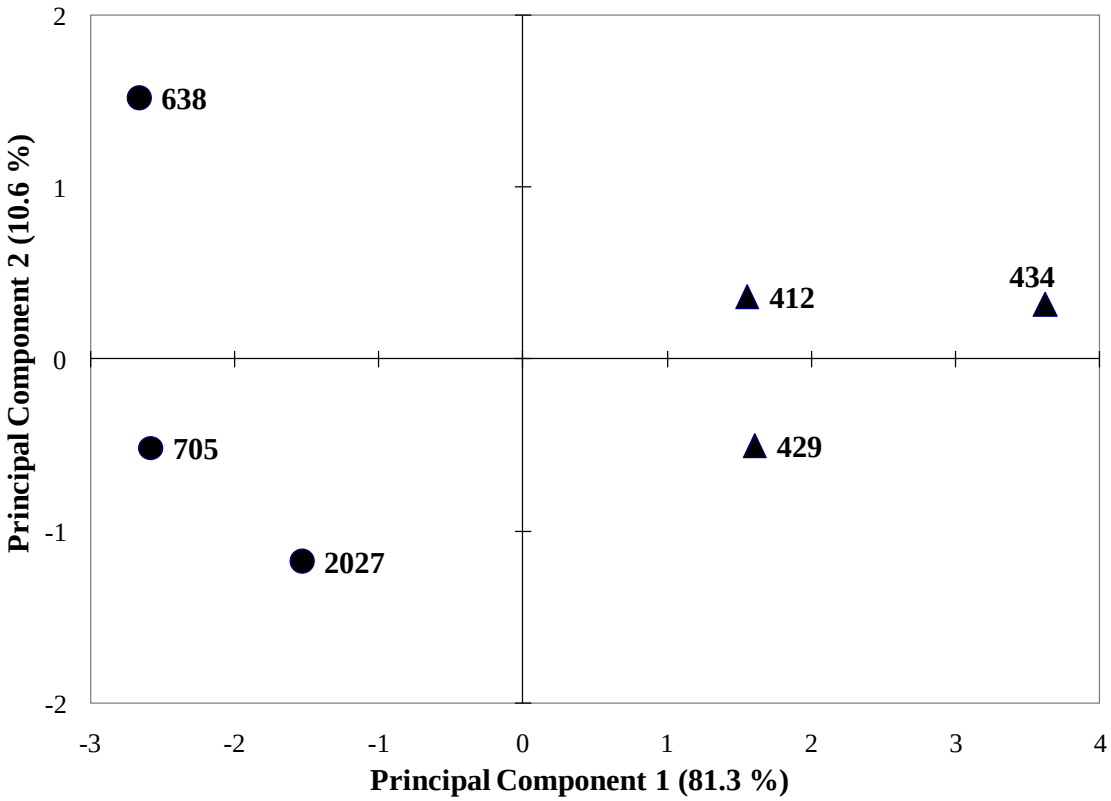

Figure 3.6 PCA of the significantly (p<0.05) modulated proteins identified between heavy smokers and non-smokers. PCA of seven proteins identified as differentially expressed between smokers with greater than or equal to 10 pack years (n=3) and age-matched non-smokers (n=3). Each marker (▲-non-smokers, ●-smokers) represents the compressed weighted average of the principal components of the proteins analyzed for each subject (number indicates the ID of the study subject) in both conditions. Figure was published in reference (260).

proteins were down-regulated in the plasma of smokers as compared to non-smokers. These results were found to be statistically significant for both proteins (p<0.05).

5.4 The effect of cigarette smoking on 14-3-3 isoforms σ and ζ expression in plasma

In our preclinical study (Chapter 2), we identified numerous potential candidate biomarkers in the NNK-A/J mouse model to monitor lung cancer progression. Of particular interest were the 14-3-3 protein isoforms, which we found to be down-regulated in the lung tissue and adenocarcinomas of NNK-treated mice. Therefore, we also wanted to determine the

expression of these proteins in the plasma of smokers and non-smokers. We selected the 14-3-3 protein isoforms σ and ζ. These proteins were selected based on their significance in human cancers (187), including those of the lung (188,266). Both 14-3-3 protein isoforms, σ and ζ, were down-regulated in the plasma of smokers compared to non-smokers by immunoblot analysis (Figure 3.8A and B). However, based on our sample size and statistical analysis they were not statistically significant.

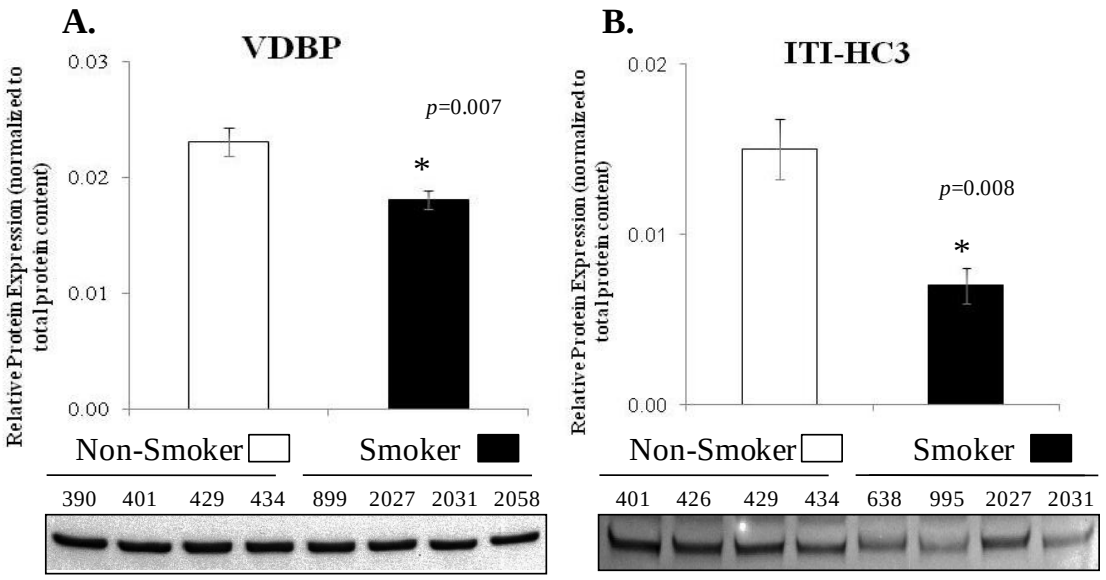

Figure 3.7 Immunoblot analysis confirming iTRAQ results for vitamin D-binding protein (VDBP) and inter-α-trypsin inhibitor heavy chain H3 (ITI-HC3) in smokers' plasma. Numbers above blots are corresponding subject IDs. (A) Relative VDBP protein expression in non-smokers (n=4) and smokers (n=4); error bars, ±SE. Corresponding VDBP protein bands are presented below bar graph and were normalized to total protein content for each subject for quantification purposes. (B) Relative ITI-HC3 protein expression in non-smokers (n=4) and smokers (n=4); error bars, ±SE. Corresponding ITI-HC3 protein bands are presented below bar graph and were normalized to total protein content for each subject for quantification purposes. *$p<0.05$ (Student's *t* test). Figure was published in reference (260).

5.5 Biological significance of proteins modulated by cigarette smoking

In order to understand the biological impact of cigarette smoking on the plasma proteome the differentially expressed proteins identified by iTRAQ were imported into the PANTHER database to identify key molecular functions and biological processes affected (262). The top six protein classes in plasma affected by cigarette smoking included transfer/carrier proteins, proteases, hydrolases, defense/immunity proteins, cell adhesion molecules, and enzyme modulators (Figure 3.9A). In addition, the proteins were found to participate in a variety of important biological processes including metabolic, immune, "response to stimulus", cellular, and transport-related processes (Figure 3.9B).

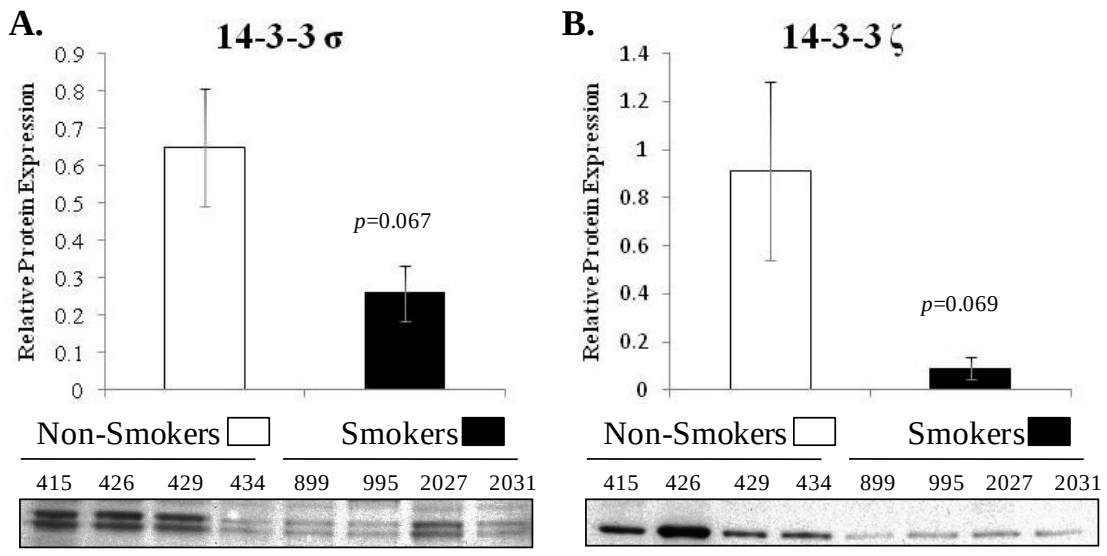

Figure 3.8 Expression of 14-3-3 protein isoforms, σ and ζ, in the plasma of smokers compared to non-smokers by immunoblot analysis. Twenty five micrograms of depleted plasma was loaded in each lane. (A) Relative 14-3-3 σ protein expression in non-smokers (n=4) and smokers (n=4); error bars, ±SE. Corresponding 14-3-3 σ protein bands are presented below bar graph. (B) Relative 14-3-3 ζ protein expression in non-smokers (n=4) and smokers (n=4); error bars, ±SE. Corresponding 14-3-3 ζ protein band is presented below bar graph. Protein expression was normalized to total protein content for each subject for quantification purposes. *p*-values were obtained by Student's *t* test.

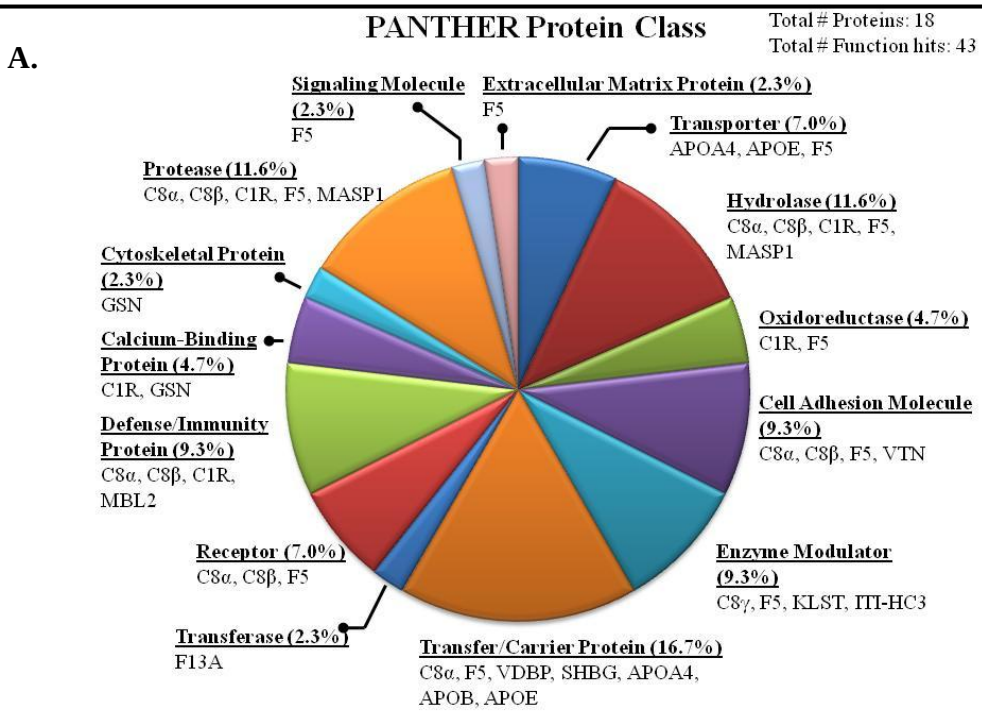

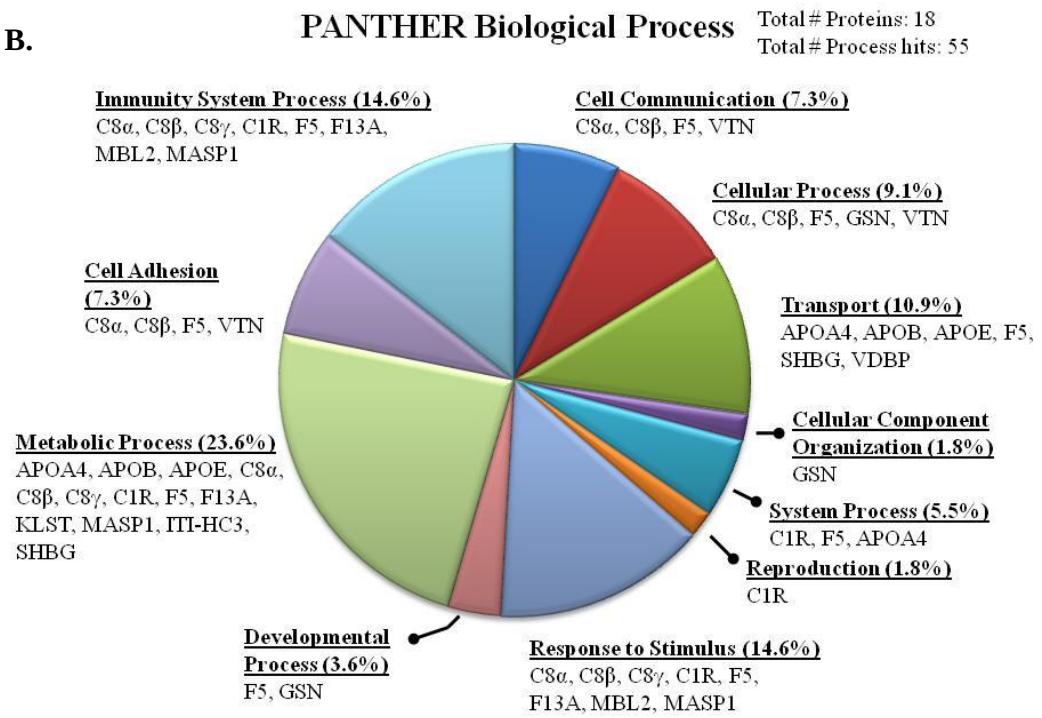

Figure 3.9 Biological impact of cigarette smoking on identified plasma proteins differentially expressed in smokers and non-smokers using the PANTHER database. Proteins were assigned to one or more profiles for both Protein Class (A) and Biological Process (B) based on gene ontology (GO). Figure was published in reference (260).

6. Discussion

In this investigation, using the iTRAQ proteomic approach, as was utilized in Chapter 2, we determined the impact of cigarette smoking on the human plasma proteome. Unlike experiments described in Chapter 2 in which we were able to evaluate the molecular effects of a specific tobacco carcinogen, NNK, on the lung, we analyzed the effect of exposure to whole tobacco smoke on surrogate tissue, i.e. plasma. Our overall goal was to identify candidate protein biomarkers in plasma that may be modulated by tobacco smoking and possibly contribute to the development of tobacco smoking-related diseases, such as lung cancer. The clinical utility of plasma is such that it provides an optimal biological fluid in which to evaluate the current health condition of an individual. However, the complexity and dynamic nature of plasma often hinders protein biomarker discovery investigations (249). A primary concern is the relatively small number of major proteins that comprise greater than 99% of the protein mass in plasma. Such major proteins tend to impede the assessment of lower abundance, and potentially more disease-related, proteins (255,256). Therefore, in this study we depleted fourteen of the most abundant plasma proteins, which represent 94% of the proteins in plasma. As a result, approximately 3.2% of the starting material was recovered. This recovery rate is in agreement with those of others that have used immunodepletion columns (267,268). Thus, we were able to detect lower abundance proteins in plasma that are typically at μg/ml to ng/ml concentrations, including mannose-binding protein C (MBL2), kallistatin (KLST), and sex hormone-binding globulin (SHBG), and tissue leakage proteins, such as gelsolin (GSN) and vitronectin (VTN) (267).

Current techniques in proteomics, including depletion procedures and mass spectrometry analysis, have only allowed us to scratch the surface of the plasma proteome; the abundance of proteins in plasma proteomes varies between proteins such as albumin at high mg/ml concentrations to the rarest of proteins exemplified by interleukins at pg/ml concentrations (255). As a result, in our pilot study we were able to identify over 100 proteins in human plasma with

high confidence under the current conditions; most, if not all of these proteins have previously been reported in human plasma (255). Although the number of proteins confidently identified represents only a relatively small fraction of proteins present in plasma this does not lessen the significance of quantitative differences in the proteins found in the current study between smokers and non-smokers.

In our study, we selected proteins that were significantly modulated between smokers and non-smokers based on a *p*-value of less than 0.05. However, while one is naturally more confident in the potential biological significance of larger fold changes, it is entirely possible for small fold changes to have large biological effects, such as the case of the eukaryotic initiation factor 2 α (eIF2α), which upon phosphorylation (10-20% of total eIF2α) results in complete shut-down of protein synthesis (269). Therefore, we included proteins such as the complement component 1 r subcomponent (CIR) that was significantly down-regulated (1.1-fold, $p<0.05$) in the plasma of smokers compared to non-smokers.

The samples used for iTRAQ (smokers, n=7; non-smokers, n=7) were depleted of the fourteen most abundant proteins in plasma, whereas the samples (n=4 in each category) used in the immunoblot analysis were from whole plasma (i.e. non-depleted). Using both techniques, VDBP and ITI-HC3 were consistently significantly down-regulated in smokers compared to non-smokers. In comparing the results (fold-change) between iTRAQ and immunoblot analysis for both VDBP and ITI-HC3 there is some degree of difference. These differences observed between the two techniques can be attributed to factors such as the use of depleted or whole plasma, sample size, and/or differences inherent in the technical approach. For example, it is now widely accepted that iTRAQ analysis very often underestimates the degree of change that is occurring between samples (270,271). However, the direction (up- or down-regulation) of the change as detected by iTRAQ is consistent with the immunoblot analysis (272).

The proteins in plasma that we discovered to be significantly modulated as a result of chronic cigarette smoking are associated with a variety of important protein classes and biological processes as depicted by PANTHER in Figure 3.9A and B, respectively. Our analysis grouped proteins according to currently known classes and biological processes associated with each protein. Many of the proteins are grouped into numerous classes and biological processes as a result of their involvement in diverse functions. However, these group associations are only assigned according to the information present in the PANTHER database (http://www.pantherdb.org/, SRI International) and do not suggest that these are all of the known classes and biological processes in which these proteins may play a role. Our results in this pilot study have however, pointed out some important classes and biological processes, such as immunity and inflammatory responses, that have been associated with the harmful effects of cigarette smoking. This was also recently observed in the urine of smokers (254). Accordingly, these results are in agreement with current knowledge concerning the capability of cigarette smoke to initiate a host of systemic effects including activation of the complement system (273), and in inducing oxidative stress and inflammatory responses (238). We identified proteins involved in both the classical and lectin complement systems of innate immunity that are responsible for initiating protective cascades in response to stimuli. These included complement component 8 polypeptide chains α (C8α), β (C8β), and γ (C8γ), complement component 1, r subcomponent (C1R), MBL2, and mannan-binding lectin serine protease 1 (MASP1). It has been hypothesized that the expression of some of these proteins may be influenced by inflammatory cytokines, such as TNF-α, IL-1β, IL-8, and IL-6, produced primarily by macrophages. Consequently, these cytokines are regulated by the transcriptional factor, NF-κB that is targeted for activation by cigarette smoke in immune cells (274). In this study, we found all but C1R to be up-regulated in the plasma of chronic cigarette smokers. Thus, the increase in immunity protein expression we observed further supports the above mentioned hypothesis.

Inflammation is a known contributing factor in a number of diseases. Here, we identified the inflammatory-associated proteins ITI-HC3 and VDBP to be down-regulated in smokers by both iTRAQ and immunoblot analysis. ITI-HC3 is part of the ITI family of plasma serine protease inhibitors, which also include HC1, HC2, HC4, and HC5, and the light chain bikunin that are primarily synthesized in the liver and are involved in extracellular matrix stabilization, and inhibition of the inflammatory protein tissue kallikrein (275,276), as well as tumor suppression (277). Interestingly, in a single report, ITI-HC3 was identified as being potentially elevated in the plasma of smokers with lung adenocarcinoma compared to healthy smokers (278). However, loss of ITI-HC3 expression is frequently found in cancerous tissue, including that of the lung (277), and therefore the discrepancy between tissue and plasma levels requires further investigation. We found ITI-HC3 in plasma to be down-regulated by as much as 2.1-fold in healthy smokers compared to non-smokers in our immunoblot analysis. However, ITI-HC4, which did not show significant changes in this study, has also been found to be up-regulated in lung adenocarcinoma patients compared to healthy subjects (278,279) and up-regulated in the urine of healthy smokers (254). Moreover, ITI-HC4 was also found to be down-regulated in plasma of smokers with COPD compared to smokers without COPD (280). The information pertaining to the expression of the ITI family of proteins, regarding smoking and respiratory diseases, such as COPD and lung cancer, is intriguing and thus, further large-scale studies in both target tissue and plasma are warranted to track this family of proteins in smokers that develop these diseases in order to fully grasp their potential clinical significance.

VDBP is a moderately abundant, multi-functional plasma protein predominately produced by hepatic parenchymal cells (281). As per its name, VDBP is better-known for its ability to bind to and transport vitamin D in the body. In addition, VDBP also mediates inflammatory and immunoregulatory activities in response to environmental challenges. VDBP mediates these activities by binding to vitamin D, scavenging for extracellular actin, providing

leukocyte C5a-mediated chemotaxis, activating macrophages, and stimulating osteoclasts (281). Given the diverse and physiologically important roles of VDBP, down-regulation could contribute to a variety of health concerns. In fact, its role in transporting vitamin D to the lung is very important, and consequently, loss of vitamin D in the lungs is associated with asthma, COPD, and lung cancer (282). VDBP has already gained support as a biomarker of lung adenocarcinoma development. It was discovered to be down-regulated by 1.3-fold in serum at an early stage of lung tumor growth and at advanced stages up-regulated greater than 2-fold (283). In this study, we identified VDBP to be down-regulated in the plasma of chronic cigarette smokers by as much as 3-fold with cumulative tobacco smoke exposure greater than or equal to 10 pack years.

Some of the low abundance proteins we indentified in the plasma in this study, including SHBG, GSN, and VTN, are normally present at concentrations of approximately 8.1 ng/ml, 190-300 µg/ml, and 200-400 µg/ml, respectively (267,284,285). SHBG is a plasma glycoprotein that binds with high affinity to steroid hormones, such as testosterone, to regulate their bioavailability (286). In contrast to previous studies (287-289), we observed a significant decrease in SHBG levels in smokers, and more so in those smokers whose cumulative tobacco smoke exposure was greater than or equal to 10 pack years. This discrepancy, however, warrants further investigation, as it was also suggested that after adjustment for levels of testosterone and estradiol, SHBG levels may no longer be significantly altered between cigarette smokers and non-smokers (290). GSN is produced by various tissues and exists as a cytoplasmic and excreted isoform. Similar to VDBP, GSN plays an important role as an actin scavenger in plasma during a variety of clinical situations involving cellular damage, such as necrotic cell death (285). Interestingly, cigarette smoke extract has been shown to cause necrosis of vascular endothelial cells (291). Therefore, increases in circulating GSN, as was observed in this study, could occur in order to provide protection against actin accumulation in the vasculature. We found VTN to be down-regulated in the

plasma of smokers compared to non-smokers. VTN is an adhesive glycoprotein in the extracellular matrix that is produced in the liver and by platelets, and is involved in important regulatory roles concerning cellular differentiation, proliferation, and morphogenesis. Loss of expression of this protein in plasma is often associated with liver damage (284).

Our results described in Chapter 2 encouraged us to investigate the expression of 14-3-3 protein isoforms in the plasma of chronic smokers compared to non-smokers. The 14-3-3 proteins are of particular interest provided their functionality and associations with diseases such as cancer (248); in Chapter 2, 14-3-3 isoforms θ, ε, σ, and ζ were down-regulated in NNK-induced lung adenocarcinomas (186). Previous studies have demonstrated the ability to detect various 14-3-3 isoforms such as σ and ζ in human blood (292,293). Therefore, in this study we determined their levels of expression in plasma related to smoke exposure. We were able to successfully detect both proteins and qualitatively both proteins appeared to be down-regulated in the plasma of smokers compared to non-smokers, however, statistical significance was not reached (*p*-value=0.067 for 14-3-3 σ and *p*-value=0.069 for 14-3-3 ζ). Although our sample size limited any means of significance for our data, it is of particular interest that 14-3-3 σ has been found to be down-regulated in the plasma of lung cancer patients (292) and 14-3-3 ζ has been described to be important for normal lung function (188). Given the decreased expression we observed in smokers compared to non-smokers, the down-regulation of proteins such as 14-3-3 σ and ζ may have important implications in suppressing tissue damage caused by cigarette smoking.

In summary, we identified key proteins in plasma involved in a variety of diverse biological functions, including immunity and inflammation, transportation of important regulatory biomolecules, sequestration of harmful cellular byproducts, and cellular processes, such as differentiation and proliferation that were modulated by cigarette smoking. Additional proteins with important functions not discussed in detail in the present investigation, including

apolipoproteins (APOA4, APOB, and APOE) and coagulation factors (F13A and F5), were also identified as being modulated by cigarette smoking, and thus, require further investigation. In particular, apolipoprotein levels and smoking are heavily associated with increased risk of coronary artery disease (294). We are also fully aware of the limitation posed by the number of subjects included in the current pilot study using the iTRAQ approach. Therefore, we combined two separate 8-plex iTRAQ experiments and incorporated a common pooled sample in each analysis for cross experiment comparison. As a result, we were able to compare fourteen individuals as opposed to eight and increase our statistical power. Since our primary goal was to determine the effect of smoking on protein profiles, we compared heavy smokers to age-matched non-smokers. By doing this, we further decreased the number of individuals (n=3) to analyze, but determined that this was an important factor to address. However, future molecular epidemiological studies should explore the impact of cigarette smoking on proteins identified in this pilot study with respect to gender and race in a larger sample size. Ultimately, identification of informative biomarkers in a non-invasive biological fluid, such as plasma, could prove to be beneficial in terms of early detection of tobacco-smoking related diseases.

Chapter 4

Development of a Novel Selenium-Containing Chemopreventive Agent

1. Objectives

Most chemopreventive agents, including *p*-XSC, are effective during the initiation stage of carcinogenesis (i.e. those categorized as blocking agents) and are weakly effective during the promotion/progression phases (i.e. those categorized as suppressing agents). Clearly, more effective agents are needed to target the latter phases of carcinogenesis, which may be more beneficial in the case of former smokers. Therefore, the aim of research described in this chapter was to develop more effective selenium-containing compounds targeting important molecular pathways involved in the lung carcinogenic process. Inducible nitric oxide synthase (iNOS) and its product nitric oxide (NO) are associated with lung cancer development. The sulfur-containing chemopreventive agent *S*,*S*'-(1,4-phenylenebis[1,2-ethanediyl])bisisothiourea (PBIT) was designed to target iNOS to limit NO production. Based on the benefits of selenium, we hypothesized that substitution of sulfur for selenium in the structure of PBIT would enhance the chemopreventive efficacy of the compound. Thus *in vitro* studies were performed using NSCLC cells to compare the effects of PBIT and the novel selenium–containing compound *Se*,*Se*'-(1,4-phenylenebis[1,2-ethanediyl])bisisoselenourea (*Se*-PBIT).

2. Background

2.1 <u>An introduction to nitric oxide (NO) and inducible nitric oxide synthase (iNOS)</u>

Nitric oxide (NO) is a short-lived ($t_{1/2}$=seconds), gaseous molecule with various cellular functions. In general, NO is known to act as a signaling molecule to regulate various physiological and pathophysiological processes such as cellular proliferation, angiogenesis, and

neurotransmission, and at relatively high concentrations it elicits cytoxic effects against invading pathogens (295). NO is generated from the terminal guanido nitrogen atom of L-arginine by the NADPH-dependent NO synthase (NOS) in the presence of molecular oxygen. There are three known isoforms of NOS: neuronal NOS (nNOS), endothelial NOS (eNOS), and inducible NOS (iNOS). Both nNOS and eNOS are constitutively expressed and require cytosolic calcium to produce low levels of NO. iNOS, however, is calcium independent and generates high concentrations of NO. iNOS is transcriptionally regulated and induced by inflammatory cytokines, bacterial endotoxin, hypoxia, oxidative stress, and cigarette smoking (296,297).

2.2 NO, iNOS, and lung cancer

Although NO plays a role in several essential processes, it is a highly reactive free radical that can also cause detrimental damage to cells. NO and NO metabolites such as nitrite (NO_2^-), nitrate (NO_3^-), *S*-nitrosothiols (RSNO, R denotes some organic group), and peroxynitrite (ONOO-) can produce cytotoxic and genotoxic effects by damaging DNA and protein resulting in gene mutations and loss of protein function, respectively. Such damage is thought to play an active role in carcinogenesis (145). In addition, the inherent role of NO has also been correlated to tumor progression. NO has shown the ability to stimulate tumor growth and metastasis by promoting migratory, invasive, and angiogenic properties of tumor cells (144,145).

Increased production of NO is associated with many cancers, including that of the lung, and all three NOS enzymes have been detected in several human tumors; the tissue type dictates which NOS enzyme is more prevalent, e.g. tumor vascular endothelial cells predominantly express eNOS (144,145). In lung cancer patients increased levels of NO are detectable in exhaled breath and increases in expression of iNOS are found in premalignant and malignant tissue, as well as alveolar and tumor-associated macrophages (298-301). In addition, iNOS overexpression has been observed in lung carcinomas of smokers compared to lungs of non-smokers (302). The activity of NOS, presumably iNOS, has been found to be highest in human lung adenocarinoma

compared to other histological types of lung tumors (303). Studies have suggested that the association between NO/iNOS and cancer is a result of mutagenic properties related to NO-mediated DNA damage or hindrance to DNA repair (145,304). For example, iNOS expression has been correlated with mutations of *P53* in tumors of the colon, oropharynx, and lung (305,306).

2.3 Targeting iNOS and NO expression

To develop effective cancer prevention strategies it is of paramount importance to design approaches to inhibit important mediators involved in the multi-step carcinogenesis process. Thus, provided NO and iNOS have a role in lung cancer development, strategies to inhibit these molecules warrant investigation. Ideally, inhibition of iNOS expression and/or activity should reduce NO production. In support of this, in a urethane-induced mouse lung tumorigenesis model, mice deficient for iNOS expression (i.e. iNOS knockouts (-/-)) exhibited an 80-87% reduction in tumor multiplicity compared to carcinogen-treated iNOS (+/+) controls (307,308). This was due, in part, to a decrease in angiogenesis as indicated by lower levels of vascular endothelial growth factor (VEGF) in tumors isolated from iNOS (-/-) mice; prior assays showed both iNOS and VEGF increased in tumors relative to surrounding tissue in wild-type mice (307). Furthermore, down-regulation of iNOS expression by the natural compound silibinin has demonstrated efficacy in lung cancer chemoprevention studies (308).

Efforts to target iNOS specifically, and thus NO production, have also led to the design of structural inhibitors of the enzyme itself. Many early inhibitors were amino acid analogs of the substrate L-arginine (Figure 4.1) such as L-Nitroarginine (L-NA) (309) designed to target the active site of NOS (310). L-NA was, however, specific and very potent for nNOS (309). Non-amino acid analogs of L-arginine were later designed such as aminoguanidine (Figure 4.1) (311) and alkylgaunidine (312) that showed selectivity towards iNOS, however, their potency was weak. Garvey et al. designed a series of structural isothiourea compounds to target human NOSs

and found that the bisisothiourea *S*,*S*'-(1,4-phenylenebis[1,2-ethanediyl])bisisothiourea (PBIT, Figure 4.1) was a potent selective inhibitor of iNOS (310). The selectivity of PBIT for iNOS was confirmed in cytokine-induced colorectal adenocarcinoma cells (310,313). PBIT has structural similarity to the guanidine and L-arginine (Figure 4.1) and is proposed to bind in the guanidinium portion of the active site of iNOS via the *S*-atom and its constituents (310).

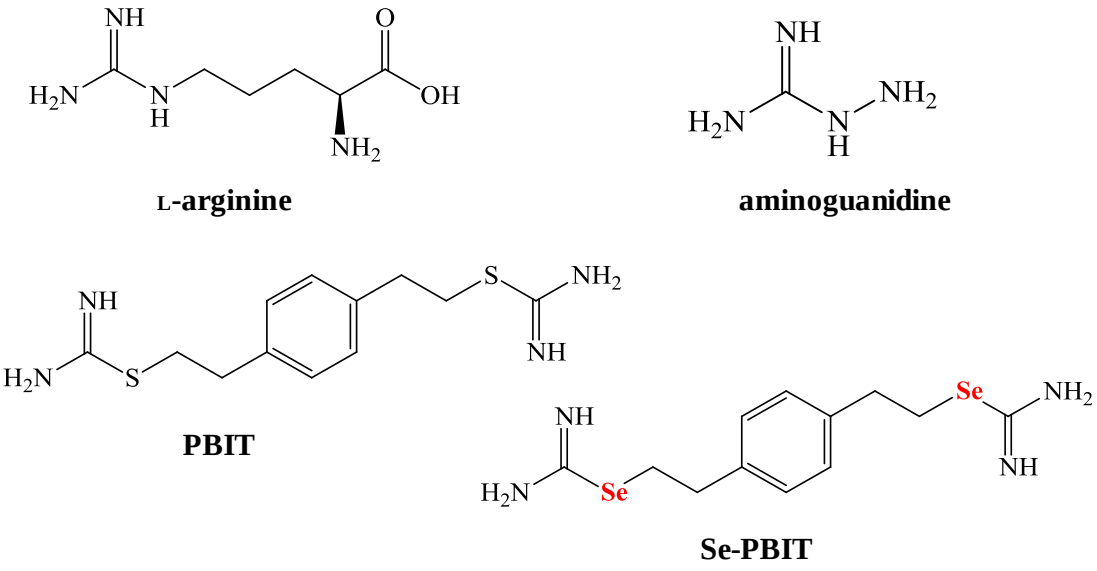

Figure 4.1 Structures of L-arginine, aminoguanidine, PBIT, and *Se*-PBIT.

The efficacy of PBIT as a chemopreventive agent to inhibit tumor development has been demonstrated in various rodent models (314,315). Chen et al. used PBIT to inhibit esophageal tumor progression (314), whereas Rao et al used PBIT to inhibit azoxymethane-induced colonic aberrant crypt foci (315). However, due to concerns such as toxicity and cellular uptake, its use in a clinical setting has been hampered (310).

As discussed in Chapter 1, our laboratory focuses on the discovery of novel selenium-containing agents that have enhanced chemopreventive efficacy, low toxicity, and can target pathways involved in the multi-step process of carcinogenesis. Our previous studies have

demonstrated that selenium substitution of sulfur-containing compounds results in more effective chemopreventive analogs (125). Of interest, is the fact that the structural makeup of PBIT is such that it contains two *S*-atoms that can be replaced with *Se*-atoms (Figure 4.1). Synthesis of the selenium analog of PBIT *Se*,*Se*'-(1,4-phenylenebis[1,2-ethanediyl])bisisoselenourea (*Se*-PBIT) was accomplished and studies thus far, have demonstrated enhanced chemopreventive efficacy against skin and colon cancer development compared to PBIT (316,317). Moreover, Desai et al. also demonstrated inhibiton of cell growth in a NSCLC cell line (317). However, the mechanisms that can account for the protective effect of *Se*-PBIT require further investigation.

3. Rationale

The primary approach to curb the lung cancer epidemic is focusing on the prevention of smoking initiation and smoking cessation. A plausible secondary approach is chemoprevention; however, there are no such agents available in the clinic for lung cancer (97,122). Based on epidemiological, preclinical, and some clinical research, selenium appears to provide some protection against cancer, including that of the lung (123,125-127). Investigations in our laboratory, as well as others, have indicated that both the dose and form in which selenium is present is an integral factor for its chemopreventive efficacy (126,134). *p*-XSC, developed in our laboratory and utilized in Chapter 2, is a potent agent against preclinical tobacco-carcinogen induced lung cancer (139,169,170); however, its effect is most notable during the initiation phases of development. In the case of a former smoker where extensive damage due to smoking is already present, such an agent may not provide protection against the latter phases of lung carcinogenesis, i.e. promotion/progression phases. Therefore, agents targeting known mechanisms involved in the carcinogenic process are needed. PBIT is a selective inhibitor of iNOS (310), and consequently NO production, both of which are associated with lung cancer (144,145,298). By substituting selenium for sulfur in the structure of PBIT we aimed to develop a novel selenium-containing chemopreventive agent. *Se*-PBIT has demonstrated efficacy against

cancers of the skin and colon (316,317). We compared the effects of *Se*-PBIT with PBIT in NSCLC cells against NO production and various cellular activities including proliferation, apoptosis, and cell-cycle control. Furthermore, to compare the effects of selenium-containing compounds to each other, we incorporated *p*-XSC into select bioassays.

4. Experimental design

4.1 Reagents and cell lines

Human NSCLC cells (NCI-H460 and A549) and normal human lung fibroblast cells (MRC-5) were obtained from the American Type Culture Collection (ATCC; Manassas, VA). The synthesis of PBIT and *Se*-PBIT shown in Figure 4.2 was described previously (310,316,317). All reagents and starting materials were of analytical grade and were obtained from Sigma-Aldrich. Briefly, methyl 1,4-phenylenediacetic acid (A) was reduced with lithium aluminum hydride ($LiAlH_4$) to produce 1,4-phenylenediethanol (B). Upon bromination with carbon tetrabromide (CBr_4) and triphenylphospine (PPh_3), compound (B) was converted to the dibromo compound 1,4-di(2-bromoethyl) benzene (C). Finally, to generate PBIT or *Se*-PBIT, compound (C) was reacted with thiourea (NH_2CSNH_2) or selenourea (NH_2CSeNH_2). The spectral and chromatographic characteristics of both compounds were in agreement with those reported in the literature (310,316,317). *p*-XSC was prepared in house as reported previously (177). Reagents for immunoblot assays were purchased from Bio-Rad Laboratories. Primary and secondary antibodies were purchased from Cayman Chemicals (Ann Arbor, MI), Cell Signaling, and Santa Cruz Biotechnology. Chemiluminescent immunodetection reagents and autoradiography films were purchased from GE Healthcare and Imaging Resources, Inc., respectively.

4.2 Treament of human NSCLC and normal lung cells with PBIT and *Se*-PBIT

Human NSCLC lung cancer cell lines (NCI-H460 and A549) were maintained in Roswell Park Memorial Institute (RPMI-1640) medium, which contained 2 mM L-glutamine, 1.5 g/L

sodium bicarbonate, 4.5 g/L glucose, 10 mM HEPES, and 1.0 mM sodium pyruvate (ATCC), supplemented with 1% penicillin/streptomycin (100 units/mL each) and 10% fetal bovine serum (FBS). Normal human lung fibroblast cells were maintained in Eagle's Minimum Essential Medium (EMEM; ATCC) with 1% penicillin/streptomycin (100 units/mL each) and 10% FBS.

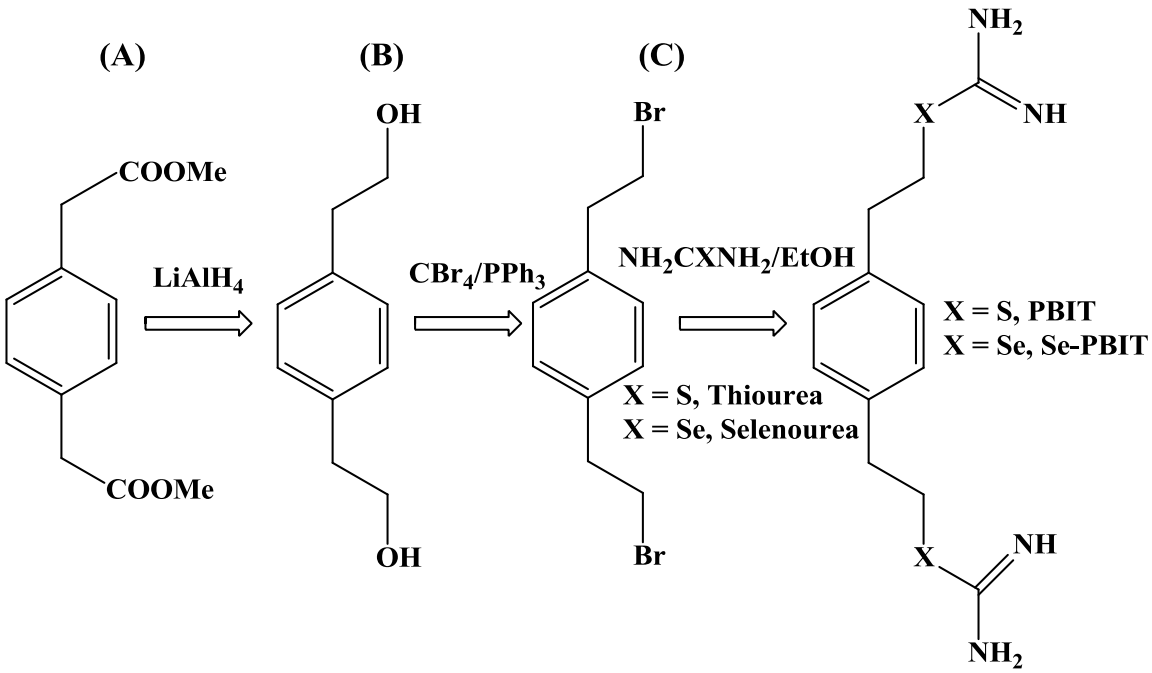

Figure 4.2 General scheme for synthesis of PBIT and *Se*-PBIT. Figure was published in reference (318).

Cells were maintained in 10 cm dishes in a humidified environment at 37°C with 5% CO_2 and were routinely passaged when they reached 70-80% confluency. To remove adherent cells, cells were incubated with 0.05-0.25% Trypsin-EDTA (Invitrogen) for 2-3 minutes.

Stock solutions of PBIT and *Se*-PBIT were prepared from lyophilized forms by resuspension in Milli-Q H_2O and stored at 4°C. Cells were treated with various concentrations of PBIT and *Se*-PBIT ranging from 1 μM to 20 μM in the cell culture medium for 24 hrs. Control cultures were treated with a corresponding volume of H_2O (up to 15 μl) and processed similarly. For enhancement of iNOS expression, cells were pretreated with a cytomix containing 10 ng/ml

interleukin-1β (IL-1β), 10 ng/ml tumor necrosis factor-α (TNF-α) and 100 ng/ml interferon-γ (IFN-γ) that was procured from Sigma-Aldrich and starved of FBS for 24 hrs. For comparsion of selenium-containing compounds, *p*-XSC was introduced in various bioassays. *p*-XSC stock solutions were prepared from a lyophilized form by resuspension in dimethyl sulfoxide **(**DMSO; Me_2SO) and stored at 4^oC. Cells were treated with *p*-XSC at concentrations of 1.25, 2.5, and 5 μM in the cell culture medium for 24 hrs. Control cultures were treated with a corresponding volume of DMSO (up to 15 μl) and processed similarly.

4.3 Measurement of NO production in NSCLC cells

We used a colorimetric assay using the Griess Reagent from Calbiochem (Darmstadt, Germany) to quantify the production of NO following treatment of cells. The assay detects the presence of only NO_2^- (in aqueous solutions NO is rapidly converted to NO_2^- and NO_3^-) using a diazotization reaction that was first described by Peter Griess (319). In this reaction sulfanilamide is converted to a deep purple azo compound in the presence of NO_2^- and *N*-(1-naphthyl)ethylenediamine dihydrochloride (NED) (Figure 4.3).

Viable (as determined by exclusion of trypan blue stain, Sigma-Aldrich) NCI-H460 and A549 cells were counted with a hemacytometer and plated in triplicate for each treatment dose at 10,000 cells/well in a 96-well plate. The cells were allowed to grow for 24 hrs and afterwards, treated with 1.0, 5.0, or 10.0 μM of PBIT or *Se*-PBIT in complete media for 24 hrs. Following treatment, the media was assayed for total NO_2^- by incubating the samples in the presence of nitrate reductase enzyme and NADPH for 20 min; to obtain an accurate measurement of total NO, both NO_2^- and NO_3^- should be measured, therefore, NO_3^- needs to be converted to NO_2^- with the NADH-dependent nitrate reductase enzyme. Sulfanilamide and NED were then added and upon reaction with NO_2^- generated the azo compound that was measured spectrophotometrically at 540 nm in a SPECTRAmax® PLUS^{384} plate reader (Molecular Devices Corporation, Sunnyvale, CA); higher absorbance values correspond to higher levels of NO_2^- in samples. Sample NO

measurements were based on a standard linear curve that was constructed by using various concentrations of standard NO_2^- supplied by the manufacturer (Figure 4.4). Contributing NO_2^- present in the media was subtracted from the samples and final values were presented as total µM of NO_2^-.

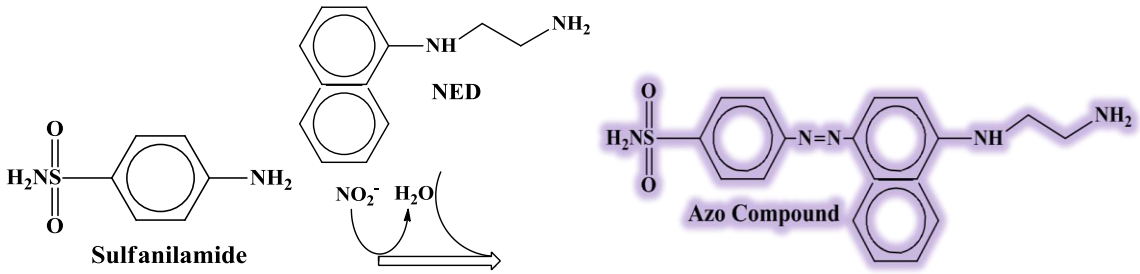

Figure 4.3 Principle concept of Griess reaction used to detect levels of total NO from NO_2^-.

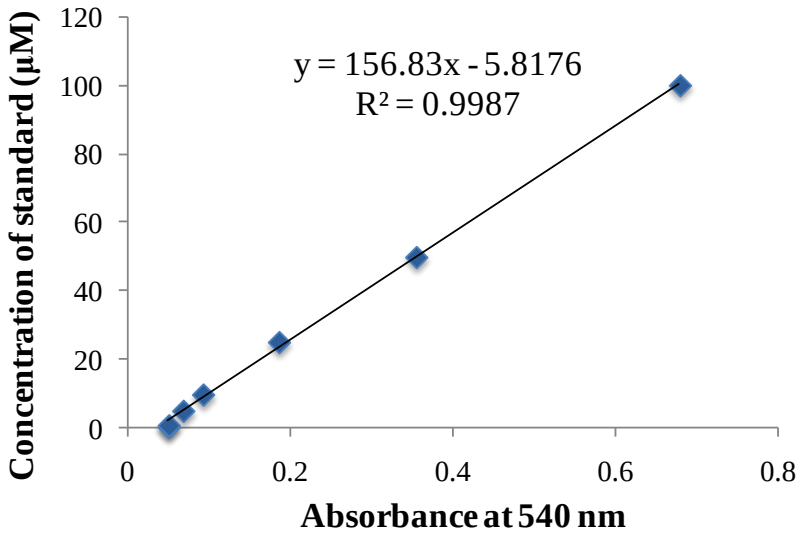

Figure 4.4 Standard curve for quantitation of NO production from samples. The standard curve was constructed using various concentrations of NO_2^-.

4.4 Assessment of cell viability by mitochondrial activity

The viability of NCI-H460, A549, and MRC-5 cells following treatments were assessed by a standard colorimetric assay using the compound MTT (3-(4,5-dimethylthiazol-2-yl)-2,5-diphenyltetrazolium bromide) (Sigma-Aldrich). MTT is a yellow tetrazolium salt that can be reduced to the purple formazan product (Figure 4.5) by mitochondrial dehydrogenase enzymes in active, hence viable, cells (320).

All viable cells (as determined by exclusion of trypan blue stain) were counted with a hemacytometer and plated in triplicate for each treatment dose at 10,000 cells/well in a 96-well plate. The cells were allowed to grow for 24 hrs and afterwards, treated with 1.25, 2.5, or 5.0 μM of PBIT or *Se*-PBIT in complete media for 24 hrs; NSCLC cells were also treated with *p*-XSC to compare with *Se*-PBIT. Following treatment, the media was aspirated and MTT (50 μg/100 μl) was prepared in PBS and added to the cells for 4 hrs at 37°C in the dark. The MTT was then aspirated and 100 μl of DMSO was added to each well and skaken to solubilize the purple formazan. Absorbance values at 570 nm were read in a SPECTRAmax® PLUS[384] plate reader; higher absorbance values indicate an increase in cell viability, and conversely, lower absorbance values indicate a reduction in cell viability. The mean of three values was determined and the results were expressed as percent of control.

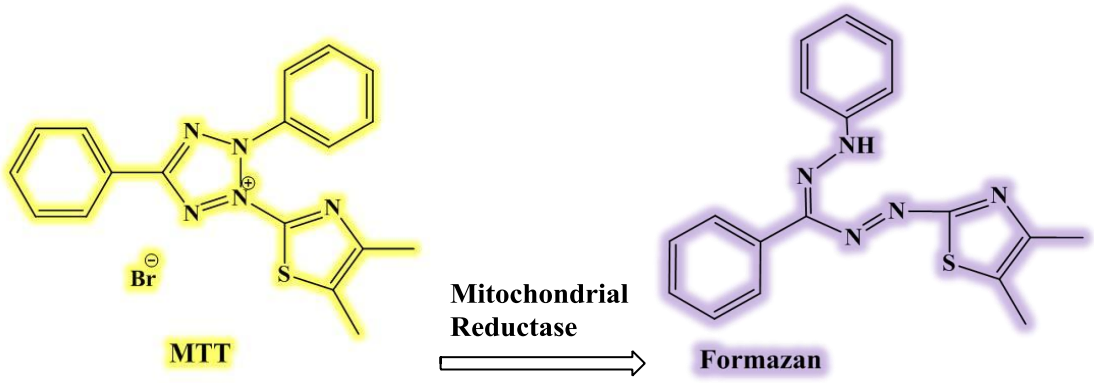

Figure 4.5 Principle concept of MTT assay to detect cell viability. MTT is converted to formazan by active mitochondrial reductases.

4.5 Analysis of cellular apoptosis

Eukaryotic cell death occurs in two ways: necrosis and apoptosis. Necrosis is a traumatic form of cell death that can be harmful, whereas apoptosis is a programmed death that is strategically carried out to end the life cycle of a cell. The process of apoptosis can be characterized in a variety of ways that include induction of proteases (e.g. caspases), membrane blebbing, and DNA fragmentation. DNA fragmentation is caused by endogenous endonucleases that cleave DNA at accessible internucleosomal linker regions not protected by histones. This results in the formation of mono- and oligonucleosomes heavily complexed with histones such as H1, H2A, H2B, H3, and H4 (321).

In this investigation, we chose to analyze apoptotic activity in NCI-H460 and A549 cells by detecting the formation of mono- and oligonucleosomes using the Roche Cell Death Detection ELISA (Indianapolis, IN). This assay is colorimetric and is based on the quantitative sandwich-enzyme-immnunoassay principle using mouse monoclonal antibodies directed against DNA and histones, including those mentioned above. In the first part of the assay, a microplate is prepared by coating the walls of the wells with anti-histone, followed by blocking of non-specific sites. Sample lysates containing nucleosomes are then added and the histone regions bind to the immobilized anti-histone antibodies. Next, an anti-DNA-peroxidase (horseradish peroxidase) conjugate is added to react with the DNA regions of the nucleosomes and unbound material is washed away. Finally, a substrate for peroxidase, ABTS (2,2'-azino-di-(3-ethylbenzthiazoline sulfonate)), is added to determine the amount of peroxidase present (Figure 4.6).

All viable cells (as determined by exclusion of trypan blue stain) were counted with a hemacytometer and plated in triplicate for each treatment dose at 50,000 cells/well in a 96-well plate. The cells were allowed to grow for 24 hrs and afterwards, treated with 1.0, 2.5, or 5.0 μM of PBIT or *Se*-PBIT in complete media for 24 hrs; NCI-H460 cells were also treated with *p*-XSC to compare with Se-PBIT. Following treatment, the cells were assayed for mono- and

oligonucleosomes according to the manufacturer's instructions. Sample absorbances were read at 410 nm in a SPECTRAmax® PLUS^{384} plate reader. The results were presented as an enrichment factor (ratio of treatment over control) of mono- and oligonucleosomes released into the cytoplasm.

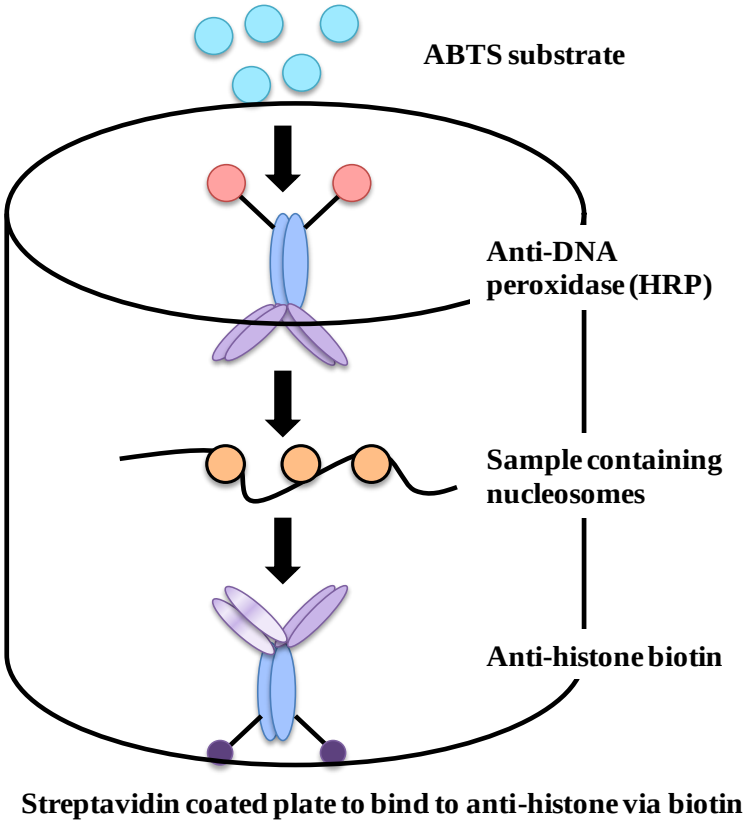

Figure 4.6 Principle concept of cell death detection sandwich ELISA in microplate format.

4.6 Cell cycle analysis by flow cytometry

Fluorescence-activated cell sorting (FACS) is a well-established flow cytometry-based laboratory procedure used to differentiate cells based on surface antigens, as well as in measuring DNA content to analyze the distribution of cells in the various phases of the cell cycle. To measure DNA content, cells are stained with intercalating agents such as propidium iodide (PI). PI intercalates into only double-stranded nucleic acids and fluoresces red when excited at 488 nm wavelength of light; when staining with PI it is important to use the enzyme ribonuclease A

(RNaseA) to degrade double-stranded RNA, so only double-stranded DNA is available for PI. Beginning from the G1 phase of the cell cycle and moving into the S phase, at which point DNA synthesis occurs, and finally ending at the G2 phase, before mitosis (M phase), the amount of DNA in a cell is doubled. Thus, double stranded DNA content varies and is dependent on what phase of the cell cycle the cell is in. Upon certain stress, cells can undergo senescence at any of these stages. As a result, the measurement of DNA content can provide an estimate of each phase of the cell cycle (Figure 4.7) (322).

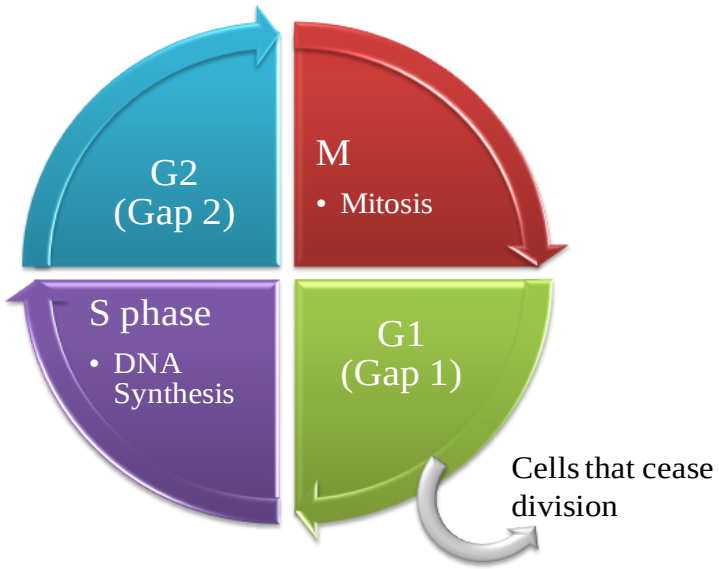

Figure 4.7 Eukaryotic cell cycle. NOTE: sizes of phases in figure are not proportional to time normally alloted in each phase.

Viable (as determined by exclusion of trypan blue stain) NCI-H460 and A549 cells were counted with a hemacytometer and plated at 500,000 cells/well in a 6-well plate and incubated for 24 hrs in RPMI-1640 medium containing 1% penicillin/streptomycin without FBS at 37^{o}C in 5% CO_2 for synchronization of the cell cycle. After cells were synchronized, they were treated for 24 hrs with PBIT or *Se*-PBIT at concentrations of 1.25, 2.5, or 5.0 μM; NSCLC cells were also

treated with *p*-XSC at similar concentrations to compare with *Se*-PBIT. The treatments were added to medium containing 10% FBS. After treatment, cells were harvested by scraping with a cell scraper (Sarstedt, Newton, NC), centrifuged at 5^{o}C for 3 min at 350 x g, and washed once with cold PBS. The cells were then fixed by adding 1 mL of cold (-20^{o}C) 70% ethanol, dropwise, while vortexing and placed at -20^{o}C. To stain with PI, cells were first pelleted by centrifugation at 5^{o}C for 3 min at 350 x g and then resuspended with 1 ml of hypotonic DNA staining buffer containing 100 μg/ml PI, 200 μg/ml RNase A, 0.1% sodium citrate, and 0.3% triton-X 100, followed by vortexing. The stained cells were then incubated at 4^{o}C for approximately 1 hr in the dark. Stained cells were then analyzed by flow cytometry in the Penn State Hershey Flow Cytometry Core Facility on a Becton Dickinson FACScan (Franklin Lakes, NJ). For each sample, 15,000 events were viewed, collected, and analyzed for cell-cycle distribution. Percentage of cells in G0/G1, S, and G2/M phases were determined using ModFit LT™ software (Verity Software House, Topsham, ME).

4.7 Immunoblot analysis to determine expression of molecular markers

We performed immunoblot analysis to determine the effect of PBIT and *Se*-PBIT on important molecular markers involved in known cellular activities related to lung carcinogenesis. NCI-H460 and A549 cells were grown to 50-60% confluency in 10 cm dishes, followed by treatment with PBIT and *Se*-PBIT for 24 hours at doses of 5.0, 10.0, and 20.0 μM. Cells were harvested by scrapping with a cell scraper and washed with PBS. To isolate cellular proteins, cells were lysed in standard cell lysis buffer (Cell Signaling) and freshly added 1mM PMSF overnight at 4^{o}C after vortexing. Protein was collected following centrifugation at 14,000 x g for 10 min at 4^{o}C and concentrations were determined using the Bio-Rad Protein Assay Dye Reagent Concentrate (Bio-Rad Laboratories). For each sample, 40 μg of total protein was denatured and resolved on a 12% or 15% SDS-PAGE gel and transferred to a nitrocellulose membrane. Equal amounts of protein (30 μg) were separated on 10% SDS-PAGE gels (100 V for 120 min) and

transferred to nitrocellulose membranes (100 V for 65 min) (Amersham Biosciences). Membranes were blocked with 5% non-fat dry milk in TBS containing 0.5% T20 overnight at 4°C. To probe for proteins of interest, membranes were cut according to the molecular weight of the proteins. The following antibodies, diluted in 0.5% non-fat dry milk in TBS-T20, were used: anti-iNOS (1:500) and anti-COX-2 (1:500) from Cayman Chemicals, anti-p53 (1:500), anti-p27 (1:500), anti-p21 (1:500), anti-cPLA2 (1:500), and anti-β-actin (1:2000) from Santa Cruz, and anti-p38 (1:1000) and anti-cleaved poly (ADP-ribose) polymerase (PARP, 1:1000) from Cell Signaling. Following incubation with primary antibodies overnight at 4°C (for anti-β-actin, 1 hr at room temperature), membranes were washed 3x with TBS-T20 and corresponding secondary antibodies conjugated to HRP were added at a 1:2000 dilution in 0.5% bovine serum albumin in TBS-T20. Membranes were again washed 3x with TBS-T20 and bands were detected using ECL (GE Healthcare) and developed with autoradiography film (Imaging Resources, Inc). For densitometric analysis, films were scanned using Bio-Rad's GS800 Calibrated Densitometer. Quantitation of protein levels was carried out using the Quantity One v4.5.0 1-D Analysis Software (Bio-Rad Laboratories) and normalized to β-actin levels.

4.8 Statistical analysis

Experiments were performed at least three times. Data for iNOS protein expression, NO production, cell growth inhibition, and induction of apoptosis were presented as average of results under given conditions and expressed as mean ± SE. Statistical comparisons between cells treated with PBIT or *Se*-PBIT or *p*-XSC versus control were based on Student's *t* test. Significant differences were considered at a $p<0.05$.

5. Results

5.1 The effect of PBIT and *Se*-PBIT on iNOS and NO production in A549 cells

Based on the selective activity of PBIT towards iNOS, we first investigated the effects of both PBIT and *Se*-PBIT on iNOS by immunoblot and production of NO by detection of total NO_2^- (Figure 4.8). Treatment with 5 μM PBIT did not inhibit the expression of iNOS compared to control treatment (Figure 4.8A). However, at doses of 10 and 20 μM, PBIT was able to significantly inhibit expression of iNOS (Figure 4.8A and B). Treatment with all doses of *Se*-PBIT (5, 10, and 20 μM) significantly inhibited the expression of iNOS (Figure 4.8A and B). The activity of iNOS, as measured by NO production, indicated that PBIT inhibited NO levels at all doses employed (1, 5, and 10 μM); however, under these experimental conditions the results were not significant (Figure 4.8C). *Se*-PBIT inhibited NO at similar doses to those of PBIT and at a concentration of 10 μM demonstrated a significant difference in reduction of NO production compared to control levels (Figure 4.8C). These results show that PBIT and *Se*-PBIT can inhibit the expression of iNOS, but are, however, weak inhibitors of NO production in A549 NSCLC cells.

5.2 The effect of PBIT and *Se*-PBIT on cell viability

We investigated the effects of PBIT and *Se*-PBIT at doses of 1.25, 2.5, and 5.0 μM on cell viability by MTT assay after 24 hr of treatment; 2.5 to 5.0 is the physiological level of selenium (128,323,324). In both NCI-H460 and A549 cells, PBIT at all doses tested did not inhibit cell viability (Figure 4.9A and B). Conversely, *Se*-PBIT significantly inhibited cell viability in NCI-H460 cells at all doses with a half maximal inhibitory concentration (defined as the concentration needed to inhibit 50% of a biological response, e.g. cell viability; IC_{50}) of 3.0 μM (Figure 4.9A) and in A549 cells at 2.5 and 5.0 μM with an IC_{50} of 2.5 μM (Figure 4.9B). In normal lung fibroblasts (MRC-5), PBIT and *Se*-PBIT had no effect on cell viability at the doses

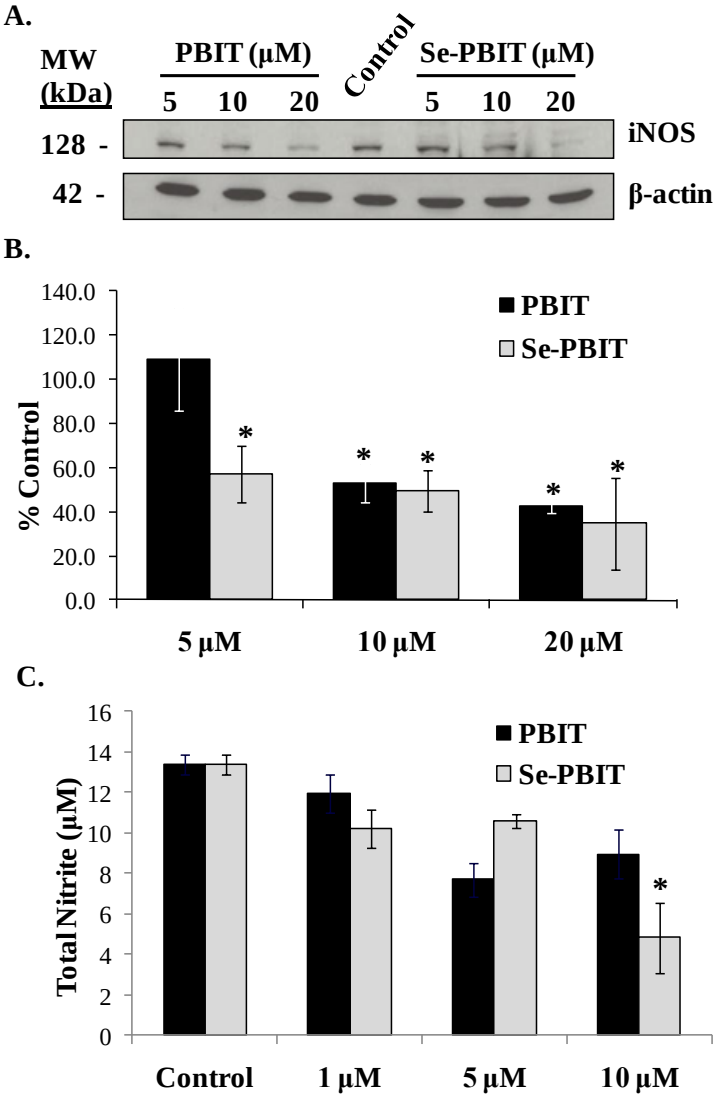

Figure 4.8 The effect of PBIT and *Se*-PBIT on iNOS protein expression and NO production in A549 cells. Cells were pretreated with cytomix (10 ng/ml IL-1β, 10 ng/ml TNF-α, and 100 ng/ml IFN-γ) and starved of FBS for 24 hr before treatment. Cells were then treated with PBIT or *Se*-PBIT at concentrations of 1, 5, 10, or 20 μM for 24 hr. (A) Representative immunoblot of iNOS protein expression after treatment; lane 4, Control, is iNOS protein expression from total cell protein lysate from A549 cells that were not treated with any compound. (B) *iNOS Protein Expression*: iNOS protein band densities were obtained by densitometric measurement from three separate immunoblot analyses. After normalizing to β-actin, PBIT- and *Se*-PBIT-treated cells were compared to non-treated (control) cells. (C) *iNOS Activity*: NO_2^- levels from three separate treatment experiments were obtained and compared to non-treated cells. Data are presented as mean ± SE. **p*<0.05 (Student's *t* test). Data were published in reference (318).

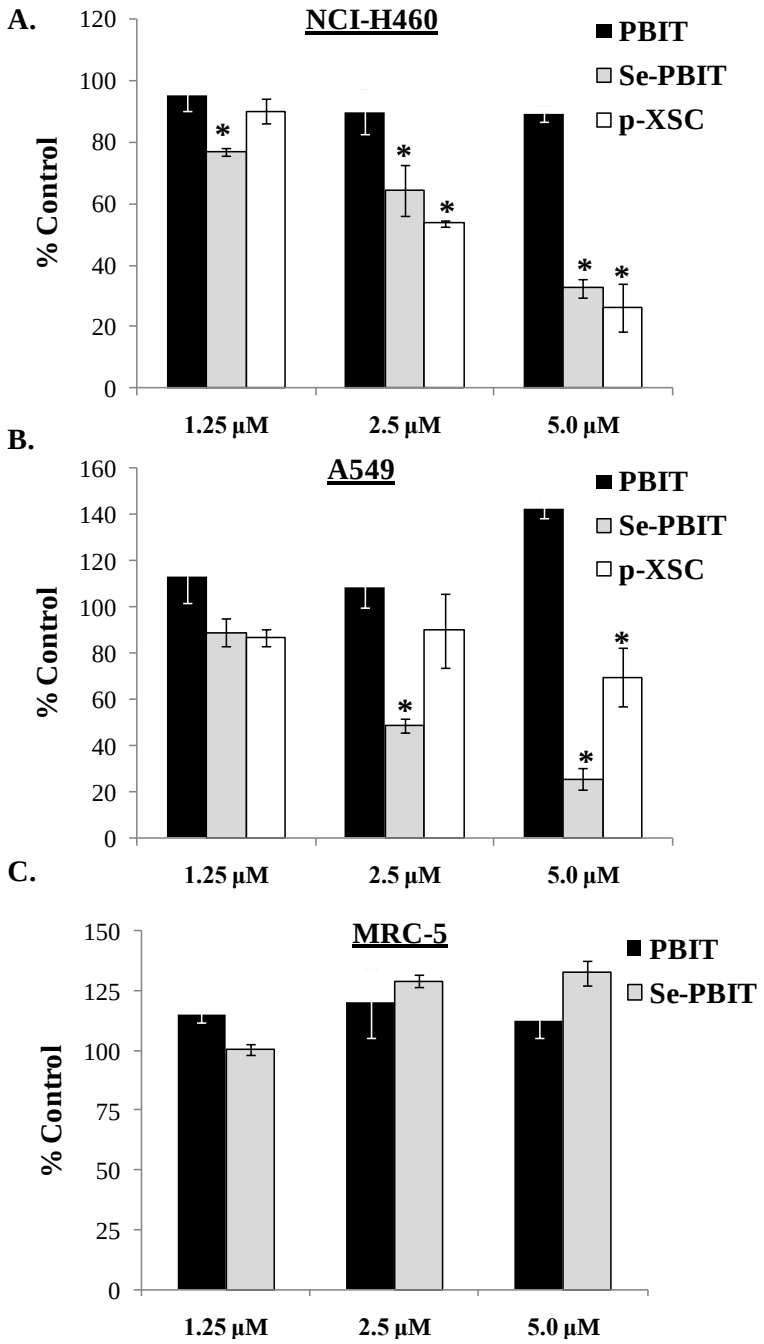

Figure 4.9 The effect of PBIT, *Se*-PBIT, and *p*-XSC on cell viability after 24 hr of treatment as determined by MTT assay. Cells (NSCLC cells NCI-H460 (A) and A549 (B) and normal lung fibroblast cells MRC-5 (C)) were treated with 1.25, 2.5 and 5.0 µM of PBIT, *Se*-PBIT, or *p*-XSC. Absorbances were obtained at 570 nm and percentage of control was quantified from three independent experiments performed in triplicate. Data are presented as mean ± SE. *$p<0.05$ (Student's *t* test). Data were published in reference (318).

tested (Figure 4.9C). By comparison, *p*-XSC was equally effective in inhibiting cell viability in NCI-H460 cells. However, in A549 cells *Se*-PBIT was more effective than *p*-XSC. *p*-XSC only significantly reduced (30%) cell viability at the highest dose (5.0 μM) tested, whereas *Se*-PBIT caused a significant reduction (50%) in cell viability at half the dose of *p*-XSC (2.5 μM). This suggests that selenium in the form of *Se*-PBIT compared to *p*-XSC is a better inhibitor of cell viability in NSCLC cells.

5.3 The effect of PBIT and *Se*-PBIT on induction of apoptosis in NSCLC cells

Based on reduction in cell viability by *Se*-PBIT in NSCLC cells, we also determined whether this was accompanied by a subsequent increase in apoptosis. We therefore, investigated the effects of PBIT and *Se*-PBIT at doses of 1.0, 2.5, and 5.0 μM on induction of apoptosis in NSCLC cells by quantifiying the levels mono- and oligonucleosomes using the Roche Cell Death Detection ELISA. In both cell lines, NCI-H460 and A549, PBIT at all doses tested did not induce apoptosis (Figure 4.10A and B). Conversely, *Se*-PBIT significantly induced apoptosis in NCI-H460 cells at all doses tested with a near seven-fold increase in apoptotic index at a dose of 5.0 μM (Figure 4.10A). Similarly, in A549 cells, *Se*-PBIT was equally effective with a greater than nine-fold increase in apoptotic index at a dose of 5.0 μM (Figure 4.10B). By comparison *p*-XSC was unable to significantly induce apoptosis with the doses tested under these experimental conditions in NCI-H460 cells; however, previous studies have demonstrated a two-fold increase in apoptotic index at doses of 2.5 and 5.0 μM *p*-XSC (142). Furthermore, apoptotic activity by *Se*-PBIT was confirmed by immunoblot detection of the 89 kDa cleavage product of PARP; during apoptosis, PARP is cleaved by caspases into 24 kDa and 89 kDa fragments. At doses of 5, 10, and 20 μM *Se*-PBIT, a strong band for the 89 kDa fragment of PARP was detected in both NCI-H460 and A549 cells (Figure 4.10C). These results show that *Se*-PBIT is a superior inducer of apoptosis.

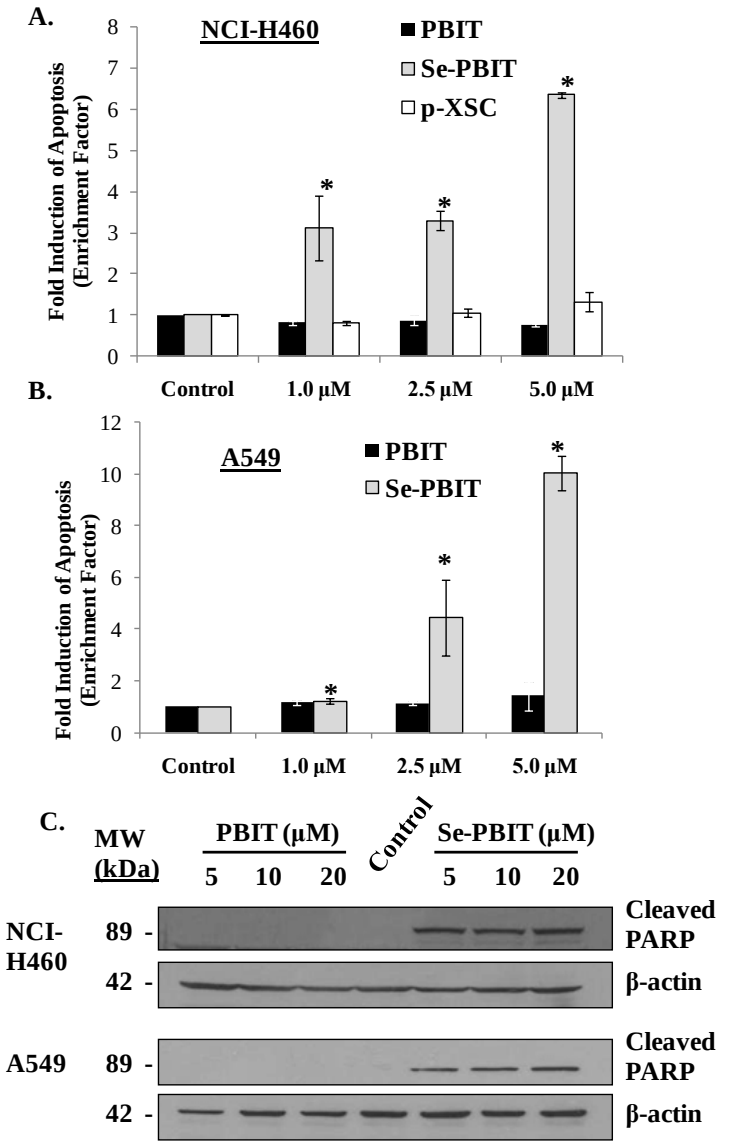

Figure 4.10 The effect of PBIT and *Se*-PBIT on induction of apoptosis in NSCLC cell lines as determined by Cell Death Detection ELISA and cleaved PARP analysis. For Cell Death Detection ELISA (A and B), cells (NCI-H460 and A549) were treated with 1.0, 2.5, or 5.0 µM PBIT or *Se*-PBIT for 24 hr; NCI-H460 cells were also treated with *p*-XSC. Percentages of apoptotic cells were quantitated from three independent experiments. The assay was performed in triplicate and the results are presented as fold induction of apoptosis (i.e. enrichment factor, ratio of treatment over control). For cleaved PARP analysis (C), cells were treated with 5, 10, or 20 µM PBIT or *Se*-PBIT for 24 hr. β-actin was used to show accurate protein loading. Data are presented as mean ± SE. **p*<0.05 (Student's *t* test) as compared with untreated controls. Data were published in reference (318).

5.4 The effect of PBIT and *Se*-PBIT on the cell cycle in NSCLC cells

Using FACS analysis, we investigated the effects of PBIT and *Se*-PBIT at doses of 1.25, 2.5, and 5.0 μM on the various phases of the cell cycle in NSCLC cells (NCI-H460 and A549). In NCI-H460 cells, PBIT had no effect on altering the percentage of cells in G1, S, or G2 phases of the cell cycle. The phase distribution was very similar to that of untreated cells (Figure 4.11A). Conversely, *Se*-PBIT, starting at a dose of 1.25 μM, caused an increase in the number of cells in the G1 phase, from 43% in untreated cells to 60% in cells treated with 1.25 μM *Se*-PBIT (Figure 4.11A). Subsequently, the number of cells in the S phase diminished rapidly and at an increasing concentration of *Se*-PBIT, the number of cells in the G2 phase increased from 23% in cells treated with 1.25 μM *Se*-PBIT to 42% in cells treated with 5.0 μM *Se*-PBIT compared to 14% in untreated cells (Figure 4.11A). In A549 cells, PBIT altered the cell cycle distribution slightly, but no consistent trend was observed (Figure 4.11B). *Se*-PBIT, however, caused an increase in the number of A549 cells in the G1 phase, from 36% in untreated cells to 78% in cells treated with 1.25 μM *Se*-PBIT (Figure 4.11B). This was also accompanied by a large loss of cells in the S phase, and however, only a slight increase in cells in the G2 phase (Figure 4.11B). These results demonstrate the ability of *Se*-PBIT to arrest NSCLC cells in the cell cycle phase. By comparison, *p*-XSC caused an increase in the number of cells in the G1 phase in both NSCLC cell lines; however, not to the extent observed in cells treated with *Se*-PBIT. In NCI-H460 cells, the number of cells in G1 increased from 43% in cells treated with DMSO to 50% in cells treated with 5 μm *p*-XSC and in A549 cells, an increase from 32% in cells treated with DMSO to 53% in cells treated with 2.5 μm *p*-XSC.

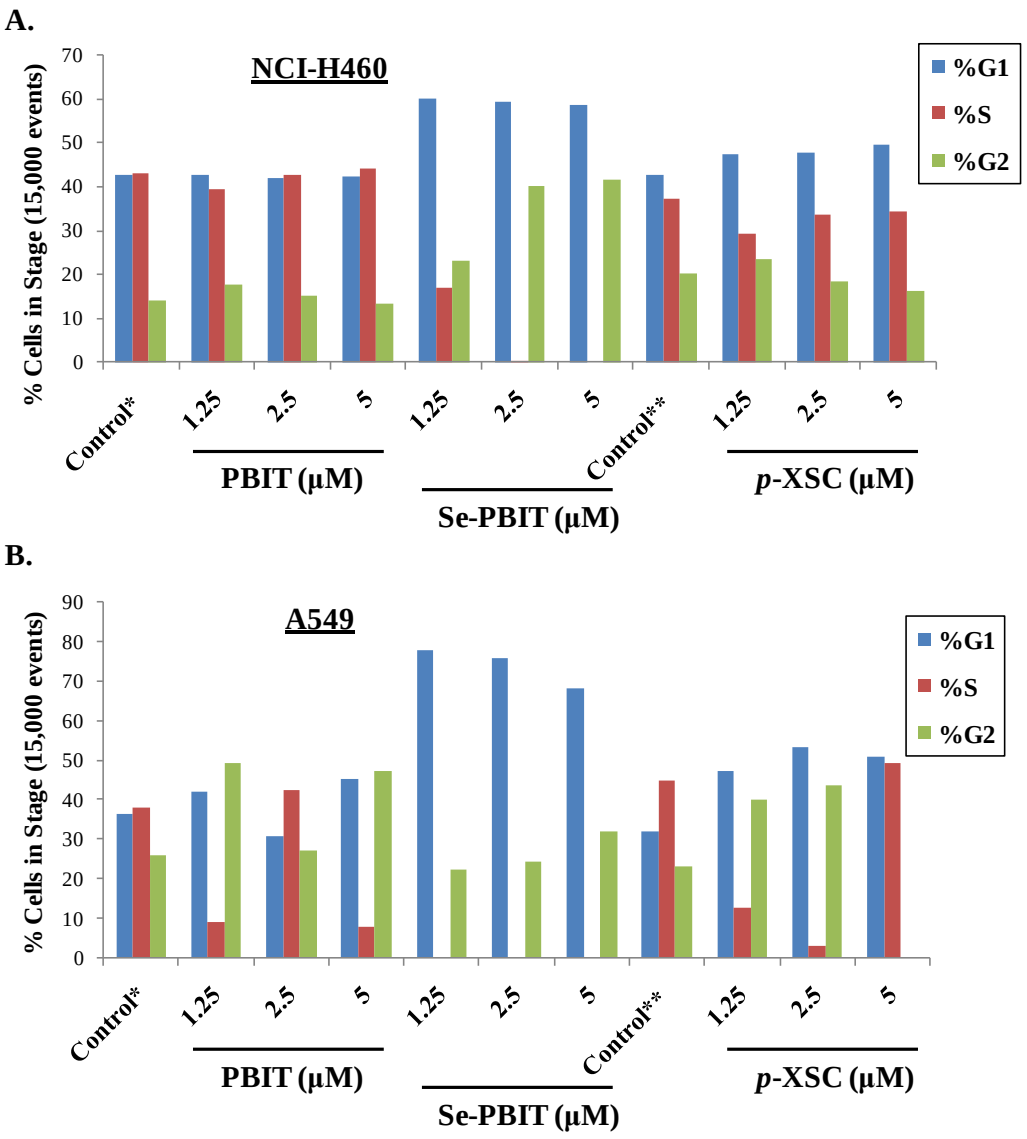

Figure 4.11 The effect of PBIT, *Se*-PBIT, and *p*-XSC on FACS cell cycle analysis in NSCLC cells. Cells (NCI-H460 (A) and A549 (B)) were treated for 24 hr at doses of 1.25, 2.5, and 5.0 μM. Control*, Milli-Q H_2O; Control**, DMSO. Data were published in reference (318).

5.5 The effect of PBIT and *Se*-PBIT on modulation of molecular markers

We investigated the effects of PBIT and *Se*-PBIT at 5, 10, and 20 μM doses on protein modulation in the NSCLC cell line A549 by immunoblot after 24 hr treatment. Proteins previously known to have a role in cellular proliferation, apoptosis, and/or lung carcinogenesis

were selected; these include cytosolic phospholipase A2 (cPLA2), cyclooxygenase-2 (COX-2), p53, p38, p27, and p21. Under the experimental conditions, PBIT had no apparent effect on any of the selected molecular markers in A549 cells (Figure 4.12). *Se*-PBIT at high doses of 10 and 20 μM, caused a reduction in cPLA2 expression and an increase in p53; no effect was observed on COX-2 expression (Figure 4.12). In comparison, similar effects have been observed with *p*-XSC regarding reduced expression of cPLA2; however, *p*-XSC has been shown to inhibit COX-2 expression at a dose of 5 μM (142). A strong induction of p38, p27, and p21 was observed in A549 cells treated with the lowest dose of *Se*-PBIT (5 μM) (Figure 4.12). These proteins are consequently known to play an integral role in cell cycle regulation and apoptosis. By comparison, p38, p27, and p21 were not induced under the same experimental conditions using *p*-XSC.

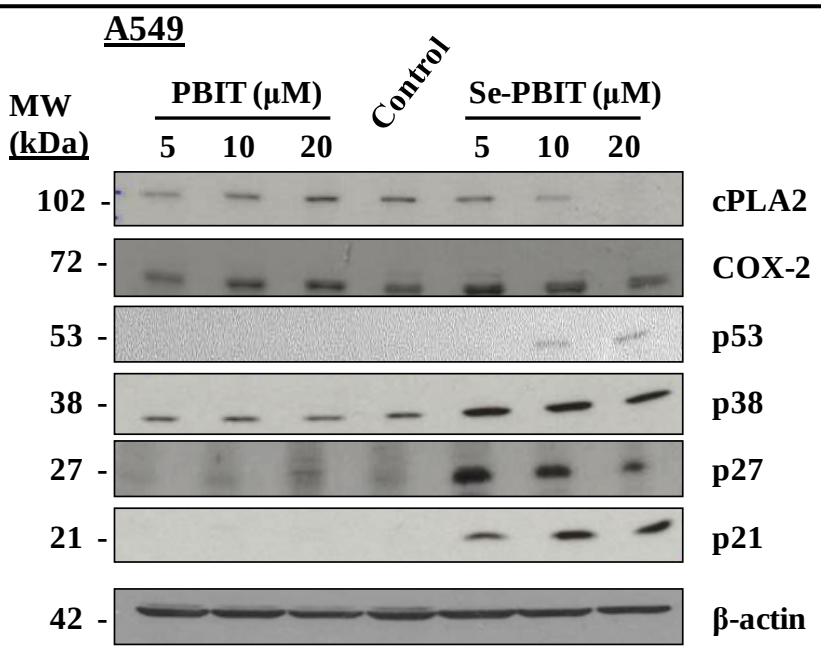

Figure 4.12 The effect of PBIT and *Se*-PBIT on molecular markers of cellular proliferation and apoptosis in A549 cells. Cells were treated with PBIT or *Se*-PBIT at doses of 5, 10, or 20 μM for 24 hr. Total cell lysate was collected from each treatment group and equal amounts of protein (30 μg) were loaded into each lane. Similar results were observed in NCI-H460 cells. Figure was published in reference (318).

6. Discussion

There is no effective chemopreventive agent against the development of lung cancer available for use in the clinic (97,122). Development of such agents will have a major impact on the management of the lung cancer epidemic.

Lung cancer is a multi-factorial disease in which various endogenous and exongenous mediators can influence its development. In particular, it has been demonstrated that dysregulation of NO may play a role in carcinogenesis and tumorigenesis and high levels of iNOS, a primary producer of NO, is elevated in lung tumors (144,145). Consequently, cigarette smoking has been shown to induce iNOS expression (297). Therefore, inhibition of iNOS and/or NO production is a viable area for lung cancer chemoprevention research.

Our laboratory, as well as others, has demonstrated the chemopreventive capabilities of various selenium containing compounds (122,125,126). A principle concept regarding research with selenium is that both the dose and form are very important factors to consider (125,126). Currently, in our laboratory, *p*-XSC is the most potent inhibitor in preclinical investigations against NSCLC. In this investigation, we evaluated the *in vitro* efficacy of a novel selenium-containing compound, *Se*-PBIT, against NSCLC. *Se*-PBIT was derived from the chemopreventive agent PBIT by substitution of its *S*-atoms with *Se*. Preclinical studies conducted in our laboratory have consistently showed that selenium substitution of sulfur in a variety of known chemopreventive agents enhances the efficacy of the parent compounds (125,178,325).

PBIT is a compound which has been shown to be an effective inhibitor of colon and esophageal cancer in rats by targeting iNOS activity and NO production (314,315). The structure of PBIT is such that it is very similar to guanidine and consequently, competitively binds to the guanidinium portion of the L-arginine active site of iNOS (310). It is proposed that the inhibition of iNOS is due to several factors including the binding of the *S*-atom in PBIT and related analogs to the active site of the enzyme (310). Considering the varied chemical

characteristics of selenium versus sulfur (nucleophilicity, atomic volume, etc.) (326), we hypothesized that selenium substitution of sulfur in the structure of PBIT (*Se*-PBIT) might result in a more effective inhibitor of the enzyme. However, based on our investigation, we found both PBIT and *Se*-PBIT to be equally effective inhibitors of NO production in NSCLC cells. This suggests that substitution of selenium for sulfur does not alter PBIT's ability to inhibit iNOS activity.

From a mechanistic standpoint, both PBIT and *Se*-PBIT are designed to inhibit iNOS activity and not expression per se. However, at higher concentrations of either compound we observed a significant decrease in protein expression. Previous *in vivo* studies using PBIT have shown no modulation of iNOS mRNA levels upon treatment with PBIT (314). However, in an inflammatory-based model administering the endotoxin lipopolysaccharide (LPS) which induces iNOS expression, decreased levels of iNOS mRNA were found in the lung tissue of rats treated with PBIT compared to LPS-alone treated mice. This result was explained, in part, by the ability of PBIT to block NO production and thus, cause a reduction of tissue inflammation (327). NFκB is an important transcriptional factor involved in the expression of iNOS and is activated during inflammation (296). Therefore, in our investigation, the reduction of iNOS expression in NSCLC cells treated with higher concentrations of PBIT or *Se*-PBIT may be caused by a reduction of NO and subsequently, the transcriptional activity of NFκB.

Although PBIT and *Se*-PBIT demonstrated similar efficacy against NO production and iNOS expression, additional inhibitory effects towards NSCLC cells were elicited by *Se*-PBIT. These effects can be largely associated with the presence of selenium. The hallmark of selenium chemoprevention activity against cancer is via inhibition of cellular growth and induction of apoptosis (126,328). In previous studies, our laboratory has shown that selenium-containing compound *p*-XSC is one of the most potent chemopreventive forms of selenium examined to inhibit cell viability and induce apoptosis of NSCLC cells NCI-H460 and A549 (142).

Furthermore, natural selenium compounds such as selenomethionine and *Se*-methylselenocysteine (components of selenized yeast) have no effect on cell viability at equal doses similar to that of *p*-XSC (142). By comparison, in this investigation, under identical conditions using the same NSCLC cell lines, selenium in the form of *Se*-PBIT was a significantly better inhibitor of cell viability and inducer of apoptosis than *p*-XSC. The IC_{50} of *p*-XSC was approximately 7.5 μM (142) compared to an IC_{50} of approximately 2.5-3.0 μM for *Se*-PBIT. In addition, the apoptotic index of treatment with 2.5 and 5.0 μM *p*-XSC and was only two-fold higher than non-treated cells (142), whereas the apoptotic index at 2.5 μM *Se*-PBIT was greater than three-fold and reached greater than seven-fold in NSCLC cells treated with 5.0 μM *Se*-PBIT compared to non-treated cells. Moreover, the effect of *Se*-PBIT on cell growth was specific to cancer cells as *Se*-PBIT had no effect on normal lung fibroblast cells at equal doses.

To elucidate the mechanism of activity of *Se*-PBIT regarding inhibition of cell viability and induction of apoptosis, we focused on determining whether alterations in the cell cycle were occurring, as well as whether specific proteins that are critical to cellular maintenance and have been implicated in the development of lung cancer were targeted by *Se*-PBIT. The cell cycle is an ordered, tightly regulated process involving multiple checkpoints that respond to extracellular growth signals and changes in cell size and DNA integrity (329). Failure of essential cell cycle arrest can cause uncontrolled cellular proliferation, as observed in cancer cells (329) and is thus, an area targeted by some chemopreventive agents, including selenium (146), to inhibit proliferation and induce apoptosis. Many organoselenium compounds have been shown to arrest the cell cycle at the G1 stage prior to entering the S phase for DNA synthesis (330-332). Based on our FACS analysis, *Se*-PBIT caused a distinct change in the cell cycle pattern in NSCLC cells by simultaneously inducing G1 and G2-M arrest. In melanoma cells treated with *Se*-PBIT a similar effect on the cell cycle was also observed (316). This indicates that *Se*-PBIT inhibits

cellular proliferation by arresting cells in G1 and G2-M phases of the cell cycle and induces apoptosis.

p21/WAF1/CIP1 and p27/KIP1 are inhibitors of cyclin/cyclin-dependent kinase (CDK) complexes and as a result, are important regulators of cell cycle progression. For example, p21/WAF1/CIP1 can specifically bind to cyclin D/CDK4 and cyclin E/CDK2 complexes early in G1 phase and also bind to the cyclin A/CDK2 complex just prior to the S phase/G2 phase transition to inhibit cell cycle progression (333). Similarly, p27/KIP1 can also bind to cyclin D or CDK4 to induce cell cycle arrest at G1 (334). Methylselenic acid has been shown to induce G1 arrest in human prostate cancer cells in association with increased expression of p21 and p27 (330). In our investigation, we also observed a strong induction of both p21 and p27 in NSCLC cells treated with the lowest dose of *Se*-PBIT (5 μM). In addition, the increased expression of p21 in the presence of *Se*-PBIT was accompanied by induction of the tumor suppressor protein p53. p53 is known to tightly manage the expression of the CDKN1A gene that encodes p21 (335). p53 is also a well-known inducer of apoptosis by induction of the pro-apoptotic BAX gene (329).

p38 MAP Kinase (MAPK) is a mitogen-activated protein kinase that responds to certain stress stimuli and is involved in cellular differentiation, growth, and apoptosis. Accordingly induction of apoptosis and inhibition of cell growth have been linked to the activation of p38 (336,337). Active MAPK has also demonstrated the ability to promote a G2-M cell cycle checkpoint through the phosphorylation and activation of p53 (338). It is well known that post-translational stabilization of p53 is achieved through phosphorylation at multiple sites by protein kinases including MAPK (339,340). Interestingly, inorganic sodium selenite has been shown to activate oxidative-stress mediated p53 and p38 pathways to induce caspase-independent cell death in cervical cancer cells (341). As mentioned above, we observed an induction of the p53 protein following *Se*-PBIT treatment in NSCLC cells. Furthermore, we also observed an

increase in MAPK protein expression. These results suggest that both proteins may play an important role in the chemopreventive efficacy of *Se*-PBIT.

In addition to iNOS, cPLA2 and COX-2 are important mediators involved in inflammation, cellular proliferation, and apoptosis and have been linked to the development of carcinogenesis (342-344). cPLA2 is a rate-limiting step in the hydrolysis of membrane phospholipids releasing arachidonic acid for eicosanoid production (345) and COX-2 converts arachidonic acid to prostaglandins and thromboxanes (342). NSCLC cells have been observed to produce high levels of inflammatory-related prostaglandins as a result of increased expression of COX-2 and cPLA2 (346,347). Furthermore, COX-2 expression and activity has been shown to be regulated by iNOS and NO in colon tumorigenesis (315), as well as in a variety of cell types (348). In previous studies, our laboratory demonstrated a dose-dependent inhibition of COX-2 expression with the selenium-containing compound *p*-XSC in NSCLC cells (142,349) and inhibition of cPLA2 at only a high dose of *p*-XSC (20 μM) in NSCLC cells (142). However, in this investigation, both PBIT and *Se*-PBIT had no effect on COX-2 expression and only at the highest concentrations of *Se*-PBIT (10 and 20 μM) was inhition of cPLA2 apparent, whereas no reduction in protein expression was observed with any concentration of PBIT. This suggests that selenium is contributing, in part, to the inhibition of cPLA2, in the form of *Se*-PBIT, but is unable to affect COX-2 expression, as demonstrated for *Se* in *p*-XSC.

In summary, we have developed a novel selenium-containing compound (*Se*-PBIT) that is superior to an established sulfur-containing chemopreventive agent (PBIT) as an inhibitor of cell growth and a potent inducer of apoptosis in NSCLC cells. We also showed that although both agents appeared to be equally effective inhibitors of NO and iNOS expression, only *Se*-PBIT altered certain proteins that are known to be important targets in the development of lung cancer. The proposed mechanism based on the results of this study and literature reports is presented in Figure 4.13. The results of this investigation are encouraging and support previous

chemoprevention studies utilizing *Se*-PBIT against cancer development (316,317). Furthermore, based on the results from this study, *Se*-PBIT appears to be a better selenium-containing chemoprevention agent than *p*-XSC. Thus future studies in our laboratory will be designed to provide additional insights into the specific details of *Se*-PBIT's mechanistic activity, as well as to evaluate the chemopreventive efficacy of *Se*-PBIT against the development of NSCLC in a well-defined animal model compared to *p*-XSC.

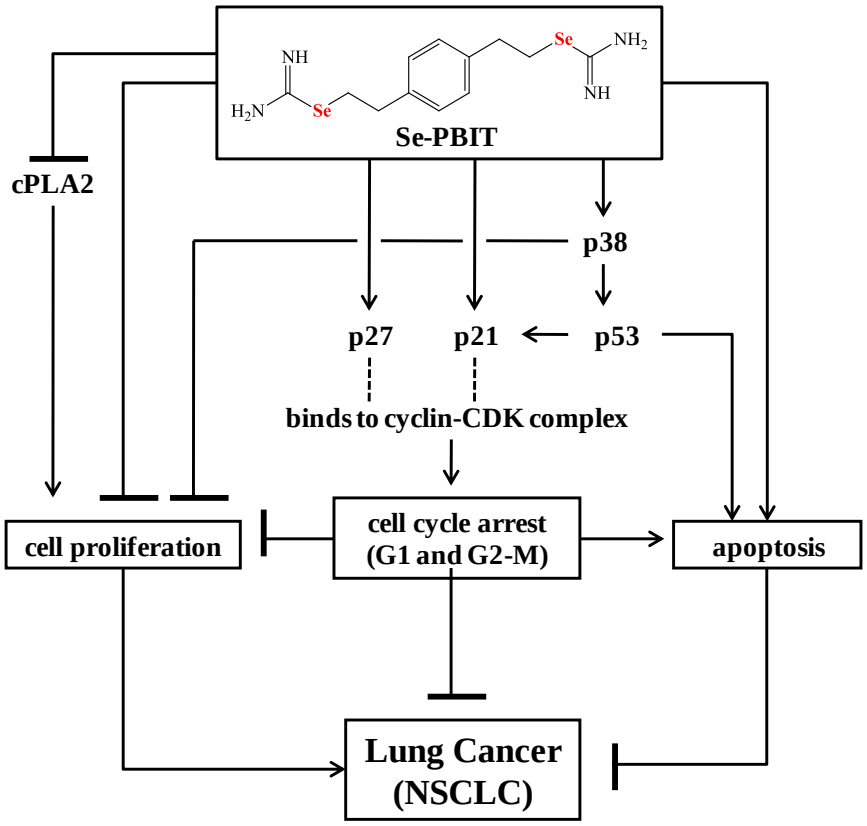

Figure 4.13 Scheme illustrating the proposed chemopreventive activity of *Se*-PBIT against NSCLC development (*in vitro*) based on the results from this study. →, leads to induction; ⊣, leads to inhibition; ---, binds.

Chapter 5

Summary and Future Directions

1. Potential strategies to curb the lung cancer epidemic

Lung cancer claims the lives of over one million people worldwide each year and is one of the most common cancers of men and women (2). Current strategies in the treatment of lung cancer include surgery, radiation therapy, chemotherapy, and targeted biological therapies. These have had minimal success and as a result the 5-year survival rate for all stages combined rests at 16% (5). The inability of current treatment strategies to increase survival stems from the late diagnosis of the disease, histologic heterogeneity, and the high recurrence rate after curative treatment has been administered (25).

Ironically, lung cancer is a potentially preventable cancer because it is strongly linked to tobacco use (11); smoking is also associated with COPD, heart disease, and cerebrovascular disease (5). Therefore, initiatives aimed at preventing people from starting to smoking and at smoking cessation must be continually reinforced. Cigarette smoke contains a variety of toxic and carcinogenic agents, including the polyaromatic hydrocarbon B[a]P and the tobacco- and organ-specific N-nitrosamine NNK. Following metabolic activation, these compounds can interact with DNA, lipids, and proteins in multiple organs to alter their normal physiological activities, and ultimately, lead to adverse health effects (11,29). In particular, NNK induces adenocarcinomas in various rodent models, independent of the route of administration (33) and has been classified as a human lung carcinogen by the IARC working group (48). In the United States, there are about 91 million current and former smokers composing about 40% of the adult population (20). Although former smokers have taken one of the greatest leaps towards health

awareness by quitting smoking, they are unfortunately still at a high risk for lung cancer development for several years following cessation (10,18).

As a result of dismal success in treatment strategies and the high number of individuals at risk for lung cancer development, there is clearly an urgent need to develop alternative approaches for management of lung cancer. The development of sensitive, specific, and reliable biomarkers for early detection of lung cancer and the discovery of novel chemopreventive agents are two strategies with promising clinical implications. Therefore, in this search we embarked upon strategies to further advance these modalities for disease management.

2. Summary of results from this study

2.1 Development of biomarkers from an animal model

Although early attempts to identify novel biomarkers characteristic of lung cancer development have been reported, no single marker has so far met sufficient specificity and sensitivity to be recognized for clinical significance (149). With the advancement of proteomic technologies a large scale view of critical molecular changes related to disease development is now possible. Well-defined animal models can be used for lung cancer biomarker discovery and allow for detection of proteins at various stages of disease development in both target and surrogate tissues (84).

In the NNK-induced lung tumorigenesis A/J mouse model utilizing the 2D-DIGE and iTRAQ proteomic techniques we identified many proteins in the lung that are involved in a variety of biological functions critical in lung carcinogenesis, including inflammation, cell cycle regulation, proliferation, and apoptosis. Proteins identified at the adenocarcinoma stage were CC10, annexin A5, and the 14-3-3 protein isoforms θ, ε, σ, and ζ. Furthermore, by targeting earlier stages of disease development, i.e. hyperplasia/atypia and adenoma, we identified additional proteins that have a strong relationship to carcinogenesis, including Cbr2 and HMGB1, that may be critical to early stages of disease development. Of particular interest is that some of

the proteins we identified by iTRAQ at earlier stages of disease development (hyperplasia/atypia and adenoma) in whole tissue have also been detected in tumors (adenomas and adenocarcinomas) with similar expression profiles; these include HSP90B1, ANXA6, PRDX6, Cbr2, LCP1, PDIA3, and P4HB (193). This suggests the potential utility of these proteins in early detection of lung cancer. It is apparent that multiple proteins – rather than a single protein – identified in this study may provide a better view of cellular changes related to disease development.

We used the organoselenium compound *p*-XSC to better understand the mechanism of lung carcinogenesis and to assess the relevance of these proteins as potential biomarkers. In lung tissue comprised primarily of adenomas or adenocarcinomas, *p*-XSC positively regulated the expression of the 14-3-3 protein isoforms θ, ε, and σ, but had no effect on CC10 expression.

2.2 Detection of blood protein biomarkers related to smoking

Cigarette smoking causes potentially harmful changes in the body leading to various diseases, including lung cancer (238). Ultimately, detection of these changes related to disease development would provide a diagnostic tool with which to detect individuals that are at high risk for health concerns.

Biomarkers in non-invasive fluids indicative of cigarette smoke's effects are urgently needed. In Chapter 3, we utilized the proteomic approach iTRAQ to identify differentially expressed plasma proteins in white male smokers compared to white male non-smokers. A total of 113 plasma proteins were confidently identified and compared between smokers and non-smokers. Subsequent analyses indicated that nine proteins were significantly up-regulated including the complement component 8 polypeptide chains α, β, and γ, mannan-binding lectin serine protease 1, and mannose-binding protein C, as well as nine proteins to be significantly down-regulated including inter-α-trypsin inhibitor heavy chain H3, vitronectin, vitamin D-binding protein, and sex-hormone binding globulin. Several proteins identified in this study are

heavily associated with immunity and inflammatory responses such as inter-α-trypsin inhibitor heavy chain H3 and vitamin D-binding protein and have been shown to have an association with tobacco-related diseases including COPD and lung cancer (277,278,282,283). Consistent with our previous preclinical study (Chapter 2) with a tobacco carcinogen (NNK)-induced lung tumorigenesis model, we also identified the 14-3-3 protein isoforms, α and ζ, to be down-regulated in the plasma of human smokers compared to non-smokers. Our results demonstrate for the first time the effect that cigarette smoking has on the human plasma proteome and the potential to find clinically relevant protein biomarkers in a non-invasive biological fluid, such as plasma, that can be indicative of tobacco-related disease development, including lung cancer.

2.3 A novel selenium-containing compound to target the promotion/progression stages of lung carcinogenesis: *Se*-PBIT

Clinically there are no effective chemopreventive agents targeting lung cancer (122). Thus, development of novel compounds that can target cellular and molecular pathways involved in the multi-step carcinogenesis process is urgently needed. One pathway which has garnered interest in the development of lung cancer is the production of NO. High levels of inducible nitric oxide synthase (iNOS) protein expression and NO have been positively correlated with the development of a number of human cancers, including lung cancer (144,145).

Our study focused on targeting iNOS by selecting an established iNOS inhibitor, PBIT, which is a sulfur-containing compound. Since we have consistently found that selenium substitution for sulfur in sulfur-containing compounds resulted in more effective chemopreventive analogs (125), we synthesized and compared PBIT and selenium substituted PBIT (*Se*-PBIT) in preclinical model systems using human NSCLC cells (NCI-H460 and A549). Furthermore, we compared the effects of *Se*-PBIT with our established organoselenium compound *p*-XSC.

Our results indicated that PBIT and *Se*-PBIT appeared to have similar activity regarding regulation of iNOS and its activity on NO production. However, at physiologically relevant doses, *Se*-PBIT was superior to PBIT as an inhibitor of cell growth and an inducer of apoptosis. Furthermore, *Se*-PBIT arrested the cell cycle at G1 and G2-M stages in both A549 and H460 cells. The arrest at G1 is consistent with previous studies using other selenium compounds and may be due in part to the decreased expression of the G1/S-specific cyclin D1 (126,316); however the effect on G2-M requires further investigation. In addition, only *Se*-PBIT significantly enhanced the levels of p53, p38, p27 and p21 protein expression and reduced the levels of cPLA2; such molecular targets are involved in cell growth inhibition, induction of apoptosis and cell cycle regulation. In comparison to *p*-XSC, *Se*-PBIT elicited a much stronger effect on inhibiton of cell proliferation and induction of apoptosis. Collectively, the results indicate that *Se*-PBIT may be considered a promising candidate for chemoprevention of NSCLC.

3. Future directions

3.1 Preclinical

3.1.1 Identification of protein modulation in select cellular compartments of the lung

The lung consists of a heterogenous mixture of various types of bronchial and alveolar cells, including type I and type II pneumocytes, alveolar macrophages, and Clara cells (41). Type II pneumocytes and Clara cells line the epithelium of the airways and are of particular interest provided their potential role as precursor cells of lung carcinogenesis, and more specifically NNK-induced tumorigenesis in rats and mice (41,164,350). In our animal model study, the use of whole tissue rather than the isolation of specific precursor lesion cells may result in under or overexpression of protein. Nevertheless, identification of protein modulation in these specific cell types would be highly useful during disease progression. Qualitatively, we could use immunohistochemical techniques to identify specific cellular regions in the lung which are

contributing to the expression changes we observed. Furthermore to study molecular changes in early stage neoplastic cells *in vivo*, we could isolate epithelial cells by protease extraction and density centrifugation or by the use of laser capture microdissection (LCM); both of which have been demonstrated in mouse models (351,352).

3.1.2 Biomarkers in surrogate tissue

In terms of clinical utility for early detection of lung cancer and evaluation of chemopreventive agents, biomarkers found in surrogate tissue such as BALF and blood need to be pursued; this provided the basis for selection of blood plasma in our clinical pilot investigation of proteomic profiling in chronic smokers in Chapter 4. Therefore, subsequent studies using the A/J mouse model should determine which of the proteins identified in mouse lung can also be found in surrogate tissue. Ideally, BALF and blood should contain a profile of proteins that are altered or are present at varying levels as a result of lung carcinogenesis. These proteins may be released directly from the target tissue, e.g. as for the case of most BALF proteins, or are present as a result of cellular insult (353). BALF is a proximal fluid that is in constant contact with the lung tissue and consequently, contains a rich source of proteins produced by various cells lining the airways and aveoli such as type II cells and Clara cells. In particular, these cells specifically secrete surfactant protein (SP)-A, SP-B, and SP-D and CC10 (211); the significance of CC10 in relation to smoking and lung cancer has been previously demonstrated (205) and was further supported in our investigations. These proteins are ideal biomarker candidates provided their lung specificity. However, other proteins that are not typically secreted by the lung have been identified in BALF such as glucose-regulated protein 1 and tropomyosin and have been shown to be involved in various lung diseases (354). The collection of BALF requires an invasive technique known as fiberoptic bronchoscopy. During this procedure a thin tube called a bronchoscope is inserted through the nose or mouth and is advanced along the back of the throat through the vocal cords and then finally into the airways. The procedure is safe, but can be

uncomfortable and thus, cannot be performed as routine in all patients (355); however, this procedure has been performed successfully in mice for proteomic studies (356). Blood, on the other hand, is less invasive and can also contain several proteins present in BALF as a result of passage through the broncho-alveolar/blood barrier, e.g. CC10 (211).

3.1.3 Use of whole tobacco smoke exposure models

Humans are ultimately exposed to whole tobacco smoke which contains a host of compounds rather than a single agent such as NNK. Therefore, further preclinical studies should be conducted in a model that incorporates whole tobacco smoke exposure to validate biomarkers discovered in this study. Several smoke inhalation animal models have been developed and the advantages and disadvantages have been described in the literature (357). In general, smoke inhalation studies using various animals including hamsters, ferrets, dogs, rabbits, and non-human primates are quite difficult to assimilate and have thus far provided either inconclusive or negative results regarding pulmonary tumor induction (357). Studies conducted in our laboratory have demonstrated that exposure of male guinea pigs to cigarette smoke (whole body exposure) by inhalation, twice a day for 28 days, induces preneoplastic lung lesions analogous to those found in human smokers, including bronchial hyperplasia, dysplasia, and squamous metaplasia (358). In addition, mice and rats exposed to environmental cigarette smoke (89% sidestream smoke and 11% mainstream smoke) for 28 days show lung carcinogenesis-related changes including DNA adduct formation, increased production of cellular proliferation markers, and cytotoxicity (359). More importantly, some of these effects have been shown to be attenuated with chemopreventive agents (359,360). Furthermore, Hutt and colleagues have developed a whole-body cigarette smoke exposure model in $B6C3F_1$ mice to induce lung tumors; $B6C3F_1$ mice typically have a low baseline incidence of pulmonary neoplasia (361). Remarkably, in this strain of mice, mainstream cigarette smoke induced lung adenomas and adenocarcinomas. The incidence of adenocarcinoma was about ten times greater in smoke-exposed mice compared to

non-exposed mice and many of the histological features and molecular alterations in the lung appeared to be similar to those found in smokers (361,362). Although many chemopreventive agents, including *p*-XSC, have been shown to be ineffective against lung tumor incidence in current whole tobacco smoke exposure models (363), *myo*-inositol in combination with dexamethasone has demonstrated efficacy (363,364). Therefore, in future studies it would be important to understand the molecular changes at the protein level occurring in the lung as a result of smoke exposure and how they are modulated to reflect the protective effects of chemopreventive agents such as as *myo*-inositol and dexamethasone.

3.1.4 Selenium-based chemoprevention

In our *in vitro* mechanistic study we were able to further support our previous findings that substitution of selenium for sulfur in a compound enhances its chemopreventive efficacy. Although PBIT has demonstrated efficacy in various cancers and may very well be effective for lung cancer, the *in vitro* results suggest that the selenium analog appears to be a better agent against the development of lung cancer. Therefore, for future studies it is also important to determine *Se*-PBIT's *in vivo* capabilities using an established animal model such as the NNK-induced lung tumorigenesis A/J mouse model used in Chapter 2, as well as a model which incorporates whole tobacco smoke exposure such as the mouse model developed by Hutt and colleagues (361). A previous *in vivo* study using *Se*-PBIT at a concentration of 2.5 ppm as selenium demonstrated its efficacy against skin tumors in mice by reducing skin tumor development by as much as 50% compared to PBIT (316). Madhunapantula et al. (316) demonstrated the ability of *Se*-PBIT to inhibit phosphorylation of the survival protein serine/threonine kinase Akt3 by abberant activation of the MAPK pathway, which at aberrant levels can lead to growth inhibition and apoptosis in melanoma cells (365). In lung cancer, mutant K-ras is responsible for activation of Akt1 and the Akt/mammalian target of rapamycin (mTOR) pathway is induced by tobacco carcinogens (366,367). Therefore, these two pathways

should also be explored in our lung cancer cells and may provide further insight as to the mechanistic activity of *Se*-PBIT against NSCLC. Furthermore, the metabolism of *Se*-PBIT may provide additional information pertaining to activity. Similar to the metabolism of *p*-XSC (136-138), *Se*-PBIT may be prone to conjugation with glutathione and subsequently produce a selenol moiety that may be an important to its chemoprevention activity (138).

Recently, researchers have begun to analyze closely the effects of using a mixture of chemopreventive agents rather than a single one. The rationale is that a combination of agents would be more effective provided that each agent is affecting different or complementary cellular pathways that are utilized by the cancer cell. In addition, by using a combination of agents, it may be possible to use lower doses of each thereby avoiding toxicity (100). This was demonstrated in a clinical study for colon cancer, in which the polyamine synthesis inhibitor, difluoromethylornithine, and the nonsteroidal anti-infllammatory drug, sulindac, prevented recurrence of colon adenomas by 70% without serious toxicity (104). Therefore, future studies should consider combining *p*-XSC or *Se*-PBIT with natural agents such as *myo*-inositol (100) to compare the combination of agents against the development of lung cancer.

3.2 Clinical studies

The prevention of smoking initiation and smoking cessation has had beneficial effects on various health concerns, including lung cancer (5,13). For example, in the United States and Canada-based Lung Health Study, smokers who had received intervention program help consisting of physician counseling and behavior modifications for up to 14.5 years and were successful in quitting had a 55% reduction in lung cancer risk as compared to continuing smokers that did not receive help (368). Moreover, the implementation of successful tobacco control programs is apparent in the United States where the California Tobacco Control Program has demonstrated success in reducing lung cancer rates in California as a result of decreasing cigarette consumption (369). Nevertheless, there is a large population that is unwilling or unable

to quit (370) and as a result require additional means of support to prevent the onset of life-threatening diseases.

Identifying the molecular profile of a smoker that constitutes a smoker's susceptibility to tobacco-related disease development compared to a non-smoker is an area of research that is of great interest. As discussed in Chapter 4, much work has been conducted in the target tissue, the lung, as well as in biological fluids such as BALF and urine to discover important molecular changes. Similary, in our clinical pilot study, we began to address the differences observed in blood plasma between smokers and non-smokers in terms of identifying protein biomarkers that may be of clinical value regarding tobacco-related diseases. Based on literature knowledge concerning the function and biological activity of the proteins we discovered, a number of potential candidates were identified that may present a vulnerability issue in smokers regarding future health concerns; however, it should be emphasized that this study was performed in a small sample set. Therefore to further validate our findings we will need to conduct a study using a larger sample size. In addition, it will be important to consider various factors when comparing smokers and non-smokers, specifically gender and race, as these are two variables which demonstrate differences in various diseases. Moreover, within the smoking population there may be a difference in plasma proteins with regards to factors such as pack-years.

4. Concluding remarks

The utility of protein biomarkers for lung cancer has the potential to help in early detection, disease monitoring, and in the evaluation of preventative and therapeutic agents, including chemotherapy. By studying a well-characterized animal model, the NNK-induced lung tumorigenesis A/J mouse model, we were able to identify potential protein biomarkers related to lung cancer development. Like all candidate biomarker development studies, intensive verification and validation studies are required. These need to be conducted with several hundreds of samples and performed with the purpose of demonstrating clinical correlations.

Although we did not have an adequate sample size of humans to perform such studies, we conducted a small clinical investigation in our laboratory in collaboration with oncologists to determine the expression level of two proteins of interest based on our preclinical studies (14-3-3 σ and annexin A5). These proteins were detected in the plasma of smokers compared to non-smokers (separate samples from those used in Chapter 4) and in the plasma of lung cancer patients compared to healthy subjects. Remarkably and consistent with our preclinical results, we found that 14-3-3 σ and annexin A5 were down-regulated in smokers compared to non-smokers (Figure 5.1A). Interestingly, we also found 14-3-3 σ and annexin A5 to be down-regulated in lung cancer patients as compared to healthy controls (Figure 5.1B); however, due to our limited sample sizes both sets of results were not evaluated statistically. Furthermore, 14-3-3 σ and annexin A5 expression were monitored in a patient receiving chemotherapeutic treatment with Paclitaxel, an anti-neoplastic agent that binds to tubulin and inhibits microtubule disassembly (371). Following treatment, these proteins were subsequently restored to levels reaching that of healthy subjects (Figure 5.2). More importantly, in conjunction with CT and PET scans, the restorations of these proteins appeared to be correlated with tumor size reduction (Figure 5.2). Furthermore, it was recently demonstrated that real-time micro-CT can be used to monitor of progression of lung tumors in small animals such as mice (308). The combination of biomarkers and CT scans will be invaluable for early detection and chemopreventive strategies against lung cancer development. As a result, models such as the NNK-A/J mouse model can facilitate the discovery of biomarkers and potentially accelerate the translation of biomarkers to viable clinical screening tools (372).

Discovery of natural agents in the diet or synthetically derived compounds will continue to advance the field of chemoprevention; however, ultimately caution should be taken to fully evaluate each agent before it reaches a clinical setting. This is best exemplified from clinical trials utilizing β-carotene (ATBC (108) and CARET (109)) discussed in Chapter 1, in which lung

cancer incidence was actually increased in smokers (112-114). Furthermore, the utility of selenium in cancer chemoprevention should also be pursued carefully based on the results of the SELECT trial which showed a non-significant increase in diabetes mellitus in subjects receiving selenomethionine (132); however, the dose and form in which selenium is administered appears to be one of the most important factors to consider (126,147). Nevertheless, our preclinical results from the present study with *Se*-PBIT suggest that selenium in this form has the potential to be an effective agent against NSCLC at physiologically relevant doses. In addition, compared to *p*-XSC studied in our laboratory, this agent may be more effective against NSCLC.

Regarding plasma biomarkers in healthy human subjects, the down-regulation of VDBP in the plasma of human smokers in our clinical pilot study provokes much interest. VDBP has an important role in transporting vitamin D and its metabolites such as 1,25-dihydroxyvitamin D (1,25-OHD) to various tissues in the body, including the lung, to help maintain cellular activities (282). Consequently, decreased levels of circulating vitamin D are associated with lung cancer incidence (373), and improved survival in early stage NSCLC has been associated with high levels of vitamin D (374). Epidemiological and preclinical studies have suggested that active metabolites of vitamin D, including 1,25-OHD, have the ability to prevent progression and metastasis of lung cancer through regulating cellular mechanisms central to the development of cancer including cell growth, differentiation, and apoptosis, as well as inhibition of angiogenesis (373,375,376). Therefore, our observation in smokers may have confounding implications regarding decreased transportation of vitamin D to an organ such as the lung which is heavily targeted by the harmful effects of cigarette smoke and suspect to cancer. Future studies evaluating expression of VDBP in healthy smokers and smokers with lung cancer are thus, strongly warranted.

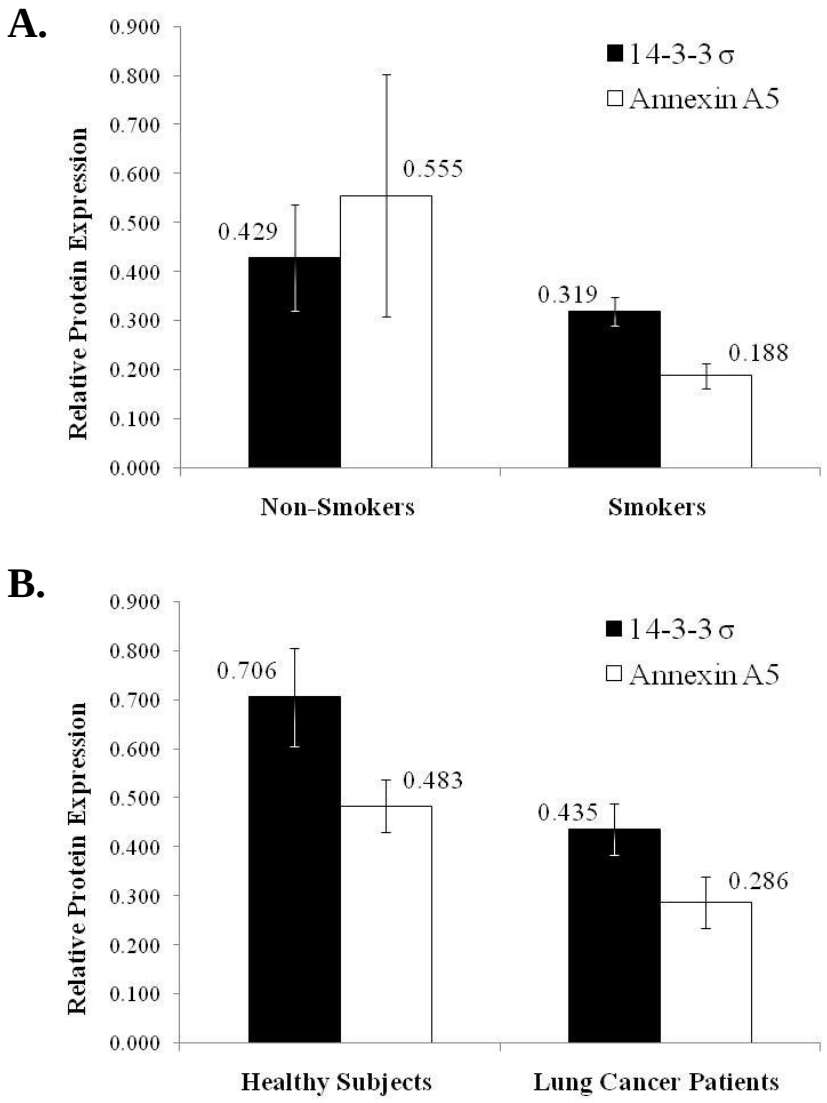

Figure 5.1 Relative expression of 14-3-3 σ and annexin A5 in human plasma. (A) Healthy non-smokers (n=3) compared to healthy smokers (n=3). (B) Healthy subjects (n=2) compared to lung cancer patients (n=4) (B). *Error bars* are ± SE. Average relative expression of 14-3-3 σ and annexin A5 in the plasma of healthy normal subjects and compared to lung cancer patients. Total protein staining with ponceau S (Sigma-Aldrich) confirmed consistent protein loading.

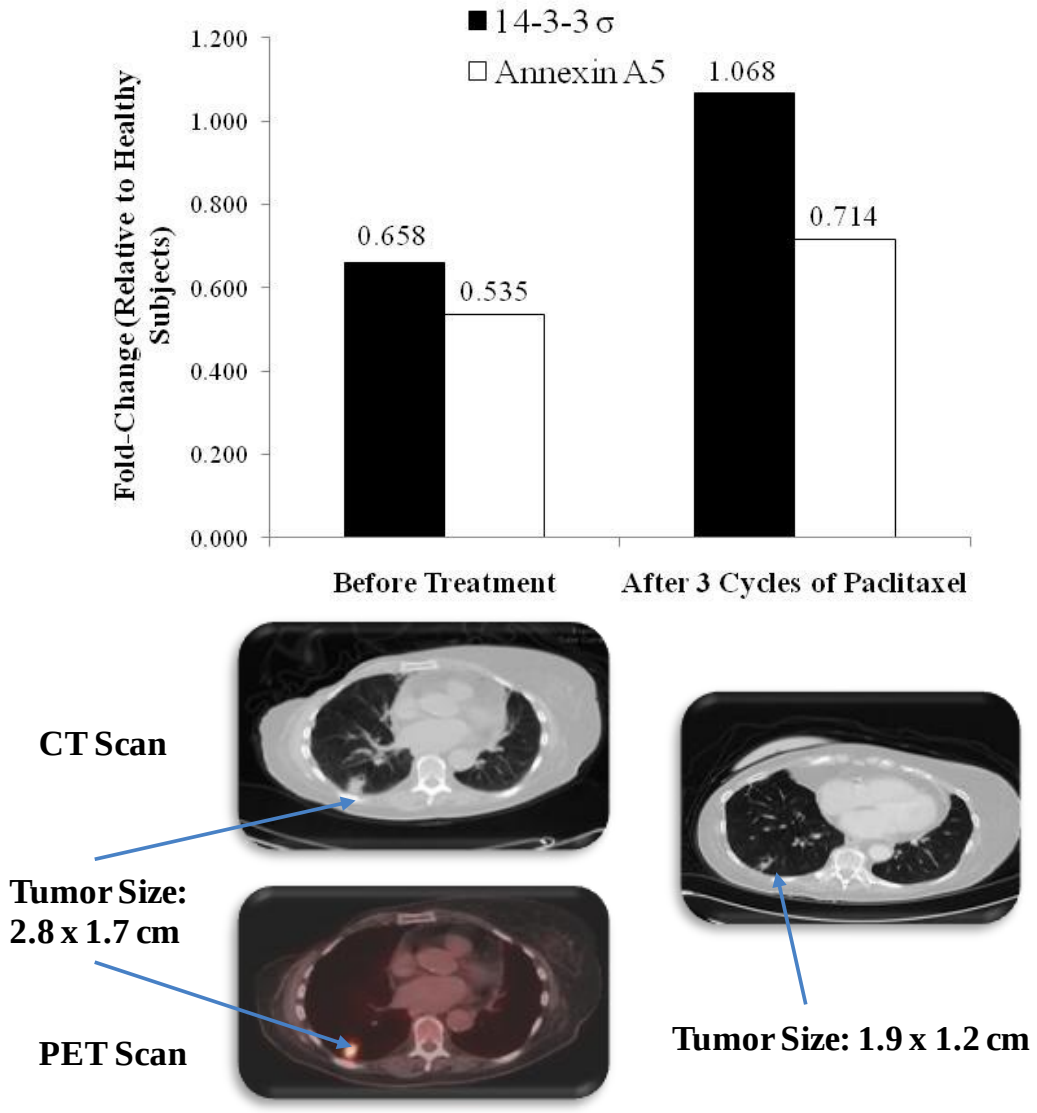

Figure 5.2 Expression of 14-3-3 σ and annexin A5 in the plasma of a lung cancer patient receiving chemotherapeutic treatment (Paclitaxel). Fold-change was calculated with n=2 healthy individuals. Classical imaging techniques (CT and PET Scans) in conjunction with molecular markers show successful reduction in tumor size. Total protein staining with ponceau S (Sigma-Aldrich) confirmed consistent protein loading.

REFERENCES

1. Garcia M, Jemal A, Ward EM, Center HM, Hao Y, Siegel RL, et al. Global Cancer Facts & Figures 2007. Atlanta, GA: American Cancer Society; 2007.

2. Parkin DM, Bray F, Ferlay J, Pisani P. Global Cancer Statistics, 2002. CA Cancer J Clin 2005;55:74-108.

3. Mackay J, Ericksen M, Shafey O. The Tobacco Atlas 2nd edition. Atlanta, GA: American Cancer Society; 2006.

4. Boffetta P, Nyberg F. Contribution of environmental factors to cancer risk. Br Med Bull 2003;68:71-94.

5. American Cancer Society. Cancer Facts & Figures 2010. Atlanta, GA: American Cancer Society; 2010.

6. Jemal A, Siegel R, Ward E, et al. Cancer statistics, 2009. CA Cancer J Clin 2009;59:225-49.

7. Ries AG, Eisner MP, Kosary CL, et al. SEER Cancer Statistics Review, 1975-2001. National Cancer Institute 2004.

8. Massion PP, Carbone DP. The molecular basis of lung cancer: molecular abnormalities and therapeutic implications. Respir Res 2003;4:12.

9. Sekido Y, Fong KM, Minna JD. Progress in understanding the molecular pathogenesis of human lung cancer. Biochim Biophys Acta 1998;1378:F21-F59.

10. El-Bayoumy K, Muscat JE, Hoffmann D. Nutrition and Tobacco-Related Cancers. In: Heber D, Blackburn GL, Go VLW, Milner J, editors. Nutr Oncol. 2nd ed. Burlington, MA: Academic Press; 2006. p. 199-217.

11. Hecht SS. Cigarette smoking and lung cancer: chemical mechanisms and approaches to prevention. Lancet Oncol 2002;3:461-9.

12. Tobacco smoke and involuntary smoking. IARC Monogr Eval Carcinog Risks Hum 2004;83:1-1438.

13. Viswanath K, Herbst RS, Land SR, Leischow SJ, Shields PG. Tobacco and cancer: an American Association for Cancer Research policy statement. Cancer Res 2010;70:3419-30.

14. Wynder EL, Graham EA. Tobacco smoking as a possible etiologic factor in bronchiogenic carcinoma; a study of 684 proved cases. J Am Med Assoc 1950;143:329-36.

15. Doll R, Hill AB. Smoking and carcinoma of the lung; preliminary report. Br Med J 1950;2:739-48.

16. U.S.Surgeon General's Advisory Committee on Smoking and Health. Smoking and health: report to the advisory committee to the surgeon general of the public health service. Washington, DC; 1964.

17. Wiencke JK, Thurston SW, Kelsey KT, et al. Early age at smoking initiation and tobacco carcinogen DNA damage in the lung. J Natl Cancer Inst 1999;91:614-9.

18. Tobacco control: reversal of risk after quitting smoking. IARC Handbooks of Cancer Prevention 2007;11.

19. Zhang H, Cai B. The impact of tobacco on lung health in China. Respirology 2003;8:17-21.

20. Centers for Disease Control and Prevention. Cigarette Smoking Among Adults and Trends in Smoking Cessation --- United States, 2008. Morb Mortal Wkly Rep 2009;58:1227-32.

21. Gilpin EA, Pierce JP. Demographic differences in patterns in the incidence of smoking cessation: United States 1950-1990. Ann Epidemiol 2002;12:141-50.

22. Alberg AJ, Brock MV, Samet JM. Epidemiology of lung cancer: looking to the future. J Clin Oncol 2005;23:3175-85.

23. Zochbauer-Muller S, Gazdar AF, Minna JD. Molecular pathogenesis of lung cancer. Annu Rev Physiol 2002;64:681-708.

24. Spira A, Ettinger DS. Multidisciplinary management of lung cancer. N Engl J Med 2004;350:379-92.

25. Travis WD. Pathology of lung cancer. Clin Chest Med 2002;23:65-81, viii.

26. Minna JD, Roth JA, Gazdar AF. Focus on lung cancer. Cancer Cell 2002;1:49-52.

27. Collins LG, Haines C, Perkel R, Enck RE. Lung cancer: diagnosis and management. Am Fam Physician 2007;75:56-63.

28. Gabrielson E. Worldwide trends in lung cancer pathology. Respirology 2006;11:533-8.

29. Hoffmann D, Hoffmann I, El-Bayoumy K. The less harmful cigarette: a controversial issue. a tribute to Ernst L. Wynder. Chem Res Toxicol 2001;14:767-90.

30. Wynder EL, Muscat JE. The changing epidemiology of smoking and lung cancer histology. Environ Health Perspect 1995;103 Suppl 8:143-8.

31. El-Bayoumy K, Hoffmann D. Nutrition and Tobacco-Related Cancer. In: Heber D, Blackburn GL, Go VLW, Holland JF, Giovannucci E, Clinton A, et al., editors. Nutritional Oncology. San Diego, CA: Academic Press; 1999. p. 299-324.

32. Benowitz NL. Nicotine addiction. N Engl J Med 2010;362:2295-303.

33. Hecht SS. Biochemistry, biology, and carcinogenicity of tobacco-specific N-nitrosamines. Chem Res Toxicol 1998;11:559-603.

34. Hecht SS. Tobacco carcinogens, their biomarkers and tobacco-induced cancer. Nature Rev 2003;3:733-44.

35. Hecht SS. Tobacco smoke carcinogens and lung cancer. J Natl Cancer Inst 1999;91:1194-210.

36. Loft S, Poulsen HE. Cancer risk and oxidative DNA damage in man. J Mol Med (Berlin, Germany) 1996;74:297-312.

37. Mayne ST. Antioxidant nutrients and chronic disease: use of biomarkers of exposure and oxidative stress status in epidemiologic research. J Nutr 2003;133 Suppl 3:933S-40S.

38. Smith CJ, Perfetti TA, Garg R, Hansch C. IARC carcinogens reported in cigarette mainstream smoke and their calculated log P values. Food Chem Toxicol 2003;41:807-17.

39. Jacob P, III, Havel C, Lee DH, et al. Subpicogram per milliliter determination of the tobacco-specific carcinogen metabolite 4-(methylnitrosamino)-1-(3-pyridyl)-1-butanol in human urine using liquid chromatography-tandem mass spectrometry. Anal Chem 2008;80:8115-21.

40. Hecht SS, Hoffmann D. The relevance of tobacco-specific nitrosamines to human cancer. Cancer Surveys 1989;8:273-94.

41. Nikitin AY, Alcaraz A, Anver MR, et al. Classification of proliferative pulmonary lesions of the mouse: recommendations of the mouse models of human cancers consortium. Cancer Res 2004;64:2307-16.

42. Hecht SS, Hoffmann D. 4-(methylnitrosamino)-1-(3-pyridyl)-1-butanone, a nicotine derived tobacco-specific nitrosamine, and cancer of the lung and pancreas in humans. In: Brugge J, Curran T, Harlow E, McCormick F, editors. The Origins of Human Cancer: A Comprehensive Review.Stone Harbor, NY: Cold Spring Harbor Lab Press; 1991. p. 745-55.

43. Carmella SG, Kagan SS, Kagan M, et al. Mass spectrometric analysis of tobacco-specific nitrosamine hemoglobin adducts in snuff dippers, smokers, and nonsmokers. Cancer Res 1990;50:5438-45.

44. Carmella SG, Akerkar S, Hecht SS. Metabolites of the tobacco-specific nitrosamine 4-(methylnitrosamino)-1-(3-pyridyl)-1-butanone in smokers' urine. Cancer Res 1993;53:721-4.

45. Hecht SS, Carmella SG, Murphy SE, et al. A tobacco-specific lung carcinogen in the urine of men exposed to cigarette smoke. N Engl J Med 1993;329:1543-6.

46. Church TR, Anderson KE, Caporaso NE, et al. A prospectively measured serum biomarker for a tobacco-specific carcinogen and lung cancer in smokers. Cancer Epidemiol Biomarkers Prev 2009;18:260-6.

47. Yuan JM, Koh WP, Murphy SE, et al. Urinary levels of tobacco-specific nitrosamine metabolites in relation to lung cancer development in two prospective cohorts of cigarette smokers. Cancer Res 2009;69:2990-5.

48. Smokeless tobacco and some tobacco-specific N-nitrosamines. IARC Monogr Eval Carcinog Risks Hum 2007;89:1-592.

49. Jalas JR, Hecht SS, Murphy SE. Cytochrome P450 enzymes as catalysts of metabolism of 4-(methylnitrosamino)-1-(3-pyridyl)-1-butanone, a tobacco specific carcinogen. Chem Res Toxicol 2005;18:95-110.

50. Brown PJ, Bedard LL, Reid KR, Petsikas D, Massey TE. Analysis of CYP2A contributions to metabolism of 4-(methylnitrosamino)-1-(3-pyridyl)-1-butanone in human peripheral lung microsomes. Drug Metab Dispos 2007;35:2086-94.

51. Wang L, Spratt TE, Liu XK, et al. Pyridyloxobutyl adduct O6-[4-oxo-4-(3-pyridyl)butyl]guanine is present in 4-(acetoxymethylnitrosamino)-1-(3-pyridyl)-1-butanone-treated DNA and is a substrate for O6-alkylguanine-DNA alkyltransferase. Chem Res Toxicol 1997;10:562-7.

52. Hecht SS, Villalta PW, Sturla SJ, et al. Identification of O2-substituted pyrimidine adducts formed in reactions of 4-(acetoxymethylnitrosamino)- 1-(3-pyridyl)-1-butanone and 4-(acetoxymethylnitros- amino)-1-(3-pyridyl)-1-butanol with DNA. Chem Res Toxicol 2004;17:588-97.

53. Hecht SS. Progress and challenges in selected areas of tobacco carcinogenesis. Chem Res Toxicol 2008;21:160-71.

54. Singer B, Grumberger D. Molecular Biology of Mutagens and Carcinogens. Plenum Press, New York and London; 1983.

55. Gentil A, Cabral-Neto JB, Mariage-Samson R, et al. Mutagenicity of a unique apurinic/apyrimidinic site in mammalian cells. J Mol Biol 1992;227:981-4.

56. Takeshita M, Eisenberg W. Mechanism of mutation on DNA templates containing synthetic abasic sites: study with a double strand vector. Nuc Acids Res 1994;22:1897-902.

57. Avkin S, Adar S, Blander G, Livneh Z. Quantitative measurement of translesion replication in human cells: evidence for bypass of abasic sites by a replicative DNA polymerase. Proc Natl Acad Sci USA 2002;99:3764-9.

58. Eadie JS, Conrad M, Toorchen D, Topal MD. Mechanism of mutagenesis by O6-methylguanine. Nature 1984;308:201-3.

59. Loechler EL, Green CL, Essigmann JM. In vivo mutagenesis by O6-methylguanine built into a unique site in a viral genome. Proc Natl Acad Sci USA 1984;81:6271-5.

60. Singer B, Essigmann JM. Site-specific mutagenesis: retrospective and prospective. Carcinogenesis 1991;12:949-55.

61. Liu XK, Spratt TE, Murphy SE, Peterson LA. Pyridyloxobutylation of guanine residues by 4-[(acetoxymethyl)nitrosamino]-1-(3-pyridyl)-1-butanone generates substrates of O6-alkylguanine-DNA alkyltransferase. Chem Res Toxicol 1996;9:949-53.

62. Peterson LA, Liu XK, Hecht SS. Pyridyloxobutyl DNA adducts inhibit the repair of O6-methylguanine. Cancer Res 1993;53:2780-5.

63. Peterson LA, Thomson NM, Crankshaw DL, Donaldson EE, Kenney PJ. Interactions between methylating and pyridyloxobutylating agents in A/J mouse lungs: implications for 4-(methylnitrosamino)-1-(3-pyridyl)-1-butanone-induced lung tumorigenesis. Cancer Res 2001;61:5757-63.

64. Belinsky SA, Foley JF, White CM, Anderson MW, Maronpot RR. Dose-response relationship between O6-methylguanine formation in Clara cells and induction of pulmonary neoplasia in the rat by 4-(methylnitrosamino)-1-(3-pyridyl)-1-butanone. Cancer Res 1990;50:3772-80.

65. Peterson LA, Hecht SS. O6-methylguanine is a critical determinant of 4-(methylnitrosamino)-1-(3-pyridyl)-1-butanone tumorigenesis in A/J mouse lung. Cancer Res 1991;51:5557-64.

66. Foiles PG, Akerkar SA, Carmella SG, et al. Mass spectrometric analysis of tobacco-specific nitrosamine-DNA adducts in smokers and nonsmokers. Chem Res Toxicol 1991;4:364-8.

67. Rosa JG, Prokopczyk B, Desai DH, Amin SG, El-Bayoumy K. Elevated 8-hydroxy-2'-deoxyguanosine levels in lung DNA of A/J mice and F344 rats treated with 4-(methylnitrosamino)-1-(3-pyridyl)-1-butanone and inhibition by dietary 1,4-phenylenebis(methylene)selenocyanate. Carcinogenesis 1998;19:1783-8.

68. Chung FL, Xu Y. Increased 8-oxodeoxyguanosine levels in lung DNA of A/J mice and F344 rats treated with the tobacco-specific nitrosamine 4-(methylnitrosamine)-1-(3-pyridyl)-1-butanone. Carcinogenesis 1992;13:1269-72.

69. Xu Y, Ho CT, Amin SG, Han C, Chung FL. Inhibition of tobacco-specific nitrosamine-induced lung tumorigenesis in A/J mice by green tea and its major polyphenol as antioxidants. Cancer Res 1992;52:3875-9.

70. Bilodeau JF, Wang M, Chung FL, Castonguay A. Effects of nonsteroidal antiinflammatory drugs on oxidative pathways in A/J mice. Free Radic Biol Med 1995;18:47-54.

71. Herzog CR, Desai D, Amin S. Array CGH analysis reveals chromosomal aberrations in mouse lung adenocarcinomas induced by the human lung carcinogen 4-(methylnitrosamino)-1-(3-pyridyl)-1-butanone. Biochem Biophys Res Commun 2006;341:856-63.

72. Razani-Boroujerdi S, Sopori ML. Early manifestations of NNK-induced lung cancer: role of lung immunity in tumor susceptibility. Am J Respir Cell Mol Biol 2007;36:13-9.

73. Akopyan G, Bonavida B. Understanding tobacco smoke carcinogen NNK and lung tumorigenesis. Int J Oncol 2006;29:745-52.

74. West KA, Brognard J, Clark AS, et al. Rapid Akt activation by nicotine and a tobacco carcinogen modulates the phenotype of normal human airway epithelial cells. Journal Clin Invest 2003;111:81-90.

75. van Zandwijk N. New methods for early diagnosis of lung cancer. Lung cancer (Amsterdam, Netherlands) 2002;38:S9-11.

76. Hardison BL. Lung Cancer Screening Using Helical CT vs. Chest X-ray Reduces Deaths among Current and Former Heavy Smokers. Benchmarks 2010; Retrieved from: http://benchmarks.cancer.gov/2010-11/lung-cancer-screening-using-helical-ct-vs-chest-x-ray-reduces-deaths-among-current-and-former-heavy-smokers/.

77. Ganti AK, Mulshine JL. Lung cancer screening. Oncologist 2006;11:481-7.

78. The National Lung Screening Trial: Overview and Study Design. Radiology 2010.

79. Yasufuku K. Early diagnosis of lung cancer. Clin Chest Med 2010;31:39-47, Table.

80. Mountain CF. Revisions in the International System for Staging Lung Cancer. Chest 1997;111:1710-7.

81. Chhatwani L, Cabebe E, Wakelee HA. Adjuvant treatment of resected lung cancer. Proc Am Thorac Soc 2009;6:194-200.

82. Biomarkers and surrogate endpoints: preferred definitions and conceptual framework. Clin Pharmacol Ther 2001;69:89-95.

83. Hanahan D, Weinberg RA. The hallmarks of cancer. Cell 2000;100:57-70.

84. Cho JY, Sung HJ. Proteomic approaches in lung cancer biomarker development. Expert Rev Proteomics 2009;6:27-42.

85. Greenberg AK, Lee MS. Biomarkers for lung cancer: clinical uses. Curr Opin Pulm Med 2007;13:249-55.

86. Matt P, Fu Z, Fu Q, Van Eyk JE. Biomarker discovery: proteome fractionation and separation in biological samples. Physiol Genomics 2008;33:12-7.

87. Chen G, Gharib TG, Huang CC, et al. Proteomic analysis of lung adenocarcinoma: identification of a highly expressed set of proteins in tumors. Clin Cancer Res 2002;8:2298-305.

88. Wu WW, Wang G, Baek SJ, Shen RF. Comparative study of three proteomic quantitative methods, DIGE, cICAT, and iTRAQ, using 2D gel- or LC-MALDI TOF/TOF. J Proteome Res 2006;5:651-8.

89. Timms JF, Cramer R. Difference gel electrophoresis. Proteomics 2008;8:4886-97.

90. Lilley KS, Friedman DB. All about DIGE: quantification technology for differential-display 2D-gel proteomics. Expert Rev Proteomics 2004;1:401-9.

91. Greengauz-Roberts O, Stoppler H, Nomura S, et al. Saturation labeling with cysteine-reactive cyanine fluorescent dyes provides increased sensitivity for protein expression profiling of laser-microdissected clinical specimens. Proteomics 2005;5:1746-57.

92. Marouga R, David S, Hawkins E. The development of the DIGE system: 2D fluorescence difference gel analysis technology. Anal Bioanal Chem 2005;382:669-78.

93. Chakravarti B, Gallagher SR, Chakravarti DN. Difference gel electrophoresis (DIGE) using CyDye DIGE fluor minimal dyes. Curr Protoc Mol Biol 2005;Chapter 10:Unit.

94. Freeman WM, Hemby SE. Proteomics for protein expression profiling in neuroscience. Neurochem Res 2004;29:1065-81.

95. Bienvenut WV, Deon C, Pasquarello C, et al. Matrix-assisted laser desorption/ionization-tandem mass spectrometry with high resolution and sensitivity for identification and characterization of proteins. Proteomics 2002;2:868-76.

96. Ross PL, Huang YN, Marchese JN, et al. Multiplexed protein quantitation in Saccharomyces cerevisiae using amine-reactive isobaric tagging reagents. Mol Cell Proteomics 2004;3:1154-69.

97. Keith RL. Chemoprevention of lung cancer. Proc Am Thorac Soc 2009;6:187-93.

98. Wattenberg LW. Chemoprevention of cancer. Cancer Res 1985;45:1-8.

99. Hursting SD, Slaga TJ, Fischer SM, DiGiovanni J, Phang JM. Mechanism-based cancer prevention approaches: targets, examples, and the use of transgenic mice. J Natl Cancer Inst 1999;91:215-25.

100. Hecht SS, Kassie F, Hatsukami DK. Chemoprevention of lung carcinogenesis in addicted smokers and ex-smokers. Nature Rev 2009;9:476-88.

101. Kinsinger LS, Harris R, Woolf SH, Sox HC, Lohr KN. Chemoprevention of breast cancer: a summary of the evidence for the U.S. Preventive Services Task Force. Ann Intern Med 2002;137:59-69.

102. Thompson IM, Goodman PJ, Tangen CM, et al. The influence of finasteride on the development of prostate cancer. N Engl J Med 2003;349:215-24.

103. Steinbach G, Lynch PM, Phillips RK, et al. The effect of celecoxib, a cyclooxygenase-2 inhibitor, in familial adenomatous polyposis. N Engl J Med 2000;342:1946-52.

104. Gerner EW, Meyskens FL, Jr. Combination chemoprevention for colon cancer targeting polyamine synthesis and inflammation. Clin Cancer Res 2009;15:758-61.

105. Block G, Patterson B, Subar A. Fruit, vegetables, and cancer prevention: a review of the epidemiological evidence. Nutr Cancer 1992;18:1-29.

106. Salgo MG, Cueto R, Winston GW, Pryor WA. Beta carotene and its oxidation products have different effects on microsome mediated binding of benzo[a]pyrene to DNA. Free Radic Biol Med 1999;26:162-73.

107. Bendich A. Carotenoids and the immune response. J Nutr 1989;119:112-5.

108. The effect of vitamin E and beta carotene on the incidence of lung cancer and other cancers in male smokers. The Alpha-Tocopherol, Beta Carotene Cancer Prevention Study Group. N Engl J Med 1994;330:1029-35.

109. Omenn GS, Goodman GE, Thornquist MD, et al. Effects of a combination of beta carotene and vitamin A on lung cancer and cardiovascular disease. N Engl J Med 1996;334:1150-5.

110. Hennekens CH, Buring JE, Manson JE, et al. Lack of effect of long-term supplementation with beta carotene on the incidence of malignant neoplasms and cardiovascular disease. N Engl J Med 1996;334:1145-9.

111. Lee IM, Cook NR, Manson JE, Buring JE, Hennekens CH. Beta-carotene supplementation and incidence of cancer and cardiovascular disease: the Women's Health Study. J Natl Cancer Inst 1999;91:2102-6.

112. Albanes D, Heinonen OP, Taylor PR, et al. Alpha-Tocopherol and beta-carotene supplements and lung cancer incidence in the alpha-tocopherol, beta-carotene cancer prevention study: effects of base-line characteristics and study compliance. J Natl Cancer Inst 1996;88:1560-70.

113. Omenn GS, Goodman GE, Thornquist MD, et al. Risk factors for lung cancer and for intervention effects in CARET, the Beta-Carotene and Retinol Efficacy Trial. J Natl Cancer Inst 1996;88:1550-9.

114. Tanvetyanon T, Bepler G. Beta-carotene in multivitamins and the possible risk of lung cancer among smokers versus former smokers: a meta-analysis and evaluation of national brands. Cancer 2008;113:150-7.

115. van ZN, Dalesio O, Pastorino U, de VN, van TH. EUROSCAN, a randomized trial of vitamin A and N-acetylcysteine in patients with head and neck cancer or lung cancer. For the EUropean Organization for Research and Treatment of Cancer Head and Neck and Lung Cancer Cooperative Groups. J Natl Cancer Inst 2000;92:977-86.

116. Lippman SM, Lee JJ, Karp DD, et al. Randomized phase III intergroup trial of isotretinoin to prevent second primary tumors in stage I non-small-cell lung cancer. J Natl Cancer Inst 2001;93:605-18.

117. Liu C, Wang XD, Bronson RT, et al. Effects of physiological versus pharmacological beta-carotene supplementation on cell proliferation and histopathological changes in the lungs of cigarette smoke-exposed ferrets. Carcinogenesis 2000;21:2245-53.

118. Liu C, Russell RM, Wang XD. Exposing ferrets to cigarette smoke and a pharmacological dose of beta-carotene supplementation enhance in vitro retinoic acid catabolism in lungs via induction of cytochrome P450 enzymes. Journal Nutr 2003;133:173-9.

119. Pastorino U. beta-Carotene and the risk of lung cancer. J Natl Cancer Inst 1997;89:456-7.

120. Wang XD, Liu C, Bronson RT, et al. Retinoid signaling and activator protein-1 expression in ferrets given beta-carotene supplements and exposed to tobacco smoke. J Natl Cancer Inst 1999;91:60-6.

121. Wright ME, Groshong SD, Husgafvel-Pursiainen K, et al. Effects of beta-carotene supplementation on molecular markers of lung carcinogenesis in male smokers. Cancer Prev Res (Phila) 2010;3:745-52.

122. van Zandwijk N. Chemoprevention in lung carcinogenesis--an overview. Eur J Cancer 2005;41:1990-2002.

123. Navarro Silvera SA, Rohan TE. Trace elements and cancer risk: a review of the epidemiologic evidence. Cancer Causes Control 2007;18:7-27.

124. Institute of Medicine FaNB. Dietary Reference Intakes for Vitamin C, Vitamin E, Selenium, and Carotenoids. Washington DC: National Academy Press; 2000 Aug 3.

125. El-Bayoumy K, Upadhyaya P, Chae YH, et al. Chemoprevention of cancer by organoselenium compounds. J Cell Biochem Suppl 1995;22:92-100.

126. El-Bayoumy K, Sinha R. Molecular chemoprevention by selenium: a genomic approach. Mutat Res 2005;591:224-36.

127. Ip C. Lessons from basic research in selenium and cancer prevention. Journal Nutr 1998;128:1845-54.

128. Clark LC, Combs GF, Jr., Turnbull BW, et al. Effects of selenium supplementation for cancer prevention in patients with carcinoma of the skin. A randomized controlled trial. Nutritional Prevention of Cancer Study Group. JAMA 1996;276:1957-63.

129. Reid ME, Duffield-Lillico AJ, Garland L, et al. Selenium supplementation and lung cancer incidence: an update of the nutritional prevention of cancer trial. Cancer Epidemiol Biomarkers Prev 2002;11:1285-91.

130. Zhuo H, Smith AH, Steinmaus C. Selenium and lung cancer: a quantitative analysis of heterogeneity in the current epidemiological literature. Cancer Epidemiol Biomarkers Prev 2004;13:771-8.

131. Karp DD, Lee SJ, Shaw Wright GL, Johnson DH, Johnston MR, Goodman GE, et al. A phase III, intergroup, randomized, double-blind, chemoprevention trial of selenium (Se) supplementation in resected stage I non-small cell lung cancer (NSCLC). J Clin Oncol 28:7s. 2010.

132. Lippman SM, Klein EA, Goodman PJ, et al. Effect of selenium and vitamin E on risk of prostate cancer and other cancers: the Selenium and Vitamin E Cancer Prevention Trial (SELECT). JAMA 2009;301:39-51.

133. Stranges S, Marshall JR, Natarajan R, et al. Effects of long-term selenium supplementation on the incidence of type 2 diabetes: a randomized trial. Ann Intern Med 2007;147:217-23.

134. El-Bayoumy K. The protective role of selenium on genetic damage and on cancer. Mutat Res 2001;475:123-39.

135. Rayman MP. Selenium in cancer prevention: a review of the evidence and mechanism of action. Proc Nutr Soc 2005;64:527-42.

136. Sohn OS, Desai DH, Das A, et al. Comparative excretion and tissue distribution of selenium in mice and rats following treatment with the chemopreventive agent 1,4-phenylenebis(methylene)selenocyanate. Chem Biol Interact 2005;151:193-202.

137. El-Bayoumy K, Upadhyaya P, Sohn OS, Rosa JG, Fiala ES. Synthesis and excretion profile of 1,4-[14C]phenylenebis(methylene)selenocyanate in the rat. Carcinogenesis 1998;19:1603-7.

138. Ganther HE. Selenium metabolism, selenoproteins and mechanisms of cancer prevention: complexities with thioredoxin reductase. Carcinogenesis 1999;20:1657-66.

139. Das A, Desai D, Pittman B, Amin S, El-Bayoumy K. Comparison of the chemopreventive efficacies of 1,4-phenylenebis(methylene)selenocyanate and selenium-enriched yeast on 4-(methylnitrosamino)-1-(3-pyridyl)-1-butanone induced lung tumorigenesis in A/J mouse. Nutr Cancer 2003;46:179-85.

140. El-Bayoumy K, Upadhyaya P, Desai DH, Amin S, Hecht SS. Inhibition of 4-(methylnitrosamino)-1-(3-pyridyl)-1-butanone tumorigenicity in mouse lung by the synthetic organoselenium compound, 1,4-phenylenebis(methylene)selenocyanate. Carcinogenesis 1993;14:1111-3.

141. Richie JP, Jr., Kleinman W, Desai DH, et al. The organoselenium compound 1,4-phenylenebis(methylene)selenocyanate inhibits 4-(methylnitrosamino)-1-(3-pyridyl)-1-butanone-induced tumorgenesis and enhances glutathione-related antioxidant levels in A/J mouse lung. Chem Biol Interact 2006;161:93-103.

142. El-Bayoumy K, Das A, Narayanan B, et al. Molecular targets of the chemopreventive agent 1,4-phenylenebis (methylene)-selenocyanate in human non-small cell lung cancer. Carcinogenesis 2006;27:1369-76.

143. Chen KM, Spratt TE, Stanley BA, et al. Inhibition of nuclear factor-kappaB DNA binding by organoselenocyanates through covalent modification of the p50 subunit. Cancer Res 2007;67:10475-83.

144. Fukumura D, Kashiwagi S, Jain RK. The role of nitric oxide in tumour progression. Nature Rev 2006;6:521-34.

145. Lala PK, Chakraborty C. Role of nitric oxide in carcinogenesis and tumour progression. Lancet Oncol 2001;2:149-56.

146. Jackson MI, Combs GF, Jr. Selenium and anticarcinogenesis: underlying mechanisms. Curr Opin Clin Nutr Metab Care 2008;11:718-26.

147. El-Bayoumy K. The negative results of the SELECT study do not necessarily discredit the selenium-cancer prevention hypothesis. Nutr Cancer 2009;61:285-6.

148. Polanski M, Anderson NL. A list of candidate cancer biomarkers for targeted proteomics. Biomark Insights 2007;1:1-48.

149. Brambilla C, Fievet F, Jeanmart M, et al. Early detection of lung cancer: role of biomarkers. Eur Respir J Suppl 2003;39:36s-44s.

150. Buhrens RI, Amelung JT, Reymond MA, Beshay M. Protein expression in human non-small cell lung cancer: a systematic database. Pathobiology 2009;76:277-85.

151. Chenau J, Michelland S, de FF, et al. The cell line secretome, a suitable tool for investigating proteins released in vivo by tumors: application to the study of p53-modulated proteins secreted in lung cancer cells. J Proteome Res 2009;8:4579-91.

152. Keshamouni VG, Michailidis G, Grasso CS, et al. Differential protein expression profiling by iTRAQ-2DLC-MS/MS of lung cancer cells undergoing epithelial-mesenchymal transition reveals a migratory/invasive phenotype. J Proteome Res 2006;5:1143-54.

153. Liu YF, Xiao ZQ, Li MX, et al. Quantitative proteome analysis reveals annexin A3 as a novel biomarker in lung adenocarcinoma. J Pathol 2009;217:54-64.

154. Meuwissen R, Berns A. Mouse models for human lung cancer. Genes Dev 2005;19:643-64.

155. Malkinson AM. Molecular comparison of human and mouse pulmonary adenocarcinomas. Exp Lung Res 1998;24:541-55.

156. Bonner AE, Lemon WJ, Devereux TR, Lubet RA, You M. Molecular profiling of mouse lung tumors: association with tumor progression, lung development, and human lung adenocarcinomas. Oncogene 2004;23:1166-76.

157. You M, Bergman G. Preclinical and clinical models of lung cancer chemoprevention. Hematol Oncol Clin North Am 1998;12:1037-53.

158. Tuveson DA, Jacks T. Modeling human lung cancer in mice: similarities and shortcomings. Oncogene 1999;18:5318-24.

159. Wakamatsu N, Devereux TR, Hong HH, Sills RC. Overview of the molecular carcinogenesis of mouse lung tumor models of human lung cancer. Toxicol Pathol 2007;35:75-80.

160. You M, Wang Y, Stoner G, et al. Parental bias of Ki-ras oncogenes detected in lung tumors from mouse hybrids. Proc Natl Acad Sci USA 1992;89:5804-8.

161. Chen B, Johanson L, Wiest JS, Anderson MW, You M. The second intron of the K-ras gene contains regulatory elements associated with mouse lung tumor susceptibility. Proc Natl Acad Sci USA 1994;91:1589-93.

162. O'Donnell EP, Zerbe LK, Dwyer-Nield LD, Kisley LR, Malkinson AM. Quantitative analysis of early chemically-induced pulmonary lesions in mice of varying susceptibilities to lung tumorigenesis. Cancer Lett 2006;241:197-202.

163. Cooper CA, Carby FA, Bubb VJ, et al. The pattern of K-ras mutation in pulmonary adenocarcinoma defines a new pathway of tumour development in the human lung. J Pathol 1997;181:401-4.

164. Belinsky SA, Devereux TR, Foley JF, Maronpot RR, Anderson MW. Role of the alveolar type II cell in the development and progression of pulmonary tumors induced by 4-(methylnitrosamino)-1-(3-pyridyl)-1-butanone in the A/J mouse. Cancer Res 1992;52:3164-73.

165. Castonguay A, Rioux N. Inhibition of lung tumourigenesis by sulindac: comparison of two experimental protocols. Carcinogenesis 1997;18:491-6.

166. Lu G, Liao J, Yang G, et al. Inhibition of adenoma progression to adenocarcinoma in a 4-(methylnitrosamino)-1-(3-pyridyl)-1-butanone-induced lung tumorigenesis model in A/J mice by tea polyphenols and caffeine. Cancer Res 2006;66:11494-501.

167. Yang G, Wang ZY, Kim S, et al. Characterization of early pulmonary hyperproliferation and tumor progression and their inhibition by black tea in a 4-(methylnitrosamino)-1-(3-pyridyl)-1-butanone-induced lung tumorigenesis model with A/J mice. Cancer Res 1997;57:1889-94.

168. Wistuba II, Mao L, Gazdar AF. Smoking molecular damage in bronchial epithelium. Oncogene 2002;21:7298-306.

169. Prokopczyk B, Amin S, Desai DH, et al. Effects of 1,4-phenylenebis(methylene)selenocyanate and selenomethionine on 4-(methylnitrosamino)-1-(3-pyridyl)-1-butanone-induced tumorigenesis in A/J mouse lung. Carcinogenesis 1997;18:1855-7.

170. Prokopczyk B, Rosa JG, Desai D, et al. Chemoprevention of lung tumorigenesis induced by a mixture of benzo(a)pyrene and 4-(methylnitrosamino)-1-(3-pyridyl)-1-butanone by the organoselenium compound 1,4-phenylenebis(methylene)selenocyanate. Cancer Lett 2000;161:35-46.

171. Alban A, David SO, Bjorkesten L, et al. A novel experimental design for comparative two-dimensional gel analysis: two-dimensional difference gel electrophoresis incorporating a pooled internal standard. Proteomics 2003;3:36-44.

172. Umstead TM, Freeman WM, Chinchilli VM, Phelps DS. Age-Related Changes in the Expression and Oxidation of Bronchoalveolar Lavage Proteins in the Rat. Am J Physiol Lung Cell Mol Physiol 2008.

173. Ringner M. What is principal component analysis? Nat Biotechnol 2008;26:303-4.

174. Somiari RI, Sullivan A, Russell S, et al. High-throughput proteomic analysis of human infiltrating ductal carcinoma of the breast. Proteomics 2003;3:1863-73.

175. Somiari RI, Sullivan A, Russell S, et al. High-throughput proteomic analysis of human infiltrating ductal carcinoma of the breast. Proteomics 2003;3:1863-73.

176. Yates JR, III, Eng JK, McCormack AL, Schieltz D. Method to correlate tandem mass spectra of modified peptides to amino acid sequences in the protein database. Anal Chem 1995;67:1426-36.

177. El-Bayoumy K, Chae YH, Upadhyaya P, et al. Inhibition of 7,12-dimethylbenz(a)anthracene-induced tumors and DNA adduct formation in the mammary glands of female Sprague-Dawley rats by the synthetic organoselenium compound, 1,4-phenylenebis(methylene)selenocyanate. Cancer Res 1992;52:2402-7.

178. El-Bayoumy K. Effects of organoselenium compounds on induction of mouse forestomach tumors by benzo(a)pyrene. Cancer Res 1985;45:3631-5.

179. Estensen RD, Jordan MM, Wiedmann TS, et al. Effect of chemopreventive agents on separate stages of progression of benzo[alpha]pyrene induced lung tumors in A/J mice. Carcinogenesis 2004;25:197-201.

180. Jiang L, He L, Fountoulakis M. Comparison of protein precipitation methods for sample preparation prior to proteomic analysis. J Chromatogr A 2004;1023:317-20.

181. Zellner M, Winkler W, Hayden H, et al. Quantitative validation of different protein precipitation methods in proteome analysis of blood platelets. Electrophoresis 2005;26:2481-9.

182. Shilov IV, Seymour SL, Patel AA, et al. The Paragon Algorithm, a next generation search engine that uses sequence temperature values and feature probabilities to identify peptides from tandem mass spectra. Mol Cell Proteomics 2007;6:1638-55.

183. Tang WH, Shilov IV, Seymour SL. Nonlinear fitting method for determining local false discovery rates from decoy database searches. J Proteome Res 2008;7:3661-7.

184. Stanley BA. Mass Spectrometry and tandem MS/MS: Calculating False Discovery Rates (FDR). Penn State Hershey Core Research Facilities 2011; Retrieved from: http://www.hmc.psu.edu/core/proteins_MassSpec/MassSpec/Calculating%20False%20Discovery%20Rates.htm.

185. Taylor CF, Paton NW, Lilley KS, et al. The minimum information about a proteomics experiment (MIAPE). Nat Biotechnol 2007;25:887-93.

186. Bortner JD, Jr., Das A, Umstead TM, et al. Down-regulation of 14-3-3 isoforms and annexin A5 proteins in lung adenocarcinoma induced by the tobacco-specific nitrosamine NNK in the A/J mouse revealed by proteomic analysis. J Proteome Res 2009;8:4050-61.

187. Moreira JM, Shen T, Ohlsson G, et al. A combined proteome and ultrastructural localization analysis of 14-3-3 proteins in transformed human amnion (AMA) cells: definition of a framework to study isoform-specific differences. Mol Cell Proteomics 2008;7:1225-40.

188. Qi W, Liu X, Qiao D, Martinez JD. Isoform-specific expression of 14-3-3 proteins in human lung cancer tissues. Int J Cancer 2005;113:359-63.

189. Koch HB, Zhang R, Verdoodt B, et al. Large-scale identification of c-MYC-associated proteins using a combined TAP/MudPIT approach. Cell Cycle 2007;6:205-17.

190. Wojcik C. Regulation of apoptosis by the ubiquitin and proteasome pathway. J Cell Mol Med 2002;6:25-48.

191. Prokopczyk B, Cox JE, Upadhyaya P, et al. Effects of dietary 1,4-phenylenebis(methylene)selenocyanate on 4-(methylnitrosamino)-1-(3-pyridyl)-1-butanone-induced DNA adduct formation in lung and liver of A/J mice and F344 rats. Carcinogenesis 1996;17:749-53.

192. Kassie F, Anderson LB, Scherber R, et al. Indole-3-carbinol inhibits 4-(methylnitrosamino)-1-(3-pyridyl)-1-butanone plus benzo(a)pyrene-induced lung tumorigenesis in A/J mice and modulates carcinogen-induced alterations in protein levels. Cancer Res 2007;67:6502-11.

193. Kassie F, Anderson LB, Higgins L, et al. Chemopreventive agents modulate the protein expression profile of 4-(methylnitrosamino)-1-(3-pyridyl)-1-butanone plus benzo[a]pyrene-induced lung tumors in A/J mice. Carcinogenesis 2008;29:610-9.

194. Fu H, Subramanian RR, Masters SC. 14-3-3 proteins: structure, function, and regulation. Annu Rev Pharmacol Toxicol 2000;40:617-47.

195. Tzivion G, Gupta VS, Kaplun L, Balan V. 14-3-3 proteins as potential oncogenes. Semin Cancer Biol 2006;16:203-13.

196. Ralhan R, Desouza LV, Matta A, et al. iTRAQ-multidimensional liquid chromatography and tandem mass spectrometry-based identification of potential biomarkers of oral epithelial dysplasia and novel networks between inflammation and premalignancy. J Proteome Res 2009;8:300-9.

197. Neal CL, Yao J, Yang W, et al. 14-3-3zeta overexpression defines high risk for breast cancer recurrence and promotes cancer cell survival. Cancer Res 2009;69:3425-32.

198. Nakanishi K, Hashizume S, Kato M, et al. Elevated expression levels of the 14-3-3 family of proteins in lung cancer tissues. Hum Antibodies 1997;8:189-94.

199. Konishi H, Sugiyama M, Mizuno K, et al. Detailed characterization of a homozygously deleted region corresponding to a candidate tumor suppressor locus at distal 17p13.3 in human lung cancer. Oncogene 2003;22:1892-905.

200. Laronga C, Yang HY, Neal C, Lee MH. Association of the cyclin-dependent kinases and 14-3-3 sigma negatively regulates cell cycle progression. J Biol Chem 2000;275:23106-12.

201. Urano T, Saito T, Tsukui T, et al. Efp targets 14-3-3 sigma for proteolysis and promotes breast tumour growth. Nature 2002;417:871-5.

202. Yang HY, Wen YY, Chen CH, Lozano G, Lee MH. 14-3-3 sigma positively regulates p53 and suppresses tumor growth. Mol Cell Biol 2003;23:7096-107.

203. van Genderen HO, Kenis H, Hofstra L, Narula J, Reutelingsperger CP. Extracellular annexin A5: functions of phosphatidylserine-binding and two-dimensional crystallization. Biochim Biophys Acta 2008;1783:953-63.

204. Boersma HH, Kietselaer BL, Stolk LM, et al. Past, present, and future of annexin A5: from protein discovery to clinical applications. J Nucl Med 2005;46:2035-50.

205. Linnoila RI, Szabo E, DeMayo F, et al. The role of CC10 in pulmonary carcinogenesis: from a marker to tumor suppression. Ann N Y Acad Sci 2000;923:249-67.

206. Chen J, Lam S, Pilon A, et al. The association between the anti-inflammatory protein CC10 and smoking status among participants in a chemoprevention trial. Cancer Epidemiol Biomarkers Prev 2007;16:577-83.

207. Chen J, Lam S, Pilon A, et al. Higher levels of the anti-inflammatory protein CC10 are associated with improvement in bronchial dysplasia and sputum cytometric assessment in individuals at high risk for lung cancer. Clin Cancer Res 2008;14:1590-7.

208. Yang Y, Zhang Z, Mukherjee AB, Linnoila RI. Increased susceptibility of mice lacking Clara cell 10-kDa protein to lung tumorigenesis by 4-(methylnitrosamino)-1-(3-pyridyl)-1-butanone, a potent carcinogen in cigarette smoke. J Biol Chem 2004;279:29336-40.

209. Halatek T, Hermans C, Broeckaert F, et al. Quantification of Clara cell protein in rat and mouse biological fluids using a sensitive immunoassay. Eur Respir J 1998;11:726-33.

210. Lindahl M, Svartz J, Tagesson C. Demonstration of different forms of the anti-inflammatory proteins lipocortin-1 and Clara cell protein-16 in human nasal and bronchoalveolar lavage fluids. Electrophoresis 1999;20:881-90.

211. Hermans C, Bernard A. Lung epithelium-specific proteins: characteristics and potential applications as markers. Am J Respir Crit Care Med 1999;159:646-78.

212. Zelvyte I, Wallmark A, Piitulainen E, Westin U, Janciauskiene S. Increased plasma levels of serine proteinase inhibitors in lung cancer patients. Anticancer Res 2004;24:241-7.

213. Yang P, Sun Z, Krowka MJ, et al. Alpha1-antitrypsin deficiency carriers, tobacco smoke, chronic obstructive pulmonary disease, and lung cancer risk. Arch Intern Med 2008;168:1097-103.

214. Sun Z, Yang P. Role of imbalance between neutrophil elastase and alpha 1-antitrypsin in cancer development and progression. Lancet Oncol 2004;5:182-90.

215. Sun Z, Yang P. Role of imbalance between neutrophil elastase and alpha 1-antitrypsin in cancer development and progression. Lancet Oncol 2004;5:182-90.

216. Gilles C, Polette M, Piette J, et al. Vimentin expression in cervical carcinomas: association with invasive and migratory potential. J Pathol 1996;180:175-80.

217. Hendrix MJ, Seftor EA, Seftor RE, Trevor KT. Experimental co-expression of vimentin and keratin intermediate filaments in human breast cancer cells results in phenotypic interconversion and increased invasive behavior. Am J Pathol 1997;150:483-95.

218. Maeda J, Hirano T, Ogiwara A, et al. Proteomic analysis of stage I primary lung adenocarcinoma aimed at individualisation of postoperative therapy. Br J Cancer 2008;98:596-603.

219. Seike M, Kondo T, Fujii K, et al. Proteomic signatures for histological types of lung cancer. Proteomics 2005;5:2939-48.

220. Poon HF, Vaishnav RA, Getchell TV, Getchell ML, Butterfield DA. Quantitative proteomics analysis of differential protein expression and oxidative modification of specific proteins in the brains of old mice. Neurobiol Aging 2006;27:1010-9.

221. Forrest GL, Gonzalez B. Carbonyl reductase. Chem Biol Interact 2000;129:21-40.

222. Doorn JA, Maser E, Blum A, Claffey DJ, Petersen DR. Human carbonyl reductase catalyzes reduction of 4-oxonon-2-enal. Biochemistry 2004;43:13106-14.

223. Lin L, Wang Y, Bergman G, et al. Detection of differentially expressed genes in mouse lung adenocarcinomas. Exp Lung Res 2001;27:217-29.

224. Rutters H, Zurbig P, Halter R, Borlak J. Towards a lung adenocarcinoma proteome map: studies with SP-C/c-raf transgenic mice. Proteomics 2006;6:3127-37.

225. Ismail E, Al-Mulla F, Tsuchida S, et al. Carbonyl reductase: a novel metastasis-modulating function. Cancer Res 2000;60:1173-6.

226. Takenaka K, Ogawa E, Oyanagi H, Wada H, Tanaka F. Carbonyl reductase expression and its clinical significance in non-small-cell lung cancer. Cancer Epidemiol Biomarkers Prev 2005;14:1972-5.

227. Agresti A, Bianchi ME. HMGB proteins and gene expression. Curr Opin Genet Dev 2003;13:170-8.

228. Lotze MT, Tracey KJ. High-mobility group box 1 protein (HMGB1): nuclear weapon in the immune arsenal. Nat Rev Immunol 2005;5:331-42.

229. Riuzzi F, Sorci G, Donato R. The amphoterin (HMGB1)/receptor for advanced glycation end products (RAGE) pair modulates myoblast proliferation, apoptosis, adhesiveness, migration, and invasiveness. Functional inactivation of RAGE in L6 myoblasts results in tumor formation in vivo. J Biol Chem 2006;281:8242-53.

230. Taguchi A, Blood DC, del TG, et al. Blockade of RAGE-amphoterin signalling suppresses tumour growth and metastases. Nature 2000;405:354-60.

231. Brezniceanu ML, Volp K, Bosser S, et al. HMGB1 inhibits cell death in yeast and mammalian cells and is abundantly expressed in human breast carcinoma. FASEB J 2003;17:1295-7.

232. Kusume A, Sasahira T, Luo Y, et al. Suppression of dendritic cells by HMGB1 is associated with lymph node metastasis of human colon cancer. Pathobiology 2009;76:155-62.

233. Shen X, Hong L, Sun H, Shi M, Song Y. The expression of high-mobility group protein box 1 correlates with the progression of non-small cell lung cancer. Oncol Rep 2009;22:535-9.

234. Nekrutenko A. Reconciling the numbers: ESTs versus protein-coding genes. Mol Biol Evol 2004;21:1278-82.

235. Ariztia EV, Lee CJ, Gogoi R, Fishman DA. The tumor microenvironment: key to early detection. Crit Rev Clin Lab Sci 2006;43:393-425.

236. Tobacco smoking: why start? Lancet 2009;374:1038.

237. van d, V, Postma DS, Timens W, ten Hacken NH. Acute effects of cigarette smoke on inflammation and oxidative stress: a review. Thorax 2004;59:713-21.

238. Yanbaeva DG, Dentener MA, Creutzberg EC, Wesseling G, Wouters EF. Systemic effects of smoking. Chest 2007;131:1557-66.

239. Pryor WA, Stone K. Oxidants in cigarette smoke. Radicals, hydrogen peroxide, peroxynitrate, and peroxynitrite. Ann N Y Acad Sci 1993;686:12-27.

240. Muscat JE, Kleinman W, Colosimo S, et al. Enhanced protein glutathiolation and oxidative stress in cigarette smokers. Free Radic Biol Med 2004;36:464-70.

241. Spira A, Beane J, Shah V, et al. Effects of cigarette smoke on the human airway epithelial cell transcriptome. Proc Natl Acad Sci USA 2004;101:10143-8.

242. Lee EJ, In KH, Kim JH, et al. Proteomic analysis in lung tissue of smokers and COPD patients. Chest 2009;135:344-52.

243. Steiling K, Kadar AY, Bergerat A, et al. Comparison of proteomic and transcriptomic profiles in the bronchial airway epithelium of current and never smokers. PLoS One 2009;4:e5043.

244. Kelsen SG, Duan X, Ji R, et al. Cigarette smoke induces an unfolded protein response in the human lung: a proteomic approach. Am J Respir Cell Mol Biol 2008;38:541-50.

245. Schembri F, Sridhar S, Perdomo C, et al. MicroRNAs as modulators of smoking-induced gene expression changes in human airway epithelium. Proc Natl Acad Sci USA 2009;106:2319-24.

246. Schroder M, Kaufman RJ. ER stress and the unfolded protein response. Mutat Res 2005;569:29-63.

247. Jorgensen E, Stinson A, Shan L, et al. Cigarette smoke induces endoplasmic reticulum stress and the unfolded protein response in normal and malignant human lung cells. BMC Cancer 2008;8:229.

248. Morrison DK. The 14-3-3 proteins: integrators of diverse signaling cues that impact cell fate and cancer development. Trends Cell Biol 2009;19:16-23.

249. Anderson NL, Polanski M, Pieper R, et al. The human plasma proteome: a nonredundant list developed by combination of four separate sources. Mol Cell Proteomics 2004;3:311-26.

250. Plymoth A, Lofdahl CG, Ekberg-Jansson A, et al. Protein expression patterns associated with progression of chronic obstructive pulmonary disease in bronchoalveolar lavage of smokers. Clin Chem 2007;53:636-44.

251. Merkel D, Rist W, Seither P, Weith A, Lenter MC. Proteomic study of human bronchoalveolar lavage fluids from smokers with chronic obstructive pulmonary disease by combining surface-enhanced laser desorption/ionization-mass spectrometry profiling with mass spectrometric protein identification. Proteomics 2005;5:2972-80.

252. Ghafouri B, Stahlbom B, Tagesson C, Lindahl M. Newly identified proteins in human nasal lavage fluid from non-smokers and smokers using two-dimensional gel electrophoresis and peptide mass fingerprinting. Proteomics 2002;2:112-20.

253. Gianazza E, Allegra L, Bucchioni E, et al. Increased keratin content detected by proteomic analysis of exhaled breath condensate from healthy persons who smoke. Am J Med 2004;117:51-4.

254. Airoldi L, Magagnotti C, Iannuzzi AR, et al. Effects of cigarette smoking on the human urinary proteome. Biochemical and biophysical research communications 2009;381:397-402.

255. Anderson NL, Anderson NG. The human plasma proteome: history, character, and diagnostic prospects. Mol Cell Proteomics 2002;1:845-67.

256. Yocum AK, Yu K, Oe T, Blair IA. Effect of immunoaffinity depletion of human serum during proteomic investigations. J Proteome Res 2005;4:1722-31.

257. de RB, Duthie SJ, Polley AC, et al. Proteomic methodological recommendations for studies involving human plasma, platelets, and peripheral blood mononuclear cells. J Proteome Res 2008;7:2280-90.

258. Hanash SM, Pitteri SJ, Faca VM. Mining the plasma proteome for cancer biomarkers. Nature 2008;452:571-9.

259. Greening DW, Simpson RJ. A centrifugal ultrafiltration strategy for isolating the low-molecular weight (<or=25K) component of human plasma proteome. J Proteomics 2010;73:637-48.

260. Bortner JD, Jr., Richie JP, Jr., Das A, et al. Proteomic profiling of human plasma by iTRAQ reveals down-regulation of ITI-HC3 and VDBP by cigarette smoking. J Proteome Res 2011;10:1151-9.

261. Richie JP, Jr., Carmella SG, Muscat JE, et al. Differences in the urinary metabolites of the tobacco-specific lung carcinogen 4-(methylnitrosamino)-1-(3-pyridyl)-1-butanone in black and white smokers. Cancer Epidemiol Biomarkers Prev 1997;6:783-90.

262. Thomas PD, Campbell MJ, Kejariwal A, et al. PANTHER: a library of protein families and subfamilies indexed by function. Genome Res 2003;13:2129-41.

263. Song X, Bandow J, Sherman J, et al. iTRAQ experimental design for plasma biomarker discovery. J Proteome Res 2008;7:2952-8.

264. Tonack S, spinall-O'Dea M, Jenkins RE, et al. A technically detailed and pragmatic protocol for quantitative serum proteomics using iTRAQ. J Proteomics 2009;73:352-6.

265. Lin JA, Yeh CC, Lee MS, et al. Prolonged injection time and light smoking decrease the incidence of fentanyl-induced cough. Anesth Analg 2005;101:670-4, table.

266. Osada H, Tatematsu Y, Yatabe Y, et al. Frequent and histological type-specific inactivation of 14-3-3sigma in human lung cancers. Oncogene 2002;21:2418-24.

267. Ernoult E, Bourreau A, Gamelin E, Guette C. A proteomic approach for plasma biomarker discovery with iTRAQ labelling and OFFGEL fractionation. J Biomed Biotechnol 2010;2010:927917.

268. Ye H, Sun L, Huang X, Zhang P, Zhao X. A proteomic approach for plasma biomarker discovery with 8-plex iTRAQ labeling and SCX-LC-MS/MS. Mol Cell Biochem 2010.

269. Hinnebusch AG. Mechanism and regulation of initiator methionyl-tRNA binding to ribosomes. In: Sonenberg N, Hershey JWB, Mathew MB, editors. Translational Control of Gene Expression.Cold Spring Harbor, NY: Cold Spring Harbo Laboratory Press; 2000. p. 185-243.

270. Karp NA, Huber W, Sadowski PG, et al. Addressing accuracy and precision issues in iTRAQ quantitation. Mol Cell Proteomics 2010;9:1885-97.

271. Ow SY, Salim M, Noirel J, et al. iTRAQ underestimation in simple and complex mixtures: "the good, the bad and the ugly". J Proteome Res 2009;8:5347-55.

272. Culnan DM, Cooney RN, Stanley B, Lynch CJ. Apolipoprotein A-IV, a putative satiety/antiatherogenic factor, rises after gastric bypass. Obesity (Silver Spring) 2009;17:46-52.

273. Robbins RA, Nelson KJ, Gossman GL, Koyama S, Rennard SI. Complement activation by cigarette smoke. Am J Physiol 1991;260:L254-L259.

274. Ahn KS, Aggarwal BB. Transcription factor NF-kappaB: a sensor for smoke and stress signals. Ann N Y Acad Sci 2005;1056:218-33.

275. Forteza R, Casalino-Matsuda SM, Monzon ME, et al. TSG-6 potentiates the antitissue kallikrein activity of inter-alpha-inhibitor through bikunin release. American journal of respiratory cell and molecular biology 2007;36:20-31.

276. Zhuo L, Hascall VC, Kimata K. Inter-alpha-trypsin inhibitor, a covalent protein-glycosaminoglycan-protein complex. J Biol Chem 2004;279:38079-82.

277. Hamm A, Veeck J, Bektas N, et al. Frequent expression loss of Inter-alpha-trypsin inhibitor heavy chain (ITIH) genes in multiple human solid tumors: a systematic expression analysis. BMC Cancer 2008;8:25.

278. Heo SH, Lee SJ, Ryoo HM, Park JY, Cho JY. Identification of putative serum glycoprotein biomarkers for human lung adenocarcinoma by multilectin affinity chromatography and LC-MS/MS. Proteomics 2007;7:4292-302.

279. Fujii K, Nakano T, Kanazawa M, et al. Clinical-scale high-throughput human plasma proteome analysis: lung adenocarcinoma. Proteomics 2005;5:1150-9.

280. Bandow JE, Baker JD, Berth M, et al. Improved image analysis workflow for 2-D gels enables large-scale 2-D gel-based proteomics studies--COPD biomarker discovery study. Proteomics 2008;8:3030-41.

281. Gomme PT, Bertolini J. Therapeutic potential of vitamin D-binding protein. Trends Biotechnol 2004;22:340-5.

282. Chishimba L, Thickett DR, Stockley RA, Wood AM. The vitamin D axis in the lung: a key role for vitamin D-binding protein. Thorax 2010;65:456-62.

283. Chatterji B, Borlak J. Serum proteomics of lung adenocarcinomas induced by targeted overexpression of c-raf in alveolar epithelium identifies candidate biomarkers. Proteomics 2007;7:3980-91.

284. Preissner KT, Seiffert D. Role of vitronectin and its receptors in haemostasis and vascular remodeling. Thromb Res 1998;89:1-21.

285. Lee WM, Galbraith RM. The extracellular actin-scavenger system and actin toxicity. N Engl J Med 1992;326:1335-41.

286. Selby C. Sex hormone binding globulin: origin, function and clinical significance. Ann Clin Biochem 1990;27 (Pt 6):532-41.

287. English KM, Pugh PJ, Parry H, et al. Effect of cigarette smoking on levels of bioavailable testosterone in healthy men. Clin Sci (Lond) 2001;100:661-5.

288. Field AE, Colditz GA, Willett WC, Longcope C, McKinlay JB. The relation of smoking, age, relative weight, and dietary intake to serum adrenal steroids, sex hormones, and sex hormone-binding globulin in middle-aged men. J Clin Endocrinol Metab 1994;79:1310-6.

289. Muller M, den T, I, Thijssen JH, Grobbee DE, van der Schouw YT. Endogenous sex hormones in men aged 40-80 years. Eur J Endocrinol 2003;149:583-9.

290. Shiels MS, Rohrmann S, Menke A, et al. Association of cigarette smoking, alcohol consumption, and physical activity with sex steroid hormone levels in US men. Cancer Causes Control 2009;20:877-86.

291. Bernhard D, Pfister G, Huck CW, et al. Disruption of vascular endothelial homeostasis by tobacco smoke: impact on atherosclerosis. FASEB J 2003;17:2302-4.

292. Xiao T, Ying W, Li L, et al. An approach to studying lung cancer-related proteins in human blood. Mol Cell Proteomics 2005;4:1480-6.

293. He Y, Wu X, Liu X, Yan G, Xu C. LC-MS/MS analysis of ovarian cancer metastasis-related proteins using a nude mouse model: 14-3-3 zeta as a candidate biomarker. J Proteome Res 2010;9:6180-90.

294. McGorrian C, Yusuf S, Islam S, et al. Estimating modifiable coronary heart disease risk in multiple regions of the world: the INTERHEART Modifiable Risk Score. Eur Heart J 2011;32:581-9.

295. Moncada S, Palmer RM, Higgs EA. Nitric oxide: physiology, pathophysiology, and pharmacology. Pharmacol Rev 1991;43:109-42.

296. Nathan C, Xie QW. Nitric oxide synthases: roles, tolls, and controls. Cell 1994;78:915-8.

297. Wright JL, Dai J, Zay K, et al. Effects of cigarette smoke on nitric oxide synthase expression in the rat lung. Lab Invest 1999;79:975-83.

298. Liu CY, Wang CH, Chen TC, et al. Increased level of exhaled nitric oxide and up-regulation of inducible nitric oxide synthase in patients with primary lung cancer. Br J Cancer 1998;78:534-41.

299. Lakari E, Soini Y, Saily M, et al. Inducible nitric oxide synthase, but not xanthine oxidase, is highly expressed in interstitial pneumonias and granulomatous diseases of human lung. Am J Clin Pathol 2002;117:132-42.

300. Tracey WR, Xue C, Klinghofer V, et al. Immunochemical detection of inducible NO synthase in human lung. Am J Physiol 1994;266:L722-L727.

301. Lee TW, Chen GG, Xu H, et al. Differential expression of inducible nitric oxide synthase and peroxisome proliferator-activated receptor gamma in non-small cell lung carcinoma. Eur J Cancer 2003;39:1296-301.

302. Chen GG, Lee TW, Xu H, et al. Increased inducible nitric oxide synthase in lung carcinoma of smokers. Cancer 2008;112:372-81.

303. Fujimoto H, Ando Y, Yamashita T, et al. Nitric oxide synthase activity in human lung cancer. Jpn J Cancer Res 1997;88:1190-8.

304. Rojas-Walker T, Tamir S, Ji H, Wishnok JS, Tannenbaum SR. Nitric oxide induces oxidative damage in addition to deamination in macrophage DNA. Chemical research in toxicology 1995;8:473-7.

305. Calmels S, Hainaut P, Ohshima H. Nitric oxide induces conformational and functional modifications of wild-type p53 tumor suppressor protein. Cancer Res 1997;57:3365-9.

306. Ambs S, Bennett WP, Merriam WG, et al. Relationship between p53 mutations and inducible nitric oxide synthase expression in human colorectal cancer. J Natl Cancer Inst 1999;91:86-8.

307. Kisley LR, Barrett BS, Bauer AK, et al. Genetic ablation of inducible nitric oxide synthase decreases mouse lung tumorigenesis. Cancer Res 2002;62:6850-6.

308. Ramasamy K, Dwyer-Nield LD, Serkova NJ, et al. Silibinin Prevents Lung Tumorigenesis in Wild-Type but not in iNOS-/- Mice: Potential of Real-Time Micro-CT in Lung Cancer Chemoprevention Studies. Clin Cancer Res 2011;17:753-61.

309. Furfine ES, Harmon MF, Paith JE, Garvey EP. Selective inhibition of constitutive nitric oxide synthase by L-NG-nitroarginine. Biochemistry 1993;32:8512-7.

310. Garvey EP, Oplinger JA, Tanoury GJ, et al. Potent and selective inhibition of human nitric oxide synthases. Inhibition by non-amino acid isothioureas. J Biol Chem 1994;269:26669-76.

311. Misko TP, Moore WM, Kasten TP, et al. Selective inhibition of the inducible nitric oxide synthase by aminoguanidine. Eur J Pharmacol 1993;233:119-25.

312. Hasan K, Heesen BJ, Corbett JA, et al. Inhibition of nitric oxide formation by guanidines. Eur J Pharmacol 1993;249:101-6.

313. Edward P, Gerald J, Jeffrey A, Eric S. Enzyme inhibitors. Geneva: Chemin des Colombettes: World Intellectual Property Organization; 1994.

314. Chen T, Nines RG, Peschke SM, Kresty LA, Stoner GD. Chemopreventive effects of a selective nitric oxide synthase inhibitor on carcinogen-induced rat esophageal tumorigenesis. Cancer Res 2004;64:3714-7.

315. Rao CV, Kawamori T, Hamid R, Reddy BS. Chemoprevention of colonic aberrant crypt foci by an inducible nitric oxide synthase-selective inhibitor. Carcinogenesis 1999;20:641-4.

316. Madhunapantula SV, Desai D, Sharma A, et al. PBISe, a novel selenium-containing drug for the treatment of malignant melanoma. Mol Cancer Ther 2008;7:1297-308.

317. Desai D, Madhunapantula SV, Gowdahalli K, et al. Synthesis and characterization of a novel iNOS/Akt inhibitor Se,Se'-1,4-phenylenebis(1,2-ethanediyl)bisisoselenourea (PBISe)--against colon cancer. Bioorg Med Chem Lett 2010;20:2038-43.

318. Das A, Bortner J, Desai D, Amin S, El-Bayoumy K. The selenium analog of the chemopreventive compound S,S'-(1,4-phenylenebis[1,2-ethanediyl])bisisothiourea is a remarkable inducer of apoptosis and inhibitor of cell growth in human non-small cell lung cancer. Chem Biol Interact 2009;180:158-64.

319. Nims RW, Cook JC, Krishna MC, et al. Colorimetric assays for nitric oxide and nitrogen oxide species formed from nitric oxide stock solutions and donor compounds. Methods Enzymol 1996;268:93-105.

320. Mosmann T. Rapid colorimetric assay for cellular growth and survival: application to proliferation and cytotoxicity assays. J Immunol Methods 1983;65:55-63.

321. Wyllie AH, Kerr JF, Currie AR. Cell death: the significance of apoptosis. Int Rev Cytol 1980;68:251-306.

322. Krishan A. Rapid flow cytofluorometric analysis of mammalian cell cycle by propidium iodide staining. J Cell Biol 1975;66:188-93.

323. El-Bayoumy K, Richie JP, Jr., Boyiri T, et al. Influence of selenium-enriched yeast supplementation on biomarkers of oxidative damage and hormone status in healthy adult males: a clinical pilot study. Cancer Epidemiol Biomarkers Prev 2002;11:1459-65.

324. Rayman MP. The use of high-selenium yeast to raise selenium status: how does it measure up? Br J Nutr 2004;92:557-73.

325. El-Bayoumy K, Sinha R, Pinto JT, Rivlin RS. Cancer chemoprevention by garlic and garlic-containing sulfur and selenium compounds. J Nutr 2006;136:864S-9S.

326. Wessjohann LA, Schneider A, Abbas M, Brandt W. Selenium in chemistry and biochemistry in comparison to sulfur. Biol Chem 2007;388:997-1006.

327. Wang D, Wei J, Hsu K, et al. Effects of nitric oxide synthase inhibitors on systemic hypotension, cytokines and inducible nitric oxide synthase expression and lung injury following endotoxin administration in rats. J Biomed Sci 1999;6:28-35.

328. Sinha R, El-Bayoumy K. Apoptosis is a critical cellular event in cancer chemoprevention and chemotherapy by selenium compounds. Curr Cancer Drug Targets 2004;4:13-28.

329. Singhal S, Vachani A, ntin-Ozerkis D, Kaiser LR, Albelda SM. Prognostic implications of cell cycle, apoptosis, and angiogenesis biomarkers in non-small cell lung cancer: a review. Clin Cancer Res 2005;11:3974-86.

330. Jiang C, Wang Z, Ganther H, Lu J. Distinct effects of methylseleninic acid versus selenite on apoptosis, cell cycle, and protein kinase pathways in DU145 human prostate cancer cells. Mol Cancer Ther 2002;1:1059-66.

331. Li GX, Lee HJ, Wang Z, et al. Superior in vivo inhibitory efficacy of methylseleninic acid against human prostate cancer over selenomethionine or selenite. Carcinogenesis 2008;29:1005-12.

332. Lu J, Jiang C. Selenium and cancer chemoprevention: hypotheses integrating the actions of selenoproteins and selenium metabolites in epithelial and non-epithelial target cells. Antioxid Redox Signal 2005;7:1715-27.

333. Bennett WP, el-Deiry WS, Rush WL, et al. p21waf1/cip1 and transforming growth factor beta 1 protein expression correlate with survival in non-small cell lung cancer. Clin Cancer Res 1998;4:1499-506.

334. Toyoshima H, Hunter T. p27, a novel inhibitor of G1 cyclin-Cdk protein kinase activity, is related to p21. Cell 1994;78:67-74.

335. el-Deiry WS, Tokino T, Velculescu VE, et al. WAF1, a potential mediator of p53 tumor suppression. Cell 1993;75:817-25.

336. Kim JY, Choi JA, Kim TH, et al. Involvement of p38 mitogen-activated protein kinase in the cell growth inhibition by sodium arsenite. J Cell Physiol 2002;190:29-37.

337. Suzuki T, Tsukamoto I. Arsenite induces apoptosis in hepatocytes through an enhancement of the activation of Jun N-terminal kinase and p38 mitogen-activated protein kinase caused by partial hepatectomy. Toxicol Lett 2006;165:257-64.

338. Pedraza-Alva G, Koulnis M, Charland C, et al. Activation of p38 MAP kinase by DNA double-strand breaks in V(D)J recombination induces a G2/M cell cycle checkpoint. EMBO J 2006;25:763-73.

339. Fuchs SY, Adler V, Pincus MR, Ronai Z. MEKK1/JNK signaling stabilizes and activates p53. Proc Natl Acad Sci USA 1998;95:10541-6.

340. Keller D, Zeng X, Li X, et al. The p38MAPK inhibitor SB203580 alleviates ultraviolet-induced phosphorylation at serine 389 but not serine 15 and activation of p53. Biochem Biophys Res Commun 1999;261:464-71.

341. Rudolf E, Rudolf K, Cervinka M. Selenium activates p53 and p38 pathways and induces caspase-independent cell death in cervical cancer cells. Cell Biol Toxicol 2008;24:123-41.

342. Brown JR, DuBois RN. Cyclooxygenase as a target in lung cancer. Clin Cancer Res 2004;10:4266s-9s.

343. Harris RE, Beebe-Donk J, Doss H, Burr DD. Aspirin, ibuprofen, and other non-steroidal anti-inflammatory drugs in cancer prevention: a critical review of non-selective COX-2 blockade (review). Oncol Rep 2005;13:559-83.

344. Soriano AF, Helfrich B, Chan DC, et al. Synergistic effects of new chemopreventive agents and conventional cytotoxic agents against human lung cancer cell lines. Cancer Res 1999;59:6178-84.

345. Leslie CC. Properties and regulation of cytosolic phospholipase A2. J Biol Chem 1997;272:16709-12.

346. Hubbard WC, Alley MC, McLemore TL, Boyd MR. Profiles of prostaglandin biosynthesis in sixteen established cell lines derived from human lung, colon, prostate, and ovarian tumors. Cancer Res 1988;48:4770-5.

347. Hubbard WC, Alley MC, Gray GN, et al. Evidence for prostanoid biosynthesis as a biochemical feature of certain subclasses of non-small cell carcinomas of the lung as determined in established cell lines derived from human lung tumors. Cancer Res 1989;49:826-32.

348. Salvemini D, Settle SL, Masferrer JL, et al. Regulation of prostaglandin production by nitric oxide; an in vivo analysis. Br J Pharmacol 1995;114:1171-8.

349. El-Bayoumy K, Rose DP, Papanikolaou N, et al. Cyclooxygenase-2 expression influences the growth of human large and small cell lung carcinoma lines in athymic mice: impact of an organoselenium compound on growth regulation. Int J Oncol 2002;20:557-61.

350. Belinsky SA, Devereux TR, White CM, et al. Role of Clara cells and type II cells in the development of pulmonary tumors in rats and mice following exposure to a tobacco-specific nitrosamine. Exp Lung Res 1991;17:263-78.

351. Betsuyaku T, Senior RM. Laser capture microdissection and mRNA characterization of mouse airway epithelium: methodological considerations. Micron 2004;35:229-34.

352. Lindberg HK, Falck GC, Catalan J, Santonen T, Norppa H. Micronucleus assay for mouse alveolar Type II and Clara cells. Environ Mol Mutagen 2010;51:164-72.

353. Teng PN, Bateman NW, Hood BL, Conrads TP. Advances in proximal fluid proteomics for disease biomarker discovery. J Proteome Res 2010;9:6091-100.

354. Magi B, Bargagli E, Bini L, Rottoli P. Proteome analysis of bronchoalveolar lavage in lung diseases. Proteomics 2006;6:6354-69.

355. Reynolds HY. Use of bronchoalveolar lavage in humans--past necessity and future imperative. Lung 2000;178:271-93.

356. Wattiez R, Falmagne P. Proteomics of bronchoalveolar lavage fluid. J Chromatogr B Analyt Technol Biomed Life Sci 2005;815:169-78.

357. Hecht SS. Carcinogenicity studies of inhaled cigarette smoke in laboratory animals: old and new. Carcinogenesis 2005;26:1488-92.

358. Fiala ES, Sohn OS, Wang CX, et al. Induction of preneoplastic lung lesions in guinea pigs by cigarette smoke inhalation and their exacerbation by high dietary levels of vitamins C and E. Carcinogenesis 2005;26:605-12.

359. De FS, D'Agostini F, Balansky R, et al. Modulation of cigarette smoke-related end-points in mutagenesis and carcinogenesis. Mutat Res 2003;523-524:237-52.

360. Izzotti A, Bagnasco M, Cartiglia C, et al. Modulation of multigene expression and proteome profiles by chemopreventive agents. Mutat Res 2005;591:212-23.

361. Hutt JA, Vuillemenot BR, Barr EB, et al. Life-span inhalation exposure to mainstream cigarette smoke induces lung cancer in B6C3F1 mice through genetic and epigenetic pathways. Carcinogenesis 2005;26:1999-2009.

362. Thun MJ, Lally CA, Flannery JT, et al. Cigarette smoking and changes in the histopathology of lung cancer. J Natl Cancer Inst 1997;89:1580-6.

363. Witschi H. Successful and not so successful chemoprevention of tobacco smoke-induced lung tumors. Exp Lung Res 2000;26:743-55.

364. Witschi H, Uyeminami D, Moran D, Espiritu I. Chemoprevention of tobacco-smoke lung carcinogenesis in mice after cessation of smoke exposure. Carcinogenesis 2000;21:977-82.

365. Michaloglou C, Vredeveld LC, Soengas MS, et al. BRAFE600-associated senescence-like cell cycle arrest of human naevi. Nature 2005;436:720-4.

366. Hollander MC, Maier CR, Hobbs EA, et al. Akt1 deletion prevents lung tumorigenesis by mutant K-ras. Oncogene 2011;30:1812-21.

367. Memmott RM, Dennis PA. The role of the Akt/mTOR pathway in tobacco carcinogen-induced lung tumorigenesis. Clin Cancer Res 2010;16:4-10.

368. Anthonisen NR, Skeans MA, Wise RA, et al. The effects of a smoking cessation intervention on 14.5-year mortality: a randomized clinical trial. Ann Intern Med 2005;142:233-9.

369. Pierce JP, Messer K, White MM, Kealey S, Cowling DW. Forty years of faster decline in cigarette smoking in California explains current lower lung cancer rates. Cancer Epidemiol Biomarkers Prev 2010;19:2801-10.

370. Warner KE, Burns DM. Hardening and the hard-core smoker: concepts, evidence, and implications. Nicotine Tob Res 2003;5:37-48.

371. Edelman MJ. Novel taxane formulations and microtubule-binding agents in non-small-cell lung cancer. Clin Lung Cancer 2009;10 Suppl 1:S30-S34.

372. Shaw AT, Kirsch DG, Jacks T. Future of early detection of lung cancer: the role of mouse models. Clin Cancer Res 2005;11:4999s-5003s.

373. Porojnicu AC, Robsahm TE, Dahlback A, et al. Seasonal and geographical variations in lung cancer prognosis in Norway. Does Vitamin D from the sun play a role? Lung cancer (Amsterdam, Netherlands) 2007;55:263-70.

374. Zhou W, Heist RS, Liu G, et al. Circulating 25-hydroxyvitamin D levels predict survival in early-stage non-small-cell lung cancer patients. J Clin Oncol 2007;25:479-85.

375. Nakagawa K, Kawaura A, Kato S, Takeda E, Okano T. 1 alpha,25-Dihydroxyvitamin D(3) is a preventive factor in the metastasis of lung cancer. Carcinogenesis 2005;26:429-40.

376. Nakagawa K, Sasaki Y, Kato S, Kubodera N, Okano T. 22-Oxa-1alpha,25-dihydroxyvitamin D3 inhibits metastasis and angiogenesis in lung cancer. Carcinogenesis 2005;26:1044-54.

VITA

James D. Bortner, Jr.

Education:

Pennsylvania Stage University College of Medicine (PSU), Hershey, PA (2005-2011)
Ph.D. – Biochemistry and Molecular Biology
Millersville University, Millersville, PA (2000-2004)
B.S. – Molecular Biology/Biotechnology

Publications (4 of 5):

1) James D. Bortner, Jr., Arunangshu Das, Anne Stanley, Bruce Stanley, Cesar Aliaga, Timothy Cooper, Christine Skibinski, Karam El-Bayoumy. Proteomic profiling during different stages of lung tumorigenesis induced by 4-(methylnitrosamino)-1-(3-pyridyl)-1-butanone in the A/J mouse and the impact of chemopreventive agents. 2011 (in preparation).
2) James D. Bortner, Jr., John P. Richie, Jr., Arunangshu Das, Jason Liao, Todd M. Umstead, Anne Stanley, Bruce A. Stanley, Chandra P. Belani, Karam El-Bayoumy. Proteomic profiling of human plasma by iTRAQ reveals down-regulation of ITI-HC3 and VDBP by cigarette smoking. *J Proteome Res* 10 (2011): 1151-1159.
3) James D. Bortner, Jr., Arunangshu Das, Todd M. Umstead, Williard M. Freeman, Richard Somiari, Cesar Aliaga, David S. Phelps, Karam El-Bayoumy. Down-regulation of 14-3-3 isoforms and annexin A5 proteins in lung adenocarcinoma – induced by the tobacco-specific nitrosamine NNK in the A/J mouse revealed by proteomic analysis. *J Proteome Res* 8 (2009): 4050-4061.
4) Arunangshu Das, James Bortner, Dhimant Desai, Shantu Amin, Karam El-Bayoumy. The selenium analog of the chemopreventive compound S,S'-(1,4-phenylenebis[1,2-ethanediyl]bisisothiourea is a remarkable inducer of apoptosis and inhibitor of cell growth in human non-small cell lung cancer. *Chem Biol Interact* 180 (2009): 158-64.

Selected Abstracts and Poster Presentations (3 of 12):

1) James D. Bortner, Jr., Arunangshu Das, Anne Stanley, Bruce Stanley, Cesar Aliaga, Timothy Cooper, Christine Skibinski, Karam El-Bayoumy. Proteomic profiling during different stages of lung tumorigenesis induced by 4-(methylnitrosamino)-1-(3-pyridyl)-1-butanone in the A/J mouse and the impact of chemopreventive agents. *102nd Annual Meeting of American Association for Cancer Research*, Orlando, FL, April 1-5, 2011.
2) James D. Bortner, Jr., John Richie, Arunangshu Das, Jason Liao, Todd M. Umstead, Anne Stanley, Bruce Stanley, Chandra Belani, Karam El-Bayoumy. Comparison of Proteomic Profiles in Human Plasma of Smokers and Non-Smokers Using the iTRAQ Approach. *101st Annual Meeting of American Association for Cancer Research*, Washington, DC, April 17-21, 2010.
3) James D. Bortner, Jr., Arunangshu Das, Todd M. Umstead, Williard Freeman, Salah Almokadem, Richard Somiari, David S. Phelps, Karam El-Bayoumy. The chemopreventive agent 1,4-phenylenebis(methylene)selenocyanate (*p*-XSC) modulates the protein expression profile of 4-(methylnitrosamino)-1-(3-pyridyl)-1-butanone (NNK)-induced lung tumors in the A/J mouse: Clinical Implication. *2008 Penn State Cancer Institute Retreat*, Hershey, PA, November 5-6, 2008. *Selected Oral and Poster Presentation.